

美国超声心动图学会指南&标准
超声心动图评估房间隔缺损和卵圆孔未闭的应用指南
美国超声心动图学会与心血管造影及介入治疗学会联合发表

中文翻译：张 丽 华中科技大学同济医学院附属协和医院

中文审阅：谢明星 华中科技大学同济医学院附属协和医院

内容提要

目标读者

目的

前言

房间隔的发育与解剖

- 正常解剖
- 房间隔缺损解剖结构及相关异常解剖
 - 卵圆孔未闭(PFO)
 - 继发孔型房间隔缺损
 - 原发孔型房间隔缺损
 - 静脉窦型缺损
 - 冠状静脉窦型缺损
 - 单心房
 - 房间隔膨出瘤
 - 欧式瓣和希阿里(氏)网

房间隔成像

- 常规成像方法
- 三维超声房间隔成像
- 超声心动图在经导管封堵术中的应用
- 房间隔经胸超声心动图成像建议
 - TTE 剑突下(四腔心)切面观
 - TTE 剑突矢状位切面观
 - TTE 左前斜位切面观
 - TTE 心尖四腔心切面
 - TTE 改良心尖四腔心切面观(介于心尖四腔心切面与胸骨旁短轴切面之间)
 - TTE 胸骨旁短轴切面
 - 高位胸骨右旁切面
- 房间隔经食道超声心动图成像建议
 - 食管上段短轴切面
 - 食管中段主动脉瓣短轴切面

- 食管中段四腔心切面

- 食管中段二腔切面

- 3D TEE PFO 与 ASD 成像建议
- 3D TTE PFO 与 ASD 成像建议
- 3D 显示
- 心腔内超声心动图 IAS 成像建议

分流的评价

- 分流成像的技术、标准和特点：TTE 与 TEE
- 经颅彩色多普勒分流的探查/分级
- 分流对右室的影响
- 肺动脉高压
- RV 功能
- LV 功能

房间隔与间隔缺损成像

- 卵圆孔未闭
- 房间隔膨出瘤
- 欧式瓣和希阿里氏网
- 房缺的评价：标准和特点

超声心动图在经导管封堵术中的应用

- 现有封堵器和封堵技术介绍
- 封堵器栓塞和磨蚀
- 经皮导管术中成像指导：TTE, TEE, ICE
- 经导管介入术的术中指导
- ICE 术中指导 PTC
- 术后房间隔即时成像
- 随访

结论

通知和免责声明

补充数据

| 缩写 | 英语全称 | 中文全称 |
|-----|---------------------------|---------------|
| 2D | Two-dimensional | 二维 |
| 3D | Three-dimensional | 三维 |
| AoV | Aortic valve | 主动脉瓣 |
| ASA | Atrial septal aneurysm | 房间隔膨出瘤 |
| ASD | Atrial septal defect | 房间隔缺损 |
| ASO | Amplatzer septal occluder | Amplatzer 封堵器 |
| AV | Atrioventricular | 房室 |

| | | |
|-------------|--|--------------|
| CS | Coronary sinus | 冠状静脉窦 |
| EV | Eustachian valve | 欧式瓣 |
| DTI | Doppler tissue imaging | 组织多普勒成像 |
| FDA | Food and Drug Administration | 食品和药物管理局 |
| IAS | Interatrial septum/septal | 房间隔 |
| ICE | Intracardiac echocardiography | 心腔内超声心动图 |
| IVC | Inferior vena cava | 下腔静脉 |
| LA | Left atrium/atrial | 左房 |
| LV | Left ventricle/ventricular | 左室 |
| PA | Pulmonary artery | 肺动脉 |
| PFO | Patent foramen ovale | 卵圆孔未闭 |
| Qp/Qs ratio | Pulmonary to systemic blood flow ratio | 肺循环/体循环血流量比值 |
| RA | Right atrium/atrial | 右房 |
| RT3DE | Real-time three-dimensional echocardiography | 实时三维超声心动图 |
| RUPV | Right upper pulmonary vein | 右上肺静脉 |
| RV | Right ventricle/ventricular | 右室 |
| SCAI | Society for Cardiac Angiography and Intervention | 心血管造影与介入协会 |
| SVC | Superior vena cava | 上腔静脉 |
| SVD | Sinus venosus defect | 静脉窦缺损 |
| TCD | Transcranial Doppler | 经颅多普勒 |
| TEE | Transesophageal echocardiography/echocardiographic | 经食管超声心动图 |
| TTE | Transthoracic echocardiography/echocardiographic | 经胸超声心动图 |
| VTI | Velocity time integral | 速度时间积分 |

目标读者

本文可供对超声心动图领域感兴趣并具有一定基础知识的学者及对房间隔异常与心脏超声应用感兴趣的其他医学专业人士阅读。这包括心血管医师、其他心血管器材供应商、心脏超声医师、外科医师、心血管介入治疗医师、神经科医师、住院医师、研究护士、临床医师、重症监护人员及其它临床工作者。

目的

在完成对本指南的阅读后，读者将能够更好地：

1. 掌握经胸超声心动图，经食管超声心动图和心腔内超声心动图等超声技术对房间隔进行最佳成像与评估的常规二维，三维和多普勒超声心动图检查方法
2. 掌握正常房间隔、房间隔缺损、房间隔膨出瘤及卵圆孔未闭的超声心动图特点。这包括测量和评估技术的最佳实践。
3. 掌握各种超声心动图技术的优缺点及根据已发表数据而定的评价房间隔的测量指标。
4. 知晓可用于房间隔缺损、房间隔膨出瘤及卵圆孔未闭超声心动图标准化评价的图像和测量指标。

5. 解释房间隔缺损、房间隔膨出瘤和卵圆孔未闭超声心动图评价的临床和预后意义，除房间隔本身的评价外，还可同时评估各房室腔的大小和功能以及肺循环。
6. 认识对于房间隔异常的患者，需符合哪些特征才能行经导管（即，装置）封堵术。
7. 掌握房间隔异常修补术或经导管介入治疗后的超声心动图特征及可能出现的声像图改变。

前言

房间隔异常相通约占所有先天性心脏缺陷病的 6%-10%，在活产新生儿中发病率约 1:1500。¹ 房间隔缺损 (atrial septal defect, ASD) 是最常见的非紫绀型先天性心脏病之一，新生儿中发病率约 0.1%，在成年人具临床意义的异常分流中占 30%-40%。²⁻⁴ 卵圆孔未闭 (patent foramen ovale, PFO) 则更为常见，存在于超过 20%-25% 的成年人中。⁵ 房间隔缺损和卵圆孔未闭的临床症状极其多变，是一重大的健康负担，横跨了儿科、成人医学、神经内科和手术。评价房间隔异常及其相关综合征需要一套标准化、系统化的方法获取其超声心动图和多普勒特征，包括经胸超声心动图 (TTE)、经食道超声心动图 (TEE)、心脏内超声心动图 (ICE) 技术、三维 (3D) 成像、多普勒和经颅多普勒 (TCD) 技术。

对 PFO 和 ASD 完整的超声心动图评价应包括对缺损的检出及量化房间隔缺损的大小与形状、缺损周围组织的边界、分流的程度与方向、心脏各房室腔的重塑与大小、功能的改变以及肺循环的情况。三维成像的出现，尤其是在经食道三维超声心动图，为

房间隔的评价提供了更多信息。^{6,7} 因此，本指南旨在将现有的诊断方法整合起来，以便协助临床实践、培训及研究。

旧版美国超声心动图学会 (ASE) 指南着重讲述了经食道检查的操作，3D 超声心动图图像的获取与成像标准，超声心动图指导房间隔缺损封堵以及对右室 (RV) 的评估。⁸⁻¹² 全面、详细的房间隔 (IAS) 评价指南可以减少超声心动图评价质量的参差不齐，更全面的评价房间隔的特点，标准化用于评估解剖结构和生理特点的测量指标与检查技术，改进对手术和介入治疗适应症的评估。

因此，临床医师、研究人员、器械制造商以及管理机构都将受益于这些标准，它们将使临床护理、临床试验设计和影像核心实验室的管理更加统一。

此外，患者手术前后及介入治疗前后的超声心动图和多普勒 IAS 评估同样需要指南与标准化的方法。治疗的转归及并发症必须由现代超声心动图中心进行充分、有效的评估、定性及报告。

房间隔的发育与解剖

正常解剖

认识房间隔相通需要对 IAS 的胚胎发育及解剖有全面的了解。¹³ 房间隔由三部分组成：原发隔、继发隔和房室 (AV) 间隔。静脉窦并非房间隔的组成部分，但其紧邻 IAS，左、右心房异常相通可发生于此。间隔缺损可根据其在 IAS 的解剖位置分类 (图 1)。

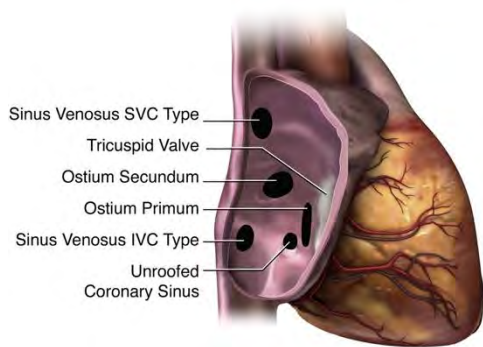


图 1 由右房侧观，房间隔相通的亚型。卵圆孔未闭未显示。

图 2 描绘了正常房间隔发育的示意图。最初心房为一个共同的腔室。在孕 28 天左右，原发隔，起于心房顶部，开始向发育中的心内膜垫迁移。在这个过程中，原发隔与心内膜垫之间的孔称为“胚胎原发孔”或者“第一房间孔”。¹⁴ 而继发隔则是由心房顶部向内折叠而形成的，并非真正的膜性结

构；它紧邻发育中的原发隔右侧，向下发育。¹⁴ 在正常心脏，原发孔由来源于原发隔的间充质细胞（即所谓的前庭脊柱充质帽）与上、下心内膜垫融合关闭。¹⁴ 继发隔的前缘成为上边缘带。孕 2 个月时，原发隔与继发隔逐渐融合，只剩下卵圆孔作为唯一残留的心房相通通道。卵圆孔周围膜性结构统称为“卵圆窝”，由继发隔、原发隔（位于左房[left atrial, LA]侧的继发隔上）及 AV 间隔构成。¹⁵ 原发隔与静脉系统相延续，构成了上、下腔静脉的流入道。静脉窦隔紧邻房间隔，将右肺静脉与上腔静脉及后方的 RA 分离开来。¹⁵ 冠状静脉窦与左房被冠状静脉窦隔分隔开来。房间隔前上部分紧邻主动脉瓣右冠窦。在附件中可以获取关于房间隔发育过程更为详细的描述。

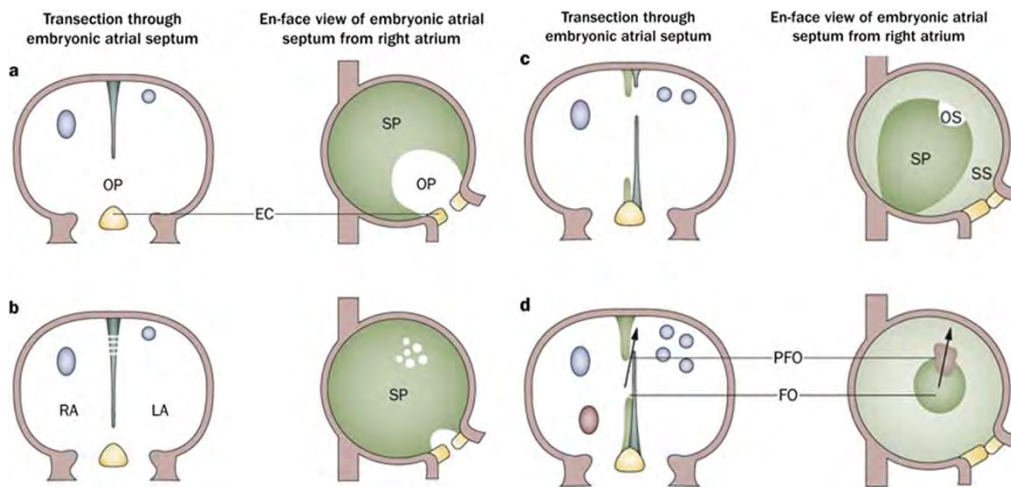


图 2 (A) 原发隔起自心房顶部。(B) 原发隔内形成窗样结构。(C) 继发隔由心房顶部内折形成。(D) 在卵圆窝的上下边缘，原发隔和继发隔仍未融合，即卵圆孔未闭的形成基础。箭头标示为血液于卵圆孔处由右房进入左房。蓝色和粉红色分别代表腔静脉与肺静脉移行为右房流入道的部位。EC，心内膜垫；FO，卵圆窝；OP，原中孔隔；OS，第二中孔隔；SP，原发隔；SS，继发隔。引自 Calvert 等。¹⁶

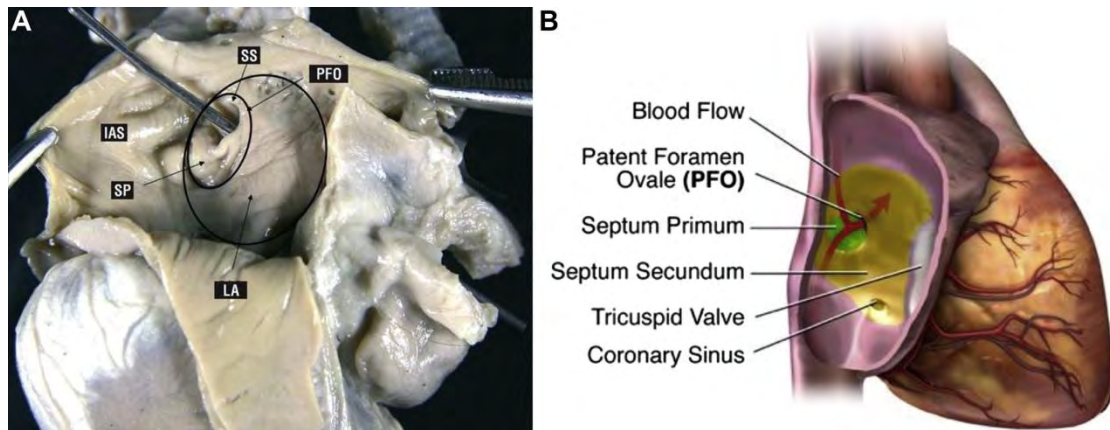


图 3 (A) 通过探针从左房侧观，动脉导管未闭解剖标本，同时也指明了动脉导管周围结构。(B) 典型卵圆孔未闭一般位于临近主动脉根部的前上缘。箭头标明了从右房分流至左房的血流通道。

房间隔缺损解剖结构及相关异常解剖

卵圆孔未闭(PFO)

PFO 并非真正房间隔组织缺损，而是位于房间隔前上部的原发隔与继发隔间一个潜在的间隙或分隔(图 3 A, B)。¹⁶ 由于 PFO 并没有真正的房间隔组织缺失，故而不认为其是真正意义上的 ASD。^{14,17} 当 LA 的压力大于 RA 时，卵圆孔呈功能性闭合的状态。在很多病例中，由于原发隔形成了瓣膜，PFO 可呈类隧道样的功能性开放状态。LA 与 RA 压力差的变化可引起间歇性的分流。PFO 也可以是两侧心房间真实存在的圆形或椭圆形缺损。部分病例中，因心房扩张和重塑而导致的继发隔前缘“伸展”也是引起 PFO 的原因之一(图 4-6)。另外部分病例中，原发隔呈瘤样结构，无法完全封闭心房间的通道¹⁸(图 7)。胎儿期，卵圆窝处的通道起到了将经胎盘获得的含氧血运输到身体各个重要器官的重要作用，其中包括发育中的中枢神经系统。¹⁸ 卵圆孔通常会在出生后两个月左右闭合。多达 20%-25%的正常人在成年期仍有 PFO。¹⁸⁻²¹

PFO 的发生率及其大小随年龄而变化。在一项 965 例人体心脏解剖的研究中发现，卵圆孔未闭的发生率约为 27.3%，但随着年龄的增长，其发生率显著降低，30 岁及 30 岁前其发生率为 34.3%，30 岁以后至 80 岁其发生率降为 25.4%，80 岁以后至 100 岁其发生率降为 20.2%。在所解剖的心脏中，PFO 的大小由 1 到 19 mm 不等(平均 4.9 mm)。其中 98%的病例的卵圆孔直径在 1 至 10 mm 之间，其大小似乎也随年龄的增长而增大，10 岁以前其平均直径约 3.4 mm，百岁其平均直径约 5.8 mm。

为了命名的一致性，将“卵圆孔未闭”定义为经多普勒超声或右心造影观察到右向左分流，但不合并真性 IAS 缺损。伴有左向右分流的 PFO 指心房内血流动力学的改变使潜在的卵圆孔通道开放，在多普勒超声检查中可见到左向右的分流信号(图 4-6)。若 PFO 是由心房内血流动力学的改变使房间隔拉伸而形成缺损，则称为“拉伸型”PFO。此时可在多普勒超声上观察到左向右或右向左的分流信号，这取决于 RA 与 LA 间的压力差。

卵圆孔由原发隔与继发隔重叠部分的组织结构融合而关闭。融合不完全可形成解剖上的袋状结构，大多数情况下，该结构与 LA 腔相通。²²“LA

房间隔袋”是指原发隔与继发隔部分重叠后未重叠部分形成的盲袋，此处易形成血栓。²³⁻²⁶其表现可类似于 LA 粘液瘤。²⁷

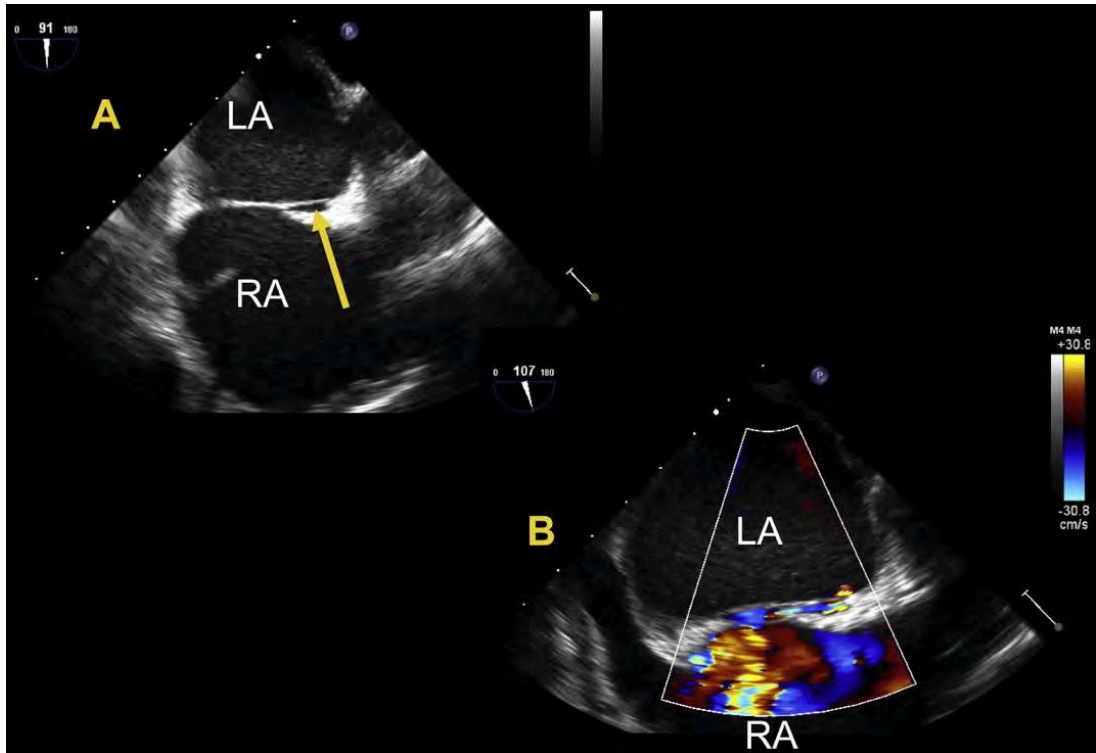


图4 二维经食道超声心动图双房切面观，显示卵圆孔未闭(PFO)(黄色箭头所示)，(A)为二维显像，(B)彩色多普勒血流显像。

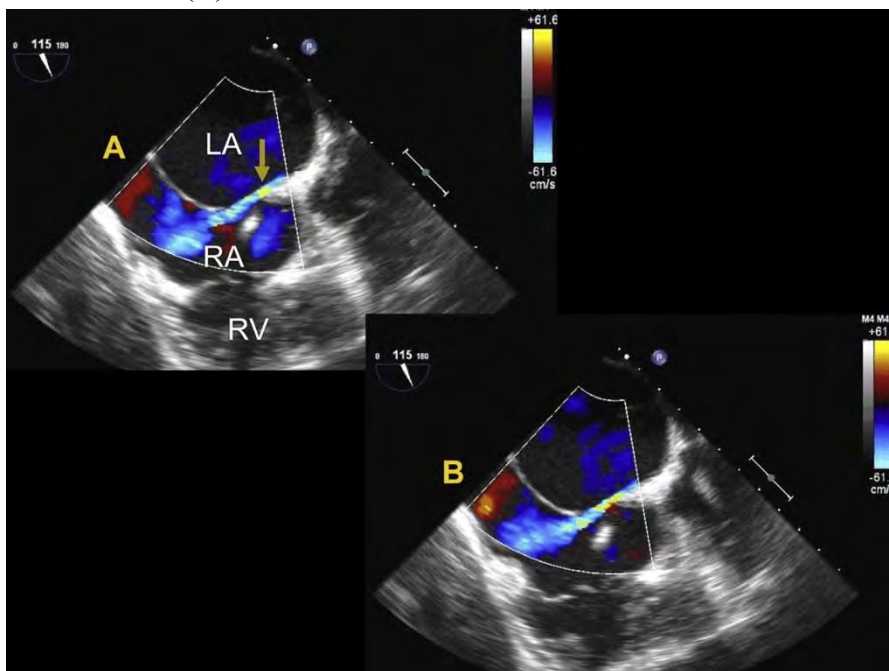


图 5 成人二维经食道超声心动图双房切面观，显示“伸展型”卵圆孔未闭图像，(黄色剪头所示)，(A 和 B) 彩色多普勒血流显像示房间隔左向右分流信号。

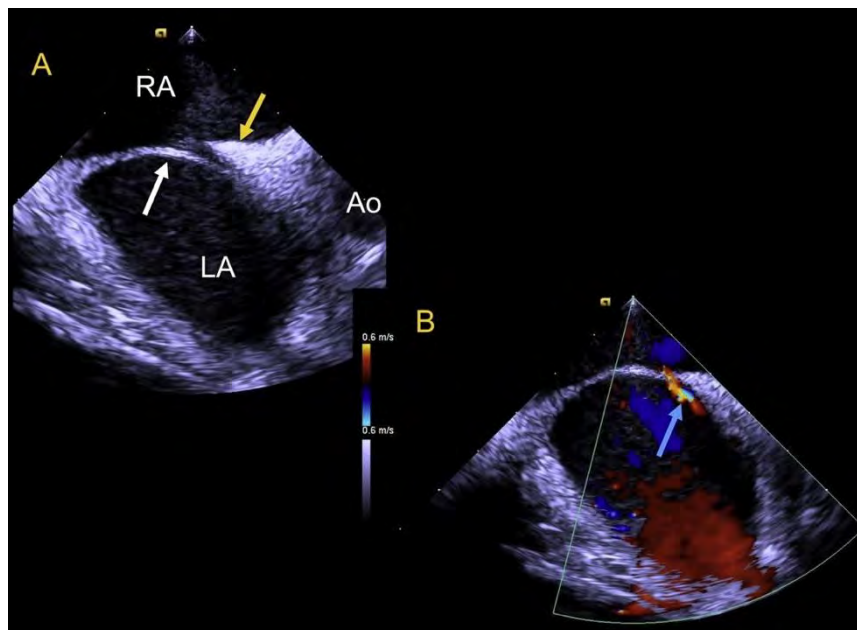


图 6(A) 成人二维经食道超声心动图，显示的“伸展型”卵圆孔未闭图像和 (B) 彩色多普勒血流显像。黄色箭头所示为继发隔；白色箭头所示为原发隔；蓝色箭头所示为卵圆孔未闭处，左向右分流信号。

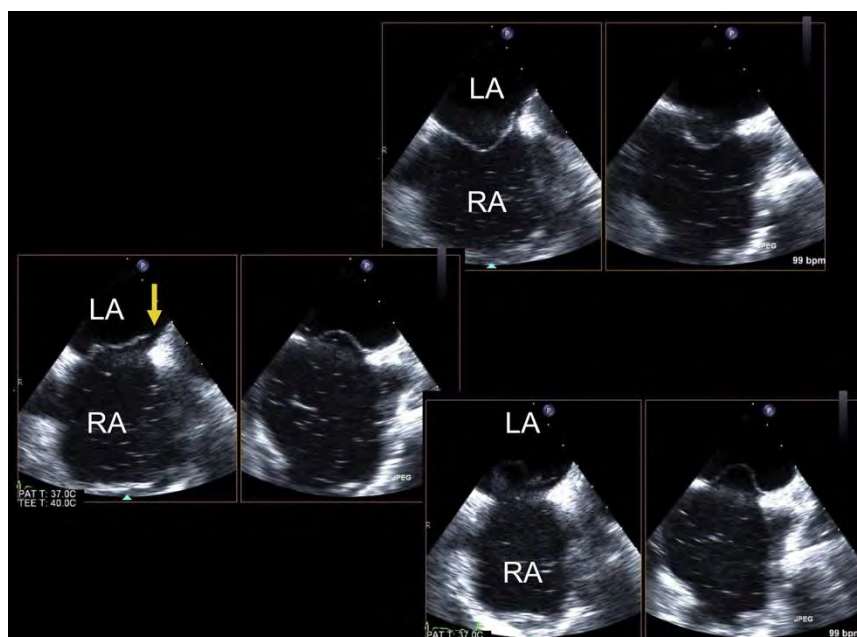


图 7 双平面经食道超声心动图显示，房间隔中部卵圆孔未闭，卵圆窝处血流丰富，组织薄弱，合并卵圆孔未闭（箭头）。从右房侧观。如同 Video3 所示。

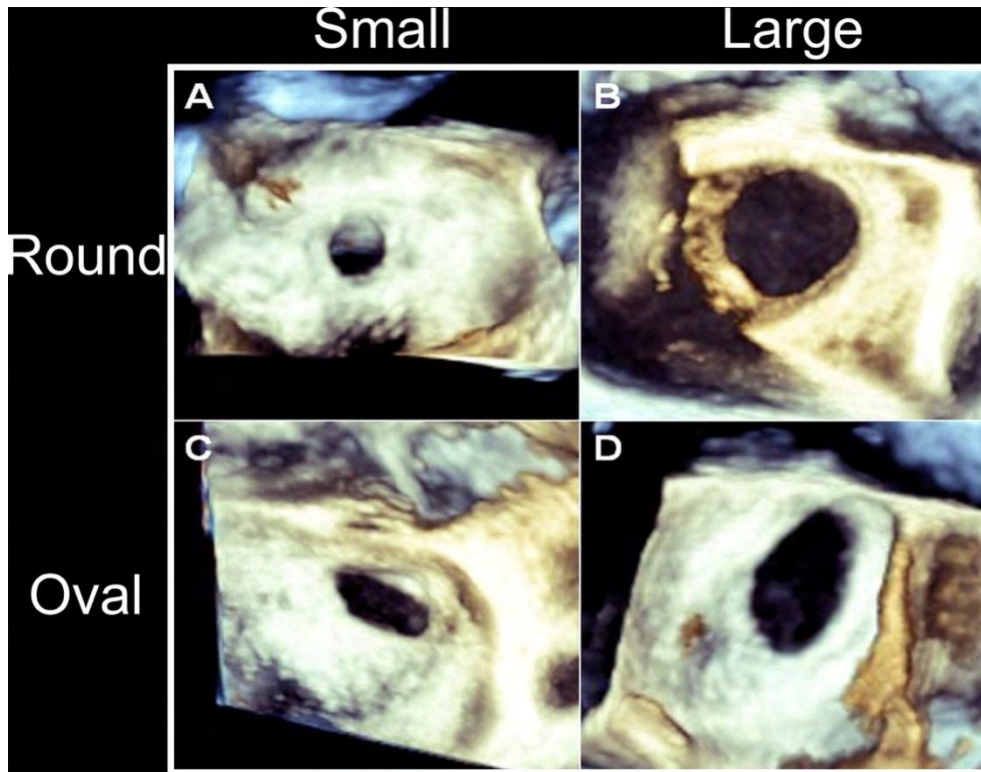


图 8 三维经食道超声心动图显示不同形状和大小的继发孔型房间隔缺损。典型病例(A)小而圆型, (B)大而圆型, (C)小孔型, (D)大孔型。如同 Video4 所示。引自 Seo 等。⁷⁷

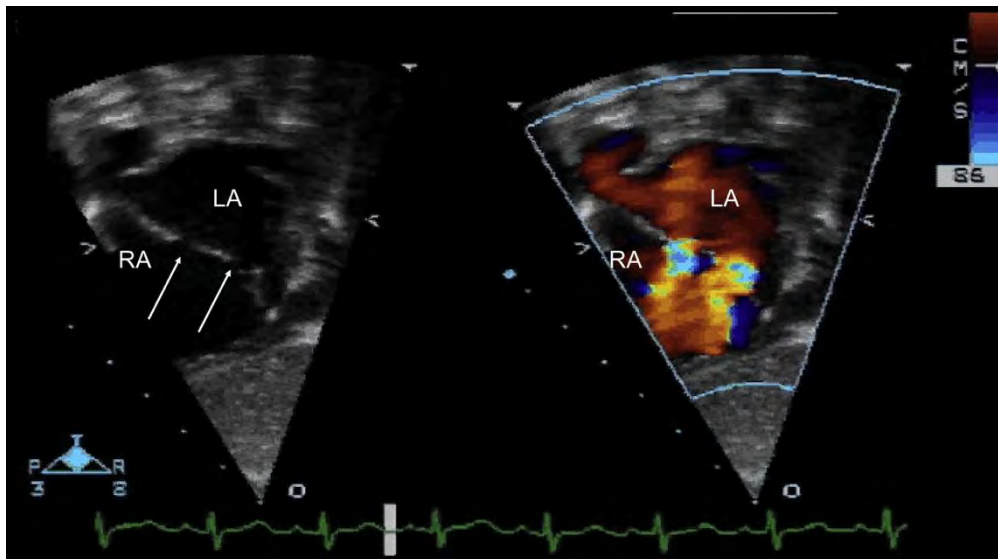


图 9 儿科患者经胸超声剑突下切面示, 多孔型房间隔二维图像, 彩色多普勒图像示左向右的分流。

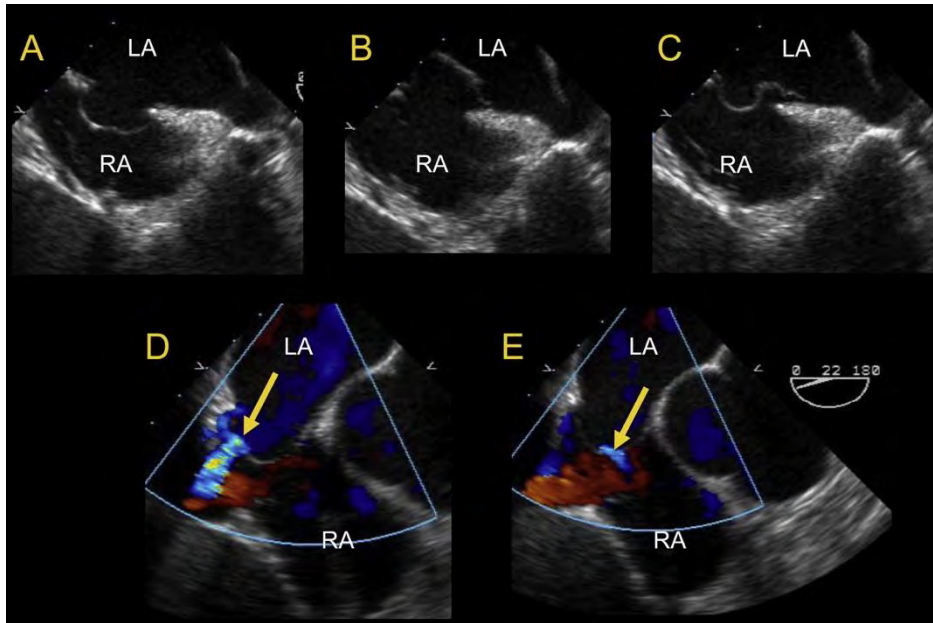


图 10 经食道二维超声（双腔平面观）下房间隔与房间隔膨隆瘤成像，示卵圆窝处动度异常并伴有多孔缺损（D-E）（黄色箭头）。

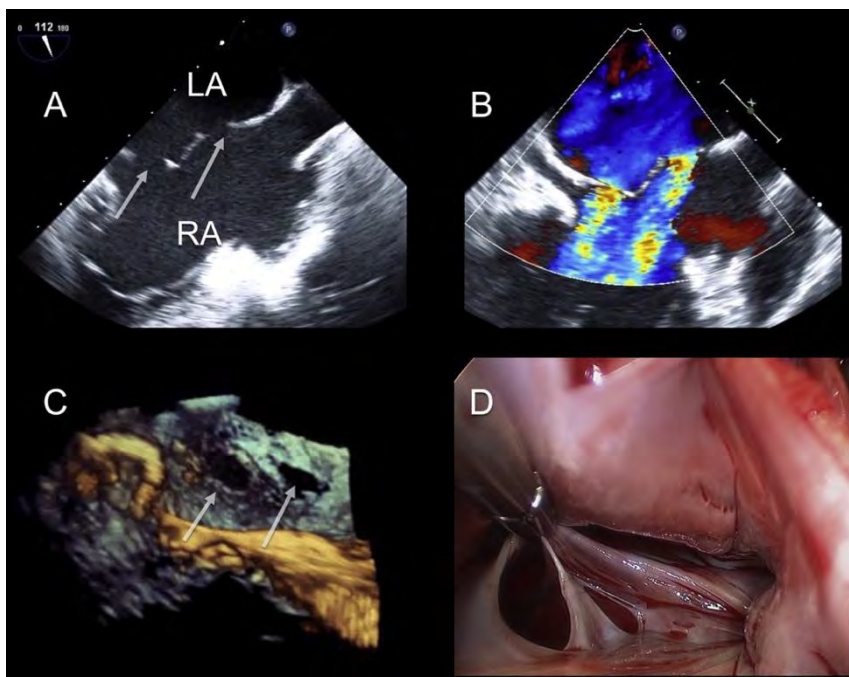


图 11 经食道三维超声提示房间隔及小继发孔型房缺（白色箭头）。（A）二腔平面观示两个不相关的都房缺。（B）彩色多普勒二腔平面观示两处不相关的左向右血液分流。（C）右房侧变焦采集两个房缺图像。（D）微创手术修补术中见与经食道三维超声所示一致的结果。

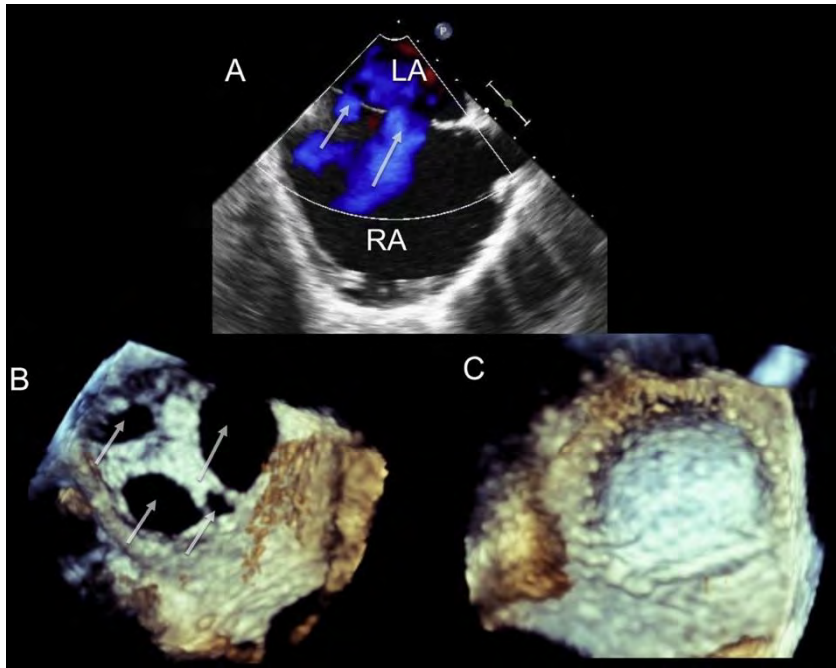


图 12 经食道三维超声下多孔型房缺（白色箭头），呈奶酪状结构。（A）彩色多普勒二腔心切面观示至少两处不相连的左向右分流信号。（B）右房侧对侧变焦采集图像示四处不相连的缺损部位。（C）微创手术修补后变焦采集图像示单一的心脏补片。

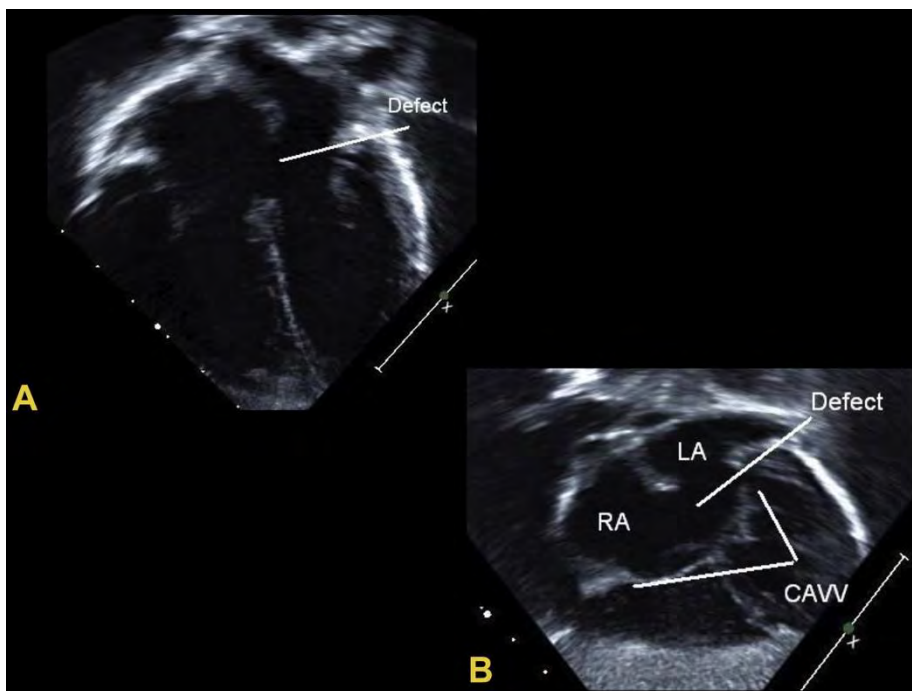


图 13 （A）经胸二维超声四腔心切面观示原发孔型房缺。（B）经胸二维超声肋下左前斜视图示原发孔型房缺。CAVV，正常主动脉瓣。

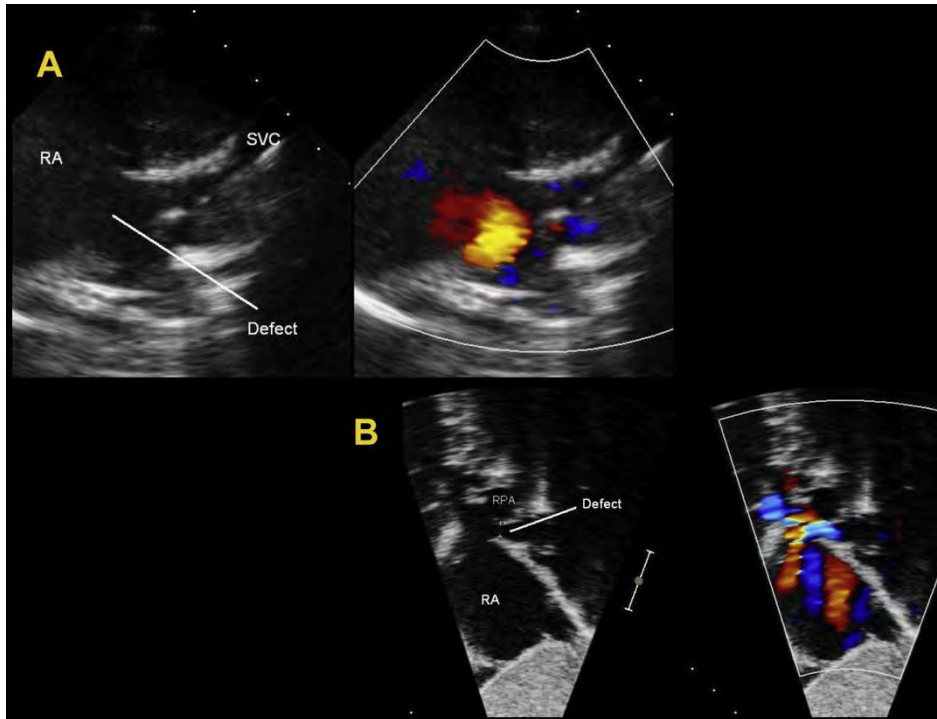


图 14 (A) 典型的上静脉型房缺经胸二维超声成像 (左) 与彩色多普勒超声成像 (右), 高右侧胸骨旁观。(B) 典型的上静脉型房缺经胸二维超声成像 (左) 与彩色多普勒超声成像 (右), 肋下切面观。RPA, 右肺动脉。

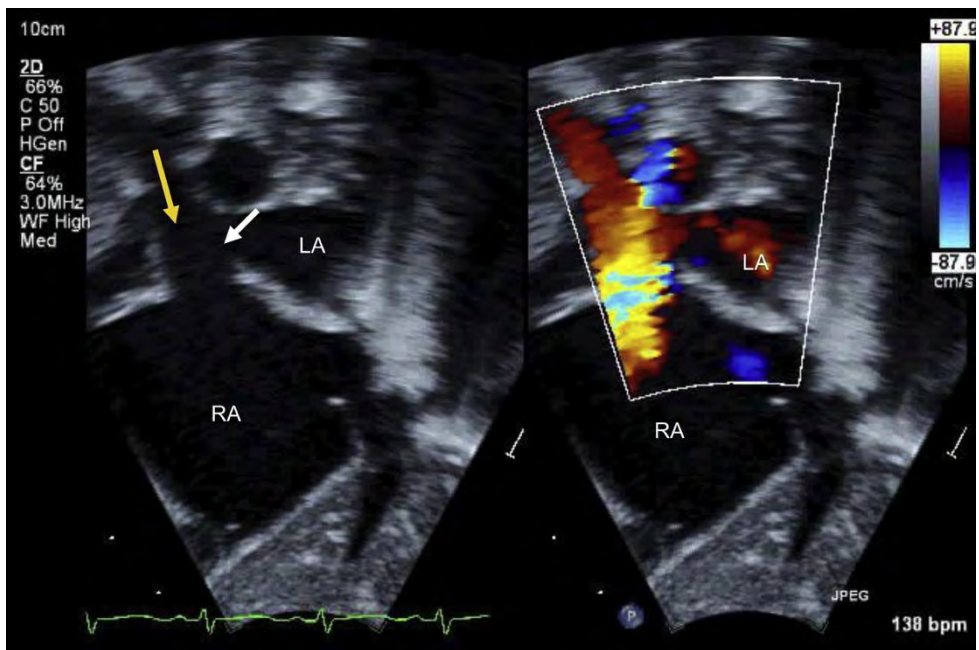


图 15 上腔静脉型房缺患儿的经胸超声心动图图像, 普通二维图像与彩色血流图像。黄色箭头示右上肺静脉, 白色箭头示房间隔缺损部位。

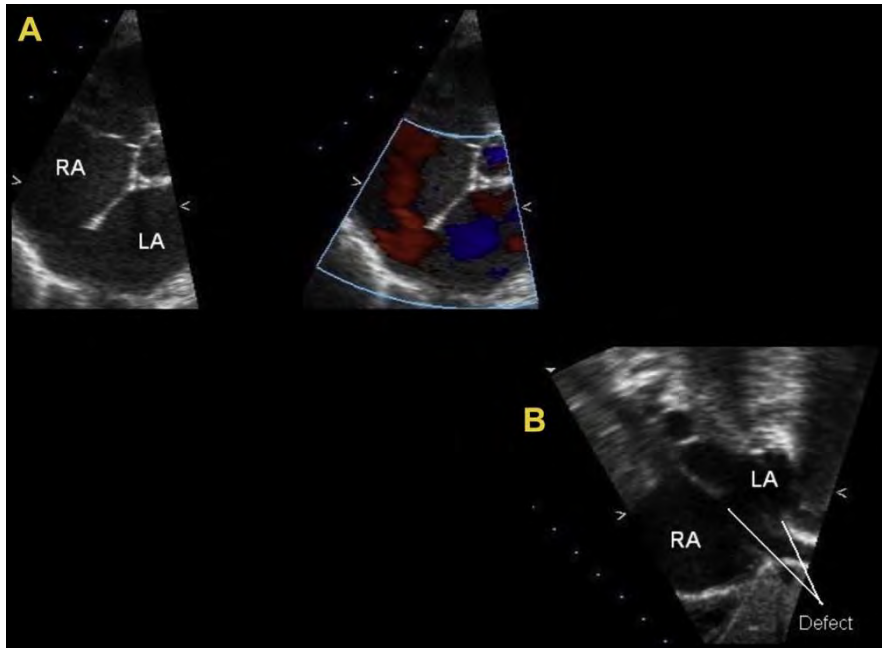


图 16 (A) 胸骨旁短轴切面观，下腔静脉型房缺的经胸二维超声图像（左）及彩色多普勒图像（右），显示左向右血液分流。（B）肋下切面观，经胸超声下腔静脉型房缺图像。

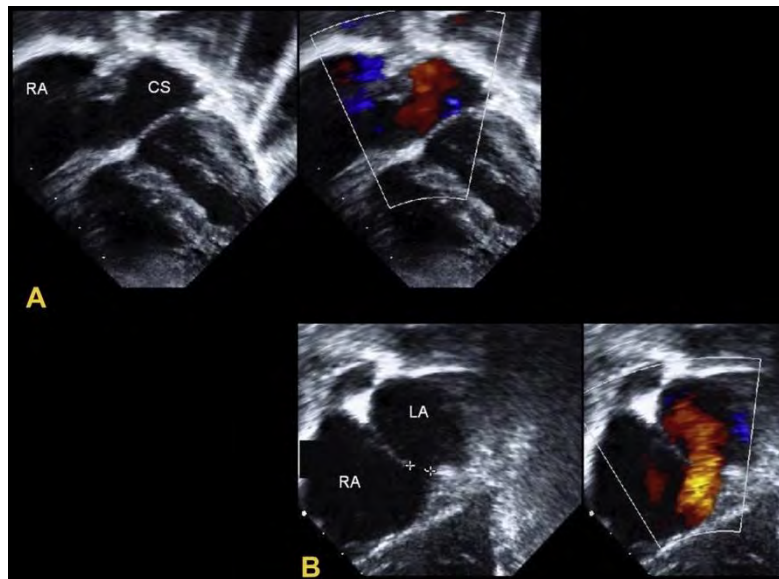


图 17 (A)四腔心切面观，冠脉顶盖缺如型房缺的经胸二维超声图像(左)和彩色多普勒图像(右)。(B)肋下左前斜面观，冠脉顶盖缺如型房缺的经胸二维超声图像(左)和彩色多普勒图像(右)。CS，冠状静脉窦。

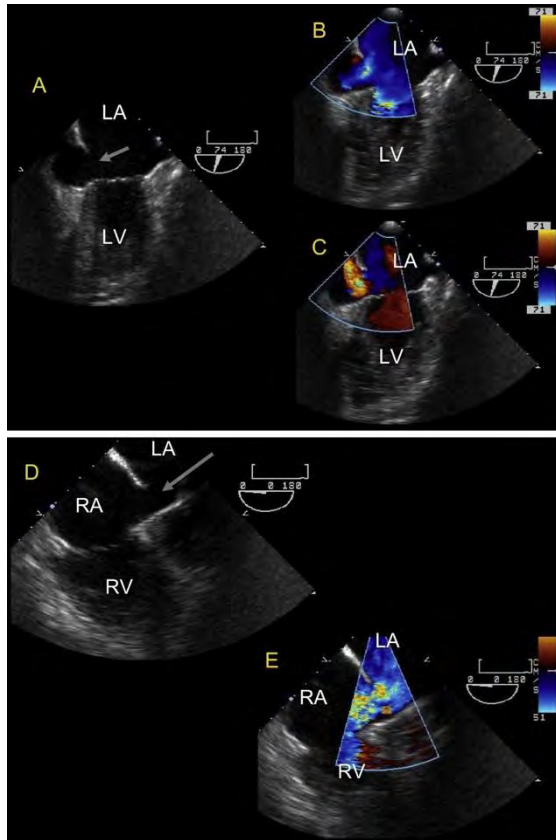


图 18 经食道超声示冠状静脉窦顶盖缺如。(A)二维超声示顶盖缺如而与左房相通的冠状静脉窦扩张。(B和C)彩色多普勒示左房内血流经冠状静脉窦进入右房，通过顶盖缺如的冠状静脉窦，房与房之间相通。(D)二维超声示顶盖缺如而与左房相通的冠状静脉窦扩张。(E和F)彩色多普勒示左房内血流经冠状静脉窦进入右房，通过顶盖缺如的冠状静脉窦，房与房之间相通。

继发孔型房间隔缺损. 继发孔型 ASD 通常存在真正的房间隔组织缺损，是最为常见的 ASD。²⁸ 缺损的上缘和后缘均为继发隔，前缘为 AV 间隔，下缘为原发隔及下腔静脉左侧静脉瓣。¹⁸ 这些缺损的大小形态各异，可以呈圆形或椭圆形（图 8）。当继发隔缺损较大时，其原发隔也往往几乎或完全缺如。部分病例中，原发隔可残存部分组织，穿过继发隔上的缺损，形成多处心房间通道，可见多孔分流（图 9-12）。这类 ASD 缺损的直径可从几毫米到 3 cm 不等。例如，在对 50 例继发孔型 ASD 患者的心脏解剖研究中发现，所有缺损可以从形态学上分为四种：（1）原发隔完全缺失，则缺损破口为整个卵圆窝（n=19, 38%）；（2）

原发隔缺损（n=16, 32%）；（3）孔型原发隔致多发 ASD（n=2, 4%）；（4）多孔型原发隔致多发 ASD（n=13, 26%）。²⁹ 缺损解剖上的不同对于封堵术的施行有极为重要的意义，可帮助决定是使用专为多孔缺损设计的封堵器进行封堵，还是使用多个封堵器进行封堵。继发孔型房间隔缺损可随着年龄的增长、心脏的增大而增大。²⁸

继发孔型房间隔缺损常可行经皮导管封堵术。³⁰⁻³³ 在这篇文章中会具体评价经皮导管封堵器的适应症。

继发隔上缘缺失是一类罕见的继发孔型 ASD。在这种病例中，房间隔的缺损部位位置较高，紧邻 SVC。应注意勿将此类缺损与下腔静脉窦型缺损混淆。值得注意的是，高位继发孔

型 ASD 并不伴有肺静脉异位引流。当左、右心耳并列位于左侧时，也可出现继发隔的缺失。心耳并列是指两侧心耳（或一侧心耳与另一心耳的一部分）彼此相邻并位于大血管同侧。这种心耳位置异常通常合并严重的先天性心脏病，包括大动脉转位。³⁴在心耳并列中，由于常有大动脉位置异常（如

原发孔型房间隔缺损。原发孔型 ASD 是一种先天性畸形，属于 AV 管缺损（图 13）。此类缺损是由于胚胎发育早期间充质细胞异常迁移，致使心内膜垫未融合而形成的。³⁵存在心内膜垫缺损时，AV 间隔及 AV 瓣膜均可受到不同程度的影响。原发孔型 ASD 也可称为部分或不完整型房室管缺损；这些名字可以互换使用。此类缺损的特点在于心房间的交通是由房间隔部分的房室管缺损所致，有一个共同房室瓣环和两组房室瓣。房室瓣组织与室间隔顶部相连，因此心室水平无分流。两组房室瓣发育异常，可见两组跨立于 RV 与左室（left ventricle, LV）之间的桥瓣，而非正常的二尖瓣前叶及三尖瓣隔瓣。桥瓣（上、下瓣）相交汇于室间隔，易被错认为“二尖瓣瓣叶裂”。这类畸形在先天性心脏病中是不可忽视。然而，由于原发孔型 ASD 患者的两组瓣叶常存在畸形，因此描述原发孔型 ASD 时用左、右 AV 瓣更为准确。由于存在瓣叶畸形或者瓣叶缺损，经所谓瓣叶裂的 AV 瓣反流极为常见。

原发孔型 ASD 的边界为原发隔的上缘与后缘及共同房室瓣环的前缘。AV 瓣裂孔是此型房间隔交通的边缘之一，不能施行经皮导管封堵术。³¹

心室双出口或大动脉转位），心房顶部的正常折叠过程（形成继发隔）往往不会出现。¹⁸虽然这类缺损并未影响腔静脉、主动脉瓣、肺静脉及冠状静脉窦，但是如若考虑行经导管封堵术，必须明确缺损部位与这些结构的位置关系。³¹

静脉窦型缺损。静脉窦型缺损较继发孔型 ASD 少见，且并非真正意义上的 ASD。²⁸此类缺损可部分或完全位于 SVC 和右上肺静脉间（SVC 型）的静脉窦隔或右下、中肺静脉与 RA 间（下腔静脉[inferior vena cava, IVC]型；图 14-16）的静脉窦隔。大多数的 SVC 型缺损患者，其右上肺静脉位置正常，但常异常引流入右房。但在部分患者中也可出现右侧部分或全部的肺静脉先异位引流入 SVC，再汇入 RA。此型缺损的分流与部分肺静脉异位引流类似，静脉血直接汇入 RA。其左向右的分流量往往较大。少数情况下，由于上腔静脉的血液可以回流入左房，患者的缺氧情况会稍有改善。LVC 型静脉窦缺损更为少见，多合并右中肺静脉与/或右下肺静脉异位引流。静脉窦型缺损不可行封堵术，通常需要用 ASD 补片将右肺静脉血流隔入 LA。如果右肺静脉直接汇入上腔静脉，则需要行上腔静脉再植术(Warden 手术)。

冠状静脉窦型缺损。冠状静脉窦间隔缺损或“无顶”冠状静脉窦是更为少见的一类房间隔交通。此型缺损中，冠状静脉窦顶部与相对的左房后之间的间隔部分或完全缺如（图 17-19）。当心脏没有其他的结构异常时，左房内血流流入冠状静脉窦，经因血流量增加而扩张的冠状静脉窦口入右房。通常

将冠状静脉窦间隔缺损合并永存左位 SVC 称为“Raghib 综合征”。³⁶

震荡生理盐水造影可帮助确定诊断。二维 (Two-dimensional, 2D) 和 3D TEE 在确定诊断上尤为重要, 并与手术结果相关性好。^{6,37} 冠状静脉窦顶盖部分缺如的患者, 有一部分也可行经导管封堵术。^{38,39}

单心房.此型缺损极为少见, 房间隔的所有结构全部缺如, 包括原发隔、继发隔及房室间隔, 只留一个单心房。^{28,40-42} 常合并内脏异位。部分患者可能会有一些残存的房间隔组织。

房间隔膨出瘤.房间隔膨出瘤 (atrial septal aneurysm, ASA) 是指房间隔中部组织冗长或呈囊袋状, 组织薄弱, 活动幅度增加。ASA 的定义为间隔组织 (尤其是卵圆窝) 向 RA 或 LA 侧偏离, 距正常房间隔的位置超过 10mm 或者左右摆动幅度超过 15mm (图 10)。ASA 的发病率约为 2%-3%。⁴³ 房间隔膨出瘤可与 PFO 并存, 且 PFO 通常较大, 不明原因的脑卒中和其它栓塞事件的发病率也增高。ASA 也常合并多发间隔缺损, 应注意运用彩色多普勒成像仔细探查。

欧式瓣和希阿里 (氏) 网.欧式瓣是胎儿期将血流自 IVC 隔入卵圆窝的 IVC 瓣的遗迹。当存在 PFO 时, 较大或较为突出的欧式瓣可阻碍卵圆孔的自然闭合而间接引起反常性栓塞。⁴⁷ 欧式瓣向前延伸至 IVC-RA 结合处。

希阿里 (氏) 网是静脉窦右瓣的遗迹, 可呈膜状或条索状位于右房的不同部位, 包括近 IVC 入口处、冠状静脉窦右房开口处 (图 20)。约 2%-3% 的人有希阿里 (氏) 网, 多与 PFO 和 ASA 同时存在。

要点

PFO

- PFO 并非真正的房间隔组织缺损, 而是位于房间隔前上部的原发隔与继发隔间一个潜在的间隙或分隔, 可见于超过 20%-25% 的人群。
- PFO 定义为经造影或彩色多普勒成像观察到右向左的分流, “拉伸型”PFO 是指心房血流动力学的改变使卵圆孔开放而导致在彩色多普勒超声中可观察到左向右或右向左的分流。

ASD

- 继发孔型 ASD 由原发隔缺损形成, 是最为常见的 ASD 类型。
- 继发孔型 ASD 通常可行经导管封堵术。
- 继发孔型 ASD 形态各异, 可呈圆形或椭圆形, 也可有多束分流。
- 原发孔型 ASD 由心内膜垫未能融合所致, 属于 AV 间隔缺损。
- 静脉窦型缺损并非真正意义上的 ASD, 由 SVC 和右上肺静脉间 (SVC 型) 的静脉窦隔或右下、中肺静脉与 RA 间 (IVC 型) 的静脉窦隔缺损所致。
- 冠状静脉窦型房缺 (或冠状静脉窦顶盖 query) 也并非真正的房缺, 其血液分流方向为左房-冠状静脉-右房。

ASA

- ASA 的定义间隔组织向 RA 或 LA 侧偏离, 距正常房间隔的位置超过 10mm 或者左右摆动幅度超过 15mm

房间隔成像

常规成像方法

TTE 是最常用于评价 IAS 的超声技术，现在仍是 PFO、ASD 和 ASA 的首选筛查和诊断方法。^{20,49-61} TTE 在小儿患者中尤为适用，他们超声图像质量好，更利于全面诊断。TTE 还可用于筛查适合行经导管 ASD 或 PFO 封堵术的小儿患者，并可实时进行术中监测。^{31,57,62-64}

TTE 可用于成人 ASD 和 PFO 患者的初步评价。然而，因 TTE 受限于患者图像质量，有时无法完整评价 IAS 的特点，此时，需要使用 TEE 对异常的 IAS 进行更全面的评价。TEE 对不考虑行经导管封堵术的 PFO 患者并不是必须的。同时，2D 和 3D TEE，与 TTE 相比，可以提供更为有价值的解剖信息，所有考虑行经导管封堵术或外科手术治疗的患者都应行 TEE 检查。^{31,65-67} 在成年患者，TEE 可用于明确 ASD 边界或边缘（参见 ASD 评估部分：标准和特征），评价 ASD 毗邻的组织结构（如，主动脉、腔静脉、肺静脉、AV 瓣和冠状静脉窦）。

ICE 已广泛用于 ASD/PFO 封堵术的术中指导，成像效果与 TEE 相当（但不相同）。后面的部分将会详细讲述关于 ICE 成像的内容（参见 IAS 的心腔内超声心动图评价指南与超声心动图成像在经导管封堵术中的应用）。使用震荡生理盐水进行超声心动图造影在评估 PFO 中有重要作用，并可用于评价经导管封堵术后有无残余分流，但其在 ASD 的诊断中作用有限。^{52,61,63,68-75} 更多关于超声心动图造影与 TCD 造影的内容，参见分流的评估：分流成像的技术、标准和特征：TTE 与 TEE；经颅多普勒分流的检出/程度分级。

表 1 根据患者的特征、成像技术、应用目的（如诊断，治疗方式的选择或知道，追踪随访），总结了推荐的房间隔异常常规成像方法。

三维超声房间隔成像

近来，普遍认为 3D TEE 改善了 PFO 与 ASD 的成像，对其边缘及毗邻结构的评价，并可用于指导经导管封堵术。^{6,7,53,63,65,66,76-81} IAS 是一个复杂的、动态的 3D 解剖结构，因此使用单一的 2D 超声心动图技术对其进行评价存在一定的局限性。IAS（及其合并的异常，如 ASD 或 PFO）并不是真正的平面结构，2D 成像不可能轻易或完整的对其进行评价。ASD 与 PFO 的大小、形状及结构各异（图 8 和 21）。而 3D 成像评价 IAS 有其独特的视角，可以直观显示 ASD 及其周围结构，可更为准确的评价 ASD 的大小与形态。此外，3D 成像可以更为全面、清晰的评估缺损随心动周期改变而出现的动态变化。同时，3D 成像也可用于评价 ASD 与其毗邻组织结构的关系及缺损边缘的情况（图 22）。

二维双平面（或三平面）成像技术，是目前市面有售的 3D 成像系统的特点之一，是在 3D 技术的基础上发展起来的一种独特的成像技术。双平面成像的优点在于它可以同时显示不同的超声心动图切面图，且图像帧频高、时间分辨率高。同时显示互相垂直的两个切面，相比与单一切面，可为诊断提供更多信息，这种成像技术尤为适合于封堵术术中指导。已有大量关于 3D TEE，包括双平面成像，在介入治疗指导中优势的报导。^{7,65,66,80,82} 图 23 展示了 ASD 经皮导管封堵术中封堵器植入前，双平面成像的应用。

此外,3D 成像有多种获取图像的模式,允许在窄角、放大和广角模式下获取不同容积的图像。获取 3D 容积图像后,可使用市面上现有的 3D 软件包,如 QLAB (Philips,Best, The Netherlands) or 4D Cardio-View (TomTec, Munich,Germany),通过切割 3D 图像,从任何一个切面观察 IAS。该技术有助于评估 ASD 的形态,并可于多个垂直切面上测量缺损的直径,减少了由于切面不标准而引起的测量误差(图 24)。注意,收缩期和舒张期的图像均需要查看,便评价可能出现的缺损大小变化。由于 3D 成像可以轻易显示邻近缺损组织结构,如主动脉,3D 正面成像还可以协助观察和测量缺损边缘的情况。呈像时,缺损与主动脉间的距离可以轻易测量出来,正如缺损面积和边缘缺失的长度一样。

超声心动图在经导管封堵术中的应用

TTE, TEE 和 ICE 在评价 ASD/PFO 及指导封堵术中起着重要作用。^{31,63,80,83}对拟施行封堵术的患者行超声心动图检查对病人的筛选、实时术中指导、封堵器有效性和并发症评估及术后长期随访均起着至关重要的作用。

TTE 可用于评价缺损的类型、血流动力学变化及合并畸形,可用于小儿患者 ASD/PFO 的诊断,病人筛选和术中监测。TTE 的优势在于可多平面转换评价房间隔,但对于已行封堵术的患者,因封堵器的声影会影响所有平面的成像,其在评价 IVC 以上房间隔组织下缘的作用有限。并且,房间隔在较大的患儿和成年患者离探头相对较远,因此图像质量往往不合格的。如果临床考虑施行封堵术,行 TEE 检查对 IAS 的解剖结构和邻近结构进行详细的评价,有助于病人的筛选及术中

指导,或者可以行 ICE 为此类患者行术中指导。

经食道超声心动图可获取房间隔、邻近组织结构、封堵术中导管及封堵器实时、详细的图像,并可观察到封堵术中的封堵器材。经食道超声需要在保持患者清醒的情况下进行镇静,仰卧位患者有误吸风险,或者使用全身麻醉,需行气管内插管,可减少误吸的风险。当介入治疗医生在施行封堵术时,也需要专业的超声心动图医师来行 TEE。3D TEE 的应用可更为详细的探查 IAS 解剖结构,可以直观观察缺损及其周围结构,完善了对 ASD 和 PFO 的评价。多平面 3D 重建技术可更为准确的测量缺损的最小和最大直径,可指导术者选择最合适的封堵器。并且,术中实时 3D TEE 可清晰显示导丝、导管、封堵器及其与邻近组织结构间的关系,并可由手术者结合术中所见加以完善(图 25)。

心腔内超声心动图已广泛 ASD/PFO 修补术中指导,很多心导管实验中心所选择的成像技术。⁸⁴⁻⁸⁸ICE 的优势在于可获得与经食道超声类相似似(但不相同)的图像质量,可更加全面的评价 IAS 及缺损的位置和形状,充分显示缺损边缘以及肺静脉的位置。并且,在显示 IAS 的下部和后部较 TEE 更为有优势。⁸⁹此外,行 ICE 时,可使用清醒镇静剂,减少了全身麻醉和气管内插管的使用。介入治疗医师在无专业超声医理师情况下也可进行 ICE 探查。但是,ICE 也有其缺点:可视范围有限,导管不稳定,ICE 导管仅能单次使用、价格高昂,需要更多的操作训练、有致心律失常的风险,单一人员难以操作。表 2 总结 TTE、

TEE 及 ICE 指导 PFO 和 ASD 封堵术中的优缺点。

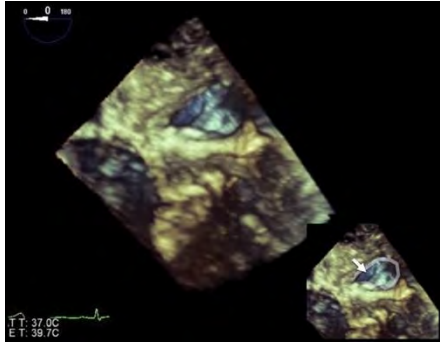


图 19 经食道三维超声心动图示：由左房观，冠状静脉窦顶盖缺如型房间隔缺损。椭圆形示冠状静脉窦在左房侧缺如部位。

房间隔经胸超声心动图成像建议

TTE 可以全面评价房间隔。要评价房间隔交通的大小、形状、位置以及其与周围组织结构的关系，需要从不同切面进行探查(图 9 和 13-17, 图 26-28)。尤为重要的一点是，在检查中应注意观察缺损与腔静脉、肺静脉、二、三尖瓣及冠状静脉窦间的关系。评估缺损周围的残边也是至关重要的。若缺损与肺静脉、主动脉瓣或下腔静脉间没有残边，则不可行经导管封堵术；在某些情况下，主动脉侧不存在残边会提高封堵器侵蚀的风险。

多切面观察心室、大动脉等结构有助于评估由 ASD 所致的血流动力学改变而引起的相关结构的继发性改变，如 RA、右室(RV)的扩大，肺动脉(PA)的扩张。在小儿患者，肋下切面是观察房间隔及其相关结构最好的切面。而在青少年及成年患者，由于探头距离房间隔太远，故肋下切面图像常不足以清晰显示房间隔。因此，需从其

他切面，如胸骨旁切面，探查房间隔。在部分患者，TTE 无法全面的评价房间隔，这时，便需行 TEE 检查。

TTE 剑突下(四腔心)切面观。剑突下(四腔心)切面可获取沿房间隔前后轴方向的图像，从 SVC 到 AV 瓣。该切面是评价房间隔的首选切面，在该切面上房间隔与超声波束几乎垂直，此时轴向分辨率最高，并可沿长轴切面测量缺损的大小。由于房间隔很薄(尤其是中间部分)，超声波束垂直入射可将真正的缺损与回声失落所造成的伪像区分开来。肋下切面亦可清楚显示附着于 ASD 边缘的原发隔组织形成的膨胀瘤。ASA 上可破口(图 9)，也可无心房水平的分流。应同时应用彩色多普勒和对比造影探查有无分流。缺损与右肺静脉间的残边也可通过该切面测量。由于此切面不能显示腔静脉的长轴，因此不适于在该切面探查腔静脉型缺损。

TTE 剑突矢状位切面观。TTE 剑突下矢状位切面是在剑突下四腔心切面基础上顺时针旋转探头 90°获得的。该切面最适于沿房间隔前后轴方向评价房间隔，垂直于剑突下四腔心切面。将探头沿着该轴从右向左扫查，可获得垂直方向上 ASD 的大小(图 15 和 17)。可该切面的缺损大小与剑下四腔心切面的缺损大小相比较，以判断缺损的形状(圆形或卵圆形)。在该切面可测量缺损距 SVC 和 IVC 的残边长度，是观察腔静脉型缺损的最佳切面(图 14B 和 15)。

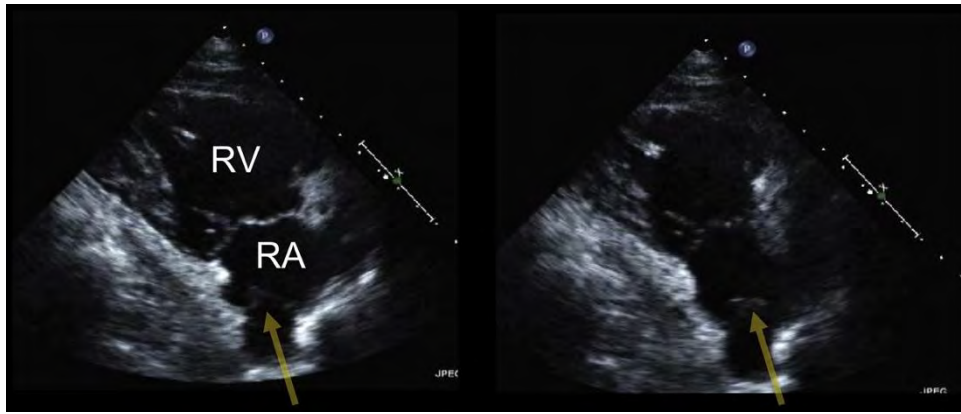


图 20 经胸超声心动图右室观示希阿里（氏）网附着于欧式脊。

表 1 评价房间隔异常的超声成像方法

| 研究对象 | ASD 或 PFO 诊断 | 封堵术指导 | 随访 |
|---------------|------------------|-------------------------------|-----|
| 儿童患者 <35-40kg | TTE 或 TEE* | TEE 或 ICE [†] | TTE |
| 儿童患者 >35-40kg | TTE, TEE, 3DTEE | TEE, 3DTEE 或 ICE [†] | TTE |
| 成年患者 | TTE, TEE 或 3DTEE | TEE, 3DTEE 或 ICE [†] | TTE |

*图像质量取决于被检查者体表面积的大小，经食道超声是评价房缺很有效的方法，但通常需要插管；如果患者体重 >35-45kg，可行经食道三维超声检查。

[†]某些心血管诊疗中心，使用经心腔内超声指导所有类型缺损的手术治疗；而某些医疗中心，将心内超声用于非复杂性小房缺的修补术，对复杂性或大房缺使用经食道超声或经食道三维超声。

TTE 左前斜位切面观。该切面是在四腔心切面的基础上将探头逆时针旋转 45° 获得的。该切面可以探查到房间隔的长轴，尤为适用于原发孔型 ASD 和

与 ASD 的位置关系。此外，该切面可用于观察右肺静脉流入心脏的位置。

TTE 心尖四腔心切面。由于在 TTE 心尖四腔心切面上，房间隔与超声波束是平行的，因此不宜用改切面诊断和测量 ASD。在该切面上常可见回声失落伪像，易导致高估缺损的大小。该切面常用于评价 ASD 引起的血流动力学改变，如 RA、RV 扩大，也可通过三尖瓣的反流速度评估 RV 压力。该切面也可用于通过震荡生理盐水造影观察右向左分流（图 29）。

冠状静脉窦扩张的评价（图 13B 和 17B）。而且，在该视图上可以评价 SVC

TTE 改良心尖四腔心切面观（介于心尖四腔心切面与胸骨旁短轴切面之间）

TTE 改良心尖四腔心切面是在心尖四腔心切面的基础上将探头滑向胸骨缘。通过提高声波束的入射角（30° -45°）使得房间隔显示的更清楚。当患者的剑突下切面显示不佳或难以获得时，该切面可在设备的纵向分辨率作用下，代替剑突下切面显示房间隔。

TTE 胸骨旁短轴切面

在 TTE 心底部胸骨旁短轴切面上，可见房间隔的前-后轴，位于主动脉根部后方。该切面尤为适于探查主动脉后方的缺损残边（图 26 和 27）。它也可

清楚显示冠状静脉窦的后缘（或缺损）和后下方的继发隔缺损。但在该切面，由于入射声波与间隔平行，易产生伪像，故而不能在该切面测量缺损的大小。

高位胸骨右旁切面

在患者取右侧卧位时进行探查，将探头从上至下扫查，可获取高位胸骨右

旁矢状切面。在该切面，入射声波束与房间隔垂直，尤其适合在剑突下切面显示不清时用来诊断腔静脉窦型缺损（图 16）。

表 3 总结了 TTE 评价 IAS 及其邻近结构的主要成像切面

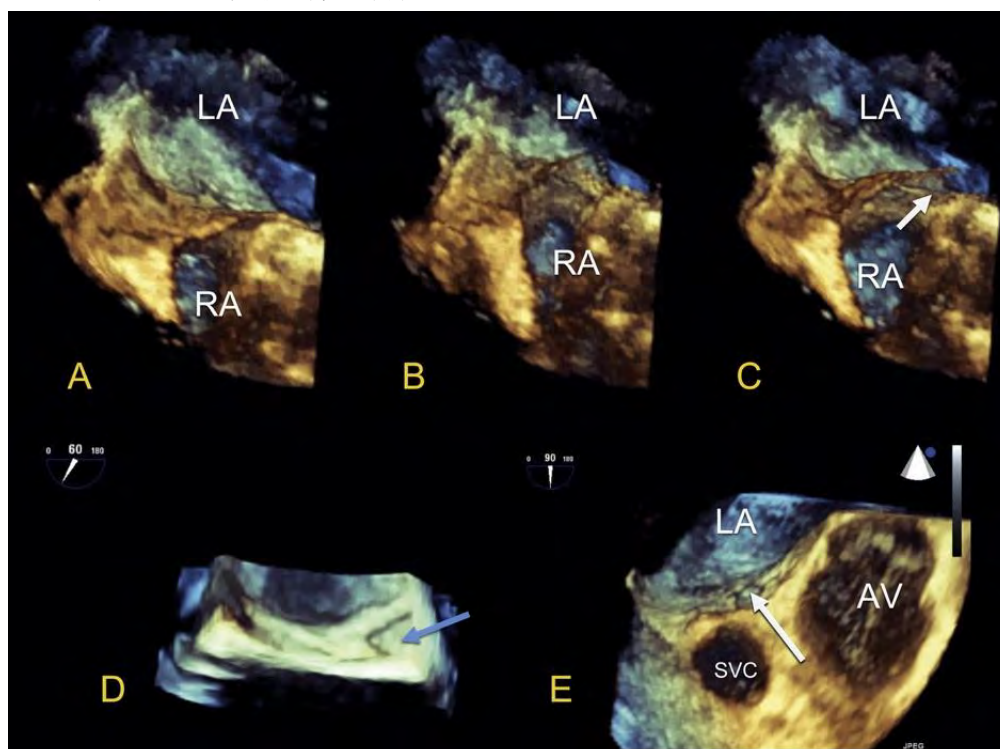


图 21 经食道三维超声卵圆孔未闭显像。（A-C）房间隔膨隆瘤和卵圆孔未闭患者中，原发隔（卵圆窝）运动度增大。白色箭头示左、右房间存在压力阶差时，卵圆孔未闭处完全开放。（D）左房侧见卵圆孔未闭的“管道样”结构。蓝色箭头显示卵圆孔未闭左房侧开口。（E）卵圆孔未闭管道样结构通向左房

房间隔经食道超声心动图成像建议

与 TTE 一样，TEE 需要多切面、连续扫查评价 IAS 及房间隔交通的大小、形状及位置。ASE 及心血管协会已发表过具体的 TEE 读平面操作指南，在具体操作 TEE 时应参考该指南。¹¹ 我们建议在操作时从标准切面开始连续扫查及存储图像，通过每 15° 顺序改变探头角度调整入射声波，探查目标部位。获取最佳二维图像，使用彩色多普勒成像。彩色多普勒增益可调低至 35-40m/sec，观测细小缺损、PFO 或小 ASD 处的低速血流信号。脉冲波

和连续波多普勒可用于在标准切面上测量血流速度、方向及时相。

存储或不伴有彩色多普勒模式的 IAS 3D 容积图像在不需要连续多平面扫查与存储的情况下也可获得更多成像信息，详细说明分别在 3D TEE PFO 与 ASD 存图指南两章。

当存在 ASD 或 PFO 时，需注意观察缺损与腔静脉、肺静脉、二、三尖瓣及冠状静脉窦之间关系。对拟行经导管封堵术的患者，缺损距邻近结构残边长度的评价非常重要。残边缺失的定义为多个连续切面测量，残边长

度均小于 5mm，而多个连续切面是指至少三个连续 15° 的过渡切面。

行 TTE 时，需加查其他切面以显示其它心脏结构，以便评价由 ASD 血流动力学改变所致的继发改变，如右心扩大及肺动脉增宽。具体请参见 ASE 关于 TEE 的评价指南及右心评价指南。⁹⁻¹¹

行 TEE 时，从五个基本切面评价 IAS 及其周围结构，具体内容总结在表四中。主要切面包括：食管上段短轴切面，食管中段主动脉瓣（AoV）短轴切面，食管中段四腔心切面。

食管上段短轴切面

食管上段短轴切面是在食管上段将探头角度由 0° 多切面扫查开始到 15°，30° 和 45° 多角度顺序扫查获取的。该切面可观察房间隔上部结构，包括继发隔，RA 与 LA 顶部以及周围的大

血管（SVC 和升主动脉）。在此切面基础上，将探头继续往下，深入食管中段，并顺时针转动可探查右肺静脉的入口（图 30）。肺静脉异位引流及 SVC 型静脉窦缺损可于该切面探查。

食管中段主动脉瓣短轴切面。食管中段 AoV 短轴切面是在食管中段将探头角度由 30° 多切面扫查开始到 45°，60° 和 75° 多角度顺序扫查获取的。随着探头的转动，可顺序观察 AoV 短轴切面到改良两腔三尖瓣切面的 IAS。AoV 短轴切面主要用于观察短轴方向的 AoV 及其邻近的间隔组织。该切面清楚的显示了房间隔的前-后平面（以及主动脉与 ASD 的后缘），ASD 的前后径，存在 PFO 时原发隔与继发隔的重叠部分（图 31 和 32）。

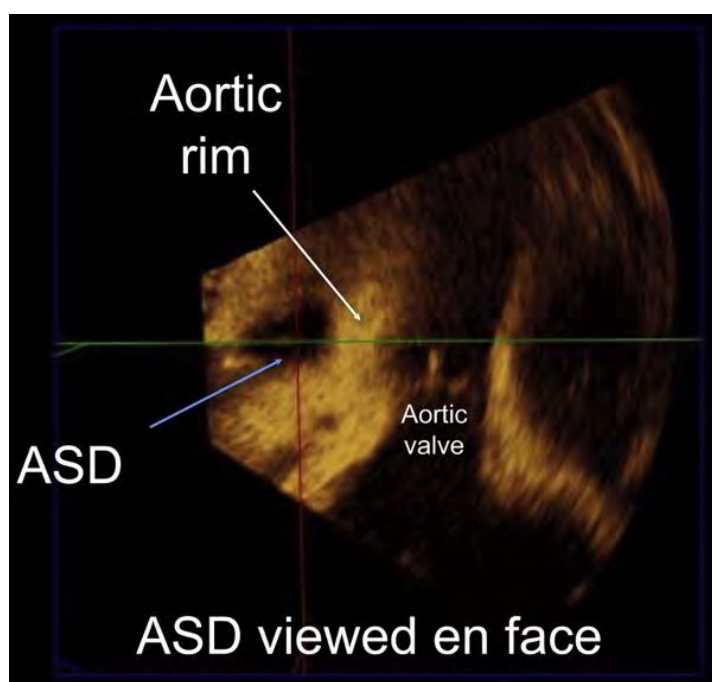


图 22：三维立体成像可清楚显示房间隔缺损（蓝色箭头）及其与毗邻结构（主动脉瓣及整个主动脉瓣环可在该视图成像）的关系。

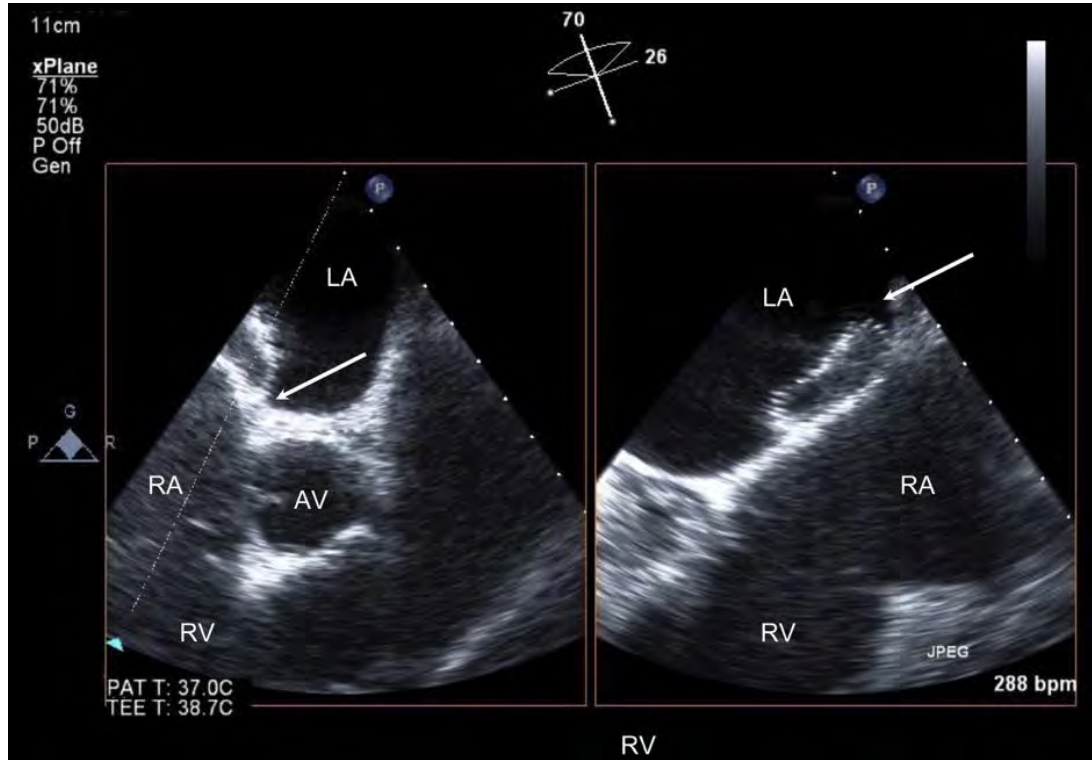


图 23: 经皮导管封堵术中双平面成像。主动脉环与其上缘（左边箭头所示），连接主动脉（左边箭头所示）与心房顶部（右边箭头所示）封堵器可同时显像

食管中段四腔心切面。食管中段四腔心切面是在食管中段将探头角度由 0°多切面扫查开始到 25°和 30°多角度顺序扫查获取的。该切面主要用于评价 AV 间隔（原发孔型 ASD）以及不同类型 ASD 与 AV 瓣的关系（图 33）。继发孔型 ASD 封堵术时，使用较大的封堵器可能影响 AV 瓣的功能，因此在封堵器置入前必须仔细评估（图 34）。

食管中段二腔切面。食管中段两腔切面是在食管中段将探头角度由 90°多切面扫查开始到 105°和 120°多角度顺序扫查获取的。该切面用于观测房间隔的上-下平面及周围结构，如 SVC 和右肺静脉（图 4,5,7,10A-C, 11A 和 B, 12A, 35,36）。该切面对于评价 SVC 型腔静脉窦缺损和右肺静脉异位引流有重要意义。同时，ASD 封堵器释放

前，必须探查 RA 顶部，而该切面在此的应用也十分重要。

食管中段长轴切面。食管中段两腔切面是在食管中段将探头角度由 120°多切面扫查开始到 135°和 150°多角度顺序扫查获取的，可用于 ASD 封堵器释放前，探查 LA 顶部（详细内容见超声心动图在经皮导管封堵术中的应用一节）。显示左心耳后，继续旋转探头可显示左肺静脉回流入 LA 的入口（图 37）。

3D TEE PFO 与 ASD 成像建议

IAS 的经食道三维图像需要从多角度、多种 3D 模式进行采集。关于 3D 图像的获取、重建及成像的具体内容可参考 2012 年的 ASE 指南。¹²

一套完整的 3D 检查通常从标准切面的实时或窄角成像开始。为了获取时间和空间分辨率高的图像，需行心电

门控、3D 宽角成像获取图像。TEE 评估 IAS 时，建议在几个主要切面行窄度，放大及宽角成像获取 3D 数据：

- 食管中段短轴切面：在食管中段从 0°开始多平面扫查获得。探头朝向 IAS 旋转。该切面尤其适合于获取窄角和宽角图像。
- 基底段短轴切面：在食管中段从 30°角旋转至 60°角多平面扫查获得。该切面尤其适合于获取窄角和宽角图像。术中指导时，该切面还可用于缩放模式成像。后处理该切面的 3D 图像可以观察 ASD 的正面及其与周围结构（如主动脉和主动脉侧的残边）的关系（图 38 和 39A 和 B）。在该切面应用宽角成像时，应同时获取有和无彩色多普勒血流成像的图像，以便线下更准确的测量 ASD 的大小、形状、血流动力学改变以及与周围结构的关系。
- 两腔视图：在食管中段水平，将探头从 90°角开始旋转至 120°角多平面扫查获得。该切面的图像也可在所有的 3D 成像模式下获取。成像时，应将锥形扇角的深度参数调至在切面中只显示房间隔的左右缘。这种特殊的参数设置可使该切面仅显示整个间隔的 3D 图像，而不显示器周围结构。将锥形扇角的角度参数设置 90°翻转，可以观察间隔整个左侧面的正面视图（图 40）。当显示出间隔的左侧面后，将探头逆时针旋转 180°后即可观察到房间隔的右侧和房间隔中部的凹陷-卵圆窝（图 41）。有时候需要在任意平面进行精细切割，以减少周围结构对房间隔的遮挡。将增益设在中等水平可以避免将卵圆窝处的回声失落误诊

为 ASD。该切面还可用于在收缩期和舒张期测量 ASD 的大小和形状。

- 矢状面两腔切面：该切面是在食道下段水平将探头由 100°角旋转至 120°角获得的。该切面与食管中段两腔切面探查的设置和操作是相同的。
- 四腔心切面：于食管中段水平，将探头自 0°角旋转至 20°角获得。

3D TTE PFO 与 ASD 成像建议。经胸 IAS 的 3D 图像可从窄角心尖四腔心切面、窄角彩色胸骨旁长轴切面和放大心尖四腔心切面获取。然而，图像的分辨率限制了其在较大的儿童和成年患者中的应用。

3D 显示。当从 LA（左）侧观察 IAS 时，应注意根据右上肺静脉的位置定为房间隔，房间隔位于右上肺静脉的 1 点钟方向。当从 RA（右）侧观察时，SVC 应位于房间隔的 11 点钟方向（图 40 和 41）。

图像的获取与存储应从将探头放置于这些位置开始，并应用这三种不同的 3D 超声心动图模式进行成像，包括窄角、放大与宽角 3D 存储模式。

在本次报告中，不同模式的图像均有举例说明。在精心切割和存储的静态图像中，常不易分辨使用的是何种 3D 超声心动图成像模式。而在动态图像中，3D 放大模式可通过其放慢的容积比率和平滑的图像中分辨出来，而如果存在拼接伪影，可以辨别出其是 3D 宽角成像模式。

经 3D 成像获得的 ASD 解剖定性评价应包括 ASD 的类型（如，继发孔型、原发孔型、静脉窦型、单心房或冠状静脉窦型），缺损的位置、形状及方位（图 8,11,12 和 39）。ASD 可

呈椭圆形、圆形、三角形，有时候也可呈鸡蛋型或梨形或轻度不规则型（图 8）。ASD 的方位是指缺损长轴的方位，可以是垂直、水平、斜前倾角或斜后倾角方向的。将缺损的直径在长轴和短轴方向上差异不超过 1mm 示为圆形。

3D 超声心动图对 ASD 进行定量评价的指标应包括心房舒张末期缺损的最大长径、最大宽径及最大面积（图 24）。同时也应在心房收缩末期测量 ASD 的大小以观察随心动周期缺损大小的变化（动态 ASD）。ASD 的大小需使用专门的定量软件从 LA 侧或 RA 侧正面视图进行测量。需要计算的参数应包括心房舒张末期到收缩末期 ASD 长度、宽度和面积的变化率。心房舒张末期定义为 ASD 最大的那一帧，心房收缩末期定义为 ASD 最小的那一帧。存在多发缺损是，应定量评价缺损的数量。

心腔内超声心动图 IAS 成像建议

对房间隔、任意类型的间隔缺损及其周围组织残边的详细评价都可使用旋转型或相控阵型 ICE 完成。表 5 中列出了 ICE 评价 IAS 的主要切面。表 6 中列出了目前可获得的 ICE 系统及他们各自的特点。目前可获得的 ICE 系统不具备电子束旋转扫描或多平面成像的能力。相反，他们提供了一个旋转扫描晶片或相控阵成像模式，通过深入和退出导管、沿轴旋转获取图像；在相控阵系统中，通过可调张力操作转向控制器，使导管可以向四个方向弯曲（前，后，左，右）。通过调节 ICE 相控阵探头的深入和退出可使由上到下的成像范围变大。沿轴旋转可以多平面成像。近来，3D ICE 也已投入商业使用。⁹⁴⁻⁹⁶但目前关于三维 ICE

在经皮导管封堵术中应用的数据有限。3D ICE 有潜力为介入治疗提供更加详细的解剖信息，但目前尚未成熟，需要进一步研究才能完善其应用。

表 5 中总结了 IAS 及其周围结构的评价标准：

- 相控阵 ICE 探头位于导管中央，最开始放置于 RA 中部，可显示三尖瓣长轴。、也被称为“主切面”（图 42A）。在该切面，可见 RA、三尖瓣、RV、RV 流出道、肺动脉瓣、肺动脉主干近端、部分 AoV 及任意一型 ASD 及其邻近间隔的部分短轴图。该切面可显示较低位置的 AV 间隔边缘。
- 在此位置，应用后-前按钮后向旋转并应用右-左按钮轻微向右旋转可获取间隔的长轴图像（图 42B）。
- 将导管头端向前推进可获得两腔切面，在该切面可以观查到 ASD 的上下缘以及缺损的直径与构成（图 42C）。
- 顺时针旋转整个导管手柄直至腔内探头接近三尖瓣，然后应用右-左按钮稍向左旋转直到显示 AoV，可以获得与经 TEE 相似的间隔短轴切面，两者的区别在于该切面上邻近的结构是 RA，而 TEE 上是 LA（图 42D 和 E）。在该切面，可测量缺损的直径和前缘（大动脉）与后缘的残边（图 43）。
- 然后，由于 ICE 导管位于 RA 内的，因此不存在真正的四腔心切面。

要点

- 表 1 根据患者自身的特点、成像模式和目的（诊断、手术方式的选择和指导、随访），选择不同的成

像方法，如 TTE、TEE 和 ICE，评价间隔异常。

- TEE 的图像质量优于 TTE。但是并不是必须要行该检查（如，并不需要手术治疗的卵圆孔未闭）。
- 三维成像可获得独特视图，尤其是，可以获得房缺及其周围结构组织的整体观，可准确观测房缺的大小和形态，划定周围组织的边缘，判断房缺与周围心脏结构之间的关系。
- 超声心动图检查对要接受手术的患者是非常重要的，可协助合适患者的选择、行实时术中指导、评价封堵器的疗效及并发症以及长期的随访。
- 表 2 总结了 TTE、TEE 和 ICE 在卵圆孔未闭与房缺封堵术中指导的优缺点。
- 表 3 用 TTE 评价房间隔和周围组织结构的主要切面。
- 表 4 用 TEE 评价房间隔和周围组织结构的主要切面。

□ 表 5 用 ICE 评价房间隔和周围组织结构的主要切面。

分流的评价

分流成像的技术、标准和特点：TTE 与 TEE

PFO 或 ASD 的分流及分流相关的血流动力学改变，需要结合结构成像、彩色多普勒成像及频谱多普勒成像来共同评价。相关改变，包括舒张期室间隔扁平与 RA、RV 及/或 PA 扩张，都是可能存在左向右分流的表現。扩张的严重程度与这些结构的顺应性及 ASD 的大小相关。

ASD 的分流方向多为左向右分流，可用彩色多普勒显示。当出现明显的肺动脉高压或 RV 顺应性明显减低时，ASD 的分流束也可呈右向左或双向分流。在彩色多普勒的基础上，可使用脉

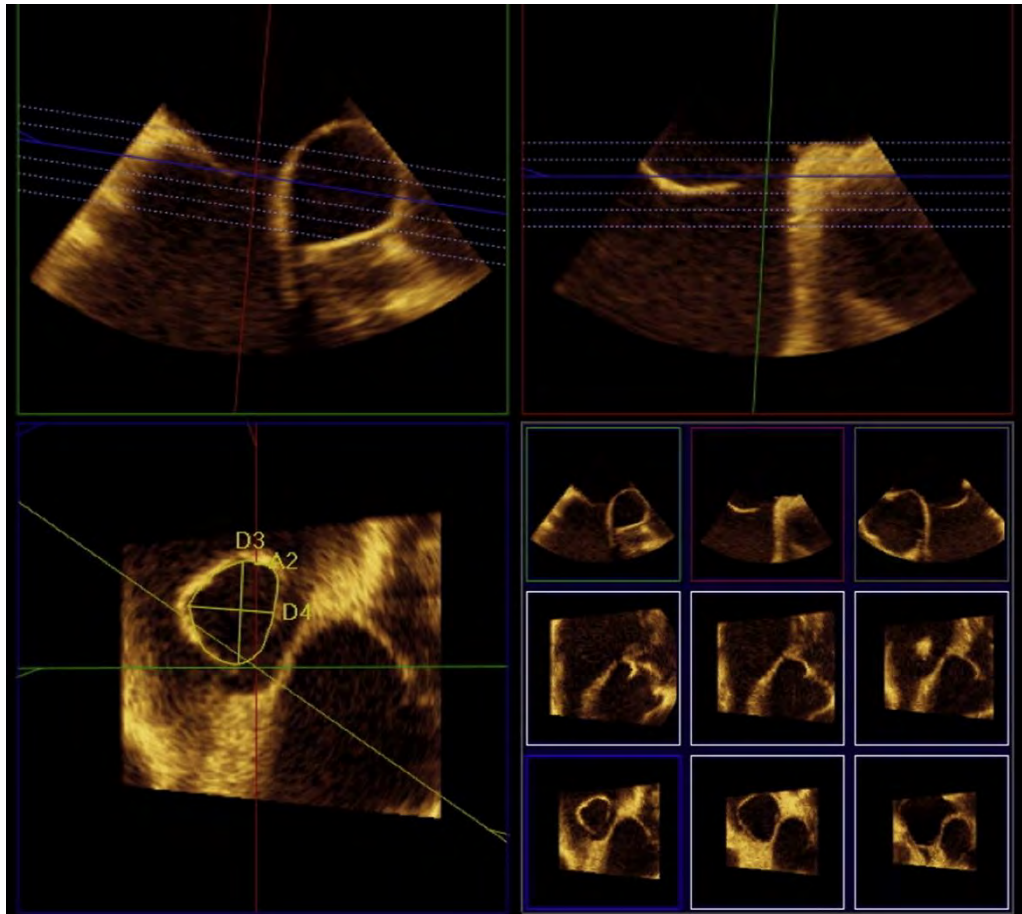


图 243D 容量图存储后，可使用商用的 3D 软件进行后处理，可将房间隔图像用 3D 平面切割成多个平面。这种技术可以在多个垂直切面上评价 ASD 的形状，在正面视图上测量缺损内径和面积，避免了由于切面的获取存在偏差而致的测量误差。详见于房间隔成像：房间隔成像。

冲多普勒探查双向分流信号。应将彩色信号增益调整至较低水平，以便探查可能存在的低速分流信号（如 25-40cm/sec）。二尖瓣狭窄、左室（left ventricular, LV）顺应性减低或左室流出道梗阻会导致 LA 高压，此时可见到高速的左向右分流。

在 ASD 患者，彩色多普勒成像测量的缺损最大径（宽度）与术中测量的缺损最大径相关。如，在一小样接受手术治疗患者的研究中发现，使用 TTE-

和 TEE-测量 ASD 彩色多普勒成像下血流束的最大径与术中测得的的存在相关性。TTE 和 TEE 彩色多普勒超声心动图测量的缺损处分流束最大径均与术中直接测量的最大径存相关性，因此，彩色多普勒可能也可用于 ASD 直径的评价。⁹⁸ 但如仅用彩色多普勒超声成像所测得的分流束宽度估计 ASD 的大小将出现很大的误差；因此，不伴彩

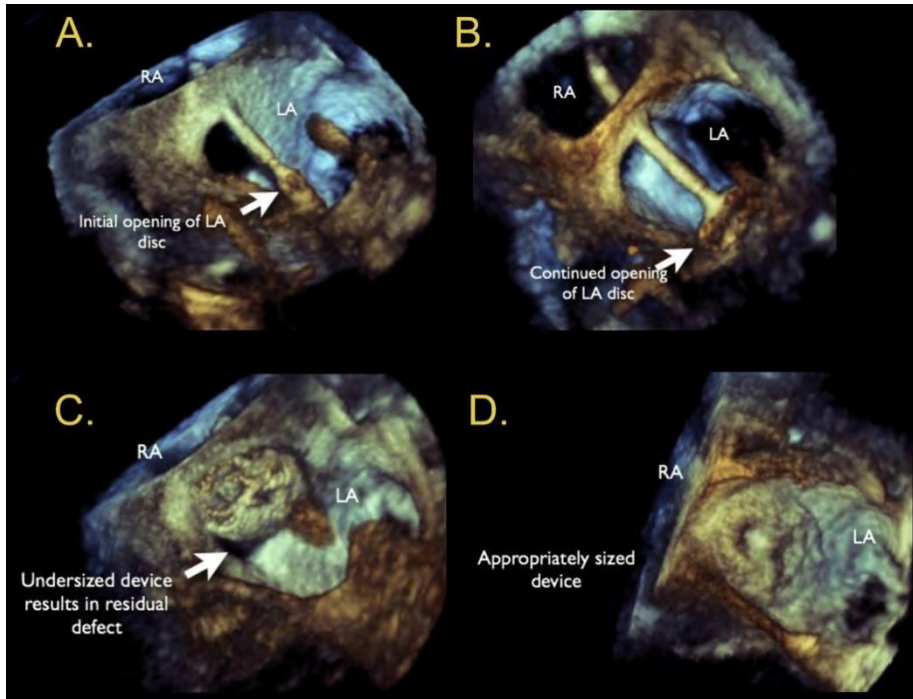


图 25 术中 RT3D TEE 可获得导线、导管、封堵器及其与毗邻结构关系高质量图像，对介入治疗者而言较 2D 超声更为直观的方式。一例继发孔型 ASD，在 RT3D TEE 引导下，行 Amplatzer 封堵器行封堵术。图像均从 LA 侧获得的。（A）LA 侧封堵器圆盘在 LA 中打开。（B）封堵器继续打开的图像。（C）封堵器偏小以致残留部分缺损。取下该封堵器并（D）装上更大的封堵器。

色成像的 2D 或 3D 测量也是必要的。不同仪器的彩色血流图像质量不同，彩色血流的设置也各不相同，可导致彩色血流信号从房间隔组织溢出，从而导致对缺损大小的高估。

分流情况可通过脉冲多普勒定量评价肺循环（ Q_p ）血流与体循环（ Q_s ）血流的比值来评价。^{99,100} 主要通过 TTE 脉冲多普勒技术推算 RV 与 LV 流出道的血流量完成。此方法包括测量 RV 和 LV 流出道的收缩期速度-时间积分（VTIs），肺动脉和 LV 流出道收缩期最大内径。该内径可用于估算相应的流出道面积，假设流出道为圆环状。用数学公式（ πr^2 ）计算出 RV 和 LV 流出道面积并乘以相应的 VTI 即可分别估测左、右室的搏出量。而 Q_p/Q_s 比值即为肺循环搏出量与体循环搏出量的比值（RV 搏出量/LV 搏出量）。此方法已通过验证，并在对继发孔型

ASD 患者小样本研究中，与血氧估测的方法进行了对比，其中包括合并肺动脉高压、二、三尖瓣反流、室间隔缺损和艾森曼格综合征的患者。⁹⁹ 不同程度半月瓣反流可不同程度的影响着搏出量，因此若有明显反流，将会限制对反流量的估测。另一类似估测方法为测量舒张期流入道血流速度和 AV 瓣环内径，与血氧估测的方法有相关性。¹⁰¹

彩色多普勒血流成像也可探查 PFO 的分流；但是，PFO 的分流常是非连续性的，彩色多普勒血流成像并非时时都可以探查。当 LA 与 RA 压不等时，PFO 受到牵拉，此时可能可以探查左向右的分流信号（图 4-6）。第一代超声心动图造影是使用震荡生理盐水作为造影剂，配合生理动作激发右向左的分流，提高了探查 PFO 的敏感度。¹⁰²⁻¹⁰⁵ 经震荡所形成的微泡直径

较大，无法通过正常的肺血管，而其回声增强，易于被超声心动图探查

（图 29）。用于提高 RA 压的激发动作有 Valsalva 动作与咳嗽。

表 2 TTE、TEE 和 ICE 在 PFO 与 ASD 经皮导管封堵术中指导的优缺点

| 方式 | 优点 | 缺点 |
|-----|--|--|
| TTE | 简单方便 价格低 评价 IAS 的切面不受限制 无创 不需任何麻醉 小儿患者图像质量好 | 成年患者图像质量可能不够好 术中需要技师或超声心动图医师进行操作 封堵器植入术后，几乎所有切面都有伪影，以致 IAS 较低的边缘显示不清 |
| TEE | 比 TTE 图像质量好 3D 技术在评价 ASD 大小、形态和位置方面优于 2D 技术； 正面成像，非专业人士可能也可更直观理解 | 需要镇静或麻醉 存在误吸和食道损伤的风险 如果手术时间较长，需要气管内插管 需要额外的超声心动图医师进行操作 患者会有不适 |
| ICE | 图像质量与 TEE 相当 可在清醒镇静的患者中进行 减少操作和透视时间 在评价 IAS 下部上优于 TEE 可由介入医师操作（不需要额外的人员协助） | 有创 8F-10F 静脉通路和导管的风险，包括血管风险和心律失常 3D 技术的应用还有待明确 一次性 ICE 导管费用高昂 某些系统的远场成像受限 需要接受专门的 ICE 操作培训 操作者需兼顾两项任务（成像与手术） |

经胸超声心动图基础上使用第一代造影剂可用于探查 PFO，且具有较高的敏感度和特异性；然而，普遍认为 TEE 是探查 PFO 的金标准。不论是使用 TEE 还是 TTE，采用标准化的操作建议，包括多次注射震荡生理盐水，并同时行激发动作瞬时提高 RA 压，可提高检查的准确性。^{50,106,107} 大多实验室都认同使用的建议示例如下：

- 静脉通路，通常置于肘前静脉，连接一个三通管
- 将 10-mL 注射器连接在三通管上，内抽取 8mL 生理盐水，1mL 患者的

血液加 1mL 空气；造影剂中加入血液可提高能被超声心动图探查的微泡的浓度¹⁰⁸

- 很多实验室避免在配制造影剂时加入患者血液，也可以达到诊断所需的浊化；在这些实验室，造影剂由 9mL 生理盐水和 1 mL 空气制备而成
- 另将一个空的 10mL 注射器连接到三通管上，在 2 个注射器之间快速来回推注液体制造微泡
- 快速经肘静脉注入造影剂，同时在超声心动图系统上存储长周期图像

(如, 10 秒); 行 TTE 检查时, 图像通常是从四腔心切面获得; 行 TEE 检查时, 探查房间隔的最佳成像角度为 30° -100°

- 双平面成像的应用可提高探查细束右向左的敏感性

在 RA 浊化后 3-6 个心动周期内, 于 LA 内见到微泡可证明存在心内分流, 如 PFO (图 29)。理想的情况下, 可见微泡经 PFO 穿过房间隔 (图 38)。静息状态下观察不到分流时, 嘱患者做可瞬时增加 RA 压力的动作, 激发微泡的右向左分流, 对于诊断 PFO 是非常必要的。Valsalva 动作即深吸气后憋住再呼出, 是常见的方法之一。Valsalva 动作要保持足够长的时间, 以使微泡充满 RA。Valsalva 动作是否有效可通过超声心动图检查时显示呼气时房间隔膨向左侧(表明 RA 压力高于 LA) 来验证。

3-6 个心动周期内于 LA 内见到微泡, 表明存在肺内分流, 如动静脉畸形。如微泡是从肺血管而非房间隔进入 LA, 可证明存在肺内分流。当存在静脉窦型间隔缺损或其他未被探查到的 ASD 或 Valsalva 动作引起暂时性肺静脉血流瘀滞而形成假性显影时, 可出现 PFO 微泡分流假阳性。

当 RA 浊化不完全、Valsalva 动作不规范、欧氏瓣将 IVC 回流的静脉血引至房间隔 (阻止自 SVC 而来的微泡不能穿过房间隔)、未能使 RA 压力高于 LA 如存在 LV 舒张功能不全与图像质量不佳时, 微泡探查也可出现假阴性。^{70,109} 对于图像质量不佳的患者, 使用二次谐波成像可改善微泡的探查。数字压缩算法会降低对心内细小分流检测的敏感性, 一些实验室仍然采用持续录像, 记录对比造影检查的结果,

以求最大限度提高检测细小分流信号的敏感性。¹¹⁰

经特定的静脉通道注射生理盐水制备的微泡进行造影检查可用于特定的临床情况中。例如, 经左侧肘前静脉注射造影剂可用于诊断引流入冠状静脉窦的永存左位 SVC。对于上腔静脉窦型 ASD 的患者, 如 ASD 封堵不完全, IVC 的血流可持续回流入 LA, 以致封堵术后患者仍持续存在发绀, 可经腿部静脉注入造影剂诊断。宽大的希阿里氏网或欧式瓣可阻碍微泡自 SVC 回流入 RA, 而经腿部静脉注射造影剂可使微泡进入 RA, 但极少应用。

镇静患者难以完成 Valsalva 动作, 正如分流成像的技术, 标准与特点: TTE 和 TEE 一节中所述。此时, 可通过增加腹部压力瞬时增加 RA 的压力。如果患者处于常规麻醉状态, 可通过控制吸气然后释放模仿 Valsalva 动作。报告内容包括了根据超声心动图静止帧图像上左心内的微泡数量, 尝试定量估测右向左的分流量; 但是, 微泡的数量取决于注入的微泡量及 Valsalva 动作的充分性。

经颅彩色多普勒分流的探查/分级

经颅彩色多普勒是检测 PFO 另一种成像方法。通过使用能量 M 型多普勒检测脑基底动脉, 从而探查因右向左分流而进入体循环的微泡。专门的设备用来聚焦超声, 并显示结果。与 TTE 和 TEE 增强造影检查一样, TCD 检查在平静呼吸时进行, 通过做 Valsalva 动作下最大限度的提高检查灵敏度和特异度。检查结果根据六级 Spencer 对数分级进行评分, 评分越高, 说明右向左分流量越大。^{111,112}

TCD 优于 TTE 和 TEE 的地方在于提高了患者的舒适度（与 TEE 相比），可以半定量评价分流量的大小并可以鉴别心外和心内分流。TCD 评价心外分流的能力也是有限的，无法提供关于分流的部位或相关结构异常的解剖信息。因此，TCD 和超声心动图可作为评价右向左分流的补充检查方法。¹¹³ 部分实验室倾向于联合 TCD 与不同的成像模式，并同时行 TTE 或 TEE 增强造影进行评价。

分流的出现和/或出现时间存在生理变化，以致不管使用何种技术进行评价

与分级都十分复杂。RA 压随呼吸时相的变化可致右向左分流的延时，易将心房内分流误诊为肺内分流。⁷⁰ LV 衰竭、二尖瓣狭窄或二尖瓣反流可引起 LA 压升高，可阻断右向左分流，因为需要更高的 RA 压才能超过增高的 LA 压。在一项将有左心疾病患者的研究中发现，有左心疾病的患者 PFO 的检出率为 5%，而无左心疾病的患者 PFO 的检出率为 29%，与正常人群中检出率相似。¹¹⁴

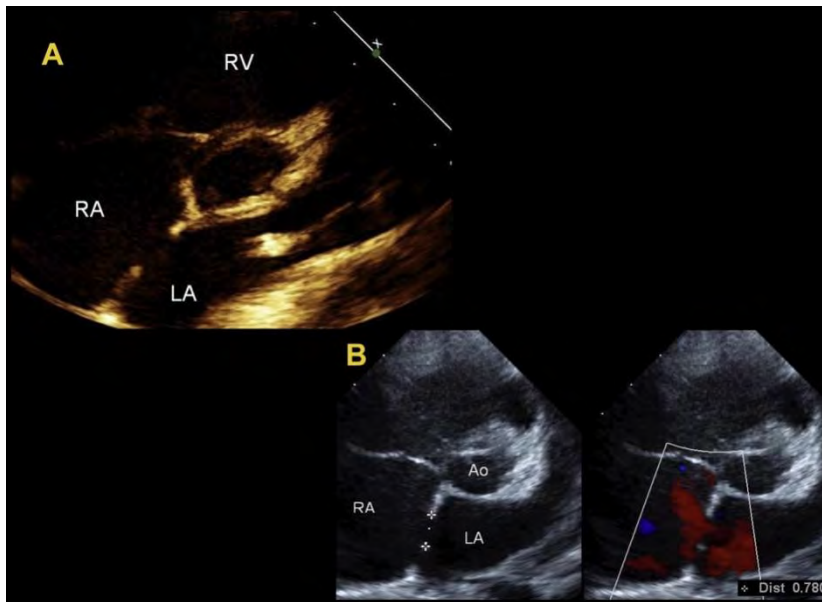


图 26 (A) 二维 TTE 胸骨旁短轴切面示继发孔型 ASD。(B) 二维 TTE (左) 及彩色多普勒 (右) 胸骨旁短轴切面示继发孔型 ASD，在缺损的上下平面测量其上下径及彩色多普勒左向右分流束。Ao，主动脉根部。

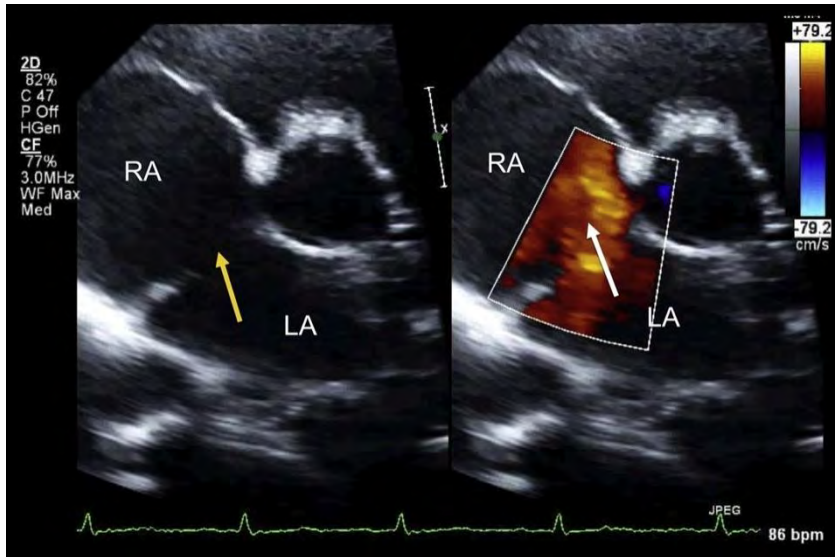


图 27 一例小儿继发孔型 ASD 患者 TTE 胸骨旁伴和不伴彩色多普勒图像。见视频 14

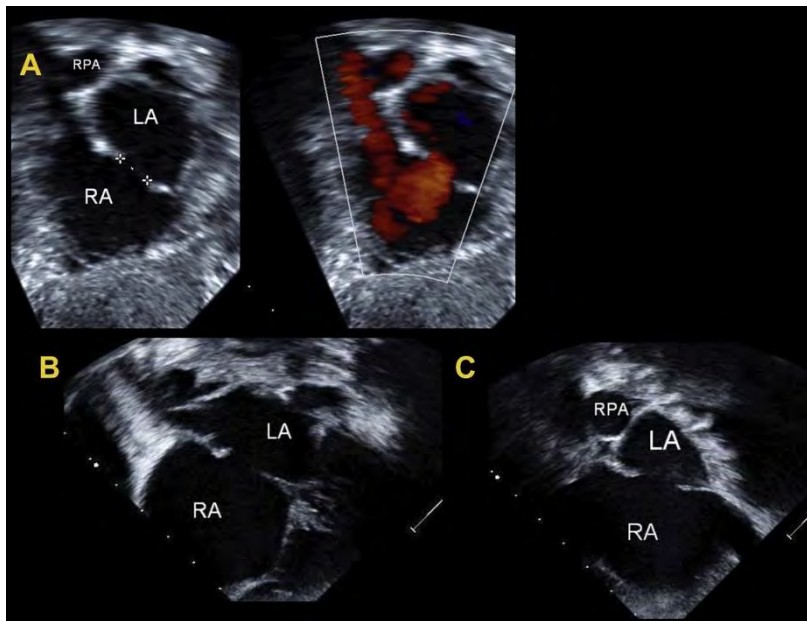


图 28 (A 和 B) 一例继发孔型缺损剑突下左前斜位切面 2D TTE (左) 与彩色多普勒图像 (右)。(A) 测量 ASD 的直径 (左), 彩色多普勒示左向右分流束 (右)。(C) 一例继发孔型 ASD 剑突下矢状切面图。RPA, 右肺动脉。

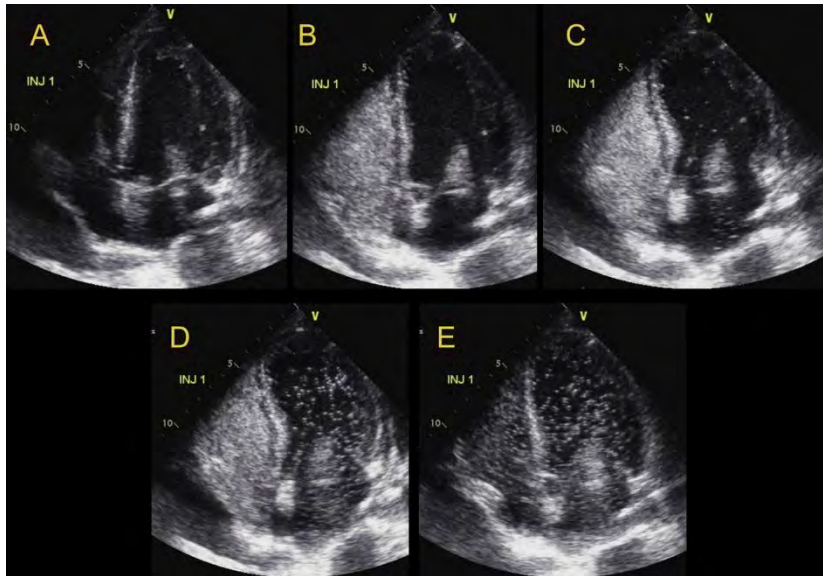
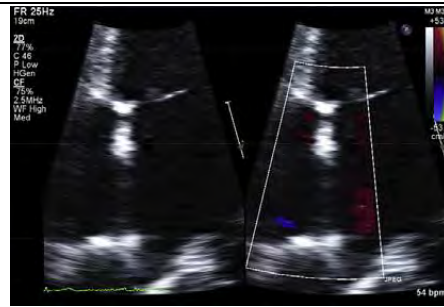


图 29 注射生理盐水增强造影时 TTE 心尖四腔心切面图。(A) 原始图像显示明显的二尖瓣伪像。(B) RA 和 RV 完全浊化。(C) 造影剂延迟进入 LA 与 LV，伴有肺动静脉畸形。如果在前三个心动周期内，微泡通过，则存在心内分流。在后面的心动周期 (D 和 E) 显示因肺内分流而致的 LA 与 LV 持续性显影。视频 14 显示了上述顺序。视频 16 显示了 PFO 的 ICE 成像，可以观察到盐水造影剂立刻由右向左分流，可清楚见到其穿过 PFO 处。INJ, injection, 注射。

表 3 评价房间隔解剖结构的 TTE 切面

| 切面 | 举例 | 房间隔解剖 | 术中评估 |
|--------------------------|----|-------------------------|-------------------------------|
| 剑突下长轴 (正面)或左前斜位 (45°) | | 右肺静脉 ASD 残边, 房缺内径和房间隔长度 | 封堵器相对于右肺静脉的位置以及残余分流的评价 |
| 剑突下短轴切面 (矢状位) | | SVC 和 IVC 残边以及和房间隔缺损的直径 | 封堵器相对于 SVC 和 IVC 的位置以及残余分流的评价 |

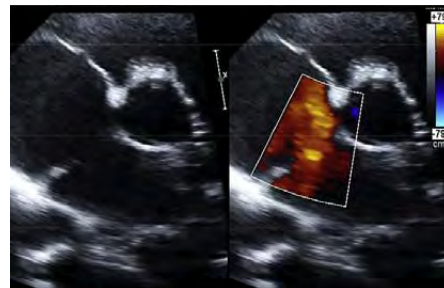
心尖四腔心切面



缺损到 AV 瓣的残边，评价 RV 增大的情况，根据三尖瓣反流估测 RV 压

封堵器相对于 AV 瓣的位置

胸骨旁短轴切面



主动脉和心房后壁残边，房间隔缺损直径，评估 RA 增大的情况

封堵器与主动脉瓣的位置关系，评估对主动脉的冲击或骑跨情况，及封堵器与后壁的位置关系

分流对右室的影响

旧版指南文件中已详细讲述了 RV 血流动力学改变的超声心动图评价。

^{9,115} ASD 对血流动力学的影响主要与分流的方向和量有关，而这取决于缺损的大小，相应 RV 和 LV 顺应性及相应的体循环和肺循环阻力。在大多数患者，RV 顺应性高于 LV，肺循环阻力低于体循环阻力，因此出现左向右的分流。左向右分流导致的最显著的超声心动图改变是 RV 的扩张。

在聚焦于 RV 的心尖四腔心切面测量 RV 的大小最为准确。要注意获取无图像缩短且可以显示 RV 最大径的图像。可以通过确保心脏的关键点和心尖可在图像中显示来完成。RV 基底段内径大于 41mm，中间段内径大于 35mm，则表明 RV 扩大。同样地，长径大于 83mm 也反应 RV 增大。¹¹⁵

RV 的面积已被证明与心脏磁共振测得的 RV 容积相关，可作为评价 RV 扩大的半定量指标。^{116,117} 与心脏磁共振相比，3D 超声心动图测量的 RV 容积是评价 RV 容积最为准确的超声

心动图方法。与 2D 的方法相比，3D 超声心动图有更好的重复性，且较少出现对 RV 容积的低估。¹¹⁸⁻¹²⁰ 用体表面积标化 RV 舒张末期容积，男性大于等于 87 mL/m²，女性大于等于 74 mL/m² 提示 RV 增大。¹²¹ 当 RV 明显扩大时，3D 容积成像常难以包绕整个 RV 用于计算其容积。

室间隔的形状/心室的形态也可反映 RV 大小。容量负荷过重导致 RV 扩大时，如 ASD 时的左向右分流，舒张期室间隔膨向 LV 侧，与正常心脏中呈现圆形外观相比，呈偏扁平的外观。除了 RV 容量负荷过重可致舒张期室间隔扁平外，对于伴有肺动脉高压的 ASD 患者，收缩期室间隔也可呈扁平状。分别于舒张期和收缩期对室间隔曲率进行评估，看是否呈“D”字型，可以用于协助诊断 RV 容积和/或压力负荷过重。即使因室间隔扁平而致的 D 型心室并非右室负荷过重的诊断依据。当其存在时，应进一步强调确认病因和右心压力或容量超负荷的严重程度。⁹ 室间隔扁平程度随右室扩大而增大，

可通过由胸骨旁短轴切面得到的 LV 短轴较小径线来计算偏心指数对其进行定量评价。¹²² 平行于室间隔的短轴较短直径与平分室间隔的短轴较短直径之比均可于舒张末期测量。当比值大于 1 时提示 RV 容量负荷过重。

肺动脉高压

因 ASD 导致血流量增加，肺血管会发生适应性改变，不伴明显的 PA 压力增高。当 RV 容量负荷持续加重，PA 血流量持续增大时，一小部分患者会出现肺动脉高压，更小一部分患者会出现不可逆的肺血管病变。¹²³ ASD 的类型与肺动脉高压的发生概率和速度也相关，腔静脉型缺损比继发孔型 ASD 更易在年轻时期就出现肺动脉高压。¹²⁴ 因此，在介入治疗前，对肺动脉高压的评估是超声心动图评价 ASD 的重要部分。RV 收缩压是评价 PA 收缩压的最佳方法，而 RV 收缩压是用三尖瓣反流峰速（velocity, V）和简化的伯努利方程进行评价： $RV \text{ 收缩压} = 4(V)^2 + \text{估测的 RA 压}$ 。正常的 RV 收缩期峰值压力应不超过 30-55mmHg。同样地，PA 舒张压可用肺动脉瓣舒张末期反流速度估算，平均 PA 压可用 PA 血流峰速估算。^{125,126} 虽然可使用非侵入性检查准确的估测 PA 压，但非侵入性检查测量的肺血管阻力更成问题。然而，现已使用三尖瓣反流峰速（米/秒）与 RV 流出道的 VTI（厘米）的比值进行评价。

RV 功能

一般来讲，ASD 的存在不会对 RV 功能（收缩或舒张）造成不利影响；然而，在部分情况下，RV 功能可受到损害，如存在明显的肺动脉高压时。可用于评价 RV 收缩功能的指标有 dP/dt 、

心肌做功指数、三尖瓣环收缩期位移，RV 面积变化率，3D 容积成像的 RV 射血分数、多普勒组织成像（Doppler tissue imaging, DTI）S' 速度、DTI 等容舒张期心肌加速度以及 RV 应变与应变率。可用于评价右室舒张功能的指标有三尖瓣 E、A 波速度、E/A 比值、DTIE'、A'速度、E/E' 比值、等容舒张时间及减速时间。更多关于各种技术的操作及其优、缺点的内容可见于最近的“超声心动图评估成人右心”指南。

LV 功能

在年长患者中，年龄相关的 LV 舒张功能减低可导致 ASD 左向右分流量增加，导致 RV 容量负荷加重，晚期才出现相应临床症状。并且，这些患者在 ASD 修补术后发生急性左心衰与肺水肿的风险性也提高了。认为是因为 ASD 修补术后，LV 舒张功能障碍才明显显现出来，左心无法承受急剧增加的容量负荷而导致了该急性变化。^{127,128} 术前通过超声心动图测量二尖瓣口血流量及瓣环运动速度评估左室舒张功能有助于筛查 ASD 修补术后有心衰和肺充血风险的患者。然而，ASD 和左、右心之间的压力平衡可以掩盖左室舒张功能障碍。¹²⁹ 在这种情况下，使用侵入性评估 ASD 封堵并测量 LA 压有助于筛查有发生肺充血风险的患者。ASD 修补术前进行利尿剂和减轻后负荷的治疗，可以帮助阻止 ASD 修补术后心衰的发生。如果药物治疗不足以减低 LA 压，可用带孔 ASD 封堵器以避免发生急性左心衰竭。

要点

- 彩色多普勒探查到的典型 ASD 分流方向为左向右。应将彩色信号增

益调整至较低水平，以便探查可能存在的低速分流信号（如 25-40cm/sec）。

- 当存在明显的费用吗高压或 RV 顺应性减低时，ASD 分流也可以是右向左或者双向的。在彩色多普勒的基础上使用脉冲波多普勒可用于探查双向分流信号。
- 当 LA 与 RA 压不等时，PFO 受到牵拉，此时可能可以探查到左向右的分流信号；然而，该分流信号通常是不连续的，不是随时都可以被彩色多普勒探查到的。
- TTE 基础上使用第一代造影剂可用于探查 PFO；然而，普遍认为 TEE 是探查 PFO 的金标准。
- 不论是使用 TEE 或 TTE，采用标准化的操作建议，包括多次注射震荡生理盐水，并同时行激发动作瞬时提高 RA 压，可提高检查的准确性。
- 3-6 个心动周期内于 LA 内见微泡，表明存在肺内分流，如动静脉畸形。
- 当 RA 浊化不完全、Valsalva 动作不规范、欧氏瓣将 IVC 回流的静脉血引至房间隔（阻止自 SVC 而来的微泡不能穿过房间隔）、未能使 RA 压力高于 LA 如存在 LV 舒张功能不全与图像质量不佳时，微泡探查也可出现假阴性。
- TCD 是检测 PFO 的另一种成像方法，TCD 优于 TTE 和 TEE 的地方在于

提高了患者的舒适度(与 TEE 相比)，可以半定量评价分流量的大小并可以鉴别心外和心内分流。

- 左向右分流导致最显著的超声心动图改变是 RV 的扩张，多种超声心动图成像方法均可以对其进行测量。
- 超声心动图通过估测 Qp/Qs 对分流程度的评价及其对 RV 功能的评价完善了 ASD 超声心动图评价。

房间隔与间隔缺损成像




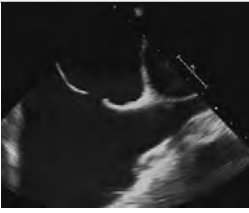

卵圆孔未闭

PFO 很普遍，发生率占人群的 20%-25%，^{5,130} 在前面的章节中已经详细介绍了其解剖结构。PFO 与隐源性卒中、潜水减压病、低氧血症综合征和偏头痛相关。¹³¹⁻¹³⁸ PFO 在这些临床病症中的所起的作用仍存在争议，现在，食品药品监督管理局（FDA）不提倡行经皮导管封堵术封堵 PFO 以尝试减少这些疾病的发生。超声心动图在评价 PFO 及 PFO 修补术，术中指导修补术起着中心作用，与其在 ASD 修补术中所起的作用相似。

使用 TTE 对 PFO 进行评价，包括使用震荡生理盐水增强造影，本质上是根据是否存在右向左分流判断是否存在 PFO。一旦探查到 PFO，且考虑行经皮导管封堵术时，则需使用 TEE 对房间隔进行详细的评价。当怀疑患者存在 PFO 时也可行 TEE 检查；然而，TTE 在技术上不足以排除 PFO 的存在。

表 4 TEE 评价 ASD 的切面

| 切面 | 举例 | 房间隔解剖 | 术中评价 | 建议多平面探查角度 | 食管部位 |
|----|----|-------|------|-----------|------|
| | | | | | |

| | | | | | |
|-------|---|------------------------|-------------------|--------------------|------------|
| 基底横切面 |  | SVA, 主动脉上, RUPV | 心房顶部封堵器与周围结构关系 | 0°, 15°, 30°, 45° | 中上段食管 |
| 四腔心切面 |  | 后侧和 AV 残边, ASD 最大直径 | 封堵器与 AV 瓣的关系 | 0°, 15°, 30° | 中段食管 |
| 短轴切面 |  | 后侧和主动脉残边, ASD 最大直径 | 封堵器与 AoV 及心房后壁的关系 | 30°, 45°, 60°, 75° | 中上段食管 |
| 两腔切面 |  | IVC 与 SVC 残边, ASD 最大直径 | 封堵器与右心房顶部的关系 | 90°, 105°, 120° | 中上段食管及深部经胃 |
| 长轴切面 |  | LA 顶部 | 封堵器与 LA 顶部的关系 | 120°, 135°, 150° | 中上段食管 |

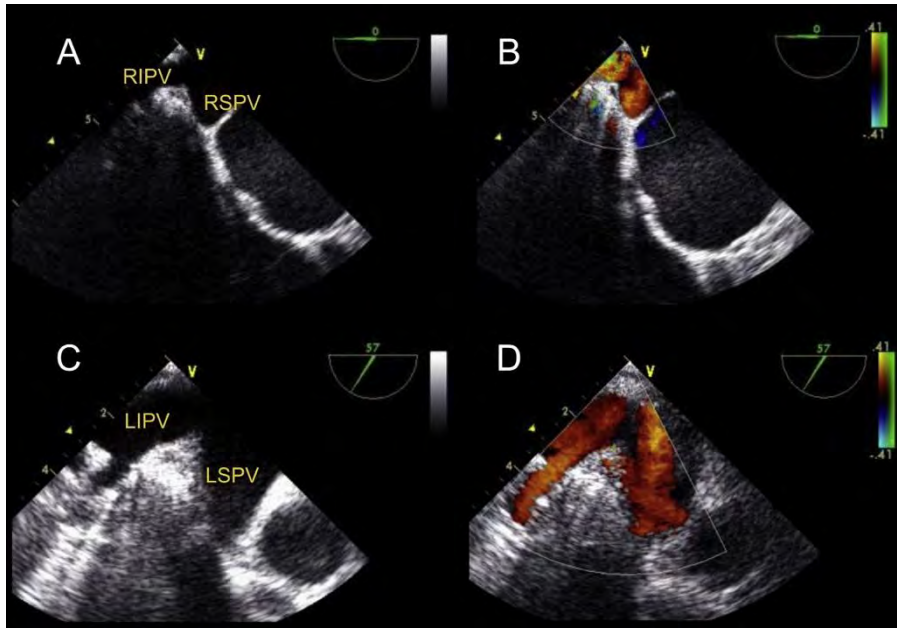


图 30 TEE 食管上段 0° 短轴切面示右肺静脉，伴 (B) 和不伴 (A) 彩色血流信号，60° 伴 (D) 和不伴 (C) 彩色血流信号。LIPV，左下肺静脉；LSPV，左上肺静脉；RIPV，右下肺静脉；RSPV，右上肺静脉

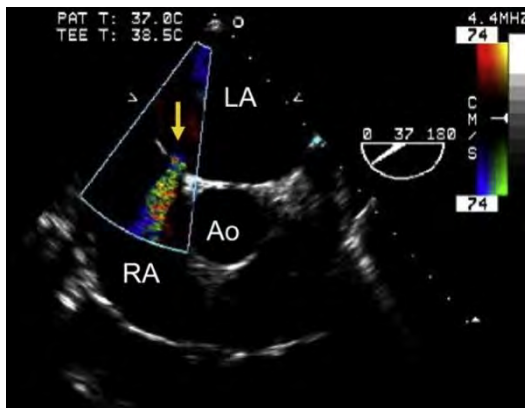


图 31 TEE 食管中段降主动脉短轴切面示小继发孔型 ASD (黄色箭头)。Ao，降主动脉。

TEE 评价 PFO 的切面与评价 ASD 的切面类似。都是从食管中段水平横切面开始，调整设置以求最优化显示房间隔，TEE 成像平面经过旋转探头获得，从 0° 开始，每次增加 15°，以完整评价房间隔。将彩色多普勒增益设



图 32 TEE 食管中段降主动脉短轴切面示大继发孔型 ASD。主动脉残边 (箭头)。AV，主动脉瓣/主动脉。

置在较低水平，使用彩色多普勒并排成像，有助于探查 PFO 处的分流与房间隔上可能存在的其它缺损。为了更好的探查 SVC 附近的房间隔，需将探头往外撤，如要探查 IVC 附近处的房间隔，则需把探头向深处推进。另外，可在横向平面对房间隔进行初步评估，从食管上段水平 SVC 处开始，将探头在食管内推进，先见到卵圆窝成像，成像最后终止于 IVC 水平。在 90° -120° 的成像切面也可完成相似的操作。

从 30° -50° 开始，在 AoV 横切面，可见 PFO 邻近主动脉。每次增加 15° 旋转平面，可使 PFO 的缝隙或通道与切面相平行。在这个角度，可以评价 PFO 通道的长度。在该切面也评价继发隔的厚度。

当探查到 PFO 后，可注射震荡生理盐水增强造影评价右向左分流，已在分流成像的技术，标准以及特点：TTE 和 TEE，一节中描述过。需要患者配合做可瞬时增加 RA 压，使其超过 LA 压的生理动作，如 Valsalva 动作。镇静患者难以完成 Valsalva 动作（详见分流成像的技术，标准以及特点：TTE 和 TEE）。

关于房间隔的重要解剖信息需要详细评价，它们影响着封堵器适用患者的筛选和封堵器类型的选择，应包括 PFO 的位置（虽然，和继发孔型 ASD 不同，PFO 的位置较为固定，一般位于卵圆窝的上部或下部）、继发隔的厚度与延伸范围、房间隔的全长、PFO 通道的长度、RA 与 LV 侧 PFO 的大小、PFO 到腔静脉的距离、是否存在 ASA（详见于 IAS 和间隔缺损成像：房间隔膨胀瘤），以及是否合并其他房间隔空洞或缺损。在 ASD 患者中，应注意排除部分型肺静脉畸形引流。

实时 3D (RT3D) TEE 较 2D TEE 可以更好的评价 PFO 的变化。⁸² RT3D TEE 已证明 PFO 呈椭圆形，而非圆形，分流束的面积从 RA 侧到 LV 侧逐渐减小。在继发孔型 ASD 患者 PFO 的面积随心动周期的变化而变化，心室收缩期面积大于心室舒张期。⁸² RT3D TEE 也可用于封堵术中指导，通过对房间隔正面成像，可显示 PFO 与封堵器及与 RA、LA 房侧毗邻结构之间的关系¹³⁹（图 44）。

当选择用于封堵 PFO 的封堵器时，应注意评价 PFO 的解剖特点。¹⁴⁰ 尤其是，卵圆窝的内径、PFO 通道的长度，是否存在 ASA 及其大小、继发隔的厚度与在整个心动周期中 PFO 的最大径，对可以行封堵术的患者的筛查都有非常重要的意义。在每一例患者，根据所有这些指标进行评价，从四种封堵器中选择合适的封堵器，相比只用单一封堵器封堵 PFO，可提高封堵的成功率，减少并发症的发生率。¹⁴⁰

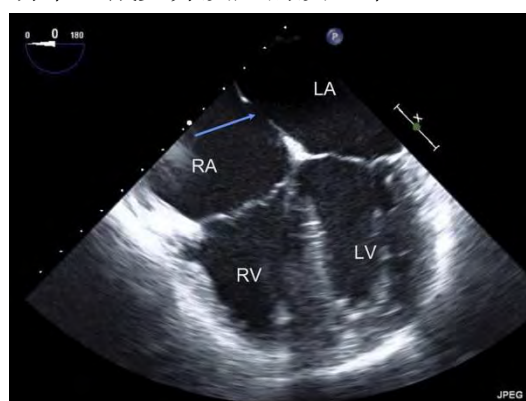


图 33 TEE 食管中段四腔心切面示大继发孔型 ASD。标记 ASD（蓝色箭头）。



图 34 TEE 食管中段四腔心切面示继发孔型 ASD 封堵器。标示与 AV 瓣的关系。标示 ASD 封堵器（蓝色箭头）。

房间隔膨胀瘤

ASA 是指房间隔冗长或呈囊袋状，且活动性增大（图 7 和 10）。ASA 的定义为间隔组织向 RA 或 LA 侧偏离，距正常房间隔的位置超过 10mm 或者左右摆动幅度超过 15mm。当光标与房间

隔平面相垂直时，可用 M 型记录此运动（图 45）。ASA 在一个更为详细的分类系统（临床上并没有广泛采用）中被分为五种类型，主

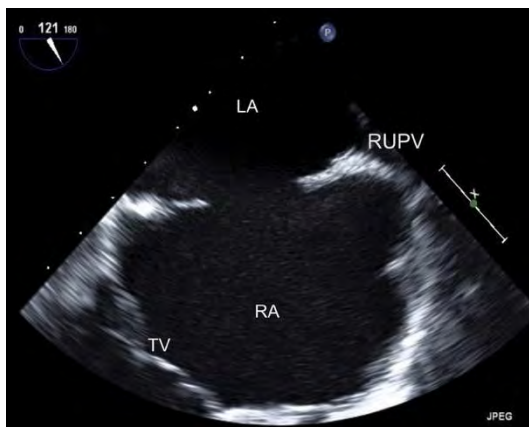


图 35 TEE 食管中段改良两腔切面（包括三尖瓣）示大继发孔型 ASD。见视频 17

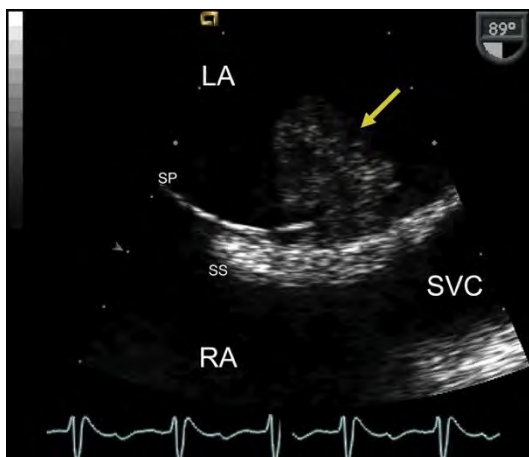


图 36 放大 TEE 两腔切面示血栓（黄色箭头）附着于左房侧 IAS 的间隔囊。这可能提示血栓穿过 PFO（反常血栓）或左房侧间隔囊原发血栓。SP，原发隔；SS，继发隔。

要是根据向 RA 或 LA 的偏移程度，主要是偏向 RA 或 LA，或者向左右的偏移程度。

ASA 常与 PFO 或 ASD、较大的 PFO，隐源性卒中和栓塞事件发生率增加有关。ASA 与多孔间隔也有关。对于 ASA 的评价，TEE 比 TTE 更敏感。存在 ASA 及其范围是选择 PFO 封堵器类型时需要考虑的因素之一。选择封堵器时，可选择相对较大的封堵器以包绕和稳定房间隔，也可选择较小较柔软的封堵器以更好的与 ASA 相贴合。

可用 2D 成像观察房间隔的偏移运动，也可将 M 型光标垂直于 IAS 平面，使用 M 型进行观察。可于 TTE 剑突下四腔心切面、TEE 两腔切面，ICE 间隔长轴切面进行观察（图 45）。

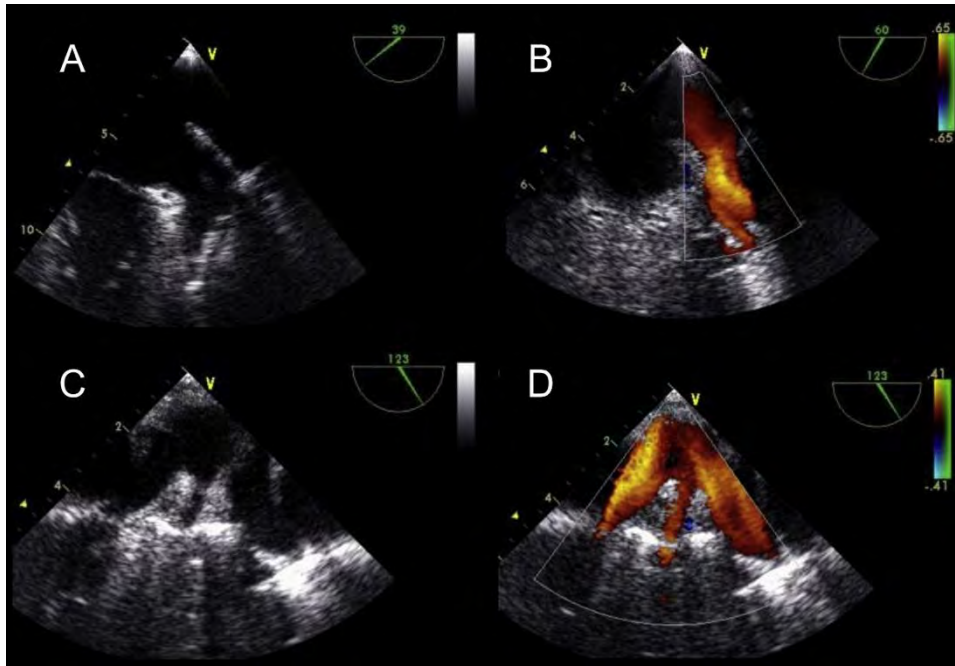


图 37 TEE 两个不同切面显示左肺静脉。食道中段不伴(A)与伴(B)彩色多普勒血流成像，在 60° 切面基础上慢慢向左旋转探头显示左侧肺静脉。食道中段长轴切面向左肺静脉旋转探头至 120°，不伴(C)和伴(D)彩色血流图像。

欧式瓣和希阿里氏网

欧式瓣自 IVC-RA 结合处向前延伸，TTE 的最佳成像切面是剑突下冠状面和矢状切面。TEE 成像时，欧式瓣的最佳成像切面是长轴切面。由于邻近 IAS 的大欧式瓣可以影响 RA 侧封堵器的释放，因此在超声心动图检查时应注意评价欧式瓣的范围及其与 IAS 之间的距离。

希阿里（氏）网是静脉窦右瓣的遗迹，可呈膜状或条索状，位于右房的不同部位，包括近 IVC 入口处及冠状静脉窦右房开口处（图 20）。希阿里氏网可干扰导线、导管、护套、导丝和封堵器穿过右房。因此，在 ASD 或 PFO 修补术前，存在希阿里氏网也应是超声心动图评价项目之一。¹⁴²

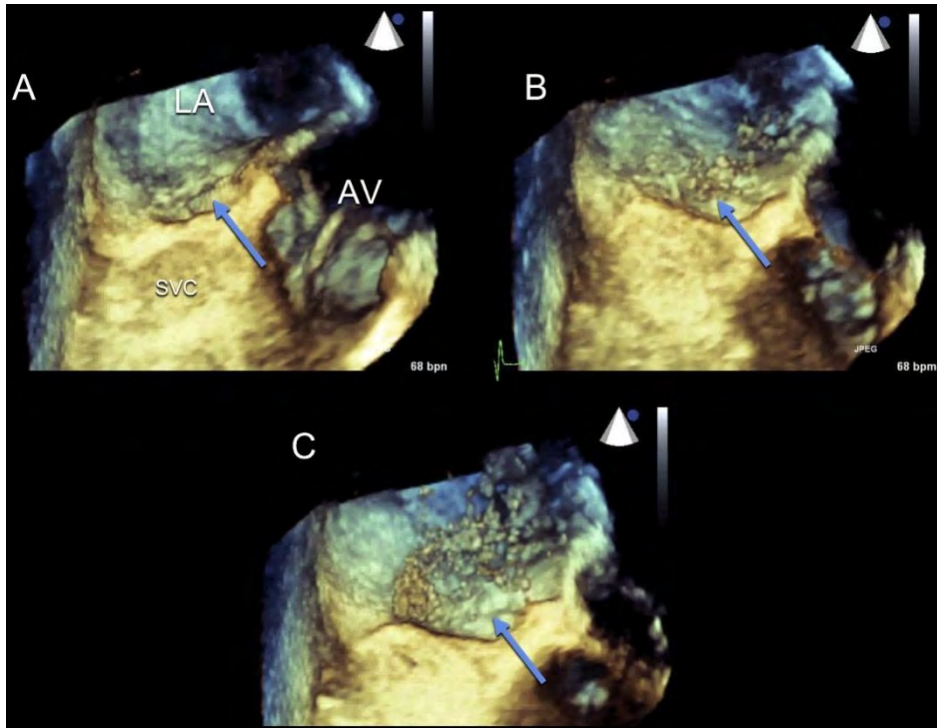


图 38 实时三维 TEE 食道中段短轴切面示生理盐水造影时 PFO 的图像。可清晰显示 PFO 进入左房的出口（蓝色箭头）。这些操作是为了显示微泡穿过房间隔进入 LA 的具体位置，而非定量评价分流量的多少。（A-C）震荡生理盐水产生的造影微泡经 PFO 进入 LA。蓝色箭头示 PFO 通道。见视频 18

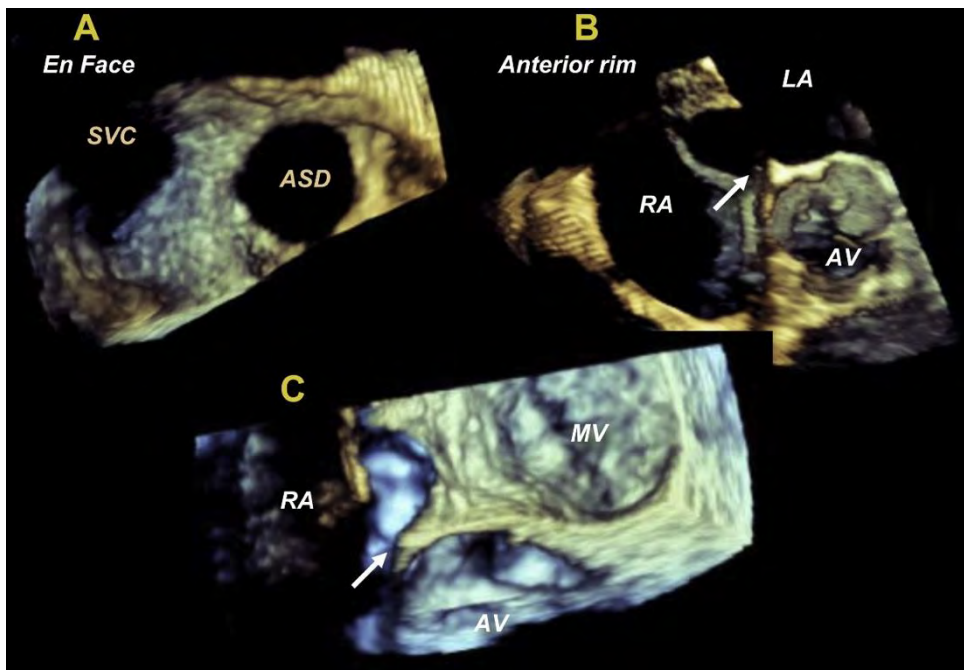


图 39 实时 TEE 食道中段短轴切面从 RA 侧(A)显示继发孔型 ASD 的正面,(B)食道中段短轴从 RA 侧显示主动脉残边（箭头），（C）四腔心切面从 LA 侧显示主动脉残边。MV，二尖瓣

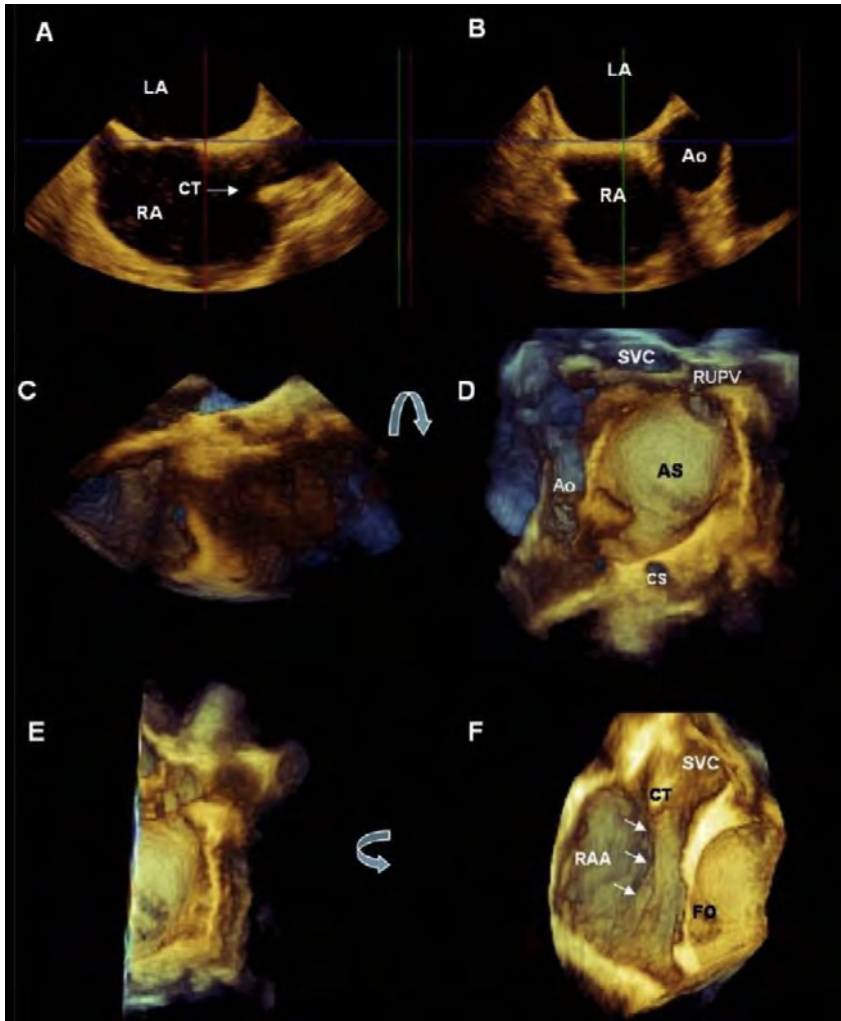


图 40 静态图像显示两个互相垂直的二维 TEE 平面(A 和 B)以获取放大的 IAS 3DE 数据(C)。将探头上-下旋转 90° (弯曲箭头)(D), 可获得房间隔左侧正面成像。可对图像 D 进行切割, 去除左侧半的房间隔(E), 逆时针旋转探头 90° (弯曲箭头)(F), 从 SVC 到 IVC 的整个界嵴(箭头)都可以显示出来。Ao, 主动脉; AS, 房间隔; CS, 冠状静脉; CT, 界嵴; FO, 卵圆窝; RAA, 右心耳。

房缺的评价：标准和特点

ASD 代表了一组可导致心内分流，解剖结构各异的病变。在前面的章节中，已详细讲述了 ASD 的分类和其它房间隔通道。表 7 列出了应对所有类型的 ASD 都系统评价和报告的共同特点。包括 ASD（原发孔型或继发孔型）或者其它心房通道（腔静脉型或无顶冠

状静脉窦）的类型、缺损处是否有彩色血流信号穿过及其方向以及其他相关的发现，如肺静脉异位引流、存在欧式瓣或希阿里氏网及其大小、缺损或缺损们的大小和形态、缺损位于房间隔的何处、是否存在多个破口与收缩末期和舒张末期 ASD 的大小。

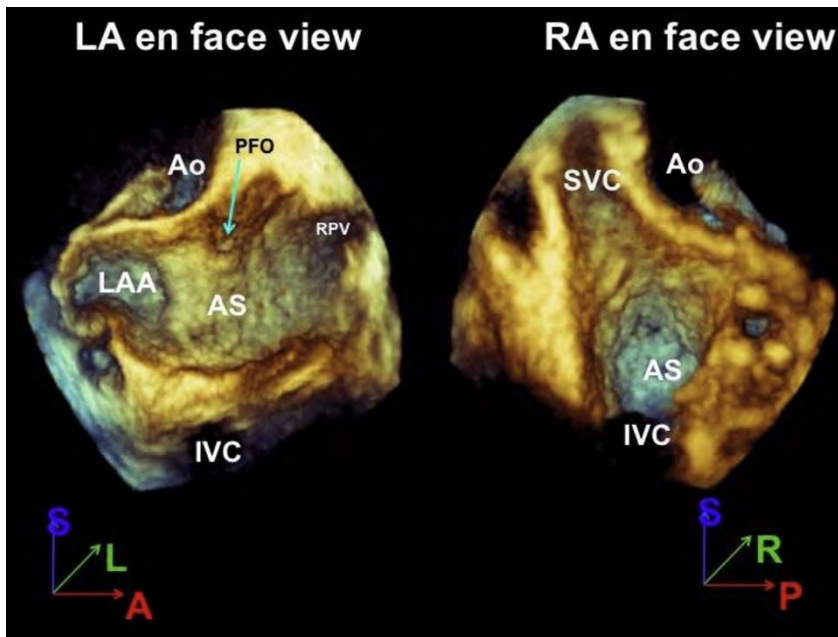


图 41 LA 侧房间隔图像（左）。在 1 点钟位置，房间隔应面向右上肺静脉。当从右房侧观察时（右），IVC 应位于其 11 点钟方向。A，前；AS，房间隔，Ao，主动脉；L，左；LAA，左心耳；P，后；R，右；S，上。

继发孔型 ASD 是最常见的缺损，也是最常发生与原发隔的缺损。²⁸ 正如前面所述，继发孔型 ASD 的大小、形态及结构各异。小 ASD 专指 ASD 的最大缺损内径小于 5mm。¹⁴³ 由于其解剖特点，继发孔型 ASD 适合行经导管封堵术。这部分内容将在本问后面的章节中详细论述。³⁰⁻³³ 继发孔型 ASD 的缺损边缘由邻近的不同组织构成，而这些“边界”根据相应的邻近结构命名。按照惯例，有六个根据解剖结构命名的周围组织。在所有患者中，都应行超声心动图仔细观测这些结构，尤其是在考虑经导管封堵术前。继发孔型 ASD 残边长度大于等于 5mm 可视为是经导管封堵术的适应症。ASD 残边小于 5mm 视为不宜行经导管封堵术或困难较大。继发孔型 ASD 的残边定义如下：

1. 主动脉残边：ASD 与主动脉环及主动脉根部之间的上/前侧残边

2. AV 瓣残边：ASD 与 AV 瓣之间的下/后侧残边

3. SVC 残边：ASD 与 SVC 之间的上/后侧残边

4. IVC 残边：ASD 与 IVC 之间的下/后侧残边

5. 后侧残边：ASD 与心房后壁之间的后侧残边

6. 右上肺静脉（RUPV）残边：ASD 与 RUPV 之间的后侧残边

ASD 经导管封堵术的成功取决于有足够长的上、下、前侧残边（SVC、RUPV、ICV、AV 瓣残边）。主动脉残边的缺失是发生侵蚀的潜在危险因素，^{103,104} 尽管它并非封堵术的绝对禁忌症。侵蚀将在封堵器栓塞与侵蚀一节中详细讲述。TEE 分别于食管上段短轴切面、食管中段短轴切面、四腔心切面及两腔切面评价这六个残边，TTE 也可获得类似切面。表 4 中列出了 TEE 成像切面及对应评价的残边。虽然在年幼的儿童患者，TTE 可充分评价这些残

边，但在年长的儿童和成人患者，其不足以全面评价这些残边。因此，建议使用 TEE 在封堵术前对这些患者的残边进行评价。ICE 已被证明在评价 ASD 残边时可获得与 TEE 相似的成像，虽然，ICE 并不能获得真正的四腔心切面。如果可以的话，应对所有考虑行经导管封堵术的患者行 3D TEE 成像--即使已经计划用 ICE 行术中指导。

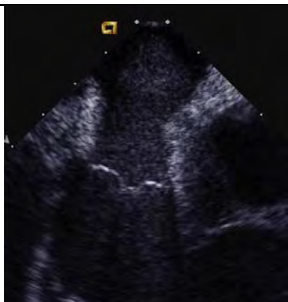
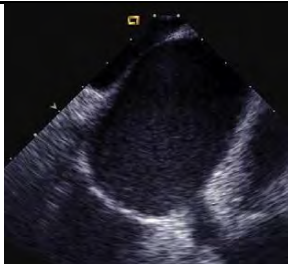
要点

- 使用 TTE 对 PFO 进行评价，包括使用震荡生理盐水增强造影，本质上是根据是否存在右向左分流判断是否存在 PFO
- 一旦探查到 PFO，如考虑行经导管封堵术，则需使用 TEE 或 ICE 对房间隔解剖进行详细的评价。
- 存在 PFO 时，注射震荡生理盐水造影是为了评价右向左分流（详见分流成像的技术，标准和特征：TTE 和 TEE）。需要患者配合做激发动作，如 Valsalva 动作，瞬时升高 RA，

使其超过 LA 压。镇静患者可能难以完成标准的 Valsalva 动作。

- 当存在 PFO 时，需常规探查的房间隔解剖信息包括：PFO 的位置、继发隔的厚度与延伸范围、房间隔的全长、PFO 通道的长度、RA 与 LV 侧 PFO 的大小、PFO 到腔静脉的距离、是否存在 ASA，以及是否合并其他房间隔空洞或缺损。
- ASA 的定义为间隔组织向 RA 或 LA 侧偏离，距正常房间隔的位置超过 10mm 或者左右摆动幅度超过 15mm。
- 表 7 列出了应对所有类型的 ASD 都系统评价和报告的共同特点
- 继发孔型 ASD 有六个明确的残边（主动脉、AV 瓣、SVC、IVC、后侧及 RUPV）。
- 继发孔型 ASD 残边小于 5mm 视为不宜接受经导管封堵术，但并非其绝对禁忌症。

表 5 心腔内超声心动图评价 IAS 的切面

| ICE 切面 | 举例 | ICE 导管位置 | 前后弯曲 | 左右弯曲 | 可显示的结构 |
|--------|---|----------|------|------|------------------------------|
| 主切面 |  | RA 中部 | 居中 | 居中 | RA, TV, RV, PV, RVOT, 低位 IAS |
| 间隔切面 |  | RA 中部 | 向后 | 向右 | IAS 下部和上部，原发隔，继发隔，与 MV 的关系 |

间隔长
轴或两
腔切面

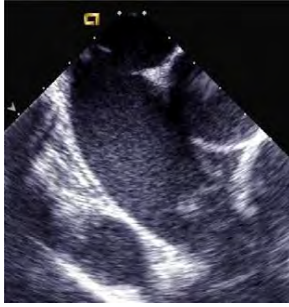


RA 上部

向后 向右

IAS, 原发隔,
继发隔, SVC

间隔短
轴



RA 中部,
转向三尖
瓣

向后 向左

AoV,
IAS, ASD 的前
后平面, 后侧
和 AV 残边

MV, mitral valve, 二尖瓣; RVOT, right ventricular outflow tract, 右室流出道; TV, tricuspid valve, 三尖瓣

表 6 现有心内超声系统的特点

| 超声技术/ 导管名称 | 导管型号 (F) | 成像频率范 围(MHz) | 成像角 度(°) | 视野深 度(cm) | 转向 (°) | 多普勒 | 可否实时三 维成像 | 费用 |
|---------------------------|-------------|-----------------|-------------|--------------|-----------------|-----|--------------------|----|
| 旋转 /UltralCE* | 9 | 9 | 360 | 5 | 无 | 无 | 否 | + |
| 相控阵 /Viewflex Plus† | 9 | 4.5-8.5 | 90 | 21 | 前-后(120) | 有 | 否 | ++ |
| 相控阵 /AcuNav‡ | 8 或 10 | 5-10 | 90 | 16 | 前、后左、 右(160) | 有 | 可(仅 10F 的 导管可以) | ++ |

超声心动图在经导管封堵术中的应用

超声心动图普遍用于 ASD 和 PFO 经导管封堵术的术中成像指导。

8,57,62,75,83,88,144-146 实时术中 TTE、TEE、3D 成像和 ICE 超声心动图检测在封堵器置入前、中、后都提供了重要的辅助信息。虽然每种模式都有其优点和缺点，超声心动图增强荧光成像为病人的筛选、封堵器的选择、术中指导、并发症监测和疗效评估都提供了重要信息。

现有封堵器和封堵技术介绍

美国心脏病学会/美国心脏协会指南建议对伴有 RA、RV 增大的 ASD 患者行封堵术，不论有无症状（I 级）。¹⁴⁷

小 ASD（如，ASD 直径小于 5mm），且不伴有 RV 增大或肺动脉高压的患者可以不行修补术，因为认为其不会影响到患者的临床进程或血流动力学。小 ASD 患者，如出现反常性栓塞或卧位低氧血症根据指南建议，也应考虑行封堵术（IIa 级）。ASD 封堵术的绝对禁忌症只有伴有不可逆的肺动脉高压（肺血管阻力大于 8 伍兹单位）和无左向右分流信号（III 级）。¹⁴⁷ 因缺乏解剖及残边特征支持，并且缺乏随机对照试验数据的支持，静脉窦型和

原发孔型缺损不宜行经导管封堵术。

表 8 中列出了 ASD 和 PFO 封堵术的适应症和禁忌症。

可用于 ASD 和 PFO 经导管封堵术的封堵器有很多种（图 46）。然而，U.S.FDA 未通过任何一种封堵器用于 PFO 经导管封堵术。在美国，目前通过的可用于继发孔型 ASD 封堵术的封堵器只有两种：the Helex (W.L. Gore, Newark, DE) 和 Amplatzer (St. Jude Medical, Plymouth, MN) 封堵器（图 46）。FDA 只允许对继发孔型 ASD 患者行经皮导管封堵器封堵术。因此，静脉窦型和原发孔型缺损，如果合适，应评估是否可行外科手术修补。

The Helex (W.L. Gore)是由单一镍钛诺线框支撑的膨体聚四氟乙烯贴片材料制成。该封堵器形成桥梁，以细胞浸润的方式关闭间隔缺损，最终完全覆盖膨体聚四氟乙烯材料。不建议将 Helex (W.L. Gore)封堵器用于直径大于 18mm 的缺损或残边缺损超过缺损周长 25%的缺损。

Amplatzer 封堵器 (Amplatzer septal occluder, ASO) 和 Amplatzer 筛状封堵器 (St. Jude Medical)是由镍钛合金网和涤纶织物制成的双盘封堵器。这种封堵器附着于缺损两侧的间

隔壁，植入后形成一个组织生长平台。ASO (St. Jude Medical)是一种自中心性封堵器，其腰部的大小可以堵单个ASD直径。筛状封堵器窄小的腰部设计是为了使其易于通过有孔间隔的中心部位而进行放置；置于间隔两侧的直径相匹配的盘状封堵器，最大化的覆盖了多孔分流。ASO (St. Jude Medical) 使用禁忌症为：缺损与右肺静脉、AV瓣或IVC之间的间隔残边缺如（定义为小于5mm）。虽然主动脉残边缺损并非使用封堵器的绝对禁忌症，但是还是认为其会增加封堵器侵蚀的风险。

很大一部分缺损常合并主动脉残边缺失或不够长，尽管这类患者ASD修补术后，封堵器侵蚀最常发生，但是绝大多数此类缺损都可以成功修补，而不发生继发侵蚀。仔细的评估房间隔和缺陷的大小后，Helex封堵器(W.L.

Gore) 和 ASOs (St. Jude Medical)，经静脉通过其独特运输系统进行放置。封堵器运输技术之间的区别及评估合适的定位将在后面的章节中讨论。

封堵器栓塞和侵蚀

PFO和ASD经皮导管封堵器的并发症很少见，包括封堵器栓塞、心脏穿孔、心包填塞和封堵器侵蚀。^{148,149} 封堵器栓塞在所有病例中的发生率约0.1%-0.4%，最常见于ASD封堵器。¹⁴⁹ 封堵器栓塞是潜在的有生命危险的并发症，需要立刻经皮导管或外科介入手术取出。通过常规TTE监测可以很容易地诊断封堵器栓塞。封堵器栓塞的危险因素包括过小的ASD封堵器、周围结构残边缺损以及封堵器错位。栓塞可在封堵器释放后立刻出现，常由封堵器错位或封堵器型号

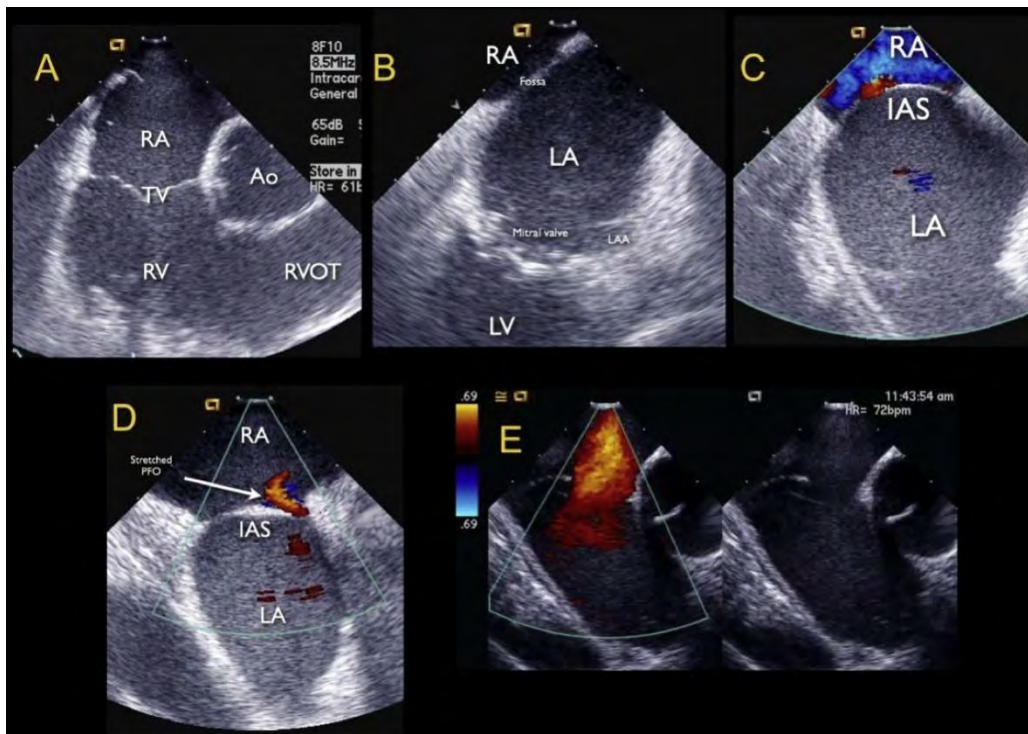


图 42 心腔内超声心动图评价 IAS(详见于心腔内超声心动图 IAS 成像建议)。(A) 主切面。(B)间隔长轴切面。(C)两腔切面。(D)间隔短轴显示 PFO 图像。(E)间隔

短轴显示继发孔型 ASD 图像。白色箭头示经伸展型 PFO 的 PFO 分流方向。LAA，左心耳；RVOT，左室流出道；TV，三尖瓣。

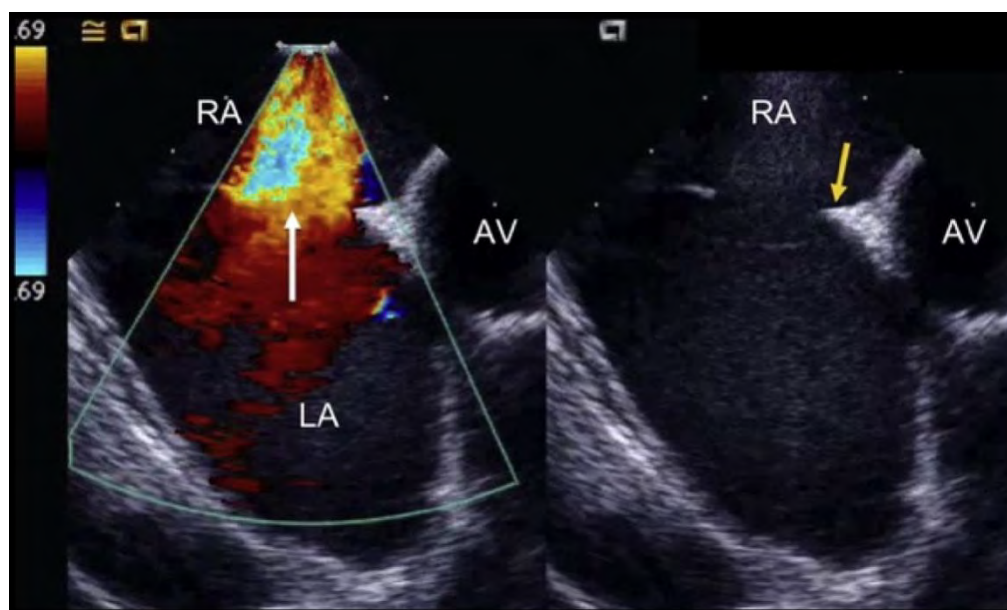


图 43 心腔内超声心动图左向右分流继发孔型 ASD 图像，伴和不伴彩色多普勒成像。白色箭头示 ASD 分流束的方向；黄色箭头示主动脉残边；AV，主动脉

表 7 应常规测量和报告的 ASD 特点

ASD 类型—PFO，原发孔型 ASD，继发孔型 ASD，或其他类型心内分流（腔静脉窦型、冠状静脉窦顶部缺如，肺静脉畸形引流）

多普勒血流—左向右、右向左或双向分流信号

ASA 存在与否

合并异常—欧式瓣或希阿里氏网

ASD 的大小—最大和最小直径（最佳测量于 3D 容积数据模式），ASD 面积

ASD 的位置（如，高位继发孔型 ASD，SVC 或 IVC 型静脉窦缺损）

测量所有残边—主动脉、RUPV、上、后、下、AV 间隔

ASD 的形状---圆形、椭圆形、不规则形

是否存在多孔分流

ASD 的血流动力学—测量缺损面积以及于收缩期末期与舒张期末期测量最大/最小直径

ASD 处分流阻断时 ASD 的直径（经皮导管封堵术球囊测量）

不对引起。TTE 和 TEE 对于评价移位封堵器的准确位置和因栓塞而遗留的生理后遗症（如，流入道/流出道梗阻，瓣叶断裂）有不可替代的作用。封堵器侵蚀是少见但潜在的致命并发症。据报道，各种封堵器均可发生侵蚀，包括 ASO(St. Jude Medical)，房间隔缺

损封堵系统，Angel-Wings 封堵器 (Microvena Corp., White Bear Lake, MN)。这些封堵器中，在美国只有 ASO (St. Jude Medical) 被批准使用。^{63,150,151} ASO (St. Jude Medical) 侵蚀的发生率约 0.1%-0.3%。^{150,152-154} 封堵器侵蚀可发生于 RA 或 LA 顶部或与主动

脉结合处，可致心包积血、心包填塞、主动脉瘘以及/或死亡。¹⁵⁴ 封堵器侵蚀可以以亚临床事件开始，伴随封堵器撞击周围结构，遮盖心房或主动脉组织，或导致亚临床心包积液。侵蚀在临床上可表现为胸痛、晕厥、呼吸急促心包积血进展、心脏压塞、血流动力学改变和死亡。

据报道，大多数侵蚀病例发生在封堵器植入后 72 小时内，但也有长达 6 年才出现侵蚀的报道。¹⁵⁵ 大多数侵蚀发生于置入术后第一周。^{63,151} 虽然并未明确说明，但多认为侵蚀是由于人体组织与封堵器之间的相互机械作用而引起的（而非炎症反应）。

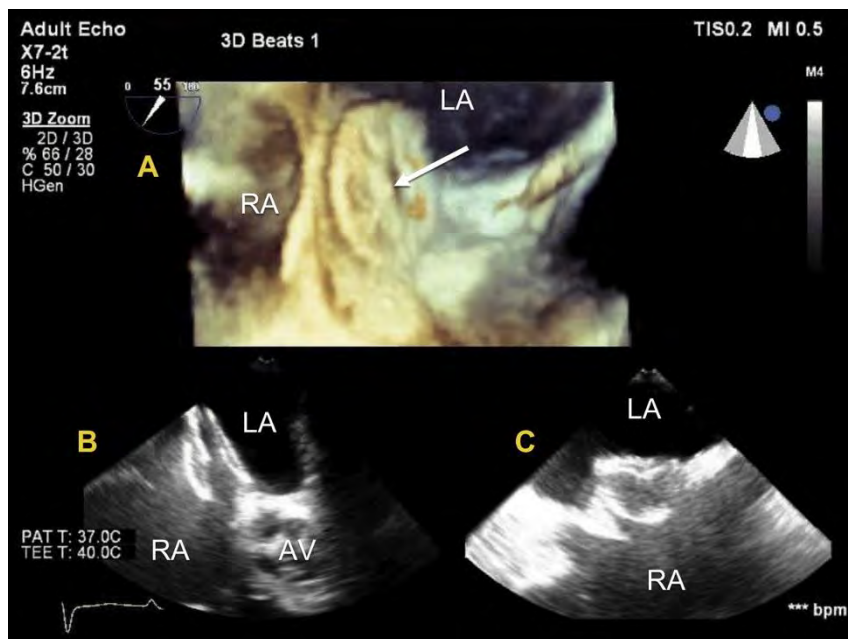


图 44 PFO 筛状封堵器封堵术中三平面图像(A,3D; B,垂直的两个短轴切面, C,垂直的两个长轴切面)。白色箭头示封堵器 LA 侧圆盘。AV, 主动脉瓣。

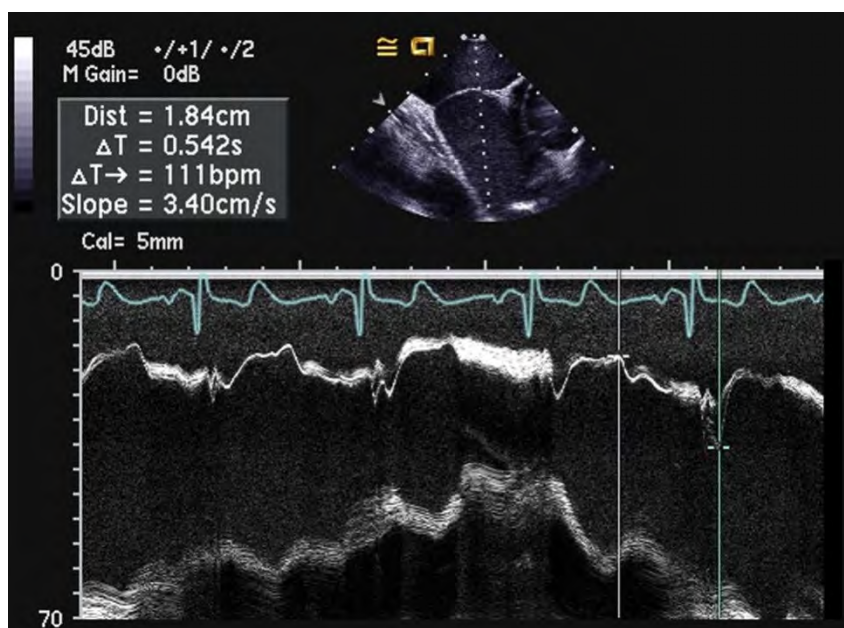


图 45 ICE M 型 ASA 成像示卵圆瓣运动幅度超过 15mm

侵蚀发生的原因不明。该并发症的少见及缺乏对照组的研究数据，对此严重并发症并没有一个全面的认识。在发生了侵蚀的一系列病例中，对其成像信息和封堵器数据进行了深入研究。从这些信息和专家共识中得出，这些因素可大致分为一些大家普遍认为更有意义的，如封堵器过大（在 40% 以上病例中出现）、主动脉残边完全缺失、缺损位于房间隔偏高/偏下的位置，以及前侧残边缺失合并后侧残边过短。¹⁵⁴ 为预测侵蚀而提出的其它形态上的危险因素包括特殊位置的 ASD，如缺损与主动脉不对称、动态 ASD（一个心动周期中大小变化超过 50%），主动脉残边缺损或缺如（90% 以上的病例中都存在），以及封堵器骑跨主动脉或围绕主动脉张开。¹⁵⁴ 然而，介入治疗协会在侵蚀发生的病因上尚未达成共识。^{31,152} 重要的是注意，如，成功行 ASO (St. Jude Medical) 封堵术的 ASD 患者中普遍存在主动脉残边缺损（最近的报道中占 40%）。^{31,153,154} 通过对已确诊病例进行回顾性分析，认为封堵器置入术后的重要危险因素包括主动脉根部封堵器的变形及置入术后 24 小时出现心包积液。表 9 中列出了 Amplatzer 封堵器侵蚀的危险因素。

没有一个危险因素或超声心动图特征可以明确侵蚀的绝对风险。因此，不存在明确的封堵术“超声禁忌症”。在一个概念框架中，例如，侵蚀可能是独特的高风险 ASD 组织结构特征合并过大的封堵器，而后引起心脏和封堵器重构。因此，超声心动图成像可帮助筛查有侵蚀风险的患者（如，主动脉残边缺损，封堵器与患者房顶部不匹配，或在释放前撞击主动脉）。¹⁵⁴ FDA 和器械商已经同意对 ASO(St.

Jude Medical) 进行批准后进一步研究，以助于更好的评价侵蚀的危险因素。评价房间隔及其相关残边的标准化文件，如本文中所述，可提高用于分析这种少见但严重的并发症的发生原因及其预防的数据的质量和可靠性。

经皮导管术中成像指导：TTE，TEE，ICE

不管何种方法，超声心动图在经皮导管术中指导和术后并发症评价中都起着重要作用。表 10 中列出了经皮导管封堵术可能出现的所有并发症及可用于协助诊断的超声成像方法。

经胸超声心动图是经皮导管封堵术创伤最小的成像方法，足以用于小儿患者的术中指导。⁶² 它的局限性在于较大的患者成像质量差，受到超声探头穿透力的影响。另外，置入的封堵器会产生伪像，常遮盖位于 IVC 上方位置较低的房间隔组织残边。

经食道超声心动图可在经皮导管封堵术中提供更为详细的成像。^{7,8,63,66,80,90,145} 行 TEE 检查时，使用常规麻醉可增加患者的舒适度，并减少误吸风险。除了麻醉支持以外，需要有经验的超声心动图医师进行术中 TEE 操作。清醒镇静用于患者筛查。

心腔内超声心动图已成为经导管封堵术中指导的另一种成像方法，在部分中心，甚至更喜欢用其行术中指导。^{65,83,85,88,91,92,146,156} ICE 成像与 TEE 相当，且在观察 LA 结构和间隔后下侧残边方面优于 TEE。ICE 检查时额外需要一根 8F-10F 的导管。如果患者的体重超过了 35kg，用于封堵器运输和 ICE 操作的导管可以置于同一侧的股静脉中，选取相隔数毫米的两个穿刺点进行穿刺。在较小的患者，ICE 导管

静脉通道应在对侧静脉穿刺。尽管超声心动图专业医师也需在术中提供帮助，但不是必须的，因为行封堵术的介入医师也可控制导管。它的优点包括不需要进行常规麻醉，术中操作时间和放射时间短以及相比于 TEE 术中指导需要行常规麻醉而言，花费较低。^{65,83,90,146}最近已引进了三维 ICE，也逐渐出现对心脏结构性疾病进行评价的初步结果。^{95,97}

实时三维 TEE 可获取房间隔的 RT3D 成像，可全面评价缺损及其与周围结构关系。可从双侧心房直视封堵器，增强了封堵器植入后有效性及潜在并发症的评价。^{6,7,31,63,65}

经导管介入术的术中指导

所有要行经皮导管封堵术的间隔缺损患者，术前都要行 TTE 或 TEE 超声心动图成像，详细评价房间隔解剖，筛查房间隔缺损是否适合行封堵器封堵。其内容应包括，如前所述，使用超声心动图连续多平面完整探查整个 IAS 及其周围结构。缺损的类型（ASD

型，ASA，PFO，拉伸型 PFO）及缺损的数量（多达 13% 的患者有一个以上的缺损），缺损的大小、位置、形态及其周围房间隔组织（残边）都应一一描述（表 7）。所有周围结构如肺静脉、上腔静脉、下腔静脉，冠状静脉，欧式瓣和主动脉瓣的相关异常都应说明或排除。

IAS 缺损及其周围心房组织残边均因仔细全面的探查。TEE 食管中段四腔心切面观（从 0° 多平面开始，每次增加 15°），可探查到前下侧残边和后上侧残边（图 47-49）。前侧（原主动脉）和后侧残边可于食道中段 AoV 短轴切面测量（自 30°-45° 多平面开始，每次增加 15°）。食道中段两腔切面（110°-130°）最适于上下侧残边的探查。3D 超声心动图成像可以获得相似的数据但不需要连续多切面逐步成像（图 50 和 51）。在部分患者中，需要行经胃成像观察 ASD 的下侧残边，评价封堵器下部和 IAS 下部的关系。

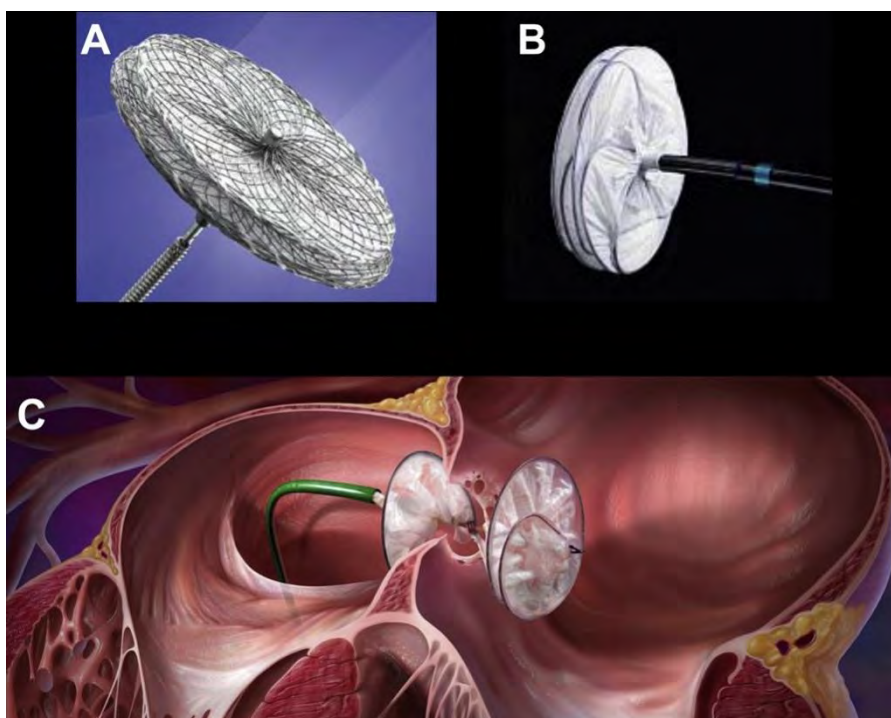


图 46 ASD 封堵器示例。(A) ASO (St. Jude Medical). (B) Helex occluder (W.L. Gore). (C) 封堵器安放的动画示意图。4C, 四腔心(切面); Ao, 主动脉; SAX, 短轴(切面)

表 8 ASD 和 PFO 封堵术的适应症和禁忌症

ASD 和 PFO 修补术的潜在适应症

单独继发孔型 ASD 并肺循环/体循环血流量(Qp/Qs)例 1.5:1, 提示右室容量负荷超载

PFO--隐源性卒中和右向左分流的证据 (目前还在研究中, FDA 并不提倡)
禁忌症 (绝对或相对)

PFO 或小 ASD 伴 Qp/Qs 比例小于 1.5:1 或没有 RV 容量负荷超载的征象
单个缺损太大, 不宜用封堵器 (>38mm)

筛孔型 ASD 不适于用经皮导管封堵术

缺损过于接近 SVC, IVC, 肺静脉, AV 瓣或冠状静脉

前、后、左或右侧残边 <5mm

肺静脉畸形引流

合并需心脏外科手术的畸形

ASD 伴重度肺动脉高压和双向或右向左分流

超声心动图诊断存在心腔内血栓

表 9 Amplatzer 封堵器侵蚀的可能危险因素

多个切面均显示主动脉残边缺损, 0°时主动脉残边缺失 (“秃主动脉”)

多个切面均显示上侧残边缺失

高位继发孔型 ASD

ASD 封堵器过大 (封堵器直径 > 分流阻断时测量缺损直径的 1.5 倍)

动态 ASD (ASD 大小改变 50%)

使用 26mm 的 ASO 封堵器

不对称缺损

封堵器放置后房间隔游离壁隆起 (突入横窦)

封堵器圆盘楔入后壁与主动脉之间

封堵器放置后出现心包积液

ICE 术中指导 PTC

使用 ICE 行术中指导时, 需全面评价缺损及其周围组织残边。探头最初定位于可以探查三尖瓣的位置。在此位置上, 使用前/后旋钮向后旋转, 左/右旋钮稍微向右旋转可获得间隔图像 (图 42C, 43)。将导管继续推进可获得两腔切面, 在该切面上可测量上、下残边, 缺损的直径和结构 (图

52A)。顺时针旋转整个手柄直到心内探头靠近三尖瓣, 接着, 稍微向左旋转右-左旋钮直到显示 AoV, 可获得类似 TEE 的短轴切面, 两切面的区别在于 ICE 下该切面上显示的邻近结构是 RA 而 TEE 是 LA (图 52B)。在该切面上, 亦可测量缺损直径、主动脉及后残边的长度。

应该从“主视图”开始行完整的“中部”扫查，然后也结束于主视图。在很多情况下，该扫查可有效的排除 SVC 型静脉窦房缺，评估主动脉瓣反流，获得完整的房间隔成像。在封堵器置入前后都应行该检查，以再次评价封堵器置入后二尖瓣和三尖瓣的反流情况。完整的两腔切面和 AoV 切面扫查，可将导管后倾并直指向右房获得。

基本的超声心动图评价应包括垂直切面上缺损直径、间隔的全长及缺损残边（原主动脉，下-IVC，及后-肺静脉）的测量。如果存在多个缺损，每个缺损的特征及缺损之间的距离都应测量。

除了超声心动图数据外，还应注意全面评价左、右心的血流动力学，以明确缺损的生理影响，排除封堵术的其他解剖或生理禁忌症。右上肺静脉成像（35°左前倾斜与 35°颅侧倾斜）可显示房间隔的侧面，并可作为封堵器置入的成像显示通路。

建议所有接受 ASD 封堵术的患者均行透视和超声心动图成像下用球囊测量缺损大小；然而，由于缺损自身的大小，部分术者不会用球囊测量面积。停流技术包括在房间隔的缺损处放置测量球囊（St. Jude 测量球囊, St. Jude Medical; or NuMED 测量球囊, NuMED Inc., Hopkinton, NY）。彩色多普勒成像时，缓慢增大球囊的面积直到经过缺损处的彩色血流完全停止

（图 53A）。当穿过缺损处的血流停止时，可多成像平面测量房间隔处球囊的直径。另外，当球囊封闭缺损时，通过两个垂直切面（短轴和双腔）观察房间隔是非常重要的，可用于确诊或排除其他缺损。

一旦完成大小的测量，ICE 导管应撤回至长轴切面，继续监测封堵术的各个步骤（图 53B-E）。

术后房间隔即时成像

超声心动图在 ASO (St. Jude Medical) 和 Helex (W.L. Gore) 封堵器术中用于监测封堵器运输的每个步骤。最有用的 TEE 切面为四腔心和短轴切面。ICE 成像时，双腔切面可获得整个 LA 的全部图像（图 53）。

对于 ASO (St. Jude Medical) 大小的选择，应在停流技术下测得的内径与在此基础上增加 2mm 之间。运输系统通过静脉鞘输送，直达左上肺静脉（图 52 和 53）。导线和扩张器需缓慢撤回，注意避免发生空气栓塞的可能。封堵器装载后输送至鞘管的尖端。然后将输送鞘重新经肺静脉送入 LA 内。介入医师固定导线，退出鞘管，从而植入 LA 侧封堵器圆盘（图 53B）。至关重要的是，在此步骤，超声心动图需要帮术者证明 LA 侧圆盘是远离肺静脉或左心耳的。当左侧圆盘与间隔只隔几毫米时，在 LA 侧释放连接腰部的一部分，并持续牵引至缺损处（图 53C）。目的是以封堵器腰部支撑缺损。接着，持续牵拉至 RA，RA 侧的圆盘也成功放置（图 53D 和 E）。当整个圆盘结构离开鞘管后，运输导丝继续向房间隔靠近，使植入的两个圆盘结构彼此贴近（图 53E）。

表 10 经皮导管封堵术的急、慢性并发症及超声心动图在其诊断和治疗的作用

| 并发症 | 结局 | 剧烈程度 | 治疗 | 超声心动图的作用 | 建议使用的超声技术 |
|---------|--------------|-------|----------|-------------|--------------------------------------|
| 心脏穿孔 | 填塞 | 急性 | 手术 | 诊断 | TTE, TEE, ICE |
| 封堵器栓塞 | 栓塞,瓣膜梗阻 | 急性或慢性 | 介入或手术探查 | 诊断,手术探查术中指导 | TTE, TEE, 或 ICE 诊断, TEE 或 ICE 用于术中探查 |
| 出血 | 低血容量,休克,死亡 | 急性 | 输血, 外科介入 | 排除其他诊断 | TTE |
| 肺栓塞 | 呼吸衰竭, 死亡 | 急性 | 抗凝 | 评价右心应变 | TTE |
| 封堵器侵蚀 | 心包积血, 填塞, 死亡 | 慢性或晚期 | 手术 | 诊断 | TTE (反流或积血), TEE (侵蚀) |
| 封堵器血栓形成 | 栓塞, 中风 | 慢性或晚期 | 抗凝 | 诊断 | TEE |
| 感染性心内膜炎 | 脓肿, 死亡 | 慢性或晚期 | 抗生素, 手术 | 诊断 | TEE |
| 封堵器断裂 | 心脏损害, 穿孔, 反流 | 慢性或晚期 | 手术探查 | 诊断 | TEE |

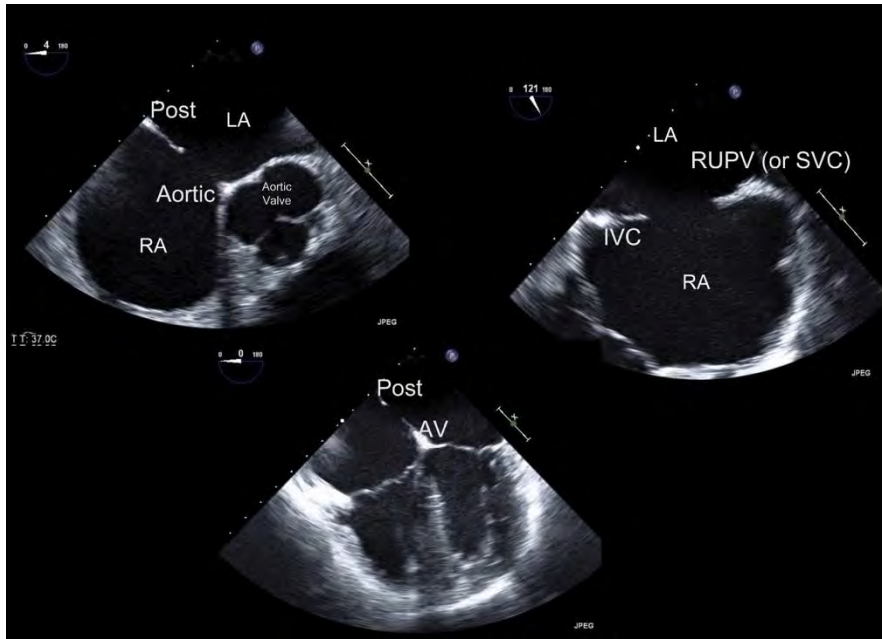


图 47 TEE 评价 ASD 的三个（五个中）重要切面。短轴切面对于评价主动脉残边及封堵器与主动脉的相互作用起着重要作用。两腔和长轴（未展示）切面对于评价封堵器与心房顶部的关系很重要。AV，房室瓣残边；Post，后侧残边。

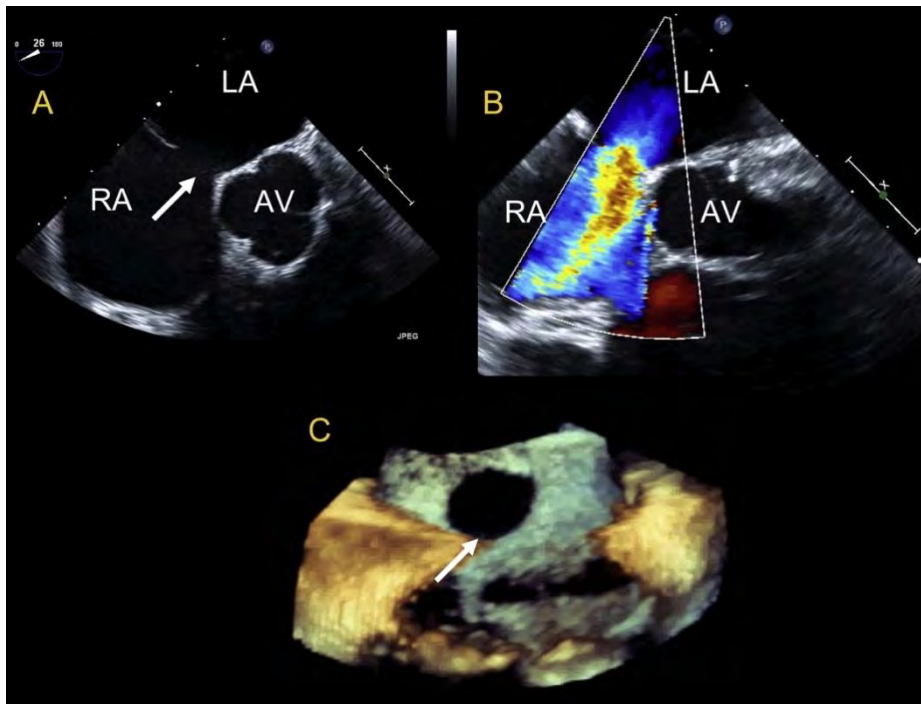


图 48 三维 TEE 成像示主动脉残边轻度缺损的中等大小继发孔型 ASD。(A)食管中段短轴切面示 ASD 和主动脉残边缺损。(B)相似的切面示左向右彩色多普勒分流束。(C)RA 侧放大 ASD 正面图像。白色箭头示 ASD。AV，主动脉瓣。

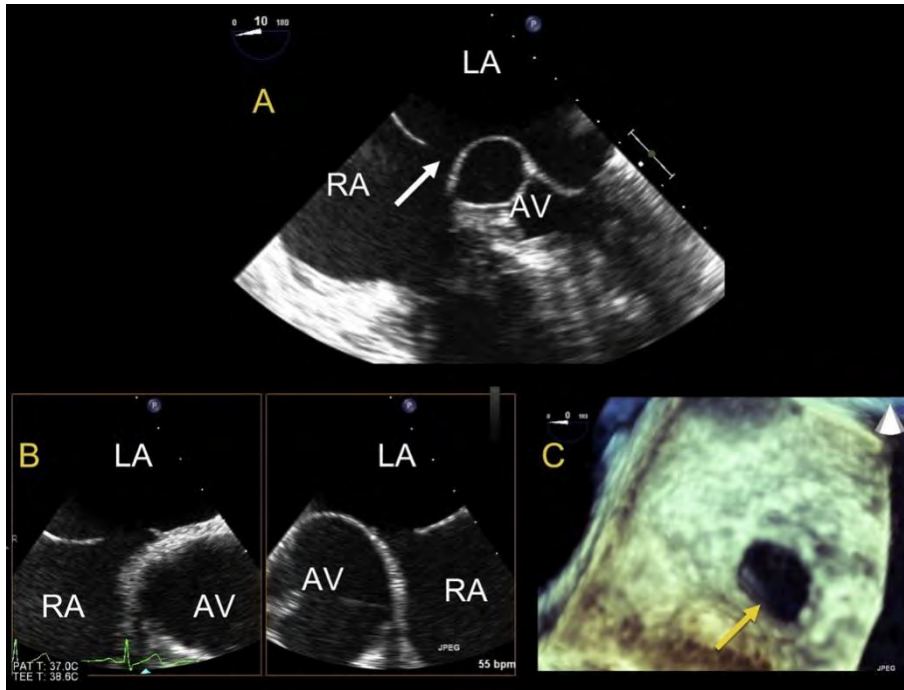


图 49 三维 TEE 是主动脉残边缺损的中等大小继发孔型 ASD。(A)改良食道中段四腔心切面。(B)双平面成像示缺损的不同面积。(C)LA 侧放大 ASD 正面图像。黄色箭头示残边缺损；白色箭头，ASD。AV，主动脉瓣。见视频 20，21

Helex 封堵器(W.L. Gore)的选择大小的选择应遵循封堵器与缺损直径的比例大于 2:1，并且选中的封堵器直径不能超过房间隔全长的 90%。在透视和超声心动图成像下，向前推进 Helex 封堵器(W.L. Gore)运输导管的尖端，直至不透射标记部位已进入 LA。左房封堵器圆盘在 LA 腔内成形。介入医师主要根据透视成像来完成这一步骤。如果正在行 TEE 检查，把探头撤离透视部位会更好。当 LA 侧圆盘成形后，则使用超声心动图成像指导 LA 侧房间隔封堵器的放置。当运输导管进入右房，RA 内圆盘成形后，LA 侧圆盘则已固定于间隔上。超声心动图探查

用于确定左、右侧圆盘均呈平面，与间隔并列，房且间隔组织位于两侧圆盘之间。

对于 Helex (W.L. Gore) 和 ASO (St. Jude Medical) 两种封堵器，在彻底释放前，需对封堵器、房间隔和周围结构作一个全面的评价。需从两个垂直切面确认 LA 与 RA 侧的圆盘已正确的置于心腔内。彩色多普勒检查用于排除封堵器边缘残余分流，当出现分流时提示封堵器大小或位置异常（图 54）。要明确 LA 与 RA 侧封堵器圆盘间是否存在房间隔组织需要进行仔细的探查。尽管主动脉残边通常易于探查到，但需仔细探查后缘、

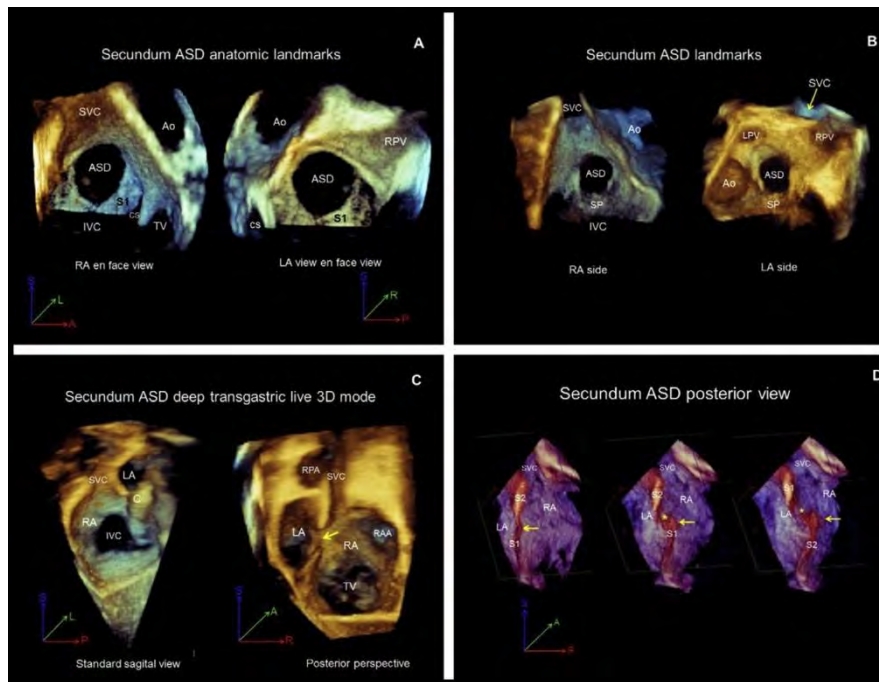


图 50 继发孔型 ASD 的典型切面和解剖标志。(A)RA 和 LA 侧正面图像。(B)另一例患者的 RA 和 LA 侧正面图像。(C)实时 3D 模式下经胃矢状两腔切面, 标准正面(左)和后面(右)图像。(D)后面图像显示原发隔与继发隔随心动周期运动的一致性。(左)原发隔(箭头)与继发隔一致的部分。房间隔各部分间轻度对和不良(中间)和明显对和不良(右)。对和不良程度加重, 心房间相通(星号)的范围增大。在定位图标上, 蓝色为 y 平面; 红, x 平面; 绿、z 平面。A, 前; Ao, 主动脉; C, 导管; CS, 冠状静脉; L, 左; LVP, 左肺静脉; RPA, 右肺动脉; S, 上; P, 后; R, 右; RAA, 右心耳; S1, 原发隔; S2, 继发隔; TV, 三尖瓣。经 Roberson 等授权⁷²

下缘的组织。在完全置入封堵器前, 需要仔细评估并排除对肺静脉、冠状静脉、AV 瓣功能造成影响, 以及主动脉根部变形。应注意可能出现的封堵器与主动脉和周围结构的之间相互作用。完全释放封堵器后, 应再次进行相同的探查。3D ICE 的作用目前尚未明确, 但在经皮导管封堵术中, 它可能可以提供更多的解剖信息。

随访

在出院前, 应行一次 TTE 检查(当使用 Amplatzer 封堵器时, 术后一周应复查一次)。应注意封堵器位置, 有无残余分流、封堵器侵蚀、不稳定或周围结构的变形。出现心包积液即使量不多也可能是存在封堵器侵蚀的指征。植入大封堵器后, 有出现心脏传导阻滞报道, 虽然罕见,

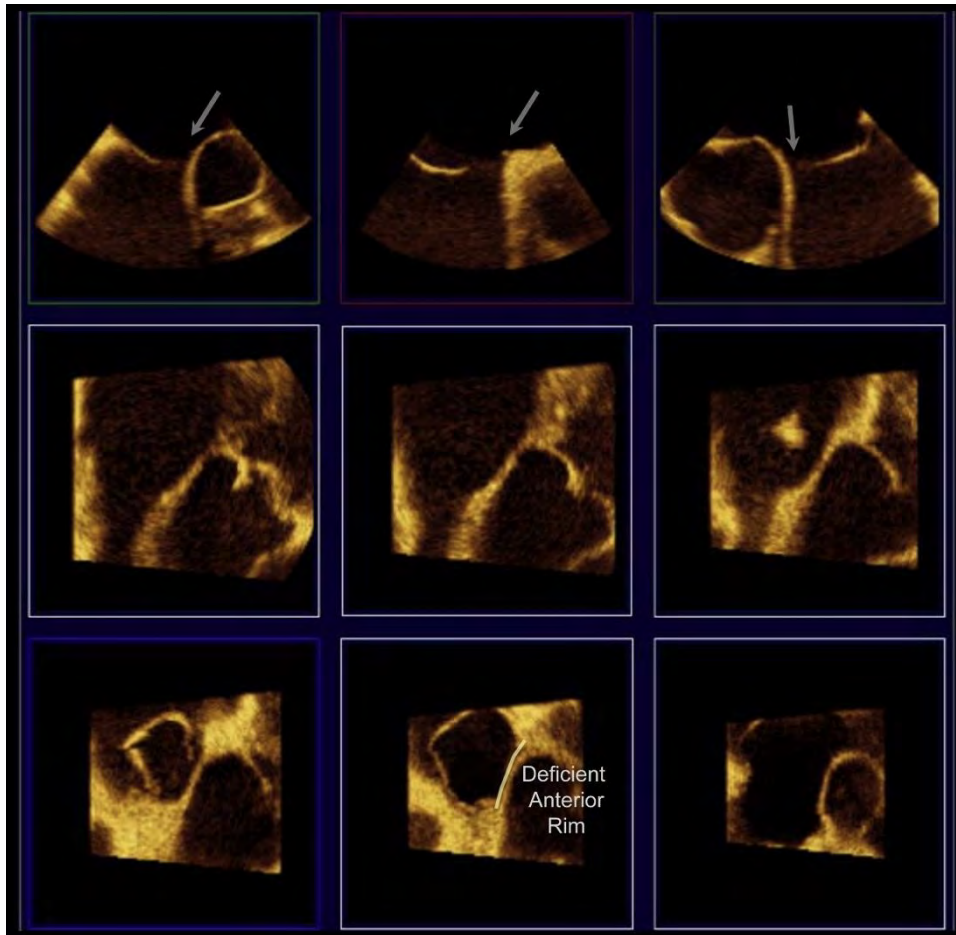


图 51 三维 TEE 可从正面评价 ASD 的形状和大小，残边缺损的特点。底部中间的图像示主动脉残边缺损。

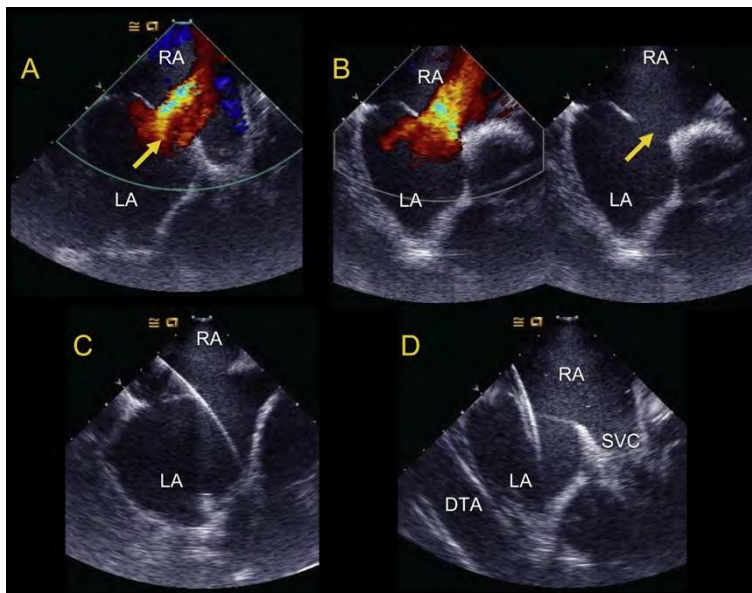


图 52 心腔内超声心动图指导继发孔型 ASD 封堵术。(A 和 B) 术前图像显示继发孔型 ASD。黄色箭头示 ASD。(C) 导丝进入左上肺静脉。(D) 导管进入左房。DTA，降主动脉。见视频 22 与 23

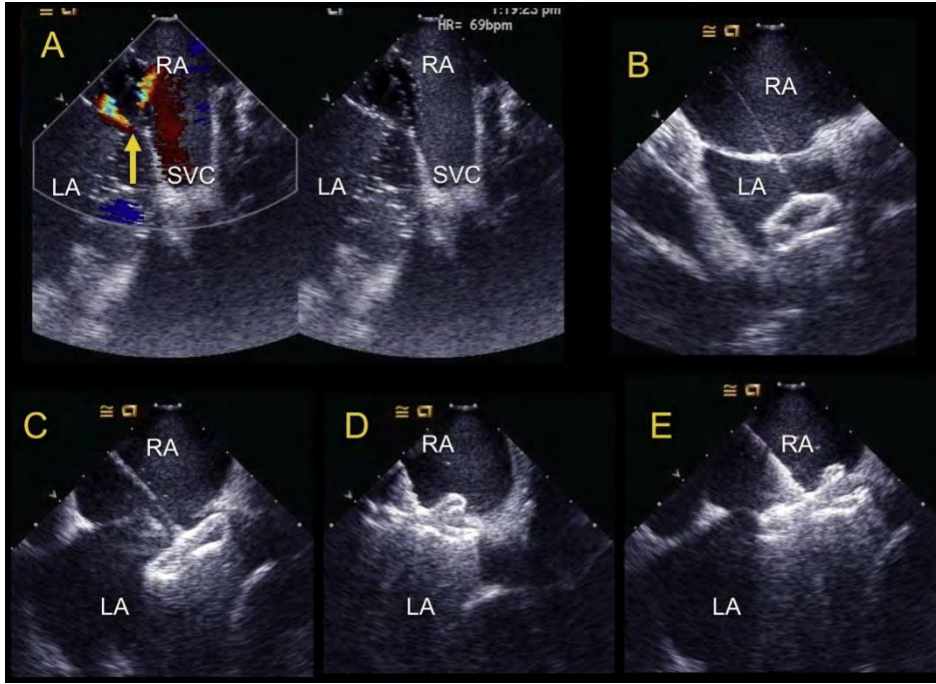


图 53 心腔内超声心动图指导继发孔型 ASD 封堵术。(A)球囊测量缺损大小，伴和不伴彩色多普勒成像。箭头示测量球囊周围少量分流束。(B)左房侧圆盘打开，向房间隔牵引。(C)向房间隔牵拉 LA 侧圆盘。(D 和 E)两侧圆盘均打开，仔细确认保证房间隔正好夹在两侧圆盘中间。见视频 24-28。视频 28 示经 ASD 的扫查显示稳定的封堵器的正面图像

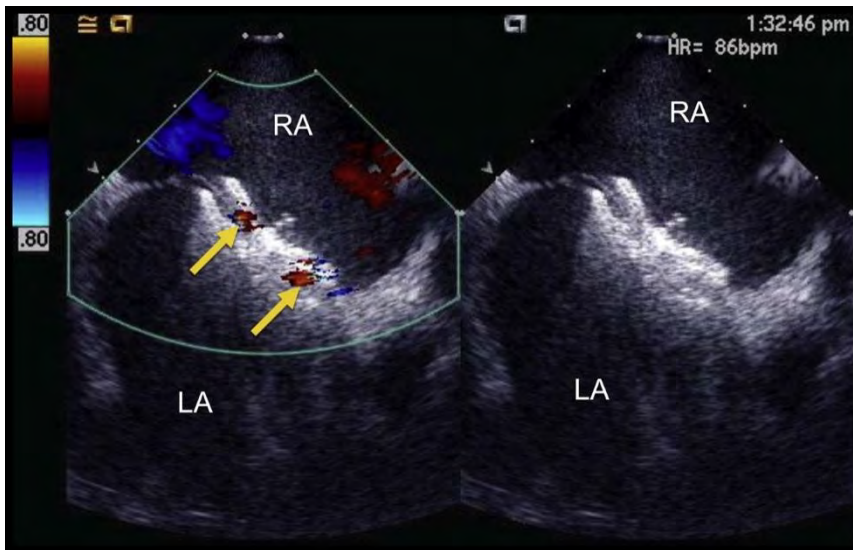


图 54 心腔内超声心动图指导继发孔型 ASD 封堵术详见术后房间隔即时成像。封堵器最后放置处（从导管释放后）可见经封堵器少许正常的残余分流（箭头）（血栓形成和内皮化之前）。

但封堵术后也有必要常规行 12 导心电图检查。^{157,158} 据报道，封堵器置入后，早期房性心律失常和传导异常的发生率增加了。¹⁵⁸

随访评估，包括 TTE，应在术后 1,6,12 月检查，以后每 1-2 年复查一次。若使用的是 Helex 封堵器，应注意封堵器的稳定性，因为封堵器的不稳定可能提示导线框架破裂。对封堵器稳定

性存疑的患者，推荐行普通透视明确和评价导线框架破裂。左向右分流阻断后第一个月，RV 大小会明显改善；但是，长期右心扩大的患者，可能恢复较慢，也可能永远无法恢复正常。

要点

- TTE 是经皮导管封堵术创伤最小的成像方法，足以用于小儿患者的术中指导
- TEE 可为经皮导管封堵术中提供更为详细的成像。
- ICE 已成为经导管封堵术中指导的另一种成像方法，在部分中心，甚至更喜欢用其行术中指导。
- 3D TEE 可获取房间隔的 RT3D 成像，可全面评价缺损及其与周围结构关系。
- 不论用何种成像方法，都应全面评估缺损及其周围的组织边缘(表 7)。
- 术前建议用球囊测量 ASD 的大小。彩色多普勒成像时，缓慢增大球囊的面积直到经过缺损处的彩色血流完全停止。当穿过缺损处的血流停止时，可多成像平面测量房间隔处球囊的直径

- 在封堵器释放前，应对封堵器、房间隔及其周围结构进行完整的评价。
- 要明确 LA 与 RA 侧封堵器圆盘间是否存在房间隔组织需要进行仔细的探查。尽管主动脉残边通常易于探查到，但需仔细探查后缘、下缘的组织。
- TTE 随访评价应在术后 1,6,12 月进行，以后每 1-2 年复查一次。

结论

正如本文所讲述的，对房间隔解剖和相关异常的详细系统化评价应包括探查及定量评价缺损的大小和形状，缺损周围的组织残边，分流的方向和分级，心脏各腔室与肺循环的重塑及大小功能的改变。对房间隔异常的全面评价需要联合分析 TTE，TEE 和/或 ICE 成像所得的结果。本文中提出了一套标准化的成像与命名，以便对这些异常进行详细的评价。

3D 技术对正常和异常间隔解剖成像和表征，对评价房间隔和指导经皮及外科介入治疗作出了巨大贡献。

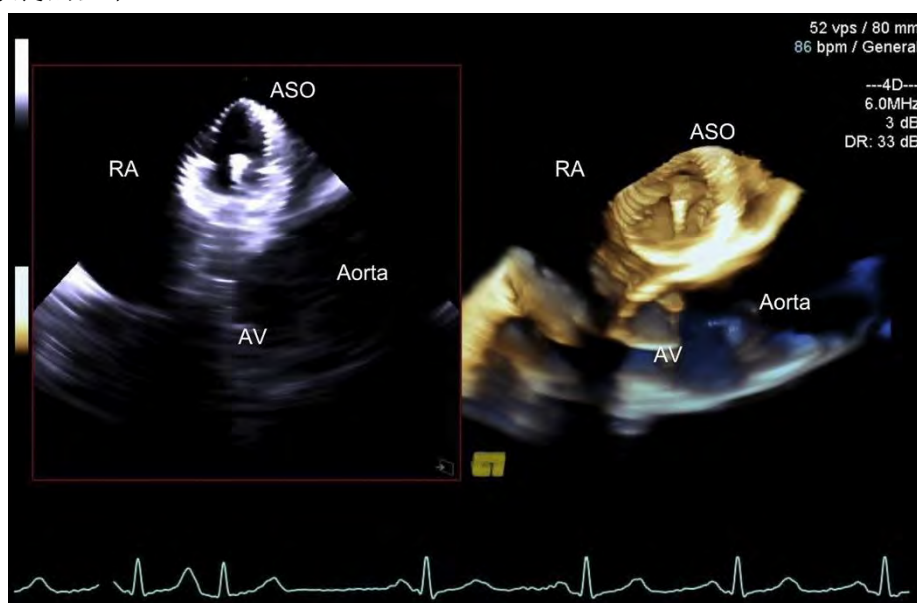


图 55 三维 ICE 示房间隔封堵器与主动脉的关系，二维（左）和三维（右）成像模式。ASO，房间隔封堵器

未来的成像方向包括完善各种成像模式下的 3D 成像技术(TTE、TEE、ICE)，联合应用超声心动图与其他成像方法如心脏电脑断层和透视进行经皮导管术进行术中指导，进一步完善评价和量化心房间分流的方法及进一步明确 PFO 与隐源性中风的生理病理关系。成像可以帮助强化对封堵器成功植入的影响因素以及侵蚀和封堵器栓塞的危险因素的认识。

通知和免责声明

本文由 ASE 和心脏造影与介入协会（Society for Cardiac Angiography and Intervention, SCAI）联合发表，作为成员们的参考来源。本文仅包含建议，不应用作临床操作或任何员工纪律处分的唯一依据。这篇文章中所包含的表述和建议主要基于专家们的观点，而非科学的研究数据。ASE 和 SCAI 对本报告中信息的完整性或准确性不作任何明示或暗示的保证，包括适销性或针对特定用途的适用性的保证。在任何情况下，ASE 或 SCAI 都无须向你、你的病人或任何其他第三方，承担您或其他组织依此文章所作的决定或采取的措施所致的责任。您对此信息的使用也不属于 ASE 或 SCAI 提供的医疗建议，也不会因 ASE 或 SCAI 与您的患者或其他任何人之间建立任何医患关系。

补充数据

本文的补充数据可以一下网址获取：
<http://dx.doi.org/10.1016/j.echo.2015.05.015>.

REFERENCE

1. Sam_ane M. Children with congenital heart disease: probability of natural survival. *Pediatr Cardiol* 1992;13:152-8.
2. Therrien J, Webb G. Clinical update on adults with congenital heart disease. *Lancet* 2003;362:1305-13.
3. Sam_ane M, Vor_iskov_aM. Congenital heart disease among 815,569 children born between 1980 and 1990 and their 15-year survival: a prospective Bohemia survival study. *Pediatr Cardiol* 1999;20:411-7.
4. BricknerME, Hillis LD, Lange RA. Congenital heart disease in adults. First of two parts. *N Engl J Med* 2000;342:256-63.
5. Hagen PT, Scholz DG, Edwards WD. Incidence and size of patent foramen ovale during the first 10 decades of life: an autopsy study of 965 normal hearts. *Mayo Clin Proc* 1984;59:17-20.
6. Pushparajah K, Miller OI, Simpson JM. 3D echocardiography of the atrial septum: anatomical features and landmarks for the echocardiographer. *JACC Cardiovasc Imaging* 2010;3:981-4.
7. Song BG, Park SW, Lee S-C, Choi J-O, Park S-J, Chang S-A, et al. Real-time 3D TEE for multiperforated IAS. *JACC Cardiovasc Imaging* 2010;3:1199.
8. Silvestry FE, Kerber RE, Brook MM, Carroll JD, Eberman KM, Goldstein SA, et al. Echocardiography-guided interventions. *J Am Soc Echocardiogr* 2009;22:213-31; quiz 316-317.
9. Rudski LG, Lai WW, Afilalo J, Hua L, Handschumacher MD, Chandrasekaran K, et al. Guidelines for the echocardiographic assessment of the right heart in adults: a report from the American Society of Echocardiography. *J Am Soc Echocardiogr* 2010;23:685-713; quiz 786-788.
10. Shanewise JS, Cheung AT, Aronson S, Stewart WJ, Weiss RL, Mark JB, et al. ASE/SCA guidelines for performing a comprehensive intraoperative multiplane transesophageal echocardiography examination: recommendations of the American Society of Echocardiography Council for Intraoperative Echocardiography and the Society of Cardiovascular Anesthesiologists Task Force for Certification in Perioperative Transesophageal Echocardiography. *J Am Soc Echocardiogr*

- 1999;12:884-900.
11. Hahn RT, Abraham T, Adams MS, Bruce CJ, Glas KE, Lang RM, et al. Guidelines for performing a comprehensive transesophageal echocardiographic examination: recommendations from the American Society of Echocardiography and the Society of Cardiovascular Anesthesiologists. *J Am Soc Echocardiogr* 2013;26:921-64.
 12. Lang RMR, Badano LPL, Tsang WW, Adams DHD, Agricola EE, Buck TT, et al. EAE/ASE recommendations for image acquisition and display using three-dimensional echocardiography. *J Am Soc Echocardiogr* 2012;25:3-46.
 13. Johri AM, Rojas CA, El-Sherief A, Witzke CF, Chitty DW, Palacios IF, et al. Imaging of atrial septal defects: echocardiography and CT correlation. *Heart* 2011;97:1441-53.
 14. Anderson RH, Brown NA, Webb S. Development and structure of the atrial septum. *Heart* 2002;88:104-10.
 15. Geva T. Anomalies of the atrial septum. In: Lai WW, Mertens L, Cohen MS, Geva T, editors. *Echocardiography in Pediatric and Congenital Heart Disease: From Fetus to Adult*. Hoboken, NJ: Wiley-Blackwell; 2009. pp. 158-74.
 16. Calvert PA, Rana BS, Kydd AC, Shapiro LM. Patent foramen ovale: anatomy, outcomes, and closure. *Nat Rev Cardiol* 2011;8:148-60.
 17. Martins JDF, Anderson RH. The anatomy of interatrial communications—what does the interventionist need to know? *Cardiol Young* 2000;10:464-73.
 18. Patel AR, DAlessandro L, Weinberg PM. Anatomy of the atrial septum. In: Hijazi ZM, Feldman T, Abdullah Al-Qbandi MH, Sievert H, editors. *Transcatheter Closure of ASD and PFO*. 1st ed. Minneapolis: Cardiotext Publishers; 2010. pp. 3-15.
 19. Schneider B, Zienkiewicz T, Jansen V, Hofmann T, Noltenius H, Meinertz T. Diagnosis of patent foramen ovale by transesophageal echocardiography and correlation with autopsy findings. *Am J Cardiol* 1996;77:1202-9.
 20. Rigatelli G, Magro B, Oliva L. Anatomic-functional characterization of IAS for catheter-based interventions. *Am J Cardiovasc Dis* 2011;1:227-35.
 21. Kedia G, Tobis J, Lee MS. Patent foramen ovale: clinical manifestations and treatment. *Rev Cardiovasc Med* 2008;9:168-73.
 22. Krishnan SC, Salazar M. Septal pouch in the left atrium: a new anatomical entity with potential for embolic complications. *JACC Cardiovasc Interv* 2010;3:98-104.
 23. Tugcu A, Okajima K, Jin Z, Rundek T, Homma S, Sacco RL, et al. Septal pouch in the left atrium and risk of ischemic stroke. *JACC Cardiovasc Imaging* 2010;3:1276-83.
 24. Strachinaru M, Morissens M, Latifyan S, Costescu I. Left atrial septal pouch thrombus assessed on three-dimensional transoesophageal echocardiography. *Eur Heart J Cardiovasc Imaging* 2012;13:967.
 25. Wong JM, Lombardo D, Handwerker J, Fisher M. Cryptogenic stroke and the left atrial septal pouch: a case report. *J Stroke Cerebrovasc Dis* 2014;23:564-5.
 26. Strachinaru M, Wauthy P, Sanoussi A, Morissens M, Costescu I, Catez E. The left atrial septal pouch as a possible location for thrombus formation. *J Cardiovasc Med* 2013;14:1-2.
 27. Shimamoto K, Kawagoe T, Dai K, Inoue I. Thrombus in the left atrial septal pouch mimicking myxoma. *J Clin Ultrasound* 2014;42:185-8.
 28. McCarthy K, Ho S, Anderson R. Defining the morphologic phenotypes of atrial septal defects and interatrial communications. *Images Paediatr Cardiol* 2003;5:1-24.
 29. Lock JE, Rome JJ, Davis R, Van Praagh S, Perry SB, Van Praagh R, et al. Transcatheter closure of atrial septal defects: experimental studies. *Circulation* 1989;79:1091-9.
 30. Wilson NJ, Smith J, Prommete B, O'Donnell C, Gentles TL, Ruygrok PN. Transcatheter closure of secundum atrial septal defects with the Amplatzer septal occluder in adults and children—follow-up closure rates, degree of mitral regurgitation and evolution of arrhythmias. *Heart Lung Circ* 2008;17:318-24.
 31. Tobis J, Shenoda M. Percutaneous treatment of patent foramen ovale and atrial septal defects. *J Am Coll Cardiol* 2012;60:1722-32.
 32. Rastogi N, Smeeton NC, Qureshi SA. Factors related to successful transcatheter closure of atrial septal defects using the Amplatzer septal occluder. *Pediatr Cardiol* 2009;30:888-92.
 33. Fu YC, Hijazi ZM. The Amplatzer septal occluder, a transcatheter device for atrial septal defect closure. *Expert Rev Med Devices* 2008;5:25-31.

34. Charuzi Y, Spanos PK, Amplatz K, Edwards JE. Juxtaposition of the atrial appendages. *Circulation* 1973;47:620-7.
35. Kirby ML. Endocardium, cardiac cushions, and valve development. In: *Cardiac Development*. Oxford UK: Oxford University Press; 2007. pp. 119-31.
36. Raghbi G, Ruttenberg HD, Anderson RC, Amplatz K, Adams P, Edwards JE. Termination of left superior vena cava in left atrium, atrial septal defect, and absence of coronary sinus: a developmental complex. *Circulation* 1965;31:906-18.
37. Sun T, Fei H-W, Huang H-L, Chen O-D, Zheng Z-C, Zhang C-J, et al. Transesophageal echocardiography for coronary sinus imaging in partially unroofed coronary sinus. *Echocardiography* 2014;31:74-82.
38. Geggel RL, Perry SB, Blume ED, Baker CM. Left superior vena cava connection to unroofed coronary sinus associated with positional cyanosis: successful transcatheter treatment using Gianturco-Grifkavascular occlusion device. *Catheter Cardiovasc Interv* 1999;48:369-73.
39. Santoro G, Gaio G, Russo MG. Transcatheter treatment of unroofed coronary sinus. *Catheter Cardiovasc Interv* 2013;81:849-52.
40. Ferdman DJ, Brady D, Rosenzweig EB. Common atrium and pulmonary vascular disease. *Pediatr Cardiol* 2011;32:595-8.
41. Gorani DR, Kamberi LS, Gorani NS. Common atrium associated with polydactyly and dwarfism in middle age male patient. *Med Arh* 2011;65:170-2.
42. Jiang H, Wang H, Wang Z, Zhu H, Zhang R. Surgical correction of common atrium without noncardiac congenital anomalies. *J Card Surg* 2013;28:580-6.
43. Agmon Y, Khandheria BK, Meissner I, Gentile F, Whisnant JP, Sicks JD, et al. Frequency of atrial septal aneurysms in patients with cerebral ischemic events. *Circulation* 1999;99:1942-4.
44. Giannopoulos A, Gavras C, Sarioglou S, Agathagelou F, Kassapoglou I, Athanassiadou F. Atrial septal aneurysms in childhood: prevalence, classification, and concurrent abnormalities. *Cardiol Young* 2014;24:453-8.
45. Scaffa R, Spaziani C, Leporace M, Leonetti S, Di Roma M, Gasparone A, et al. Voluminous atrial septal aneurysm may mask a large double atrial septal defect. *Ann Thorac Surg* 2012;93:e41.
46. Krumsdorf U, Keppeler P, Horvath K, Zadan E, Schrader R, Sievert H. Catheter closure of atrial septal defects and patent foramen ovale in patients with an atrial septal aneurysm using different devices. *J Interv Cardiol* 2001;14:49-55.
47. Schuchlenz HW, Saurer G, Weihs W, Rehak P. Persisting eustachian valve in adults: relation to patent foramen ovale and cerebrovascular events. *J Am Soc Echocardiogr* 2004;17:231-3.
48. Schneider B, Hofmann T, Justen MH, Meinertz T. Chiari's network: normal anatomic variant or risk factor for arterial embolic events. *J Am Coll Cardiol* 1995;26:203-10.
49. Lu J-H, Hsu T-L, Hwang B, Weng Z-C. Visualization of secundum atrial septal defect using transthoracic three-dimensional echocardiography in children: implications for transcatheter closure. *Echocardiography* 1998;15:651-60.
50. Attaran RR, Ata I, Kudithipudi V, Foster L, Sorrell VL. Protocol for optimal detection and exclusion of a patent foramen ovale using transthoracic echocardiography with agitated saline microbubbles. *Echocardiography* 2006;23:616-22.
51. Lange A, Walayat M, Turnbull CM, Palka P, Mankad P, Sutherland GR, et al. Assessment of atrial septal defect morphology by transthoracic three-dimensional echocardiography using standard grey scale and Doppler myocardial imaging techniques: comparison with magnetic resonance imaging and intraoperative findings. *Heart* 1997;78:382-9.
52. Konstantinides S, Kasper W, Geibel A, Hofmann T, Koster W, Just H. Detection of left-to-right shunt in atrial septal defect by negative contrast echocardiography: a comparison of transthoracic and transesophageal approach. *Am Heart J* 1993;126:909-17.
53. Monte I, Grasso S, Licciardi S, Badano LP. Head-to-head comparison of real-time three-dimensional transthoracic echocardiography with transthoracic and transesophageal two-dimensional contrast echocardiography for the detection of patent foramen ovale. *Eur J Echocardiogr* 2010;11:245-9.
54. Daniels C, Weytjens C, Cosyns B, Schoors D, De Sutter J, Paelinck B, et al. Second harmonic transthoracic echocardiography: the new reference screening method for the detection of patent foramen ovale. *Eur J Echocardiogr* 2004;5:449-52.

55. Mesihovi_c-Dinarevi_c S, Begi_c Z, Halimi_c M, Kadi_c A, Gojak R. The reliability of transthoracic and transesophageal echocardiography in predicting the size of atrial septal defect. *Acta Med Acad* 2012;41:145-53.
56. Mehta RH, Helmcke F, Nanda NC, Pinheiro L, Samdarshi TE, Shah VK. Uses and limitations of transthoracic echocardiography in the assessment of atrial septal defect in the adult. *Am J Cardiol* 1991;67:288-94.
57. Oto A, Aytemir K, Ozkutlu S, Kaya EB, Yorgun H, Canpolat U, et al. Transthoracic echocardiography guidance during percutaneous closure of patent foramen ovale. *Echocardiography* 2011;28:1074-80.
58. Siostrzonek P, Zangeneh M, Gossinger H, Lang W, Rosenmayr G, Heinz G, et al. Comparison of transesophageal and transthoracic contrast echocardiography for detection of a patent foramen ovale. *Am J Cardiol* 1991;68:1247-9.
59. Kronzon I, Tunick PA, Freedberg RS, Trehan N, Rosenzweig BP, Schwinger ME. Transesophageal echocardiography is superior to transthoracic echocardiography in the diagnosis of sinus venosus atrial septal defect. *J Am Coll Cardiol* 1991;17:537-42.
60. Zhu W, Cao QL, Rhodes J, Hijazi ZM. Measurement of atrial septal defect size: a comparative study between three-dimensional transesophageal echocardiography and the standard balloon sizing methods. *Pediatr Cardiol* 2000;21:465-9.
61. Belohlavek M, Foley DA, Gerber TC, Greenleaf JF, Seward JB. Three-dimensional ultrasound imaging of the atrial septum: normal and pathologic anatomy. *J Am Coll Cardiol* 1993;22:1673-8.
62. Zaqout M, Suys B, De Wilde H, De Wolf D. Transthoracic echocardiography guidance of transcatheter atrial septal defect closure in children. *Pediatr Cardiol* 2009;30:992-4.
63. Yared K, Baggish AL, Solis J, Durst R, Passeri JJ, Palacios IF, et al. Echocardiographic assessment of percutaneous patent foramen ovale and atrial septal defect closure complications. *Circ Cardiovasc Imaging* 2009;2:141-9.
64. Bhan A, Kapetanakis S, Pearson P, Dworakowski R, Monaghan MJ. Percutaneous closure of an atrial septal defect guided by live three-dimensional transesophageal echocardiography. *J Am Soc Echocardiogr* 2009;22:753.e1-3.
65. Bartel T, Müller S. Device closure of interatrial communications: periinterventional echocardiographic assessment. *Eur Heart J Cardiovasc Imaging* 2013;14:618-24.
66. Taniguchi M, Akagi T, Watanabe N, Okamoto Y, Nakagawa K, Kijima Y, et al. Application of real-time three-dimensional transesophageal echocardiography using a matrix array probe for transcatheter closure of atrial septal defect. *J Am Soc Echocardiogr* 2009;22:1114-20.
67. Belkin RN, Pollack BD, Ruggiero ML, Alas LL, Tatini U. Comparison of transesophageal and transthoracic echocardiography with contrast and color flow Doppler in the detection of patent foramen ovale. *Am Heart J* 1994;128:520-5.
68. Topcuoglu MA, Palacios IF, Buonanno FS. Contrast M-mode power Doppler ultrasound in the detection of right-to-left shunts: utility of submandibular internal carotid artery recording. *J Neuroimaging* 2003;13:315-23.
69. Corrado G, Massironi L, Torta D, Rigo F, Beretta S, Sansalone D, et al. Contrast transthoracic echocardiography versus transcranial Doppler for patent foramen ovale detection. *Int J Cardiol* 2011;150:235-7.
70. Woods TD, Patel A. A critical review of patent foramen ovale detection using saline contrast echocardiography: when bubbles lie. *J Am Soc Echocardiogr* 2006;19:215-22.
71. Thanigaraj S, Valika A, Zajarias A, Lasala JM, Perez JE. Comparison of transthoracic versus transesophageal echocardiography for detection of right-to-left atrial shunting using agitated saline contrast. *Am J Cardiol* 2005;96:1007-10.
72. Draganski B, Bliersch W, Holmer S, Koch H, May A, Bogdahn U, et al. Detection of cardiac right-to-left shunts by contrast-enhanced harmonic carotid duplex sonography. *J Ultrasound Med* 2005;24:1071-6.
73. Rosenzweig BP, Nayar AC, Varkey MP, Kronzon I. Echo contrast enhanced diagnosis of atrial septal defect. *J Am Soc Echocardiogr* 2001;14:155-7.
74. Soliman OI, Geleijnse ML, Meijboom FJ, Nemes A, Kamp O, Nihoyannopoulos P, et al. The use of contrast echocardiography for the detection of cardiac shunts. *Eur J Echocardiogr* 2007;8:S2-12.

75. Vigna C, Marchese N, Zanchetta M, Chessa M, Inchingolo V, Pacilli MA, et al. Echocardiographic guidance of percutaneous patent foramen ovale closure: head-to-head comparison of transesophageal versus rotational intracardiac echocardiography. *Echocardiography* 2012;29:1103-10.
76. Abdel-Massih T, Dulac Y, Taktak A, Aggoun Y, Massabuau P, Elbaz M, et al. Assessment of atrial septal defect size with 3D-transesophageal echocardiography: comparison with balloon method. *Echocardiography* 2005;22:121-7.
77. Seo J-S, Song J-M, Kim Y-H, Park D-W, Lee S-W, Kim W-J, et al. Effect of atrial septal defect shape evaluated using three-dimensional transesophageal echocardiography on size measurements for percutaneous closure. *J Am Soc Echocardiogr* 2012;25:1031-40.
78. Roberson DA, Cui W, Patel D, Tsang W, Sugeng L, Weinert L, et al. Three-dimensional transesophageal echocardiography of atrial septal defect: a qualitative and quantitative anatomic study. *J Am Soc Echocardiogr* 2011;24:600-10.
79. Magni G, Hijazi ZM, Pandian NG, Delabays A, Sugeng L, Laskari C, et al. Two- and three-dimensional transesophageal echocardiography in patient selection and assessment of atrial septal defect closure by the new DAS-Angel Wings device: initial clinical experience. *Circulation* 1997;96:1722-8.
80. Vaidyanathan B, Simpson JM, Kumar RK. Transesophageal echocardiography for device closure of atrial septal defects: case selection, planning, and procedural guidance. *JACC Cardiovasc Imaging* 2009;2:1238-42.
81. Price MJ, Smith MR, Rubenson DS. Utility of on-line three-dimensional transesophageal echocardiography during percutaneous atrial septal defect closure. *Catheter Cardiovasc Interv* 2010;75:570-7.
82. Tanaka J, Izumo M, Fukuoka Y, Saitoh T, Harada K, Harada K, et al. Comparison of two-dimensional versus real-time three-dimensional transesophageal echocardiography for evaluation of patent foramen ovale morphology. *Am J Cardiol* 2013;111:1052-6.
83. Kim SS, Hijazi ZM, Lang RM, Knight BP. The use of intracardiac echocardiography and other intracardiac imaging tools to guide noncoronary cardiac interventions. *J Am Coll Cardiol* 2009;53:2117-28.
84. Zanchetta M, Onorato E, Rigatelli G, Pedon L, Zennaro M, Carrozza A, et al. Intracardiac echocardiography-guided transcatheter closure of secundum atrial septal defect: a new efficient device selection method. *J Am Coll Cardiol* 2003;42:1677-82.
85. Luxenberg DM, Silvestry FE, Herrmann HC, Cao Q-L, Rohatgi S, Hijazi ZM. Use of a new 8 French intracardiac echocardiographic catheter to guide device closure of atrial septal defects and patent foramen ovale in small children and adults: initial clinical experience. *J Invasive Cardiol* 2005;17:540-5.
86. Boccalandro F, Baptista E, Muench A, Carter C, Smalling RW. Comparison of intracardiac echocardiography versus transesophageal echocardiography guidance for percutaneous transcatheter closure of atrial septal defect. *Am J Cardiol* 2004;93:437-40.
87. Rigatelli G, Dell'Avvocata F, Cardaioli P, Giordan M, Dung HT, Nghia NT, et al. Safety and long-term outcome of modified intracardiac echocardiography-assisted „no-balloon“ sizing technique for transcatheter closure of ostium secundum atrial septal defect. *J Interv Cardiol* 2012;25:628-34.
88. Rigatelli G, Dell'Avvocata F, Cardaioli P, Giordan M, Vassiliev D, Nghia NT, et al. Five-year follow-up of intracardiac echocardiography-assisted transcatheter closure of complex ostium secundum atrial septal defect. *Congenit Heart Dis* 2012;7:103-10.
89. Koenig PR, Abdulla R-I, Cao Q-L, Hijazi ZM. Use of intracardiac echocardiography to guide catheter closure of atrial communications. *Echocardiography* 2003;20:781-7.
90. Rao PS. Why, when and how should atrial septal defects be closed in adults. In: Rao PS, editor. *Atrial Septal Defects*; 2012;. pp. 121-38.
91. Awad SM, Cao Q-L, Hijazi ZM. Intracardiac echocardiography for the guidance of percutaneous procedures. *Curr Cardiol Rep* 2009;11:210-5.
92. Kim NK, Park S-J, Shin JI, Choi JY. Eight-French intracardiac echocardiography—safe and effective guidance for transcatheter closure in atrial septal defects. *Circ J* 2012;76:2119-23.

93. Mallula K, Amin Z. Recent changes in instructions for use for the Amplatzer atrial septal defect occluder: how to incorporate these changes while using transesophageal echocardiography or intracardiac echocardiography. *Pediatr Cardiol* 2012;33:995-1000.
94. Stapf D, Franke A, Schreckenber M, Schummers G, Mischke K, Marx N, et al. Beat to beat 3-dimensional intracardiac echocardiography: theoretical approach and practical experiences. *Int J Cardiovasc Imaging* 2013; 29:753-64.
95. Kadakia MB, Silvestry FE, Herrmann HC. Intracardiac echocardiography-guided transcatheter aortic valve replacement. *Catheter Cardiovasc Interv* 2015;85:497-501.
96. Lee W, Griffin W, Wildes D, Buckley D, Topka T, Chodakauskas T, et al. A 10-Fr ultrasound catheter with integrated micromotor for 4-D intracardiac echocardiography. *IEEE Trans Ultrason Ferroelectr Freq Control* 2011;58:1478-91.
97. Silvestry FE, Kadakia MB, Willhide J, Herrmann HC. Initial experience with a novel real-time three-dimensional intracardiac ultrasound system to guide percutaneous cardiac structural interventions: a phase I feasibility study of volume intracardiac echocardiography in the assessment of patients with structural heart disease undergoing percutaneous transcatheter therapy. *J Am Soc Echocardiogr* 2014;27:978-83.
98. Faletta F, Scarpini S, Moreo A, Ciliberto GR, Austoni P, Donatelli F, et al. Color Doppler echocardiographic assessment of atrial septal defect size: correlation with surgical measurements. *J Am Soc Echocardiogr* 1991;4: 429-34.
99. Kitabatake A, Inoue M, Asao M, Ito H, Masuyama T, Tanouchi J, et al. Noninvasive evaluation of the ratio of pulmonary to systemic flow in atrial septal defect by duplex Doppler echocardiography. *Circulation* 1984;69:73-9.
100. Rufino Nascimento LG, Dehant P, Jimenez M, Dequeker JL, Castela E, Choussat A. Calculation of the pulmonary to systemic flow ratio using echo-Doppler in septal defects—correlation with oximetry. *Rev Port Cardiol* 1989;8:35-40.
101. Lin YF, Awa S, Hishi T, Akagi M, Dodo H, Ishii T, et al. Two-dimensional pulsed Doppler echocardiographic technique for estimating pulmonary to systemic blood flow ratio in children with atrial septal defect and patent ductus arteriosus. *Acta Paediatr Jpn* 1989;31:314-22.
102. Joyner CR. In: *Ultrasound in the Diagnosis of Cardiovascular Pulmonary Disease*. Chicago: Year Book Medical Publishers; 1974.
103. Gramiak R, Shah PM, Kramer DH. Ultrasound cardiography: contrast studies in anatomy and function. *Radiology* 1969;92:939-48.
104. Fraker TD, Harris PJ, Behar VS, Kisslo JA. Detection and exclusion of interatrial shunts by two-dimensional echocardiography and peripheral venous injection. *Circulation* 1979;59:379-84.
105. Di Tullio M, Sacco RL, Venketasubramanian N, Sherman D, Mohr JP, Homma S. Comparison of diagnostic techniques for the detection of a patent foramen ovale in stroke patients. *Stroke* 1993;24:1020-4.
106. Johansson MC, Helgason H, Dellborg M, Eriksson P. Sensitivity for detection of patent foramen ovale increased with increasing number of contrast injections: a descriptive study with contrast transesophageal echocardiography. *J Am Soc Echocardiogr* 2008;21:419-24.
107. Marriott K, Manins V, Forshaw A, Wright J, Pascoe R. Detection of right-to-left atrial communication using agitated saline contrast imaging: experience with 1162 patients and recommendations for echocardiography. *J Am Soc Echocardiogr* 2013;26:96-102.
108. Fan S, Nagai T, Luo H, Atar S, Naqvi T, Birnbaum Y, et al. Superiority of the combination of blood and agitated saline for routine contrast enhancement. *J Am Soc Echocardiogr* 1999;12:94-8.
109. Johansson MC, Eriksson P, Guron CW, Dellborg M. Pitfalls in diagnosing PFO: characteristics of false-negative contrast injections during transesophageal echocardiography in patients with patent foramen ovals. *J Am Soc Echocardiogr* 2010;23:1136-42.
110. Rahmouni HW, Keane MG, Silvestry FE, St John Sutton MG, Ferrari VA, Scott CH, et al. Failure of digital echocardiography to accurately diagnose intracardiac shunts. *Am Heart J* 2008;155:161-5.
111. Spencer MP, Moehring MA, Jesurum J, Gray WA, Olsen JV, Reisman M. Power M-mode transcranial Doppler for diagnosis of patent foramen ovale and assessing transcatheter closure. *J Neuroimaging* 2004;14: 342-9.

112. Lao AY, Sharma VK, Tsvigoulis G, Frey JL, Malkoff MD, Navarro JC, et al. Detection of right-to-left shunts: comparison between the international consensus and Spencer logarithmic scale criteria. *J Neuroimaging* 2008;18:402-6.
113. Caputi L, Carriero MR, Falcone C, Parati E, Piotti P, Materazzo C, et al. Transcranial Doppler and transesophageal echocardiography: comparison of both techniques and prospective clinical relevance of transcranial Doppler in patent foramen ovale detection. *J Stroke Cerebrovasc Dis* 2009;18:343-8.
114. Siostrzonek P, Lang W, Zangeneh M, Gossinger H, Stumpflen A, Rosenmayr G, et al. Significance of left-sided heart disease for the detection of patent foramen ovale by transesophageal contrast echocardiography. *J Am Coll Cardiol* 1992;19:1192-6.
115. Lang RM, Badano LP, Mor-Avi V, Afilalo J, Armstrong A, Ernande L, et al. Recommendations for cardiac chamber quantification by echocardiography in adults: an update from the American Society of Echocardiography and the European Association of Cardiovascular Imaging. *J Am Soc Echocardiogr* 2015;28:1 e14-3914.
116. Alghamdi MH, Grosse-Wortmann L, Ahmad N, Mertens L, Friedberg MK. Can simple echocardiographic measures reduce the number of cardiac magnetic resonance imaging studies to diagnose right ventricular enlargement in congenital heart disease? *J Am Soc Echocardiogr* 2012;25:518-23.
117. Brown DW, McElhinney DB, Araoz PA, Zahn EM, Vincent JA, Cheatham JP, et al. Reliability and accuracy of echocardiographic right heart evaluation in the U.S. Melody valve investigational trial. *J Am Soc Echocardiogr* 2012;25:383-4.
118. Gopal AS, Chukwu EO, Iwuchukwu CJ, Katz AS, Toole RS, Schapiro W, et al. Normal values of right ventricular size and function by real-time 3-dimensional echocardiography: comparison with cardiac magnetic resonance imaging. *J Am Soc Echocardiogr* 2007;20:445-55.
119. Lu X, Nadvoretzkiy V, Bu L, Stolpen A, Ayres N, Pignatelli RH, et al. Accuracy and reproducibility of real-time three-dimensional echocardiography for assessment of right ventricular volumes and ejection fraction in children. *J Am Soc Echocardiogr* 2008;21:84-9.
120. Jenkins C, Chan J, Bricknell K, Strudwick M, Marwick TH. Reproducibility of right ventricular volumes and ejection fraction using real-time three-dimensional echocardiography: comparison with cardiac MRI. *Chest* 2007;131:1844-51.
121. Tamborini G, Marsan NA, Gripari P, Maffessanti F, Brusoni D, Muratori M, et al. Reference values for right ventricular volumes and ejection fraction with real-time three-dimensional echocardiography: evaluation in a large series of normal subjects. *J Am Soc Echocardiogr* 2010;23:109-15.
122. Ryan T, Petrovic O, Dillon JC, Feigenbaum H, Conley MJ, Armstrong WF. An echocardiographic index for separation of right ventricular volume and pressure overload. *J Am Coll Cardiol* 1985;5:918-27.
123. Steele PM, Fuster V, Cohen M, Ritter DG, McGoon DC. Isolated atrial septal defect with pulmonary vascular obstructive disease—long-term follow-up and prediction of outcome after surgical correction. *Circulation* 1987;76:1037-42.
124. Vogel M, Berger F, Kramer A, Alexi-Meskishvili V, Lange PE. Incidence of secondary pulmonary hypertension in adults with atrial septal or sinus venosus defects. *Heart* 1999;82:30-3.
125. Abbas AE, Fortuin FD, Schiller NB, Appleton CP, Moreno CA, Lester SJ. A simple method for noninvasive estimation of pulmonary vascular resistance. *J Am Coll Cardiol* 2003;41:1021-7.
126. Masuyama T, Kodama K, Kitabatake A, Sato H, Nanto S, Inoue M. Continuous-wave Doppler echocardiographic detection of pulmonary regurgitation and its application to noninvasive estimation of pulmonary artery pressure. *Circulation* 1986;74:484-92.
127. Schubert S, Peters B, Abdul-Khaliq H, Nagdyman N, Lange PE, Ewert P. Left ventricular conditioning in the elderly patient to prevent congestive heart failure after transcatheter closure of atrial septal defect. *Catheter Cardiovasc Interv* 2005;64:333-7.
128. Gruner C, Akkaya E, Kretschmar O, Roffi M, Corti R, Jenni R, et al. Pharmacologic preconditioning therapy prior to atrial septal defect closure in patients at high risk for acute pulmonary edema. *J Interv Cardiol* 2012;25:505-12.

129. Masutani S, Senzaki H. Left ventricular function in adult patients with atrial septal defect: implication for development of heart failure after transcatheter closure. *J Card Fail* 2011;17:957-63.
130. Homma S, Sacco RL. Patent foramen ovale and stroke. *Circulation* 2005;112:1063-72.
131. Calvet D, Mas J-L. Closure of patent foramen ovale in cryptogenic stroke: a never ending story. *Curr Opin Neurol* 2014;27:13-9.
132. Dao CN, Tobis JM. PFO and paradoxical embolism producing events other than stroke. *Catheter Cardiovasc Interv* 2011;77:903-9.
133. Blanche C, Noble S, Roffi M, Testuz A, Müller H, Meyer P, et al. Platypnea-orthodoxia syndrome in the elderly treated by percutaneous patent foramen ovale closure: a case series and literature review. *Eur J Intern Med* 2013;24:813-7.
134. Tobis J. Management of patients with refractory migraine and PFO: Is MIST I relevant? *Catheter Cardiovasc Interv* 2008;72:60-4.
135. Ailani J. Migraine and patent foramen ovale. *Curr Neurol Neurosci Rep* 2014;14:426.
136. Azarbal B, Tobis J, Suh W, Chan V, Dao C, Gaster R. Association of interatrial shunts and migraine headaches: impact of transcatheter closure. *J Am Coll Cardiol* 2005;45:489-92.
137. Volman M, Mojadidi MK, Gevorgyan R, Kaing A, Agrawal H, Tobis J. Incidence of patent foramen ovale and migraine headache in adults with congenital heart disease with no known cardiac shunts. *Catheter Cardiovasc Interv* 2013;81:643-7.
138. Khessali H, Mojadidi MK, Gevorgyan R, Levinson R, Tobis J. The effect of patent foramen ovale closure on visual aura without headache or typical aura with migraine headache. *JACC Cardiovasc Interv* 2012;5:682-7.
139. Rana BS, Shapiro LM, McCarthy KP, Ho SY. Three-dimensional imaging of the atrial septum and patent foramen ovale anatomy: defining the morphological phenotypes of patent foramen ovale. *Eur J Echocardiogr* 2010;11:i19-25.
140. Rigatelli G, Dell'Avvocata F, Daggubati R, Dung HT, Nghia NT, Nanjiundappa A, et al. Impact of interatrial septum anatomic features on short- and long-term outcomes after transcatheter closure of patent foramen ovale: single device type versus anatomic-driven device selection strategy. *J Interv Cardiol* 2013;26:392-8.
141. Olivares-Reyes A, Chan S, Lazar EJ, Bandlamudi K, Narla V, Ong K. Atrial septal aneurysm: a new classification in two hundred five adults. *J Am Soc Echocardiogr* 1997;10:644-56.
142. Cooke JC, Gelman JS, Harper RW. Chiari network entanglement and herniation into the left atrium by an atrial septal defect occluder device. *J Am Soc Echocardiogr* 1999;12:601-3.
143. Hausmann D, Daniel WG, Mügge A, Ziemer G, Pearlman AS. Value of transesophageal color Doppler echocardiography for detection of different types of atrial septal defect in adults. *J Am Soc Echocardiogr* 1992;5:481-8.
144. Chen FL, Hsiung MC, Hsieh KS, Li YC, Chou MC. Real time three-dimensional transthoracic echocardiography for guiding Amplatzer septal occluder device deployment in patients with atrial septal defect. *Echocardiography* 2006;23:763-70.
145. Mazic U, Gavora P, Masura J. The role of transesophageal echocardiography in transcatheter closure of secundum atrial septal defects by the Amplatzer septal occluder. *Am Heart J* 2001;142:482-8.
146. Ali S, George LK, Das P, Koshy SKG. Intracardiac echocardiography: clinical utility and application. *Echocardiography* 2011;28:582-90.
147. Warnes CA, Williams RG, Bashore TM, Child JS, Connolly HM, Dearani JA, et al. ACC/AHA 2008 Guidelines for the Management of Adults with Congenital Heart Disease: Executive Summary: a report of the American College of Cardiology/American Heart Association Task Force on Practice Guidelines (writing committee to develop guidelines for the management of adults with congenital heart disease). *Circulation* 2008;118:e714-833.
148. Chessa M, Carminati M, Butera G, Bini RM, Drago M, Rosti L, et al. Early and late complications associated with transcatheter occlusion of secundum atrial septal defect. *J Am Coll Cardiol* 2002;39:1061-5.
149. Abaci A, Unlu S, Alsancak Y, Kaya U, Sezenoz B. Short and long term complications of device closure of atrial septal defect and patent foramen ovale: meta-analysis of 28,142 patients from 203 studies. *Catheter Cardiovasc*

Interv 2013;82:1123-38.

150. Amin Z, Hijazi ZM, Bass JL, Cheatham JP, Hellenbrand WE, Kleinman CS. Erosion of Amplatzer septal occluder device after closure of secundum atrial septal defects: review of registry of complications and recommendations to minimize future risk. *Catheter Cardiovasc Interv* 2004;63:496-502.
151. Ivens E, Hamilton-Craig C, Aroney C. Early and late cardiac perforation by Amplatzer atrial septal defect and patent foramen ovale devices. *J Am Soc Echocardiogr* 2009;22:1067-70.
152. El-Said HG, Moore JW. Erosion by the Amplatzer septal occluder: experienced operator opinions at odds with manufacturer recommendations? *Catheter Cardiovasc Interv* 2009;73:925-30.
153. Diab K, Kenny D, Hijazi ZM. Erosions, erosions, and erosions! Device closure of atrial septal defects: how safe is safe? *Catheter Cardiovasc Interv* 2012;80:168-74.
154. Amin Z. Echocardiographic predictors of cardiac erosion after Amplatzer septal occluder placement. *Catheter Cardiovasc Interv* 2014;83:84-92.
155. Taggart NW, Dearani JA, Hagler DJ. Late erosion of an Amplatzer septal occluder device 6 years after placement. *J Thorac Cardiovasc Surg* 2011;142:221-2.
156. Ilkhanoff L, Naidu SS, Rohatgi S, Ross MJ, Silvestry FE, Herrmann HC. Transcatheter device closure of interatrial septal defects in patients with hypoxia. *J Interv Cardiol* 2005;18:227-32.
157. Al-Anani SJ, Weber H, Hijazi ZM. Atrioventricular block after transcatheter ASD closure using the Amplatzer septal occluder: risk factors and recommendations. *Catheter Cardiovasc Interv* 2010;75:767-72.
158. Hill SL, Berul CI, Patel HT, Rhodes J, Supran SE, Cao QL, et al. Early ECG abnormalities associated with transcatheter closure of atrial septal defects using the Amplatzer septal occluder. *J Interv Card Electrophysiol* 2000;4:469-74.
159. Veldtman GR, Razack V, Siu S, El-Hajj H, Walker F, Webb GD, et al. Right ventricular form and function after percutaneous atrial septal defect device closure. *J Am Coll Cardiol* 2001;37:2108-13.

Guidelines for the Echocardiographic Assessment of Atrial Septal Defect and Patent Foramen Ovale: From the American Society of Echocardiography and Society for Cardiac Angiography and Interventions

Frank E. Silvestry, MD, FASE, Chair, Meryl S. Cohen, MD, FASE, Co-Chair, Laurie B. Armsby, MD, FSCAI, Nitin J. Burkule, MD, DM, FASE, Craig E. Fleishman, MD, FASE, Ziyad M. Hijazi, MD, MPH, MSCAI, Roberto M. Lang, MD, FASE, Jonathan J. Rome, MD, and Yan Wang, RDSCS, *Philadelphia, Pennsylvania; Portland, Oregon; Thane, India; Orlando, Florida; Doha, Qatar; and Chicago, Illinois*

(J Am Soc Echocardiogr 2015;28:910-58.)

TABLE OF CONTENTS

| | | | |
|--|-----|---|-----|
| Target Audience | 911 | Left Anterior Oblique TTE View | 924 |
| Objectives | 911 | Apical Four-Chamber TTE View | 924 |
| Introduction | 911 | Modified Apical Four-Chamber TTE View (Half Way in Between Apical Four-Chamber and Parasternal Short-Axis View) | 924 |
| Development and Anatomy of the Atrial Septum | 912 | Parasternal Short-Axis TTE View | 924 |
| Normal Anatomy | 912 | High Right Parasternal View | 924 |
| Anatomy of Atrial Septal Defects and Associated Atrial Septal Abnormalities | 912 | Transesophageal Echocardiography Imaging Protocol for the Interatrial Septum | 925 |
| Patent Foramen Ovale | 912 | Upper Esophageal Short-Axis View | 925 |
| Ostium Secundum Atrial Septal Defect | 913 | Midesophageal Aortic Valve Short-Axis View | 926 |
| Ostium Primum Atrial Septal Defect | 915 | Midesophageal Four-Chamber View | 926 |
| Sinus Venosus Defects | 915 | Midesophageal Bicaval View | 926 |
| Coronary Sinus Defects | 916 | Mid-Esophageal Long-Axis View | 926 |
| Common Atrium | 916 | 3D TEE Acquisition Protocol for PFO and ASD | 927 |
| Atrial Septal Aneurysm | 916 | 3D TTE Acquisition Protocol for PFO and ASD | 927 |
| Eustachian Valve and Chiari Network | 916 | 3D Display | 927 |
| Imaging of the Interatrial Septum | 917 | Intracardiac Echocardiographic Imaging Protocol for IAS | 928 |
| General Imaging Approach | 917 | Assessment of Shunting | 928 |
| Three-Dimensional Imaging of the Interatrial Septum | 917 | Techniques, Standards, and Characterization Visualization of Shunting: TTE and TEE | 928 |
| Role of Echocardiography in Percutaneous Transcatheter Device Closure | 917 | Transcranial Doppler Detection/Grading of Shunting | 931 |
| Transthoracic Echocardiography Imaging Protocol for Imaging the Interatrial Septum | 924 | Impact of Shunting on the Right Ventricle | 932 |
| Subxiphoid Frontal (Four-Chamber) TTE View | 924 | Pulmonary Artery Hypertension | 935 |
| Subxiphoid Sagittal TTE View | 924 | RV Function | 935 |

From the Hospital of the University of Pennsylvania, Perelman School of Medicine, Philadelphia, Pennsylvania (F.E.S.); Children's Hospital of Philadelphia, Perelman School of Medicine, Philadelphia, Pennsylvania (M.S.C., J.J.R., Y.W.); Doernbecher Children's Hospital, Oregon Health and Sciences University, Portland, Oregon (L.B.A.); Jupiter Hospital, Thane, India (N.J.B.); Arnold Palmer Hospital for Children, University of Central Florida College of Medicine, Orlando, Florida (C.E.F.); Sidra Medical and Research Center, Doha, Qatar (Z.M.H.); and University of Chicago Hospital, University of Chicago School of Medicine, Chicago, Illinois (R.M.L.).

The following authors reported no actual or potential conflicts of interest in relation to this document: Frank E. Silvestry, MD, FASE Chair, Meryl S. Cohen, MD, FASE Co-Chair, Laurie B. Armsby, MD, FSCAI, Nitin J. Burkule, MD, DM, FASE, Jonathan J. Rome, MD, and Yan Wang, RDSCS. The following authors reported relationships with one or more commercial interests: Craig E. Fleishman, MD, FASE, has served as a consultant for W.L. Gore Medical; Ziyad M. Hijazi MD, MPH, MSCAI has served as a consultant for Occlutech; Roberto M. Lang, MD, FASE, has

received grant support and served on the speakers bureau and advisory board for Philips.

Attention ASE Members:

The ASE has gone green! Visit www.aseuniversity.org to earn free continuing medical education credit through an online activity related to this article. Certificates are available for immediate access upon successful completion of the activity. Nonmembers will need to join the ASE to access this great member benefit!

Reprint requests: American Society of Echocardiography, 2100 Gateway Centre Boulevard, Suite 310, Morrisville, NC 27560 (E-mail: ase@asecho.org).

0894-7317/\$36.00

Copyright 2015 by the American Society of Echocardiography.

<http://dx.doi.org/10.1016/j.echo.2015.05.015>

| Abbreviations |
|---|
| 2D = Two-dimensional |
| 3D = Three-dimensional |
| AoV = Aortic valve |
| ASA = Atrial septal aneurysm |
| ASD = Atrial septal defect |
| ASO = Amplatzer septal occluder |
| AV = Atrioventricular |
| CS = Coronary sinus |
| EV = Eustachian valve |
| DTI = Doppler tissue imaging |
| FDA = Food and Drug Administration |
| IAS = Interatrial septum/ septal |
| ICE = Intracardiac echocardiography |
| IVC = Inferior vena cava |
| LA = Left atrium/atrial |
| LV = Left ventricle/ventricular |
| PA = Pulmonary artery |
| PFO = Patent foramen ovale |
| Qp/Qs ratio = Pulmonary to systemic blood flow ratio |
| RA = Right atrium/atrial |
| RT3DE = Real-time three-dimensional echocardiography |
| RUPV = Right upper pulmonary vein |
| RV = Right ventricle/ventricular |
| SCAI = Society for Cardiac Angiography and Intervention |
| SVC = Superior vena cava |
| SVD = Sinus venosus defect |
| TCD = Transcranial Doppler |
| TEE = Transesophageal echocardiography/echocardiographic |
| TTE = Transthoracic echocardiography/echocardiographic |
| VTI = Velocity time integral |

LV Function 935
Imaging of IAS and Septal Defects 935
Patent Foramen Ovale 935
Atrial Septal Aneurysm 938
Eustachian Valve and Chiari Network 938
Assessment of ASDs: Standards and Characterization 939
Role of Echocardiography in Transcatheter Device Closure 941
Description of Available Transcatheter Devices and Techniques 942
Device Embolization and Erosion 944
Imaging Modalities in Transcatheter Guidance: TTE, TEE, ICE 947
Intraprocedural Guidance of Transcatheter Interventions 949
ICE Guidance of PTC 950
Imaging the IAS Immediately After the Procedure 951
Follow-Up 953
Conclusion 953
Notice and Disclaimer 954
References 954

TARGET AUDIENCE

This document is designed for those with a primary interest and knowledge base in the field of echocardiography and for other medical professionals with a specific interest in the abnormalities of the interatrial septum and the use of cardiac ultrasonography. This includes cardiovascular physicians, other cardiovascular providers, cardiac sonographers, surgeons, cardiac interventionalists, neurologists, residents, research nurses, clinicians, intensivists, and other medical professionals.

OBJECTIVES

On completing the reading of the proposed guideline, the participants will better be able to

1. Describe the conventional two-dimensional, three-dimensional,

cardiographic, transesophageal echocardiographic, and intracardiac echocardiographic ultrasound technologies.

2. Describe the echocardiographic parameters to characterize the normal interatrial septum and the abnormalities of atrial septal defect, atrial septal aneurysm, and patent foramen ovale. This will include the best practices for measurement and assessment techniques.
3. Identify the advantages and disadvantages of each echocardiographic technique and measurements of the interatrial septum as supported by the available published data.
4. Recognize which images should be used and measurements that should be included in the standard echocardiographic evaluation of patients with atrial septal defect, atrial septal aneurysm, and patent foramen ovale.
5. Explain the clinical and prognostic significance of the echocardiographic assessment of atrial septal defect, atrial septal aneurysm, and patent foramen ovale, including not only the interatrial septum assessment, but also evaluation of the chamber size and function and the pulmonary circulation.
6. Recognize what are the relevant features used to evaluate patients for potential transcatheter (i.e., device) closure of atrial septal abnormalities.
7. Describe the important features and potential findings in the echocardiographic assessment of the patient after surgical and transcatheter interventions for atrial septal abnormalities.

INTRODUCTION

Atrial septal communications account for approximately 6%–10% of congenital heart defects, with an incidence of 1 in 1,500 live births.¹ The atrial septal defect (ASD) is among the most common acyanotic congenital cardiac lesions, occurring in 0.1% of births and accounting for 30%–40% of clinically important intracardiac shunts in adults.^{2–4} The patent foramen ovale (PFO) is more common and is present in greater than 20%–25% of adults.⁵ The clinical syndromes associated with ASD and PFO are extremely variable and represent a significant health burden that spans pediatric and adult medicine, neurology, and surgery. The evaluation of abnormalities of the interatrial septum and their associated syndromes require a standardized, systematic approach to their echocardiographic and Doppler characterization, including the use of transthoracic echocardiographic (TTE), transesophageal echocardiographic (TEE), and intracardiac echocardiographic (ICE) ultrasound, three-dimensional (3D) imaging, Doppler, and transcranial Doppler (TCD) modalities.

A thorough echocardiographic evaluation of PFO and ASD includes the detection and quantification of the size and shape of the septal defects, the rims of tissue surrounding the defect, the degree and direction of shunting, and the remodeling and changes in size and function of the cardiac chambers and pulmonary circulation. The emergence of 3D visualization, especially with the TEE-based characterization of septal abnormalities has contributed incremental information in the evaluation of the interatrial septum.^{6,7} As such, a guideline document to integrate the available diagnostic modalities is presented to aid clinical practice, training, and research.

Previous American Society of Echocardiography (ASE) guidelines have focused on the description of performing a comprehensive transesophageal examination, standards for acquisition and presentation of 3D echocardiographic imaging, echocardiographic guidance of interatrial defect device closure, and assessment of the right ventricle (RV).^{8–12} Guidelines for the comprehensive assessment of the interatrial septum (IAS) have the potential to reduce variation in the quality of echocardiographic studies, guide the complete characterization of defects, standardize the measurements and techniques used to describe the anatomy and physiology, and improve the assessment of suitability for surgical and transcatheter therapies.

and Doppler echocardiographic methodology required for optimal evaluation and characterization of the interatrial septum from transthoracic echo-

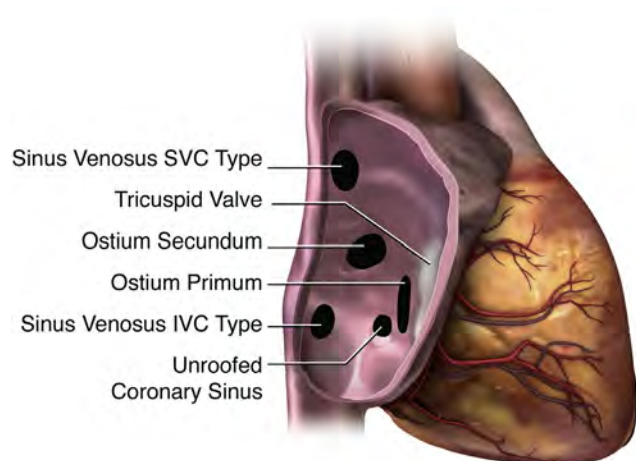


Figure 1 Subtypes of atrial septal communications when viewed from RA. PFO not illustrated.

As such, clinicians and researchers, device manufacturers, and regulatory agencies all stand to benefit from these standards, because they will bring greater uniformity into clinical care, clinical trial design, and the conduct of imaging core laboratories.

Finally, the echocardiographic and Doppler study of patients before and after surgical and transcatheter therapies involving the IAS also requires guidelines and standardization of the methodology. The results of these therapies and their complications must be fully and competently assessed, characterized, and reported by the modern echocardiography laboratory.

DEVELOPMENT AND ANATOMY OF THE ATRIAL SEPTUM

Normal Anatomy

Understanding atrial septal communications requires comprehension of the underlying development and anatomy of the IAS.¹³ The atrial septum has three components: the septum primum, septum secundum, and atrioventricular (AV) canal septum. The sinus venosus is not a component of the true atrial septum but is an adjacent structure through which an atrial communication can occur.¹⁴ Septal defects can be classified according to their anatomic location in the IAS (Figure 1).

Figure 2 depicts a schematic of normal atrial septal development. The atria first develop as a common cavity. At approximately 28 days of gestation, the septum primum, derived from the atrial roof, begins to migrate toward the developing endocardial cushions. During this transition, the space between the septum primum and the endocardial cushion is termed the “embryonic ostium primum” or the “foramen primum.”¹⁴ The septum secundum, in contrast, is an infolding of the atrial roof rather than a true membranous structure; it develops adjacent to the developing truncus and to the right of the septum primum.¹⁴ In the normal heart, the ostium primum closes by fusion of the mesenchymal cells of the septum primum (the so-called mesenchymal cap of the vestibular spine) with the superior and inferior endocardial cushions.¹⁴ The leading edge of the septum secundum becomes the superior limbic band. By 2 months into gestation, the septum secundum and septum primum fuse, leaving the foramen ovale as the only residual communication. The flap of

the foramen ovale is termed the “fossa ovalis” and is formed by the septum secundum, septum primum (which attaches on the left atrial [LA] side of the septum secundum), and the AV canal septum.¹⁵ The septum primum becomes contiguous with the systemic venous tributaries to form the inflow of the superior and inferior vena cavae. The sinus venosus septum is an adjacent structure to the atrial septum that separates the right pulmonary veins from the superior vena cava (SVC) and posterior right atrium (RA).¹⁵ The coronary sinus is separated from the LA by a wall of tissue called the coronary sinus septum. The anterosuperior portion of the atrial septum is adjacent to the right aortic sinus of Valsalva. A more detailed description of atrial septum development is available for additional information.¹⁴

Anatomy of Atrial Septal Defects and Associated Atrial Septal Abnormalities

Patent Foramen Ovale. A (PFO is not a true deficiency of atrial septal tissue but rather a potential space or separation between the septum primum and septum secundum located in the anterosuperior portion of the atrial septum (Figure 3A,B).¹⁶ It is not considered a true ASD, because no structural deficiency of the atrial septal tissue is present.^{14,17} The foramen remains functionally closed as long as the LA pressure is greater than the RA pressure. In many cases, a PFO might be only functionally patent and have a tunnel-like appearance, because the septum primum forms a flap valve. The relative differences in left and RA pressure can result in intermittent shunting of blood. A PFO can also be a circular or elliptical true opening between the two atria. Some cases of PFO result from “stretching” of the superior limbic band of the septum secundum from atrial dilation and remodeling (Figures 4–6). In other cases, the septum primum is truly aneurysmal and as such cannot completely close the atrial communication¹⁸ (Figure 7). In fetal life, patency of the foramen ovale is essential to provide oxygenated blood from the placenta to the vital organs, including the developing central nervous system.¹⁸ After birth, the foramen ovale generally closes within the first 2 months of age. Up to 20%–25% of the normal population has a PFO present in adulthood.^{18–21}

The incidence and size of a PFO can change with age. In an autopsy study of 965 human hearts, the overall incidence of PFO was 27.3%, but it progressively declined with increasing age from 34.3% during the first 3 decades of life to 25.4% during the 4th through 8th decades and 20.2% during the 9th and 10th decades.⁵ The size of a PFO on autopsy in that series ranged from 1 to 19 mm in the maximal diameter (mean 4.9 mm). In 98% of these cases, the foramen ovale was 1–10 mm in diameter. The size tended to increase with increasing age, from a mean of 3.4 mm in the first decade to 5.8 mm in the 10th decade of life.⁵

For purposes of consistency in nomenclature, a “patent foramen ovale” has been referred to when right to left shunting of blood has been demonstrated by Doppler or saline contrast injection without a true deficiency of the IAS. A “PFO with left to right flow” has been referred to when the atrial hemodynamics have resulted in opening the potential communication of the foramen, resulting in left to right shunting of blood demonstrated by Doppler imaging (Figures 4–6). When a PFO is stretched open by atrial hemodynamics, thus creating a defect in the septum, it is referred to as a “stretched” PFO. This can result in left to right or right to left shunting of blood flow demonstrated by Doppler, depending on the differences in the right and LA pressure.

Closure of the foramen ovale occurs by fusion of the septum primum and septum secundum at the caudal limit of the zone of overlap

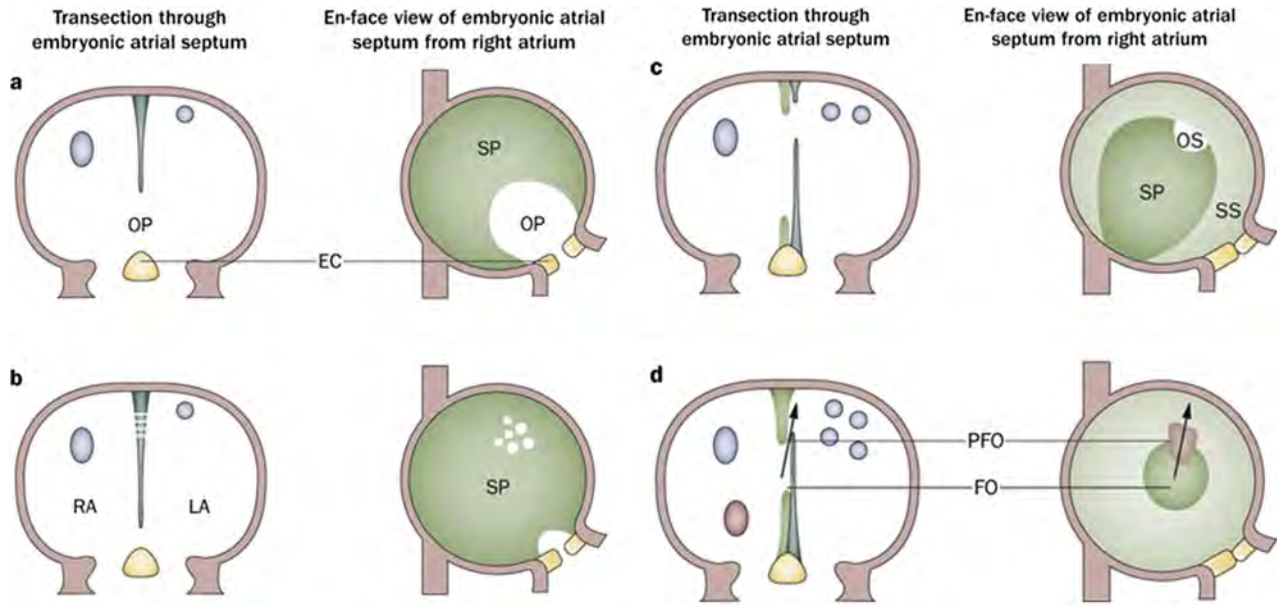


Figure 2 (A) The septum primum grows from the roof of the atria. (B) Fenestrations develop within the septum primum. (C) The septum secundum develops by an infolding of the atrial walls. The ostium secundum acts as a conduit for right-to-left shunting of oxygenated blood. (D) At the anterior superior edge of the fossa ovalis, the primum and secundum septa remain unfused, which constitutes a PFO. Arrow denotes blood flowing through the PFO from the embryonic RA to the LA. The blue and pink dots represent the development of the caval and pulmonary venous inflow to the atria. EC, endocardial cushion; FO, fossa ovalis; OP, ostium primum; OS, ostium secundum; SP, septum primum; SS, septum secundum. Reproduced with permission from Calvert et al.¹⁶

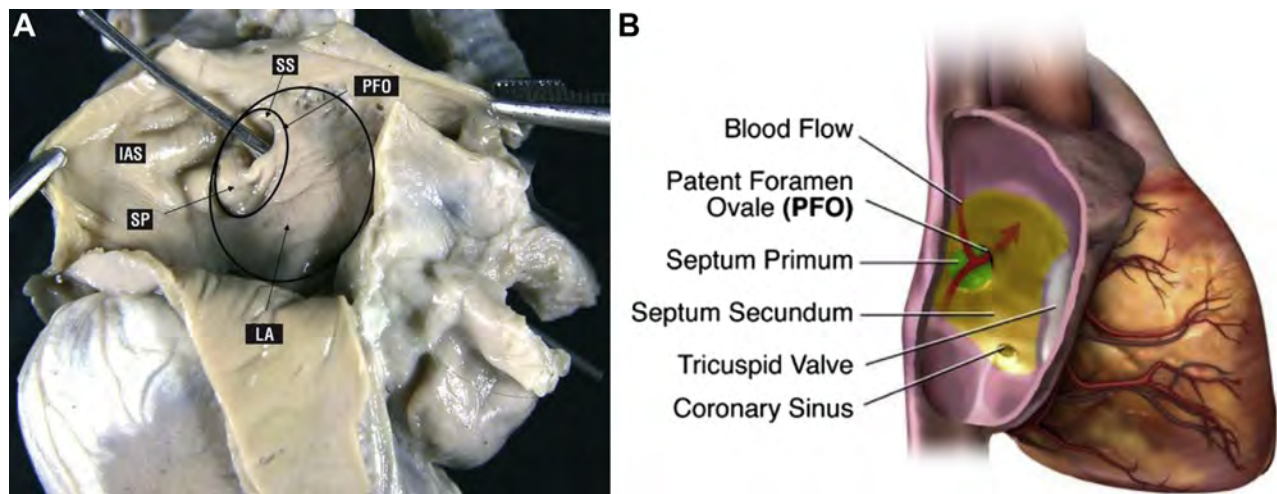


Figure 3 (A) Photograph of autopsy specimen from LA perspective demonstrating PFO by way of the passage of a metal probe; it also demonstrates adjacent structures. SP, septum primum; SS, septum secundum. Reprinted with permission from Cruz-González I, Solís J, Inglessis-Azuaje I, Palacios IF. Patent foramen ovale: current state of the art. Rev Esp Cardiol 2008;61:738-751. (B) The septum primum is dark green, and the septum secundum is light green. A PFO typically exists at the anterior superior border adjacent to the aortic root. The arrow denotes the passage of blood through the PFO from the right to left atrium.

of these structures. Incomplete fusion results in a pouch-like anatomic region that, in most instances, communicates with the LA cavity.²² The phrase “LA septal pouch” refers to the blind pouch from the residual overlap of the septum primum and septum secundum and has been suggested as a possible location for thrombus formation and embolism.²³⁻²⁶ This can mimic LA myxoma.²⁷

Ostium Secundum Atrial Septal Defect. An ostium secundum ASD most often occurs as the result of a true deficiency of septum pri-

imum tissue; it is the most common form of a true ASD.²⁸ The superior and posterior margins of the defect are composed of the septum secundum, the anterior margin is composed of the AV canal septum, and the inferior margin is composed of the septum primum and left venous valve of the inferior vena cava.¹⁸ These defects can vary in shape and can be elliptical or round (Figure 8). With large ostium secundum defects, the septum primum is often nearly or completely absent. In some cases, persistent strands of septum primum will be present and will cross the defect, resulting in multiple

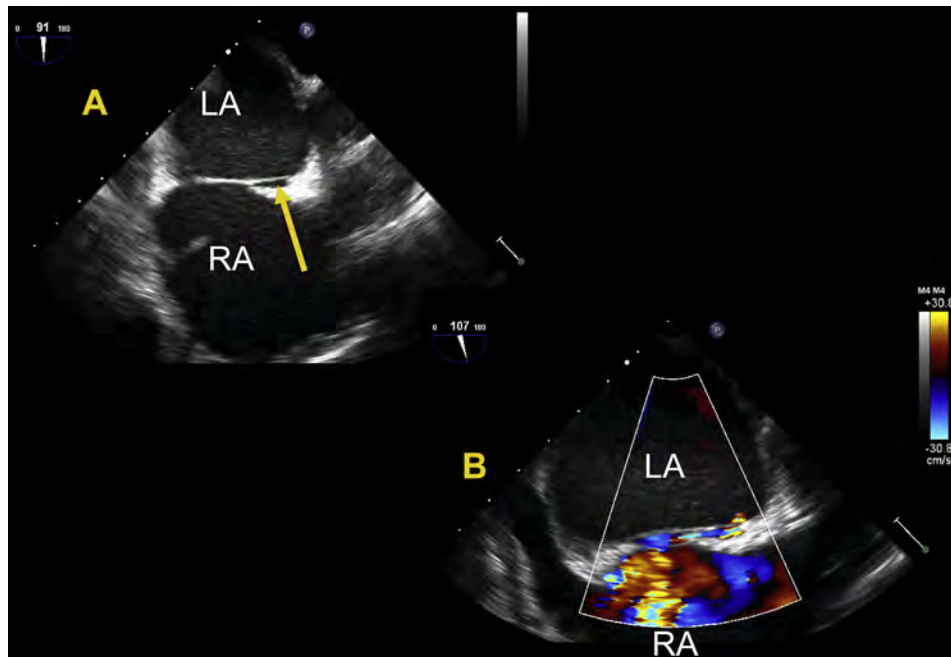


Figure 4 Two-dimensional TEE of a PFO (yellow arrow) in bicaval views (A) without and (B) with color Doppler in an adult patient.

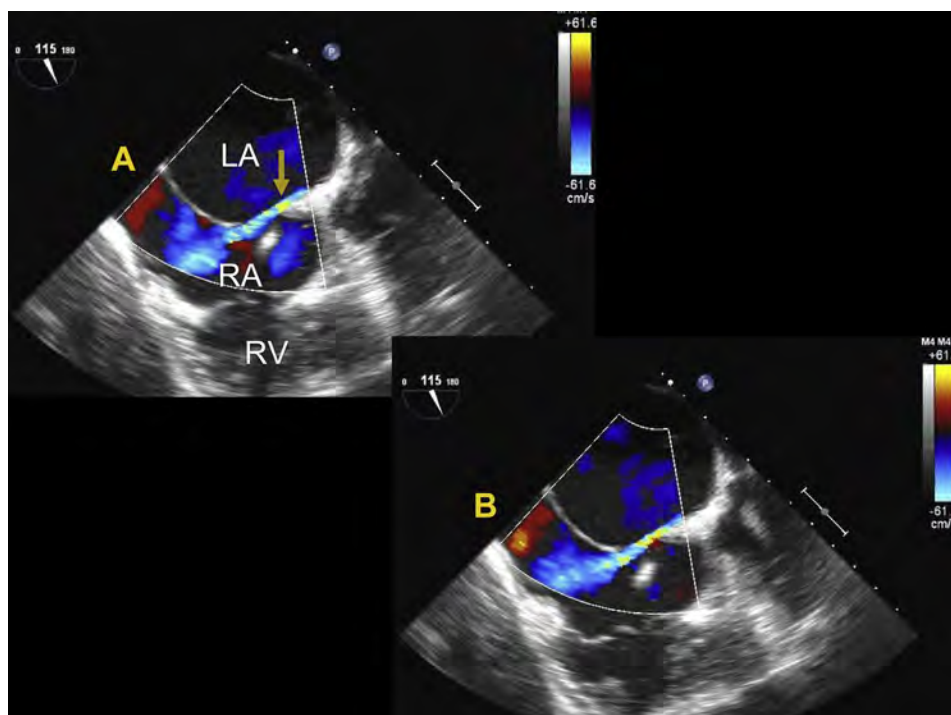


Figure 5 Two-dimensional TEE of a “stretched” PFO (yellow arrow) in bicaval views (A and B) with color Doppler flow from left to right in an adult patient. See also [Video 1](#).

communications and creating multiple fenestrations (Figures 9–12). These ASDs typically range in size from several millimeters to as large as more than 3 cm in diameter. For example, in an autopsy series of 50 patients with secundum ASD, all the defects were classifiable into one of four morphologic categories: (1) virtual absence of the septum primum such that the ASD was the entire fossa ovalis ($n = 19$, 38%); (2) deficiency of the septum primum

($n = 16$, 32%); (3) a fenestrated septum primum creating multiple ASDs ($n = 2$, 4%); and (4) fenestrations in a deficient septum primum creating multiple ASDs ($n = 13$, 26%).²⁹ These anatomic variations can have significant implications for device closure and could favor the use of devices designed for multiple fenestrations or require multiple devices for closure. Secundum ASDs can enlarge over time with age and cardiac growth.²⁸

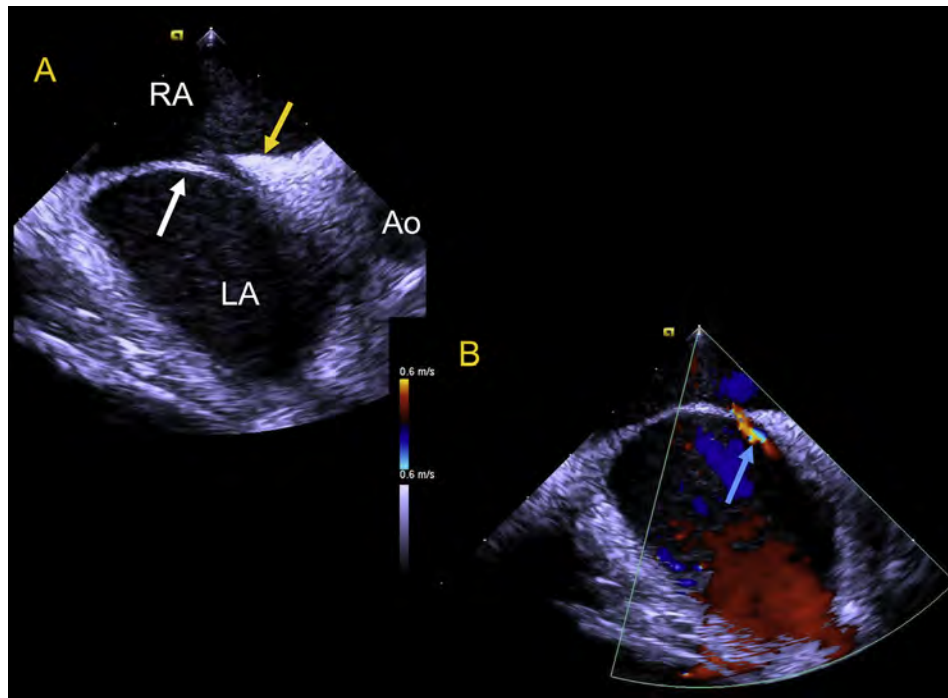


Figure 6 (A) Two-dimensional ICE of a “stretched” PFO and (B) with color Doppler in an adult patient. Yellow arrow indicates the septum secundum; white arrow, septum primum; blue arrow, left to right flow through PFO. See also [Video 2](#).

An ostium secundum ASD is often amenable to percutaneous transcatheter closure.³⁰⁻³³ The evaluation for the suitability of transcatheter closure is reviewed in detail in the present document.

A rare form of ostium secundum ASD occurs when the superior limbic band of the septum secundum is absent. In such cases, the atrial communication is “high” in the septum, in close proximity to the SVC. However, these defects should not be confused with the sinus venosus defect of the SVC type. Importantly, the high ostium secundum ASD is not associated with anomalous pulmonary venous return. An absence of the septum secundum can also occur in the presence of left-sided juxtaposition of the atrial appendages. Juxtaposition of the atrial appendages describes the condition in which both atrial appendages (or one appendage and part of the other) lie beside each other and to one side of the great arterial vessels. The juxtaposition is commonly associated with significant congenital heart disease, including transposition of the great vessels.³⁴ In juxtaposition, the normal infolding of the atrial roof (that forms the septum secundum) often does not occur because the great arteries are positioned abnormally (such as is seen with a double outlet ventricle or transposition of the great arteries).¹⁸ Although these defects do not involve the vena cavae, AV valves, pulmonary veins, or coronary sinus, it is important to recognize how close the defect is to these surrounding structures when considering catheter-based device closure.³¹

Ostium Primum Atrial Septal Defect. An ostium primum ASD is a congenital anomaly that exists within the spectrum of an AV canal defect (Figure 13). In early embryologic development, these defects occur when the endocardial cushions fail to fuse because of abnormal migration of mesenchymal cells.³⁵ With an endocardial cushion defect, the canal portion of the AV septum and the AV valves can all be variably affected. Ostium primum ASD is otherwise known as partial or incomplete AV canal defect; these names are used interchangeably. The defect is characterized by an atrial communication resulting from absence of the AV canal portion of the atrial septum in

association with a common AV valve annulus and two AV valve orifices. The AV valve tissue is adherent to the crest of the ventricular septum such that no ventricular level shunt is present. The leaflets of the two AV valves are abnormal with two bridging leaflets that straddle from the RV to the left ventricle (LV) rather than a normal anterior mitral valve leaflet and septal tricuspid valve leaflet. The bridging leaflets (superior and inferior) meet at the ventricular septum and are thus often erroneously termed “cleft mitral valve.” This term is indelibly in the lexicon of congenital heart disease. However, it is more accurate to use the left and right AV valves when describing an ostium primum ASD because both valves will always be abnormal in this setting. AV valve regurgitation through the so-called cleft is extremely common because of an abnormality or absence of valve tissue.

The borders of an ostium primum ASD include the septum primum superiorly and posteriorly and the common AV valve annulus anteriorly. Because these communications have the AV valve orifice as one of the margins, percutaneous transcatheter device closure is not possible.³¹

Sinus Venosus Defects. Sinus venosus defects are less common than ostium secundum ASDs and are not true ASDs.²⁸ These defects occur as a result of a partial or complete absence of the sinus venosus septum between the SVC and the right upper pulmonary vein (SVC type) or the right lower and middle pulmonary veins and the RA (inferior vena cava [IVC] type; Figures 14–16). In most cases of sinus venosus defects of the SVC type, the right upper pulmonary vein is connected normally but drains anomalously to the RA. However, in some cases, the right pulmonary vein or veins will be abnormally connected to the SVC superior to the RA. The shunt that occurs is therefore similar to that seen in a partial anomalous pulmonary venous connection in that the pulmonary venous flow is directed toward the RA. The resulting left-to-right shunt is typically large. Occasionally, the patient will be mildly desaturated because SVC blood is able to enter the LA. Sinus venosus defects of the IVC type

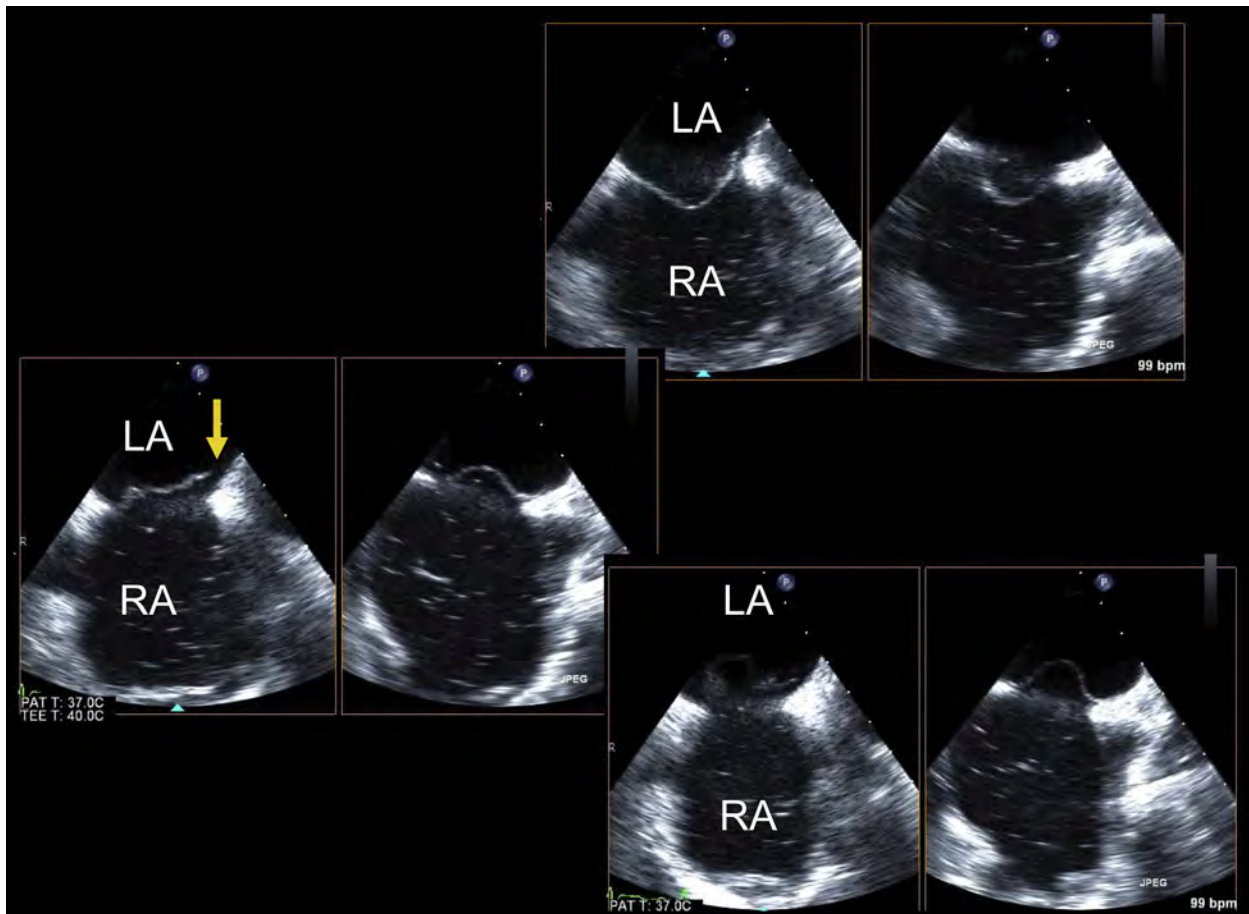


Figure 7 Biplane TEE of IAS with PFO demonstrating excessive mobility of the fossa ovalis and an associated PFO (arrow). Contrast is seen in the RA. See also [Video 3](#).

are more unusual and typically involve anomalous drainage of the right middle and/or lower pulmonary veins. Sinus venosus defects cannot be closed by device and typically require baffling of the right pulmonary veins to the LA by way of an ASD patch. Reimplantation of the SVC (Warden procedure) is sometimes required if the right pulmonary veins are connected directly to the SVC.

Coronary Sinus Defects. A coronary sinus septal defect or an “unroofed” coronary sinus is one of the more rare forms of atrial communication. In this defect, the wall of the coronary sinus within the LA is deficient or completely absent (Figures 17–19). In a heart without other major structural anomalies, LA blood enters the coronary sinus and drains into the RA through the coronary sinus os, which is typically enlarged to accommodate the increased flow. When a patent left SVC is associated with a coronary sinus septal defect, it is termed “Raghib syndrome.”³⁶

Contrast injection with agitated saline is often helpful to make the diagnosis. Two-dimensional (2D) and 3D TEE could be particularly useful in establishing the diagnosis and correlating with the surgical findings.^{6,37} In the setting of partial coronary sinus unroofing, percutaneous transcatheter device closure might be possible in some cases.^{38,39}

Common Atrium. Rarely, all components of the atrial septum, including the septum primum, septum secundum, and AV canal septum are absent, resulting in a common atrium.^{28,40–42} This is

typically seen in association with heterotaxy syndrome. Some remnants of tissue might still be present in these patients.

Atrial Septal Aneurysm. An atrial septal aneurysm (ASA) is a redundancy or saccular deformity of the atrial septum and is associated with increased mobility of the atrial septal tissue. ASA is defined as excursion of the septal tissue (typically the fossa ovalis) of greater than 10 mm from the plane of the atrial septum into the RA or LA or a combined total excursion right and left of 15 mm (Figure 10). The prevalence of ASA is 2%–3%.⁴³ ASA has been associated with the presence of a PFO, as well as an increased size of a PFO, and an increased prevalence of cryptogenic stroke and other embolic events. ASA has also been associated with multiple septal fenestrations, and this should be evaluated for carefully using color Doppler imaging.^{44–46}

Eustachian Valve and Chiari Network. The eustachian valve is a remnant of the valve of the IVC that, during fetal life, directs IVC flow across the fossa ovalis. A large or prominent eustachian valve in the setting of a PFO might indirectly contribute to paradoxical embolism by preventing spontaneous closure of the foramen.⁴⁷ The eustachian valve extends anterior from the IVC–RA junction.

A Chiari network is a remnant of the right valve of the sinus venosus and appears as a filamentous structure in various places in the RA, including near the entry of the IVC and coronary sinus into the RA (Figure 20). A Chiari network is present in 2%–3% of the general population and is associated with the presence of PFO and ASA.⁴⁸

KEY POINTS

PFO

- PFO is not a true deficiency of atrial septal tissue but rather a potential space or separation between the septum primum and septum secundum that occurs in up to 20%–25% of the population.
- PFO is defined by the demonstration of right to left shunting by contrast or color Doppler, and a “stretched” PFO is present when atrial hemodynamics have opened the foramen and result in left to right or right to left shunting demonstrated by Doppler imaging.

ASD

- Ostium secundum ASD occurs as a deficiency in septum primum and is the most common form of ASD.
- Ostium secundum ASD is often amenable to percutaneous transcatheter closure.
- Ostium secundum ASD defects can vary in shape and can be elliptical or round and can contain multiple fenestrations.
- Ostium primum ASD occur as a result a failure of fusion of the endocardial cushions and are within the spectrum of AV septal defects.
- Sinus venosus defects are *not* true ASDs and result from the absence of sinus venosus septum between right upper pulmonary veins and SVC (SVC type) or right middle and lower pulmonary veins and RA (IVC type).
- Coronary sinus defects (or unroofed coronary sinus) are not true ASDs and permit a left-to-right shunt from the LA to coronary sinus to the RA.

ASA

- ASA is defined as an excursion of septal tissue of >10 mm from the plane of the atrial septum into the atrium or a total excursion of >15 mm.

IMAGING OF THE INTERATRIAL SEPTUM

General Imaging Approach

The most widely used ultrasound modality to evaluate the IAS is TTE, which remains the preferred initial diagnostic modality for the detection and diagnosis of PFO, ASD, and ASA.^{20,49-61} TTE is especially useful in small children in whom the ultrasound image quality will typically permit a full diagnostic study. It can also be used for patient selection and real-time transcatheter ASD or PFO closure procedural guidance in pediatric patients.^{31,57,62-64}

TTE can be used for the initial evaluation of ASD and PFO in adults; however, TEE is required to further characterize the atrial septal abnormalities, because the TTE image quality will not always permit a comprehensive evaluation of the IAS. TEE is not invariably required for assessment of a PFO if transcatheter closure is not being considered. Also, 2D and 3D TEE offers significant incremental anatomic information compared with TTE and should be performed in all adult patients being evaluated for percutaneous transcatheter closure or surgical therapy.^{31,65-67} In adults, TEE can identify the margins or rims of the ASD (see section on Assessment of ASDs: Standards and Characterization) and assess the surrounding structures (e.g., aorta, cavae, pulmonary veins, AV valves, and coronary sinus).

ICE has been used extensively to guide percutaneous ASD/PFO closure procedures and provides comparable (but not identical) imaging to TEE. ICE is discussed extensively in the subsequent sections (see sections on Intracardiac Echocardiographic Imaging Protocol for IAS and Role of Echocardiography in Transcatheter Device Closure).

Contrast echocardiography with agitated saline plays an important role in the evaluation of PFO and assessing residual shunts after transcatheter closure and has a more limited role in the diagnosis of ASD.^{52,61,63,68-75} Contrast echocardiography and contrast TCD is discussed further in sections on Assessment of Shunting; Techniques, Standards, and Characterization Visualization of Shunting: TTE and TEE; and Transcranial Doppler Detection/Grading of Shunting.

Table 1 summarizes the recommended general imaging approach to atrial septal abnormalities stratified by the patient characteristics, imaging modality, and intended application (e.g., diagnosis, procedure selection or guidance, follow-up).

Three-Dimensional Imaging of the Interatrial Septum

Most recently, 3D TEE has been described to improve the visualization of PFO and ASD, their surrounding tissue rims, and surrounding structures and can be used for guidance during percutaneous transcatheter closure.^{6,7,53,63,65,66,76-81} Because the IAS is a complex, dynamic, and 3D anatomic structure, limitations exist in its evaluation using any single form of 2D echocardiography. The IAS (and associated abnormalities such as ASD or PFO) does not exist in a true flat plane that can be easily aligned or interrogated using 2D imaging. Both ASD and PFO exist in a wide variety of heterogeneous sizes, shapes, and configurations (Figures 8 and 21). Also, 3D imaging provides unique views of the IAS and, in particular, allows for en face viewing of the ASD and surrounding fossa, allowing for accurate determination of the ASD size and shape. Furthermore, 3D imaging offers the potential to clearly and comprehensively define the dynamic morphology of the defect, which has been shown to change during the cardiac cycle. Also, 3D imaging delineates the relationship of the ASD to the surrounding cardiac structures and the rims of tissue surrounding it (Figure 22).

Two-dimensional biplane (or triplane) imaging, a feature of currently commercially available 3D imaging systems, is a unique modality that takes advantage of 3D technology. The advantages of biplane imaging include the display of simultaneous additional echocardiographic views, with high frame rates and excellent temporal resolution. Complimentary simultaneously displayed orthogonal plane imaging provides incremental information compared with that from a single plane, and this imaging modality is uniquely suited to transcatheter procedure guidance. Numerous reports of the advantages of 3D TEE in guiding catheter interventions have been published and include the use of biplane imaging.^{7,65,66,80,82} Figure 23 illustrates the use of biplane imaging during percutaneous transcatheter closure of ASD before deployment of the device.

Also, 3D imaging allows for multiple acquisition modes, including narrow-angle, zoomed, and wide-angle gated acquisition of multiple volumes. Once 3D volumes are acquired, postprocessing using commercially available 3D software packages such as QLAB (Philips, Best, The Netherlands) or 4D Cardio-View (TomTec, Munich, Germany) is performed to align the plane of the IAS with multiple 3D plane slices. This approach facilitates an assessment of the shape of an ASD and allows for measurement of the en face diameters in multiple orthogonal views, without the potential for bias due to malalignment of the ultrasound planes (Figure 24). The images should be reviewed in both systole and diastole to assess for the dynamic change in size that can occur. This 3D en face display can also aid in the recognition and quantification of rim deficiencies, because the extent of the deficiency relative to the surrounding structures such as the aorta can be easily demonstrated and quantified. The distance between the defect and the aorta can be easily measured, just as can the area of the defect and length of rim deficiency when present.

Role of Echocardiography in Percutaneous Transcatheter Device Closure

The role of TTE, TEE, and ICE during the assessment and transcatheter management of ASD/PFO is essential.^{31,63,80,83}

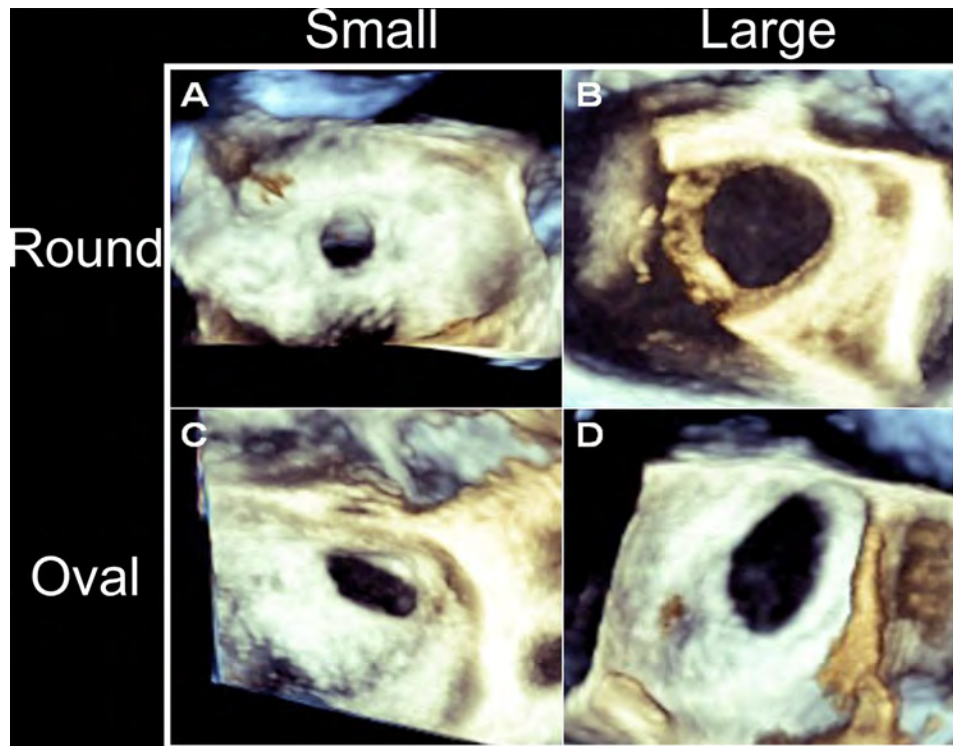


Figure 8 Three-dimensional TEE images of various shapes and sizes of ostium secundum ASD. Representative examples of (A) round, small, (B) round, large, (C) oval, small, and (D) oval, large secundum ASD. See also [Video 4](#). Reprinted with permission from Seo et al.⁷⁷

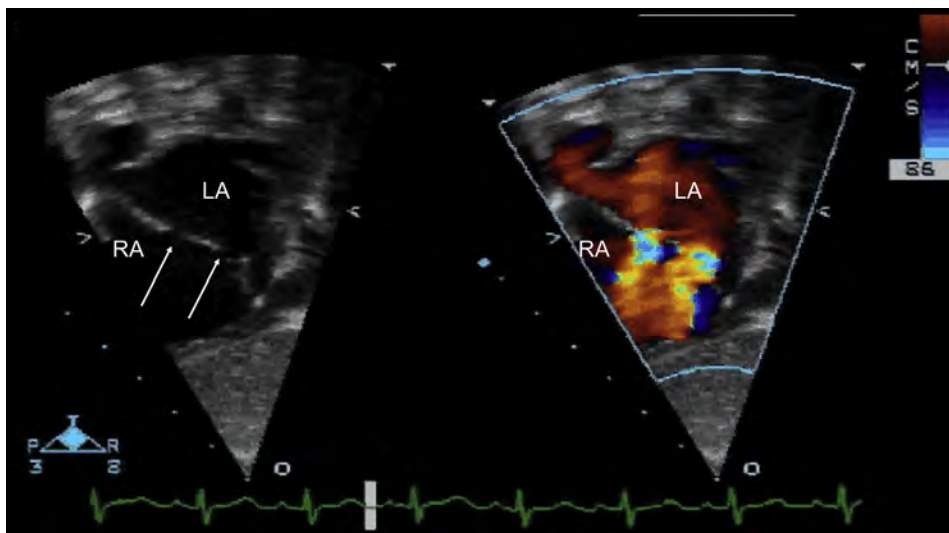


Figure 9 Subxiphoid TTE demonstrating multifenestrated IAS without and with color Doppler flow from left to right in a pediatric patient. See also [Video 5](#).

Echocardiography in patients undergoing transcatheter closure is critically important for appropriate patient selection, real-time procedure guidance, assessment of device efficacy and complications, and long-term follow-up.

TTE provides information about the type of defect, its hemodynamic significance, and any associated anomalies and can be used comprehensively in smaller pediatric patients for the diagnosis of ASD and PFO and for patient selection and procedure guidance. TTE has the advantage of offering unlimited multiple planes to eval-

uate the atrial septum, but it has limited ability to interrogate the lower rim of atrial septal tissue above the IVC after device placement because the device shadowing interferes with imaging in virtually all planes. In addition, because the septum is relatively far from the transducer, the image quality is often suboptimal in larger pediatric and adult patients. If percutaneous closure is clinically indicated, a detailed assessment of the IAS anatomy and surrounding structures using TEE is typically required for patient selection and procedure guidance or ICE for procedure guidance in such patients.

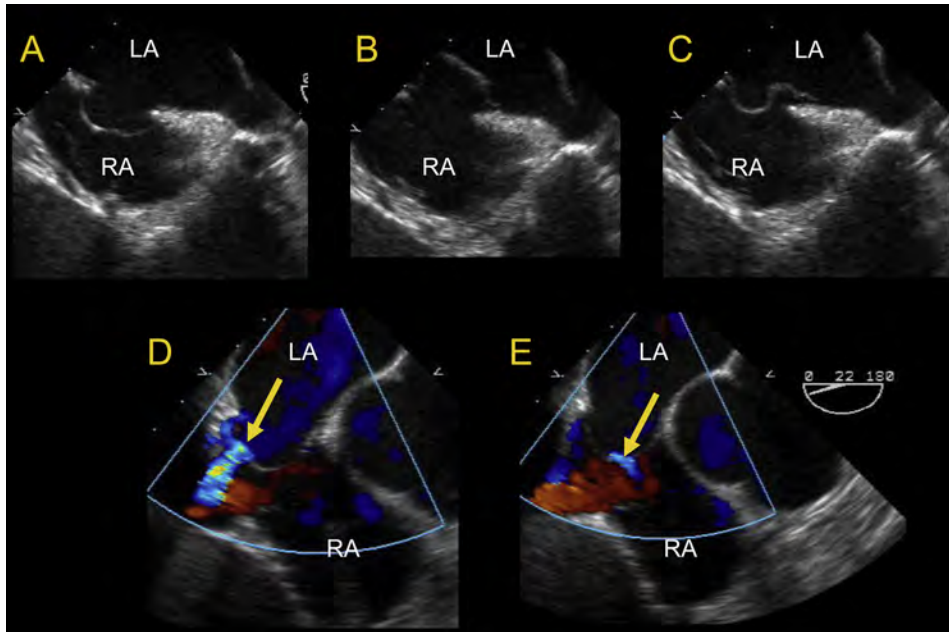


Figure 10 Two-dimensional TEE (bicaval view) of IAS with ASA demonstrating excessive mobility of the fossa ovalis (**A–C**) and associated multiple fenestrations (**D–E**) (yellow arrows).

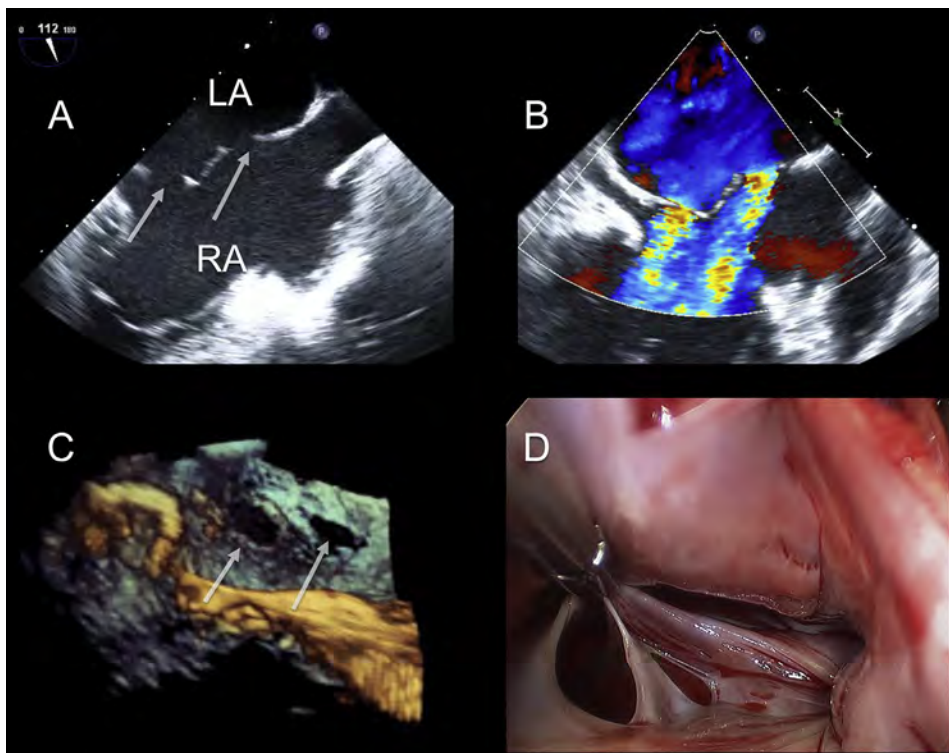


Figure 11 Three-dimensional TEE of one medium and one small ostium secundum ASDs (white arrows). (**A**) Bicaval view demonstrating two discrete ASDs. (**B**) Bicaval view with color Doppler demonstrating two discrete left to right shunts. (**C**) Zoom acquisition of both ASDs en face from RA perspective. (**D**) Minimally invasive surgical repair demonstrating identical pathologic findings to 3D TEE.

Transesophageal echocardiography provides real-time, highly detailed imaging of the IAS, surrounding structures, catheters, and closure device during transcatheter closure. It requires either conscious sedation, with the attendant aspiration risk in a supine pa-

tient, or general anesthesia, with an endotracheal tube placed to minimize aspiration risk. This approach also requires a dedicated echocardiographer to perform the TEE, while the interventionalist performs the transcatheter closure procedure. The advent of 3D

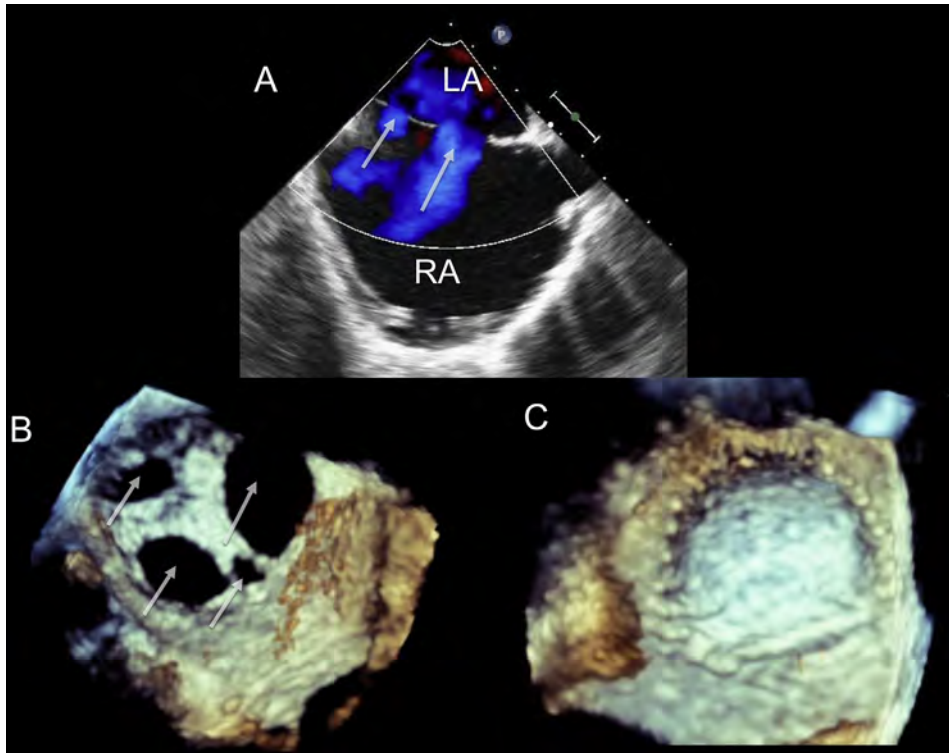


Figure 12 Three-dimensional TEE of multiple secundum ASDs (*white arrows*) resulting in a “Swiss cheese” configuration. **(A)** Bicaval view demonstrating at least two discrete ASDs with left to right color Doppler flow. **(B)** En face zoom acquisition from RA perspective demonstrating four discrete ASDs. **(C)** Zoom acquisition after minimally invasive surgical repair with a single pericardial patch. See also [Videos 6 and 7](#).

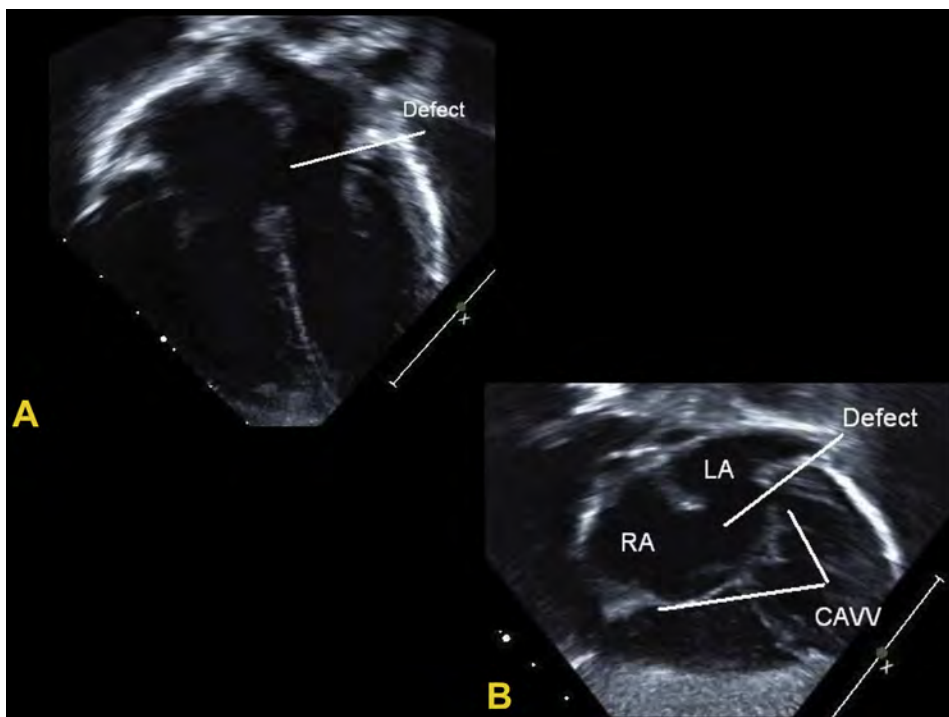


Figure 13 (A) Primum ASD by 2D TTE in apical four-chamber view. **(B)** Primum ASD by 2D TTE in subcostal left anterior oblique view. CAVV, common AV valve.

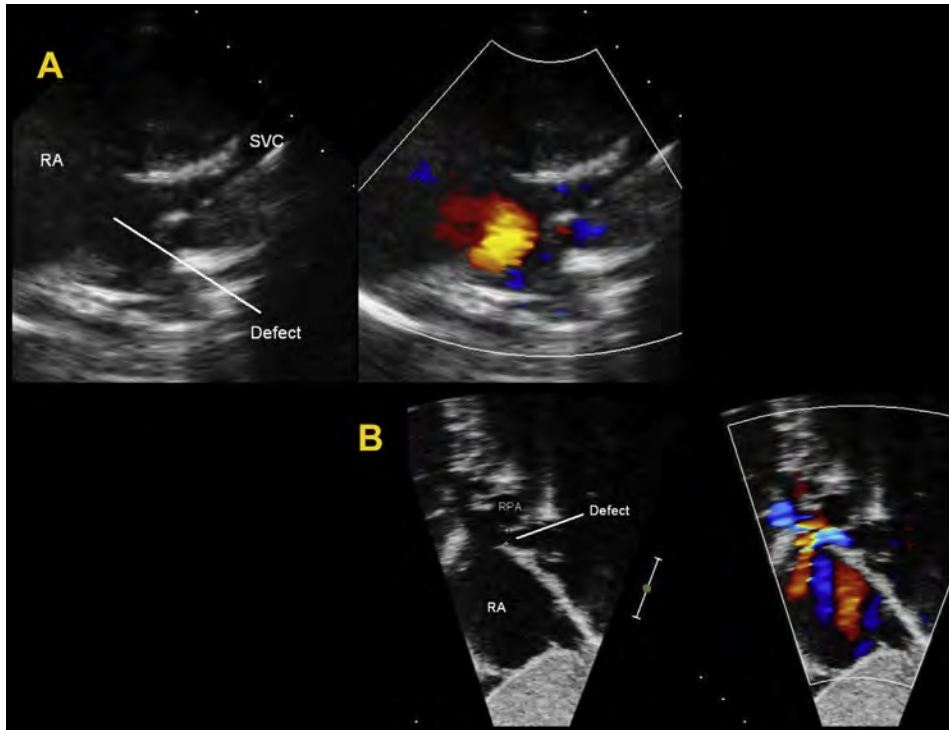


Figure 14 (A) Representative example of 2D TTE (*left*) and with color Doppler (*right*) of an SVC type sinus venosus ASD from the high right parasternal view. (B) Representative example of 2D TTE (*left*) and with color Doppler (*right*) of an SVC type sinus venosus ASD from the subcostal sagittal view. RPA, right pulmonary artery. See also [Video 8](#).

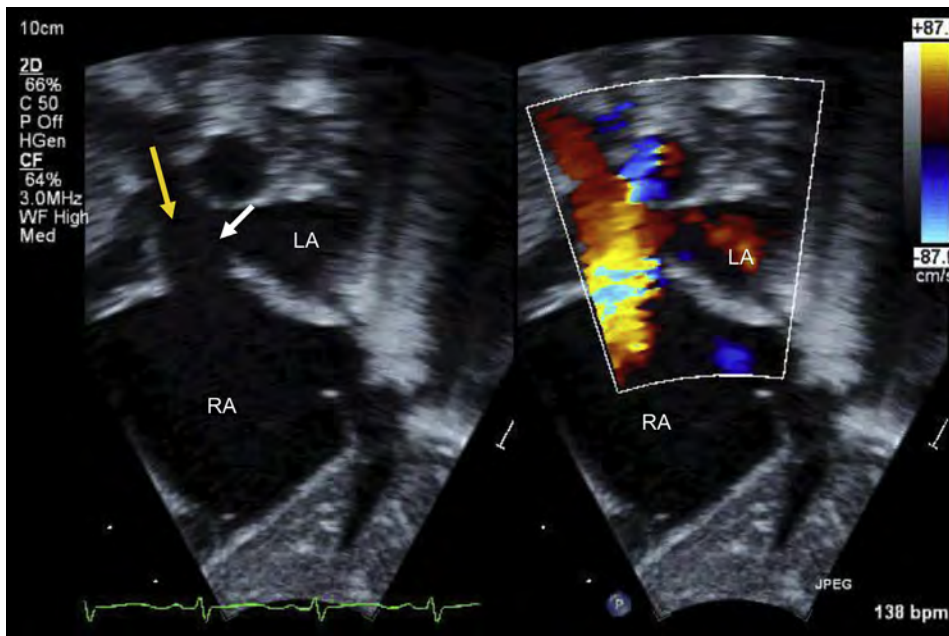


Figure 15 Transthoracic echocardiogram of a SVC type venosus ASD in subxiphoid sagittal view without and with color in a pediatric patient. The *yellow arrow* represents the right superior pulmonary vein and the *white arrow*, the defect entering the atrium. See also [Video 9](#).

TEE has enhanced the evaluation of ASD and PFO by clearly defining the IAS anatomy and enables an en face view of the defect and its surrounding structures. Multiplanar reconstruction of the 3D data set allows accurate measurement of the minimum and maximum dimensions of the defect or defects, facilitating selection of the optimal

size and type of closure device. Moreover, intraprocedural real-time 3D TEE provides superior visualization of wires, catheters and devices, and their relationships to neighboring structures in a format that is generally more intuitively comprehended by the interventional cardiologist ([Figure 25](#)).

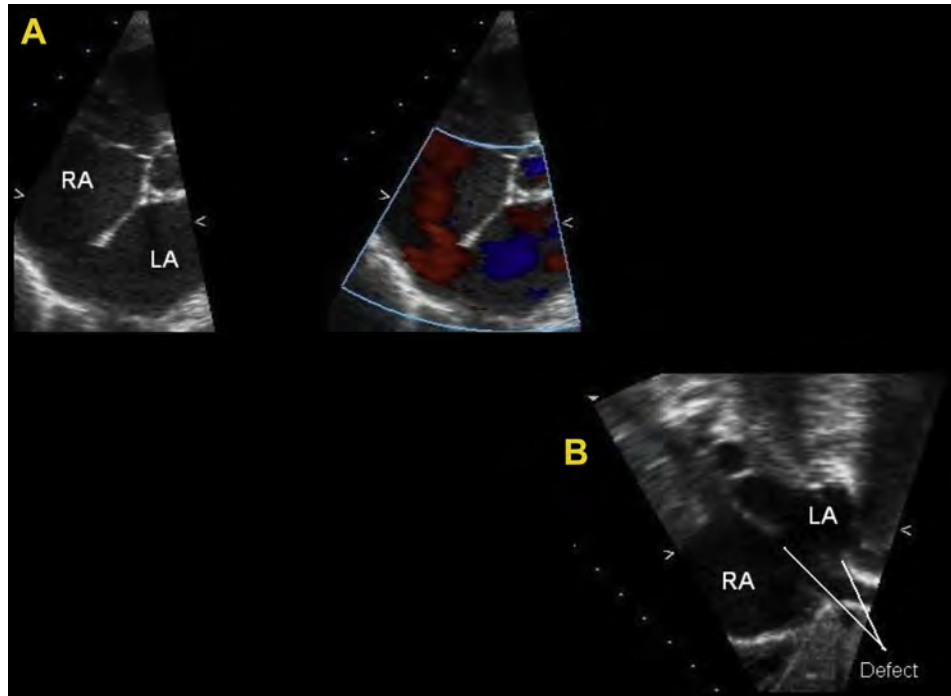


Figure 16 (A) Inferior vena cava type sinus venosus ASD by 2D TTE (*left*) and with color Doppler (*right*) in the parasternal short-axis view with left to right flow. (B) IVC type sinus venosus ASD by 2D TTE in the subcostal view. See also [Video 10](#).

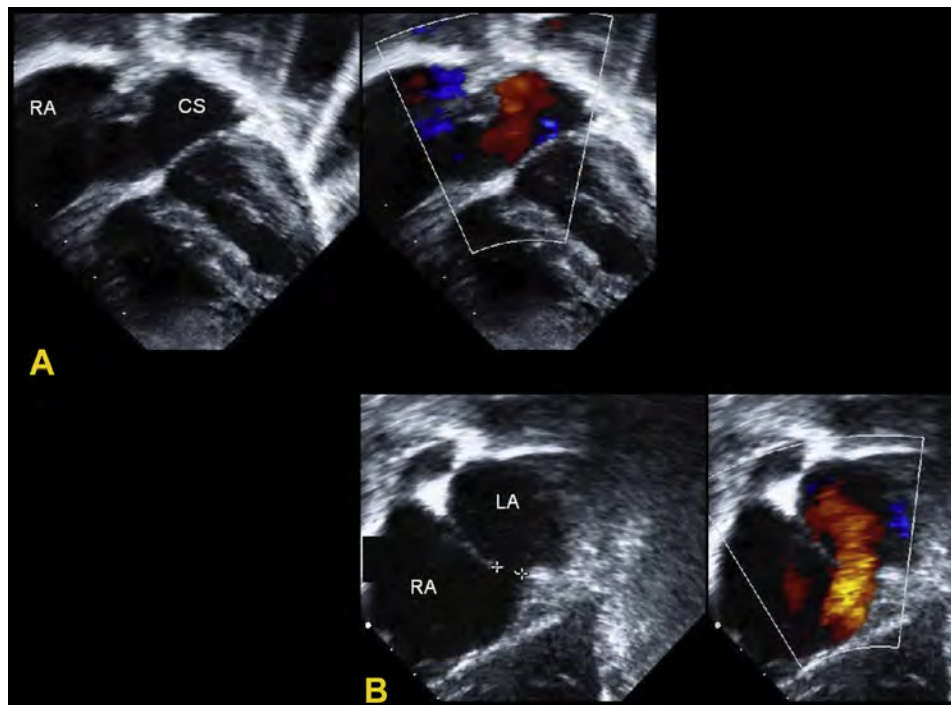


Figure 17 (A) Two-dimensional TTE (*left*) and with color Doppler (*right*) demonstrating unroofed coronary sinus interatrial communication in four-chamber view. Note dilated CS. (B) Two-dimensional TTE (*left*) and with color Doppler (*right*) demonstrating unroofed coronary sinus interatrial communication in subcostal left anterior oblique view. CS, coronary sinus. See also [Videos 11 and 12](#).

Intracardiac echocardiography has been used extensively to guide percutaneous ASD/PFO closure procedures and is the imaging modality of choice in many centers in the cardiac catheterization laboratory.⁸⁴⁻⁸⁸ The advantages of ICE include an image quality

that is similar (but not identical) to that of TEE, facilitating a comprehensive assessment of the IAS, location and size of the defects, the adequacy of the rims, and location of the pulmonary veins. It also retains an advantage compared with TEE in imaging

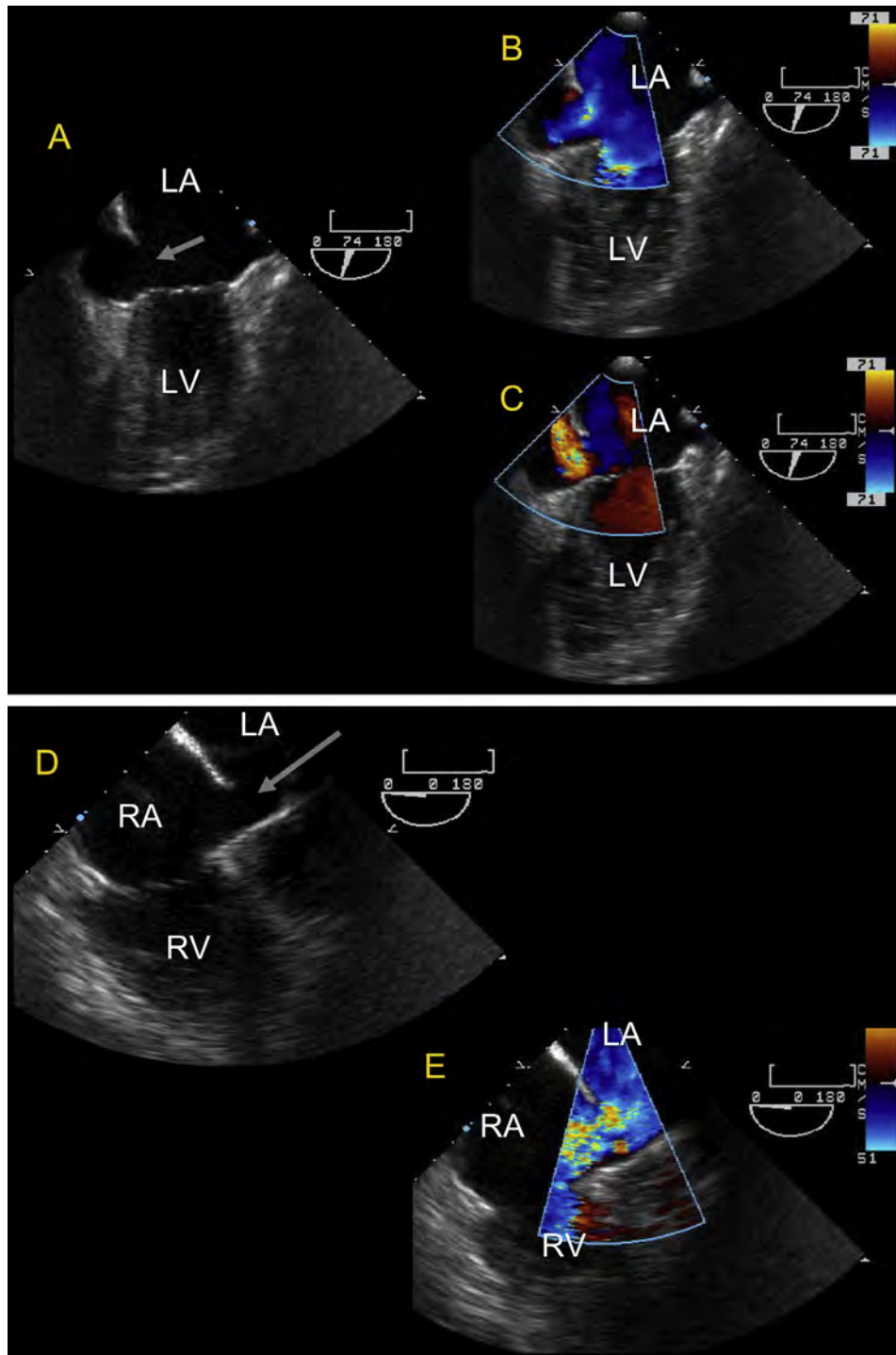


Figure 18 Two-dimensional TEE of unroofed coronary sinus. **(A)** Two-dimensional image demonstrating enlarged coronary sinus with unroofing communicating with LA (*arrow*). **(B and C)** Color Doppler flow into the coronary sinus from the LA and into the RA, creating an interatrial communication through the unroofed coronary sinus. **(D)** Two-dimensional image demonstrating enlarged coronary sinus with unroofing communicating with LA (*arrow*). **(B and E)** Color Doppler flow into the coronary sinus from the LA and into the RA, creating an interatrial communication through the unroofed coronary sinus. See also [Video 13](#).

the inferior and posterior portions of the IAS.⁸⁹ Finally, the use of ICE eliminates the need for general anesthesia and endotracheal intubation and can be performed with the patient under conscious sedation. An interventionalist can perform ICE without the need for additional

echocardiography support personnel. However, the potential disadvantages of ICE include a limited far-field view, catheter instability, the expense of single-use ICE catheters, the need for additional training, the risk of provocation of atrial arrhythmias, and increased

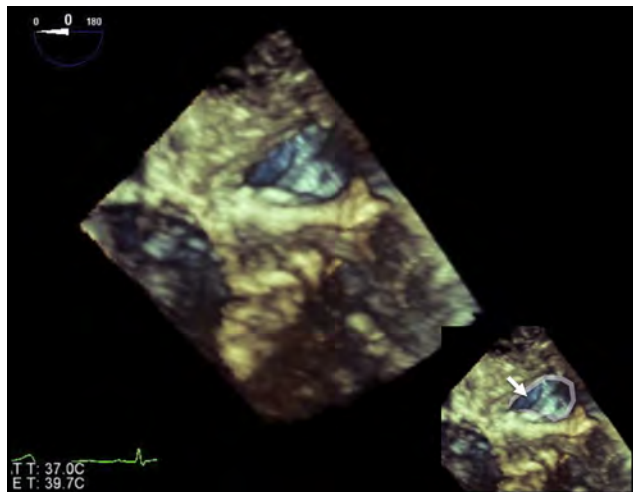


Figure 19 Unroofed coronary sinus on 3D TEE image as viewed from LA aspect. Oval indicates perimeter of unroofed portion of sinus in LA.

technical difficulty for a single operator. Table 2 provides a summary of the advantages and disadvantages of TTE, TEE, and ICE in percutaneous transcatheter guidance of PFO and ASD.

Transthoracic Echocardiography Imaging Protocol for Imaging the Interatrial Septum

The atrial septum can be evaluated fully using TTE. Ideally, multiple views should be used to evaluate the size, shape, and location of an atrial communication and the relationship of the defect to its surrounding structures (Figures 9 and 13–17 and 26–28). In particular, special attention must be paid to determine the relationship of the defect to the venae cavae, pulmonary veins, mitral and tricuspid valves, and coronary sinus. Assessment of the amount of the surrounding rims of tissue present is crucial. A deficiency of rim tissue between the defect and pulmonary veins, AV valve, or IVC will preclude transcatheter closure, and a deficiency of aortic rim can increase the risk of device erosion in certain circumstances.

Additional views of other structures such as the ventricles and great arteries are necessary to assess for secondary findings related to the hemodynamic consequences of an ASD such as RA, right ventricular (RV), and pulmonary artery (PA) dilation. In the pediatric population, the subxiphoid window typically allows the best visualization of the atrial septum and its related structures. In adolescence and adulthood, the subxiphoid window is often inadequate because of the distance from the probe to the atrial septum. Thus, other views such as the parasternal windows should be used to assess the atrial septum. In some cases, a full assessment of the atrial septum might not be possible with TTE. Thus, TEE could be required.

Subxiphoid Frontal (Four-Chamber) TTE View. The subxiphoid frontal (four-chamber) view allows imaging of the atrial septum along its anterior–posterior axis from the SVC to the AV valves. This is the preferred view for imaging the atrial septum, because the atrial septum runs near perpendicularly to the ultrasound beam, providing the highest axial resolution and permitting measurement of the defect diameter along its long axis. Because the septum is thin (especially in its midportion), placing the septum perpendicular to the ultrasound beam helps distinguish a true defect from dropout resulting from an artifact. Aneurysms of the atrial septum primum composed of tissue

attached to the edges of the ASD are also well visualized from the subcostal frontal view. ASAs could be fenestrated (Figure 9) but also can be intact with no resultant atrial level shunt. Color Doppler interrogation and contrast studies should be used to detect shunting. The surrounding rim from the defect to the right pulmonary veins can be measured in this view. Sinus venosus defects will be difficult to visualize because the venae cavae are not viewed longitudinally in this view.

Subxiphoid Sagittal TTE View. The subxiphoid sagittal TTE view is acquired by turning the transducer 90° clockwise from the frontal view. This view is ideal for imaging the atrial septum along its superior–inferior axis in a plane orthogonal to the subxiphoid frontal four-chamber view. Sweeping the transducer from right to left in this axis allows determination of the orthogonal dimension of the ASD (Figures 15 and 17). This dimension can be compared with the dimension measured in the subxiphoid frontal view to help determine the shape (circular or oval) of the defect. This view can be used to measure the rim from the defect to the SVC and IVC and is an excellent window to image a sinus venosus type defect (Figures 14B and 15).

Left Anterior Oblique TTE View. The left anterior oblique TTE view is acquired by turning the transducer approximately 45° counterclockwise from the frontal (four-chamber) view. This view allows imaging of the length of the atrial septum and is therefore ideal to identify ostium primum ASDs and for assessment of coronary sinus dilation (Figures 13B and 17B). In addition, it allows evaluation of the relation of the SVC to the defect. Furthermore, this view can be used to evaluate the entrance of the right-sided pulmonary veins into the heart.

Apical Four-Chamber TTE View. In the apical four-chamber TTE view, the diagnosis and measurement of ASDs should be avoided because the atrial septum is aligned parallel to the ultrasound beam. Thus, artifactual dropout is frequently seen in this view, which could result in overestimation of the defect size. This view is used to assess the hemodynamic consequences of ASDs, such as RA and RV dilation, and to estimate RV pressure using the tricuspid valve regurgitant jet velocity. This view is also used to evaluate for right-to-left shunting with agitated saline (Figure 29).

Modified Apical Four-Chamber TTE View (Half Way in Between Apical Four-Chamber and Parasternal Short-Axis View). The modified apical four-chamber TTE view is obtained by sliding the transducer medially from the apical four-chamber view to the sternal border. This view highlights the atrial septum at an improved incidence angle to the sound beam (30°–45°). In the patients in whom the subcostal views are difficult to obtain, the modified apical four-chamber view is an alternative method for imaging the atrial septum in the direction of the axial resolution of the equipment.

Parasternal Short-Axis TTE View. In the parasternal short-axis TTE view at the base of the heart, the atrial septum is visualized posterior to the aortic root running in an anterior–posterior orientation. This view is ideal to identify the aortic rim of the defect (Figures 26 and 27). It also highlights the posterior rim (or lack thereof) in sinus venosus and posteroinferior secundum defects. The size of the defect itself should not be measured in this view, because the beam orientation is parallel to the septum, and dropout resulting from artifact can occur.

High Right Parasternal View. The high right parasternal view is a parasagittal view performed with the patient in the right lateral decubitus position with the probe in the superior–inferior orientation. In

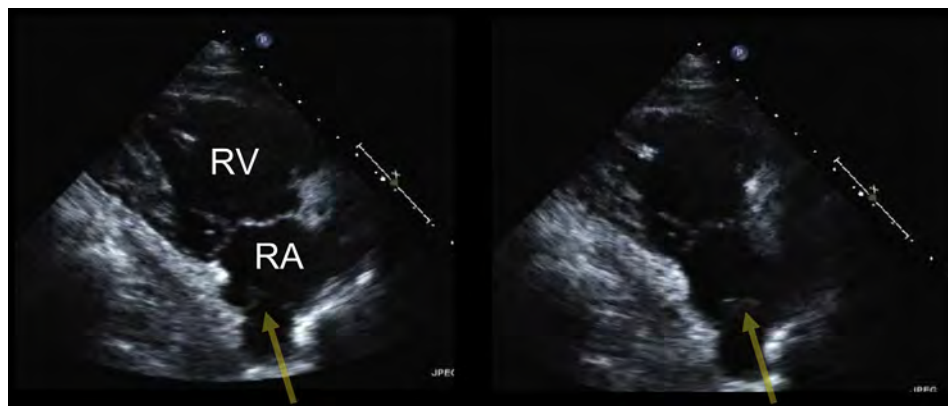


Figure 20 Transthoracic echocardiogram from the RV inflow view demonstrating mobile Chiari network (yellow arrows) attached to eustachian ridge.

Table 1 Imaging strategy in overall evaluation of atrial septal abnormalities

| Patient population | Establishing diagnosis of ASD or PFO | Imaging for transcatheter procedure guidance | Routine postprocedure follow-up study |
|------------------------------|--------------------------------------|--|---------------------------------------|
| Pediatric patients <35–40 kg | TTE or TEE* | TEE or ICE† | TTE |
| Pediatric patients >35–40 kg | TTE, TEE, 3D TEE | TEE, 3D TEE, or ICE† | TTE |
| Adult patients | TTE, TEE, or 3D TEE | TEE, 3D TEE, or ICE† | TTE |

*Depending on body surface area and adequacy of image quality, TEE is highly recommended for assessment of an ASD but is generally performed in intubated patients; if the weight is >35–40 kg, 3D TEE can be performed.

†Some centers use ICE for procedure guidance of all defects; others use ICE for uncomplicated small ASD closure only, reserving TEE or 3D TEE for complicated or larger septal defects.

this view, the atrial septum is aligned perpendicular to the beam and is ideal for diagnosing sinus venosus defects, particularly when the sub-siphoid windows are inadequate (Figure 16).

Table 3 summarizes the key imaging views for TTE for the evaluation of the IAS and surrounding structures.

Transesophageal Echocardiography Imaging Protocol for the Interatrial Septum

As with TTE, multiple and sequential TEE views should be used to completely and systematically evaluate the IAS, the size, shape, and location of any atrial communication present, and the relationship of the defect to its surrounding structures. A comprehensive guide to performing multiplane TEE has been previously published by the ASE and the Society of Cardiovascular Anesthesiologists, and should be referred to for recommendations on performing a comprehensive TEE examination.¹¹

We recommend sequential interrogation and the digital capture of images starting from the standard views and then by stepwise increases in the transducer angle in a series of 15° increments to pan or sweep the ultrasound beam through the areas of interest. Two-dimensional images should be optimized and color Doppler mapping subsequently applied. The color Doppler scale can be reduced slightly to approximately 35–40 cm/sec to capture low-velocity flow across a small fenestration, PFO, or smaller ASD. Pulsed and continuous wave Doppler should then be used to measure the velocity, direction, and timing of flow in the representative views.

Capturing 3D volumes with and without color Doppler of the IAS allows for even greater data acquisition without the need for sequen-

tial multiplane interrogation and acquisition and is discussed separately in the section on 3D TEE Acquisition Protocol for PFO and ASD.

When an ASD or PFO is present, attention must be given to determining the relationship of the defect to the venae cavae, pulmonary veins, mitral and tricuspid valves, and coronary sinus. An assessment of the amount of the surrounding rims of tissue is critical for evaluation of patient candidacy for percutaneous transcatheter closure. A deficient rim is defined as less than 5 mm in multiple sequential views, and this should be evaluated in at least three sequential related multiplane views in 15° increments.

As with TTE, additional views of the other cardiac structures are necessary to assess for secondary findings related to the hemodynamic consequences of an ASD such as right heart and pulmonary arterial dilation. Please refer to the ASE guidelines on comprehensive TEE assessment and the assessment of the right heart.⁹⁻¹¹

When using TEE, five base views are used to assess the IAS and surrounding structures, which are summarized in Table 4. These key views include the upper esophageal short-axis view, midesophageal aortic valve (AoV) short-axis view, midesophageal four-chamber view, midesophageal bicaval view, and midesophageal long-axis view.

Upper Esophageal Short-Axis View. The upper esophageal short-axis view is obtained from the upper esophagus starting at multiplane angles of 0°, with stepwise sweeping and recording at 15°, 30°, and 45°. This view facilitates imaging of the superior aspects of the atrial septum, including the septum secundum, the roofs of the RA and LA, and the surrounding great vessels (SVC and ascending aorta). Entry of the right pulmonary veins can be demonstrated by insertion

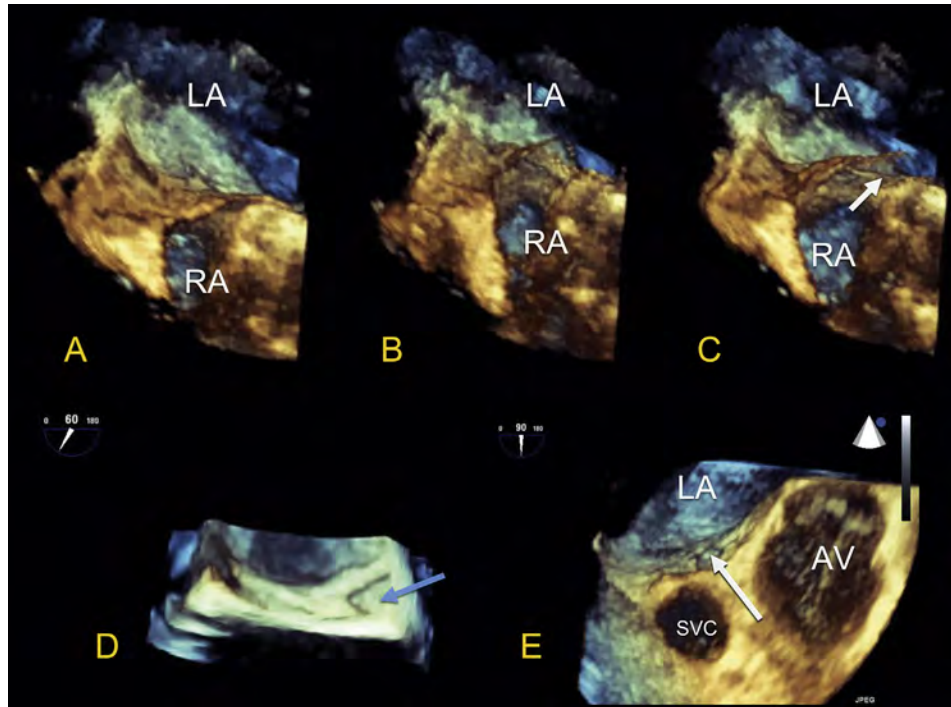


Figure 21 Three-dimensional TEE images of a PFO. (A–C) Excessive movement of the septum primum (fossa ovalis) in a patient with an ASA and a PFO. *White arrow* indicates PFO opened fully under influence of pressure difference between RA and LA. (D) PFO “tunnel” as viewed from the LA perspective. *Blue arrow* indicates the PFO exit into the LA. (E) PFO tunnel exiting into LA (*white arrow*).

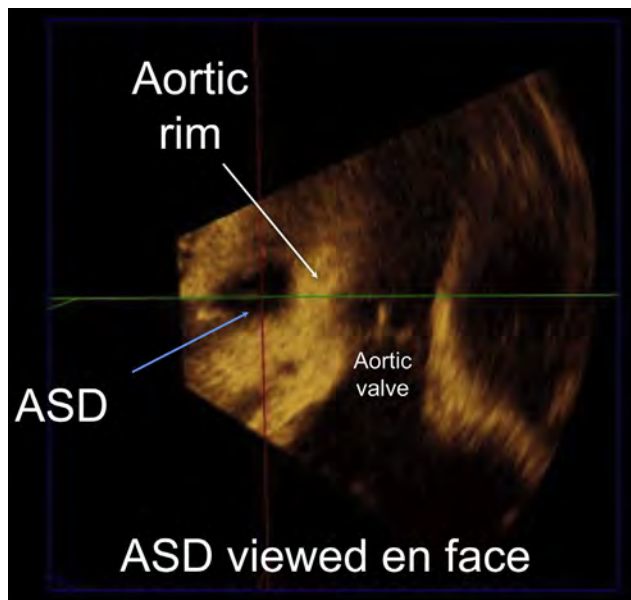


Figure 22 Three-dimensional ASD assessment allows for delineation of an ASD (*blue arrow*) and its relationship between adjacent structures—the aortic valve is seen and the entire aortic rim (*white arrow*) is visualized en face.

into the mid-esophagus and by clockwise rotation of the probe in these views (Figure 30). Anomalous pulmonary venous drainage and an SVC type sinus venosus defect can be noted in this view.

Midesophageal Aortic Valve Short-Axis View. The midesophageal AoV short-axis view is obtained from the mid-esophagus

starting with a multiplane angle of approximately 30° and stepwise sweeping through and recording additional views at 45°, 60°, and 75°. This progression of transducer angles allows transitional interrogation of the IAS from the AoV short-axis view to the modified bicaval tricuspid valve view. The AoV short-axis view is typically obtained to present short-axis views of the AoV and its surrounding septum. This view facilitates imaging of the anterior and posterior planes of the atrial septum (and aortic and posterior rims if an ASD is present), the anteroposterior diameter of the ASD, and the overlap of septum primum and septum secundum when a PFO is present (Figures 31 and 32).

Midesophageal Four-Chamber View. The midesophageal four-chamber view is obtained from the mid-esophagus beginning with a multiplane angles of 0° and stepwise increases of the multiplane angle to 15° and 30°. This view is used to evaluate the AV septum (deficient in primum ASD) and the relationship of any ASD to the AV valves (Figure 33). Larger devices used to close secundum ASD can interfere or impinge on AV valve function, and this must be carefully evaluated before device deployment (Figure 34).

Midesophageal Bicaval View. The midesophageal bicaval view is obtained from the mid-esophagus with multiplane angles of 90°, 105°, and 120°. It is used to image the inferior and superior plane of the atrial septum and the surrounding structures, such as the SVC and right pulmonary veins (Figures 4, 5, 7, 10A–C, 11A and B, 12A, 35, and 36). This view is important for evaluating sinus venosus defects of the SVC type and to evaluate for anomalous pulmonary vein insertion. This view is also important in evaluating the roof or dome of the RA, which must be visualized before release of ASD closure devices.

Mid-Esophageal Long-Axis View. The midesophageal long-axis view is obtained from the mid-esophagus with multiplane angles of

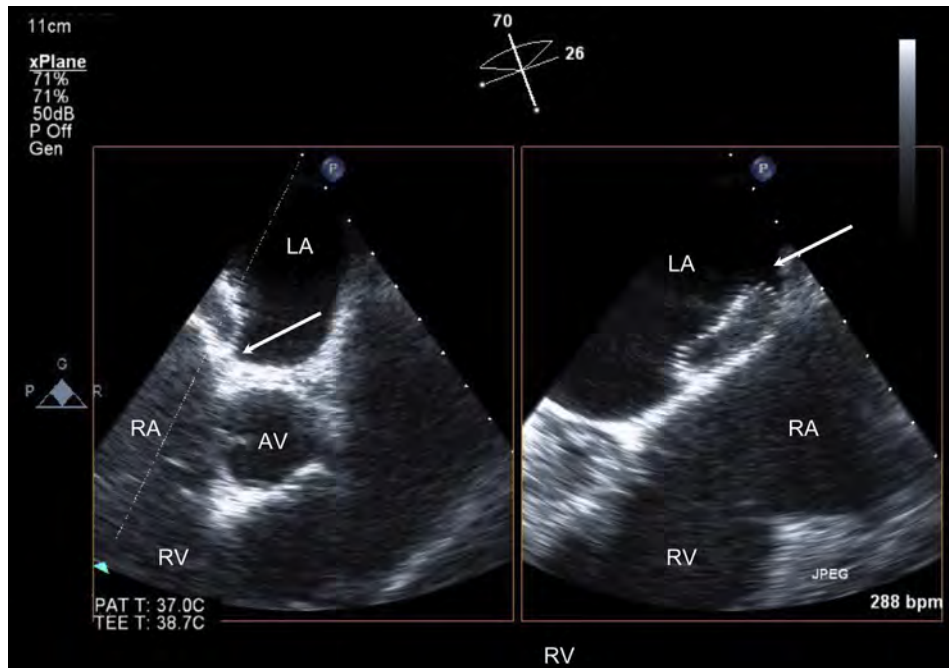


Figure 23 Biplane imaging performed during percutaneous transcatheter closure imaging of multiple planes simultaneously. The aortic rim and superior rim is seen (*left arrow*) and device interaction with the aorta (*left arrow*) and atrial roof (*right arrow*) can be assessed simultaneously.

120°, 135°, and 150° to evaluate the roof or dome of the LA when a percutaneous device is placed (see the section on the Role of Echocardiography in Percutaneous Transcatheter Device Closure). Rotation past the LA appendage demonstrates the entry of the left pulmonary veins into the LA (Figure 37).

3D TEE Acquisition Protocol for PFO and ASD

Three-dimensional transesophageal images of the IAS should be acquired from multiple views and multiple 3D imaging modes for analysis. A comprehensive description of overall 3D image acquisition, formatting, and presentation can be found in the 2012 ASE guidelines.¹²

A comprehensive 3D examination usually begins with a real-time or narrow-angled acquisition from the standard imaging views. To obtain images with higher temporal and spatial resolution, electrocardiographically gated, 3D wide-angled acquisitions are then performed. When evaluating the IAS using TEE, we recommend narrow-angled, zoomed, and wide-angled acquisition of 3D data from several key views:

- Midesophageal short-axis view: acquired from the mid-esophagus starting at a multiplane angle of 0°. The probe is rotated toward the IAS. This view is particularly suited to narrow- and wide-angled acquisitions.
- Basal short-axis view: acquired from the mid-esophagus starting at 30° to 60° multiplane angles. This view is particularly suited to narrow- and wide-angled acquisitions. This view can also be used for zoom mode imaging during procedure guidance. Processing the 3D images from this view facilitates the demonstration of an ASD en face and demonstrates the relationship to the surrounding structures (e.g., the aorta and aortic rim) (Figures 38 and 39A and B). Wide-angled acquisition from this view should be acquired with and without color Doppler flow mapping for precise off-line measurements of ASD size, shape, dynamic change, and relationship to surrounding structures.
- Bicaval view: acquired from the midesophageal level with the transducer starting at the 90° to 120° multiplane orientation. This view can also be

captured by each of the 3D imaging modalities. The depth of pyramidal data sets should be adjusted to include only the left and right sides of the atrial septum in this view. This specific setting will allow the entire septum to be acquired in a 3D format without incorporating the surrounding structures. With a 90° up-down angulation of the pyramidal data set, the entire left-sided aspect of the septum can be shown in an “en face perspective” (Figure 40). Once the left side of the atrial septum has been acquired, a 180° counterclockwise rotation will show the right side of the atrial septum and the fossa ovalis as a depression on the septum (Figure 41). Sometimes the use of fine cropping using the arbitrary crop plane will be necessary to remove the surrounding atrial structures that can obscure the septum. A gain setting at medium level is usually required to avoid the disappearance of the fossa ovalis and creating a false impression of an ASD. This view is also used to measure the size and shape of the ASD in systole and diastole.

- Sagittal bicaval view: can be obtained from the deep transgastric position with a transducer orientation of 100° to 120°. The recommendations for the settings and processing are identical to the midesophageal bicaval view.
- Four-chamber view: acquired from the midesophageal level starting at 0° to 20° transducer orientations.

3D TTE Acquisition Protocol for PFO and ASD. Transthoracic 3D images of the IAS can be obtained from the narrow-angle apical four-chamber, narrow-angle parasternal long-axis color, and apical four-chamber zoom views. However, image resolution can limit its utility in larger pediatric and adult patients.

3D Display. When the IAS is viewed from the LA (left), the atrial septum should be oriented with the right upper pulmonary vein at the 1-o’clock position. When displayed as viewed from the RA (right), the SVC should be located at the 11-o’clock position (Figures 40 and 41).

Images should be acquired from these transducer positions as an initial starting point using all three different 3D echocardiographic modes, including narrow-angled, zoomed, and wide-angled gated 3D acquisition modes.

Multiple examples of images from each modality are provided in the present report. In still images that are carefully acquired and

cropped, it will not always be apparent which 3D echocardiographic mode was used. In video images, the 3D zoomed acquisition mode will be noticeable by its slow volume rate and smooth images, and the 3D wide-angled gated acquisition mode will be noticeable by stitch artifacts, if present.

The qualitative anatomic parameters delineated from the 3D data set should include the type of ASD (e.g., secundum, primum, sinus venosus, common atrium, or coronary sinus), location within the atrial septum, shape, and orientation (Figures 8, 11, 12, and 39). The ASD shape can be defined as oval, round, or triangular or, at times, shaped somewhat like an egg or a pear or slightly irregular (Figure 8). The ASD orientation is defined according to the long-axis orientation of the defect as vertical, horizontal, oblique with an anterior tilt, or oblique with a posterior tilt. Defects in which the lengths of the long-axis and short-axis dimensions are within 1 mm should be designated as round.

Quantitative analysis of ASD using 3D echocardiography should include the maximum length, width, and area measured at atrial end-diastole (Figure 24). The ASD dimensions should also be measured at atrial end-systole to determine the change in the dimensions during the cardiac cycle (dynamic ASD). The ASD dimensions are measured in en face views from either the RA or LA perspective using dedicated quantitative software. The parameters calculated can include the percentage of change in ASD length, width, and area from atrial end-diastole to atrial end-systole. Atrial end-diastole is defined as the frame with the largest ASD dimension and atrial end-systole as the frame with the smallest ASD dimension. The number of defects in the atrial septum should be quantified if multiple.

Intracardiac Echocardiographic Imaging Protocol for IAS

A comprehensive assessment of the atrial septum, any septal defects, and surrounding tissue rims can be performed with radial or phased array ICE.^{83,90-93} The key ICE views used in the evaluation of the IAS as described are listed in Table 5. The currently available ICE systems and their present specifications are listed in Table 6. The currently available ICE systems do not have electronic beam steering or multi-plane transducer angle capabilities. Instead, they offer a radial rotational or phased area imaging plane that is manipulated by insertion and withdrawal of the catheter, axial rotation, and, in the case of the phased array systems, by manipulating the steering controls with adjustable tension, such that the catheter can be held in a flexed position in up to four directions (anterior, posterior, left, and right). Insertion and withdrawal of the phased array ICE probe will result in imaging more superiorly and inferiorly. Axial rotation allows for sweeping of the image through multiple planes. Three-dimensional ICE has recently become commercially available.⁹⁴⁻⁹⁶ Limited data exist regarding the role of 3D ICE in percutaneous transcatheter procedures at present. The use of 3D ICE offers the potential to provide greater anatomic information during structural interventions but requires additional investigation to fully define its role.^{95,97}

A standard assessment of the IAS and surrounding structures is presented here and summarized in Table 5:

- The phased array ICE probe is initially positioned in the mid-RA in a neutral catheter position to visualize the tricuspid valve in the long axis. This is referred to as the "home view" (Figure 42A). In this view, the RA, tricuspid valve, RV, RV outflow tract, pulmonary valve, proximal main PA, a portion of the AoV, and any ASD that is present with adjacent septum in the partial short-axis view can be seen. This view visualizes the lower portion of the AV septal rim.
- From this position, applying posterior deflection of the posterior-anterior knob and applying slight rightward rotation of the right-left knob will obtain the septal long-axis view (Figure 42B).

- Advancing the catheter cephalad will produce a bicaval view from which the superior and inferior rims of an ASD and the defect diameter and configuration can be measured (Figure 42C).
- Rotation of the entire catheter handle clockwise until the intracardiac transducer is near the tricuspid valve, followed by slight leftward rotation of the right-left knob until the AoV appears creates a septal short-axis view similar to the TEE short-axis plane, with the difference being the near field in the present view is the RA compared with TEE showing the LA (Figure 42D and E). From this view, the diameter of the defect and the anterior (aortic) and posterior rims can be measured (Figure 43).
- There is, however, no true four-chamber view, because the ICE catheter sits in the RA.

The initial echocardiographic assessment includes measurement of the defect diameter in multiple orthogonal planes, the overall septal length, and defect rims. If multiple defects are present, each should be characterized and the distance separating them measured. Please refer to the section on Imaging of IAS and Septal Defects: Assessment of ASDs: Standards and Characterization, for the features of an ASD that should be routinely described on imaging (Table 7).

KEY POINTS

- Table 1 summarizes the recommended general imaging approach using TTE, TEE, and ICE for evaluation of atrial septal abnormalities stratified by patient characteristics, imaging modality, and intended application (diagnosis, procedure selection or guidance, follow-up).
- TEE provides superior image quality to TTE but is not always required (e.g., a PFO that is not being contemplated for closure).
- 3D imaging provides unique views of the IAS and, in particular, allows for en face viewing of an ASD and the surrounding structures for accurate determination of ASD size and shape, to delineate the rims of surrounding tissue, and to determine the relationship of the ASD to the surrounding cardiac structures.
- Echocardiography in patients undergoing transcatheter closure is critically important for appropriate patient selection, real-time procedure guidance, assessment of device efficacy and complications, and long-term follow-up.
- Table 2 summarizes the advantages and disadvantages of TTE, TEE, and ICE in percutaneous transcatheter guidance of PFO and ASD.
- Table 3 summarizes the key imaging views using TTE for the evaluation of the IAS and surrounding structures.
- Table 4 summarizes the key views using TEE to assess the IAS and surrounding structures.
- Table 5 summarizes the key views using ICE to assess the IAS and surrounding structures.

ASSESSMENT OF SHUNTING

Techniques, Standards, and Characterization Visualization of Shunting: TTE and TEE

Shunting, and the hemodynamic significance of shunting, across an ASD or PFO is evaluated through a combination of structural imaging, color flow Doppler mapping, and spectral Doppler interrogation. Associated findings, including diastolic flattening of the ventricular septum and dilatation of the RA, RV, and/or PA, are all potential signs of significant left-to-right shunting. The severity of dilatation is related to the relative compliance of these structures, as well as to the size of the ASD.

The direction of shunting through an ASD is usually left to right and is visualized using color flow Doppler. ASD shunt flow can be right to left or bidirectional in the setting of significant pulmonary hypertension or significant impairment of RV compliance. Pulse wave spectral Doppler can be used for the detection of bidirectional shunting, in addition to color Doppler. The color scale settings should be adjusted to optimize for the expected low velocity of shunting (i.e., 25–40 cm/sec). Occasionally, higher velocity left-to-right shunting will be present

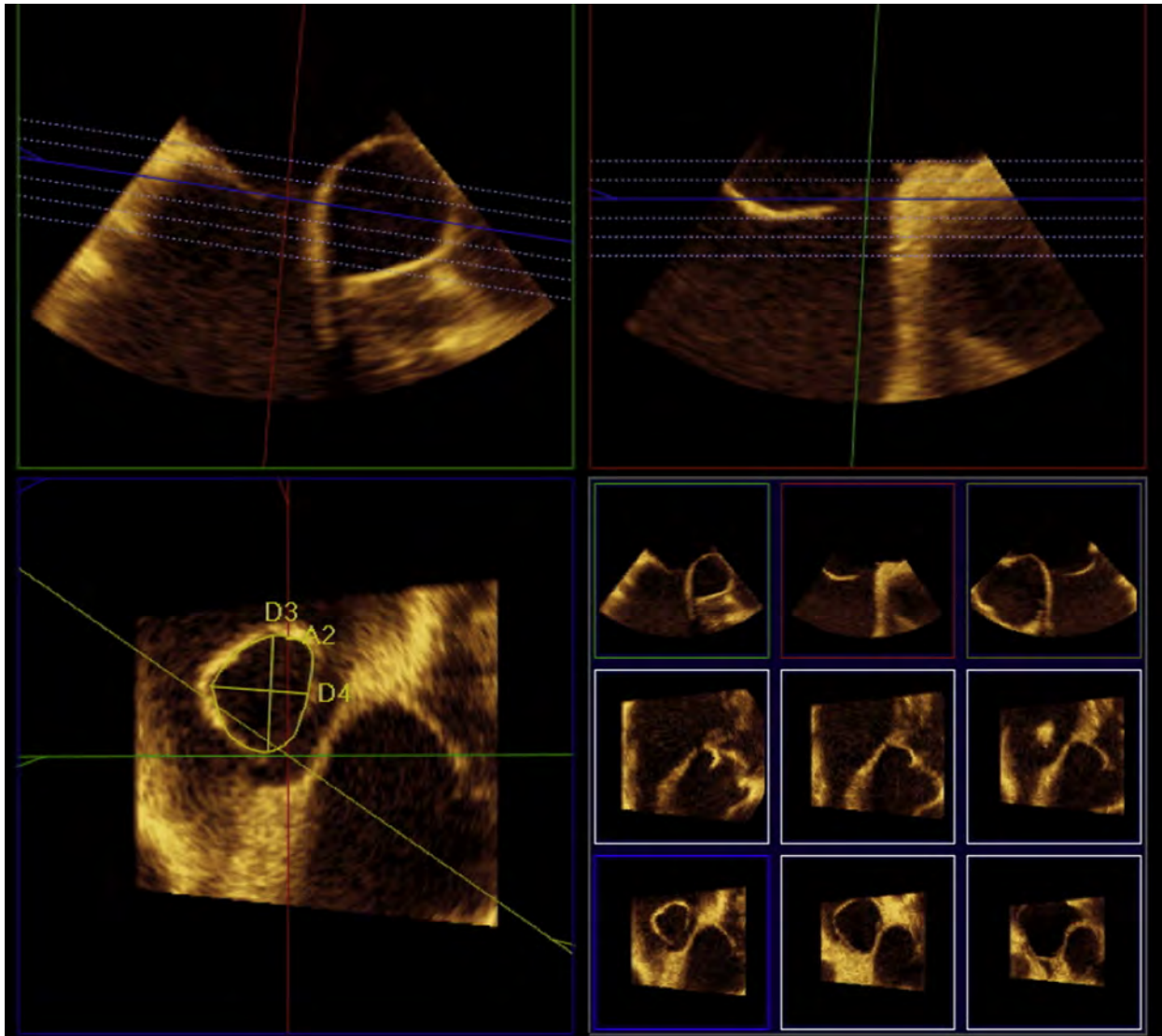


Figure 24 Once 3D volumes are acquired, postprocessing using commercially available 3D software packages will align the plane of the interatrial septum with multiple 3D plane slices. This approach facilitates an assessment of the shape of an ASD and allows for measurement of en face diameters and area in multiple orthogonal views, without the potential for bias due to malalignment of the ultrasound planes. See the section on Imaging of the Interatrial Septum: Imaging of the Interatrial Septum for more details.

owing to LA hypertension from mitral stenosis, impaired left ventricular (LV) compliance, or LV outflow obstruction.

In patients with ASD, measurement of the maximal dimension (width) using color Doppler has been correlated with the maximal dimension of the defect orifice when measured surgically. For example, in a small series of patients undergoing surgery, the TTE- and TEE-measured ASD color flow Doppler jet width measurements demonstrated correlation with the anatomic maximal dimension observed at surgery. Both TTE and TEE color flow Doppler echocardiography of the maximal jet width correlates with direct surgical measurement of the defect and, therefore, might provide an estimation of the ASD diameter.⁹⁸ Significant pitfalls exist when solely using the diameters measured by color Doppler to evaluate the size of an ASD; therefore, 2D or 3D measurements without color should be relied on. The variability in color quality between machine vendors and the variable color settings can result in excessive color bleed over the atrial septal tissue, resulting in an overestimation of the true defect size.

Shunt flow can be estimated by pulsed Doppler quantification of the pulmonary (Q_p) to systemic (Q_s) blood flow ratio.^{99,100} This is typically performed by pulse wave Doppler using TTE by interrogation of the RV and LV outflow tracts. The method involves measurement of the systolic velocity time integrals (VTIs) of the RV and LV outflow, and the maximal systolic diameters of the pulmonary and LV outflow regions. The diameters are then used for calculation of the corresponding outflow tract areas, assuming the outflow region to be circular. The mathematical estimation of the area of the RV and LV outflow tract (πr^2) multiplied by the corresponding VTI estimates the stroke volume for the right and left ventricle, respectively. The Q_p/Q_s ratio estimation is then the ratio of the pulmonary to systemic stroke volumes (RV stroke volume/LV stroke volume). This method has been validated and compared with oximetric methods in a small number of patients with secundum ASD, including those with pulmonary hypertension, mitral and tricuspid regurgitation, ventricular septal

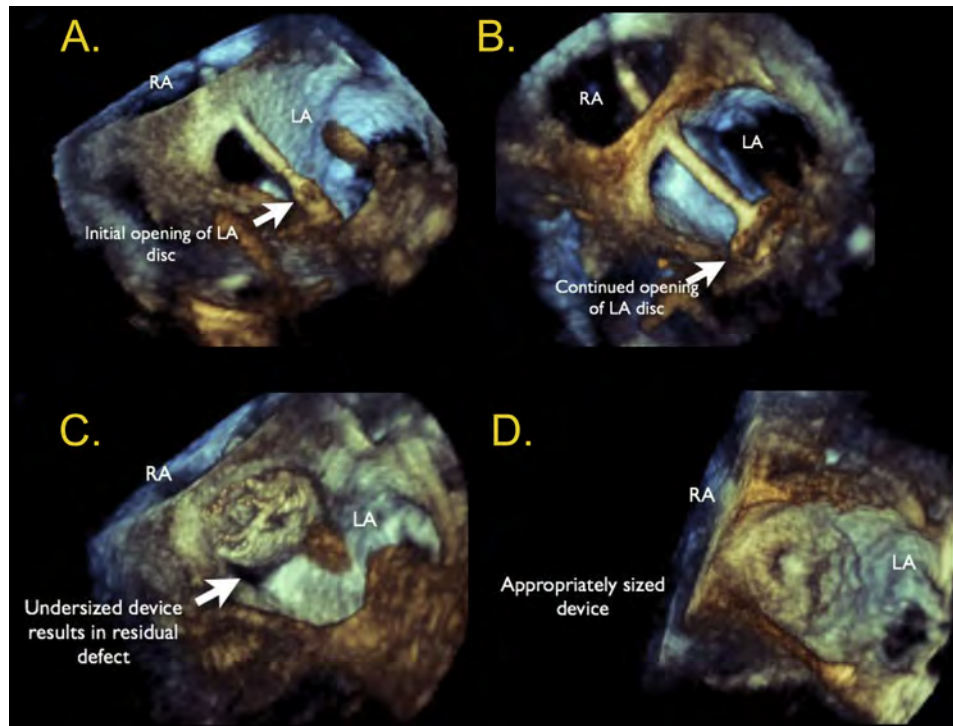


Figure 25 Intraprocedural RT3D TEE provides superior visualization of wires, catheters, and devices and their relationships to neighboring structures in a format that is generally more intuitively comprehended by the interventional cardiologist than 2D echocardiography. An ostium secundum ASD has been closed with an Amplatzer device under RT3D TEE guidance. All views are shown from the LA perspective. **(A)** The LA disc of the device opening in the LA. **(B)** View showing continued opening of the device. **(C)** An undersized device with a residual defect. This device was removed and **(D)** a larger closure device used.

Table 2 Advantages and disadvantages of TTE, TEE, and ICE in percutaneous transcatheter guidance of PFO and ASD

| Modality | Advantages | Disadvantages |
|----------|---|--|
| TTE | <ul style="list-style-type: none"> Readily available Low cost Unlimited multiple planes to evaluate IAS Noninvasive Does not require any additional sedation Excellent image quality in pediatric patients | <ul style="list-style-type: none"> Image quality in larger patients could be suboptimal Requires technologist or echocardiographer to perform study during closure Lower rim of IAS not well seen after device placement owing to shadowing in virtually all views |
| TEE | <ul style="list-style-type: none"> Improved image quality over TTE 3D technique adds incremental value over 2D technique in evaluating ASD size, shape, location Provides en face imaging that might be more intuitively understood to nonimagers | <ul style="list-style-type: none"> Requires additional sedation or anesthesia to perform Risks include aspiration and esophageal trauma Could require endotracheal intubation if prolonged procedure performed Requires additional echocardiographic operator to perform Patient discomfort |
| ICE | <ul style="list-style-type: none"> Comparable image quality to TEE Can be performed with patient under conscious sedation Reduces procedure and fluoroscopy times Superior to TEE for evaluating inferior aspects of IAS Interventionalist autonomy (can perform without additional support) | <ul style="list-style-type: none"> Invasive Risks of 8F–10F venous access and catheter, including vascular risk and arrhythmia Role of 3D technique to be defined Cost of single-use ICE catheters Limited far field views with some systems Need for additional training of ICE operator Operator might have two tasks (imaging and procedure) |

defect, and Eisenmenger complex.⁹⁹ Semilunar valve regurgitation modifies the stroke volume in proportion to the degree of regurgitation and can limit the estimation of shunt flow when a significant degree of regurgitation is present. A similar method has been used with

inflow velocity and AV valve annular dimensions in diastole and also correlated with oximetric methods.¹⁰¹

Color flow Doppler can also detect shunting across a PFO; however, the shunting is often intermittent and might not be readily detectable

using color flow Doppler. When a PFO is stretched by differences in the LA and RA pressure, a left-to-right color Doppler shunt might be seen (Figures 4–6). First-generation contrast echocardiography with agitated saline combined with physiologic maneuvers to provoke right-to-left shunting, increases the sensitivity of PFO detection.^{102–105} The microbubbles generated with agitation are too large to pass through normal pulmonary vasculature and are easily detected by echocardiographic imaging because of their increased echogenicity (Figure 29). The provocative maneuvers used to transiently increase RA pressure include the Valsalva maneuver and cough.

Transthoracic echocardiography with first-generation contrast can be used to detect PFOs with reasonable sensitivity and specificity; however, TEE is considered the reference standard for detection of a PFO. Whether using TTE or TEE, the accuracy of the test will be improved by the use of a standardized protocol that includes multiple injections of agitated saline with provocative maneuvers to transiently increase the RA pressure.^{50,106,107} An example of a protocol used by many laboratories is presented:

- Intravenous catheter, typically placed in antecubital vein, connected to a three-way locking stopcock
- Combine in 10-mL syringe connected to the stopcock 8 mL of saline plus 1 mL of blood from the patient plus 1 mL air; the addition of blood to the contrast solution results in increased intensity of the microbubbles detected by echocardiography¹⁰⁸
- Many laboratories prefer to avoid the use of the patient's blood in the contrast mixture preparation, and this can result in diagnostic quality opacification; in such cases, approximately 9 mL of saline and 1 mL of air are used
- Rapidly mix back and forth with an empty 10-mL syringe attached to the stopcock to manufacture bubbles
- Inject rapidly into the antecubital vein while acquiring a long clip length (i.e., 10 seconds) with the echocardiography system; the echocardiographic images are usually recorded from the four-chamber view for TTE, and the angle best profiling the atrial septum is used for TEE, usually 30°–100°
- The use of biplane imaging might enhance detection of a small right-to-left shunt

The appearance of microbubbles in the LA within 3–6 cardiac beats after opacification of the RA is considered positive for the presence of an intracardiac shunt such as a PFO (Figure 29). Ideally, bubbles will be visualized crossing the atrial septum through the PFO (Figure 38). Physiologic maneuvers to transiently increase RA pressure are typically required to promote right-to-left shunting of microbubbles to identify a PFO when no shunting is present without provocation. The Valsalva maneuver using held expiration and release is one common maneuver performed. The Valsalva strain must be held long enough for microbubbles to fill the RA. The effectiveness of the Valsalva maneuver can be assessed echocardiographically by the presence of a leftward shift of the atrial septum with release of Valsalva, indicating the achievement of RA pressure greater than LA pressure.

The appearance of microbubbles in the LA after 3–6 cardiac beats indicates intrapulmonary shunting, such as an arteriovenous malformation. Intrapulmonary shunting is confirmed when the bubbles are visualized entering the LA from the pulmonary veins and not visualized crossing the atrial septum. Other reasons for a false-positive bubble study for PFO are sinus venosus septal defect or other unidentified ASD or pseudocontrast caused by the strain phase of Valsalva with transient stagnation of blood in the pulmonary veins.

Bubble studies can result in false-negative findings because of inadequate opacification of the RA, an inadequate Valsalva maneuver, the presence of a eustachian valve directing venous return from the IVC to the atrial septum (preventing microbubbles entering from the SVC to cross the atrial septum), an inability to increase the RA pressure

above the LA pressure such as in the presence of LV diastolic dysfunction, and poor image quality.^{70,109} In patients with poor image quality, the use of second-harmonic imaging can improve the identification and detection of microbubbles. Digital compression algorithms can decrease the sensitivity for detection of small intracardiac shunts, and some laboratories have continued to record contrast studies on analogue videocassette to maximize the sensitivity for the detection of small shunts.¹¹⁰

Specific routes of saline contrast administration for bubble studies can be used in specific clinical scenarios. For example, a left antecubital vein saline contrast injection can be used to diagnose a persistent left SVC draining into the coronary sinus. Leg vein saline contrast administration can be used in the adult patient who has undergone ASD closure but has persistent cyanosis after the procedure, because an inferior sinus venosus ASD might have been incompletely closed, with persistence of IVC flow into the LA. A leg vein injection also can rarely be used to overcome a very large Chiari or eustachian network that might impede the bubbles entering the RA from the SVC.

Sedated patients can have difficulty performing an adequate Valsalva maneuver, as described in the section on Techniques, Standards, and Characterization Visualization of Shunting: TTE and TEE. In that circumstance, pressure on the abdomen can be applied to transiently increase the RA pressure. If the patient is under general anesthesia, the Valsalva maneuver can be mimicked by held inspiration and then release. Reports have included attempted quantification of right-to-left shunting based on the number of microbubbles appearing in the left heart on an echocardiographic still frame; however, this number is dependent on the amount of microbubbles injected and the adequacy of the Valsalva maneuver.

Transcranial Doppler Detection/Grading of Shunting

Transcranial Doppler is an alternative imaging method for the detection of a PFO. This method uses power M-mode Doppler interrogation of the basal cerebral arteries to detect microbubbles that have crossed right to left into the systemic circulation. Specialized equipment is used to focus the ultrasound system and display the results. As with contrast-enhanced TTE and TEE, TCD studies are performed with normal respiration and with the Valsalva maneuver to maximize the sensitivity and specificity of the test. The results are reported referenced to a six-level Spencer logarithmic scale, and higher grades have been associated with larger right-to-left shunts.^{111,112}

The advantages of TCD over TEE and TTE include increased patient comfort (compared with TEE), semiquantitative assessment of shunt size, and the ability to identify extracardiac and intracardiac shunting. The identification of extracardiac shunts is also a limitation of TCD, because no anatomic information is provided regarding the location of the shunt or associated abnormalities. Hence, TCD and contrast echocardiography can be complementary techniques for the evaluation of right-to-left shunting.¹¹³ Some laboratories prefer to combine modalities and perform simultaneous contrast-enhanced TTE or TEE with TCD.

The detection and grading of shunting by any technique is complicated by physiologic variations in the presence and/or timing of the shunting. Respiratory phasic changes in RA pressure can result in delayed right-to-left shunting and misclassification of interatrial flow as an intrapulmonary shunt.⁷⁰ Elevated LA pressure from LV failure, mitral stenosis, or mitral regurgitation can prevent right-to-left shunting, because higher RA pressure is required to overcome the elevated LA pressure. In a study comparing patients with versus without left heart disease, the detection of PFO was 5% in the patients with left

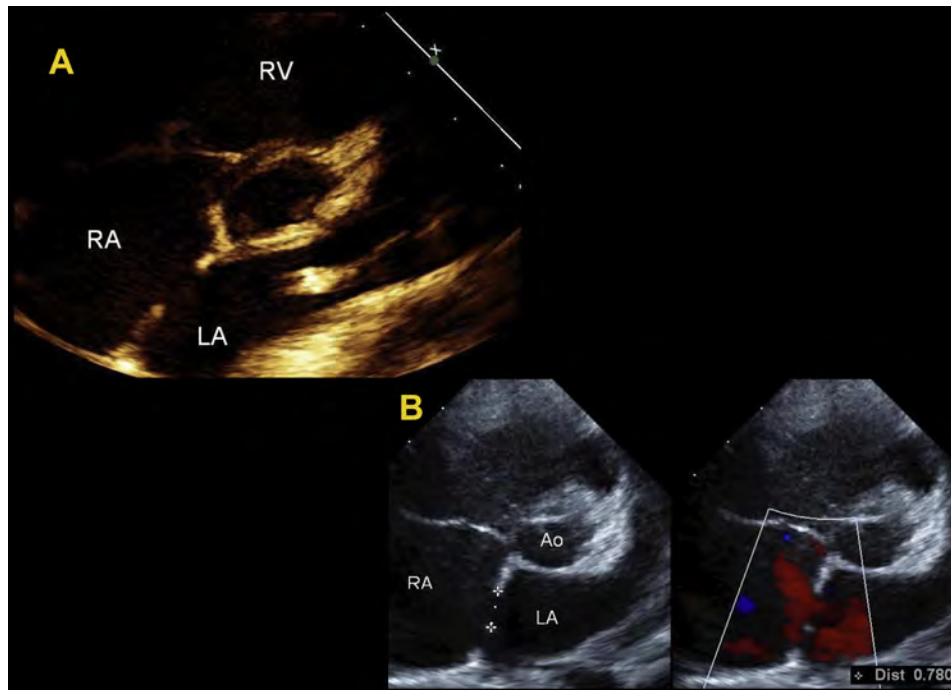


Figure 26 (A) Two-dimensional TTE of ostium secundum ASD from parasternal short-axis view. (B) Two-dimensional TTE (*left*) and with color Doppler (*right*) of an ostium secundum ASD from the parasternal short-axis view with measurement of the diameter in the anterior–posterior orientation and left to right flow by color Doppler. Ao, aortic root.

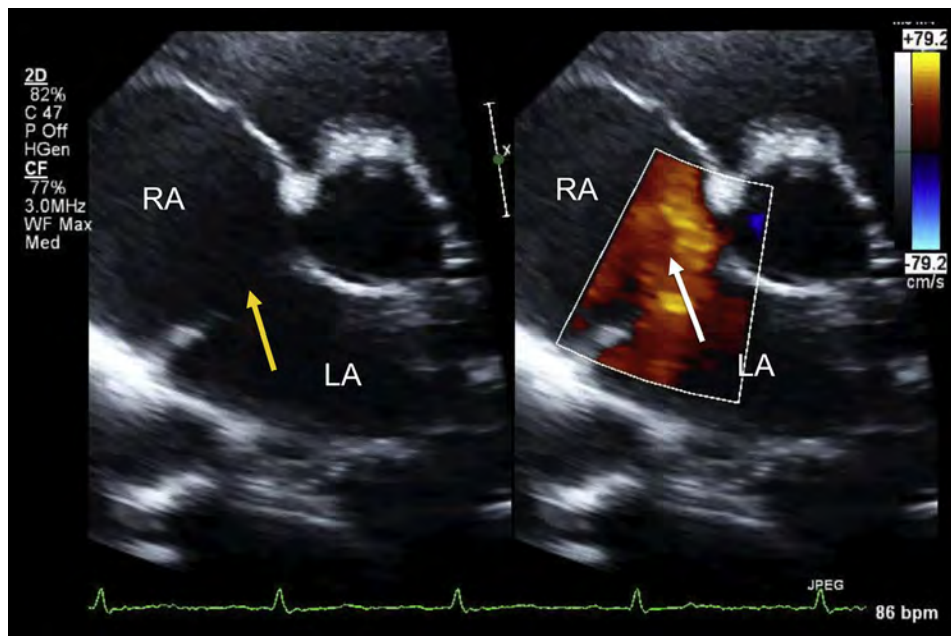


Figure 27 TTE of a secundum type ASD in the parasternal short-axis view without and with color Doppler in pediatric patient. See also Video 14.

heart disease and 29% in those without left heart disease, similar to that in the general population.¹¹⁴

Impact of Shunting on the Right Ventricle

Echocardiographic evaluation of hemodynamic changes to the RV has been described in detail in previous Guidelines documents.^{9,115}

The hemodynamic effects of ASD are primarily related to the direction and magnitude of shunting, which is determined by the size of the defect, the relative compliance of the RVs and LVs, and the relative systemic and pulmonary vascular resistances. In most patients, the greater compliance of the RV compared with the LV, and the lower resistance of the pulmonary compared with the systemic circulation, results in a net left-to-right shunt. The most

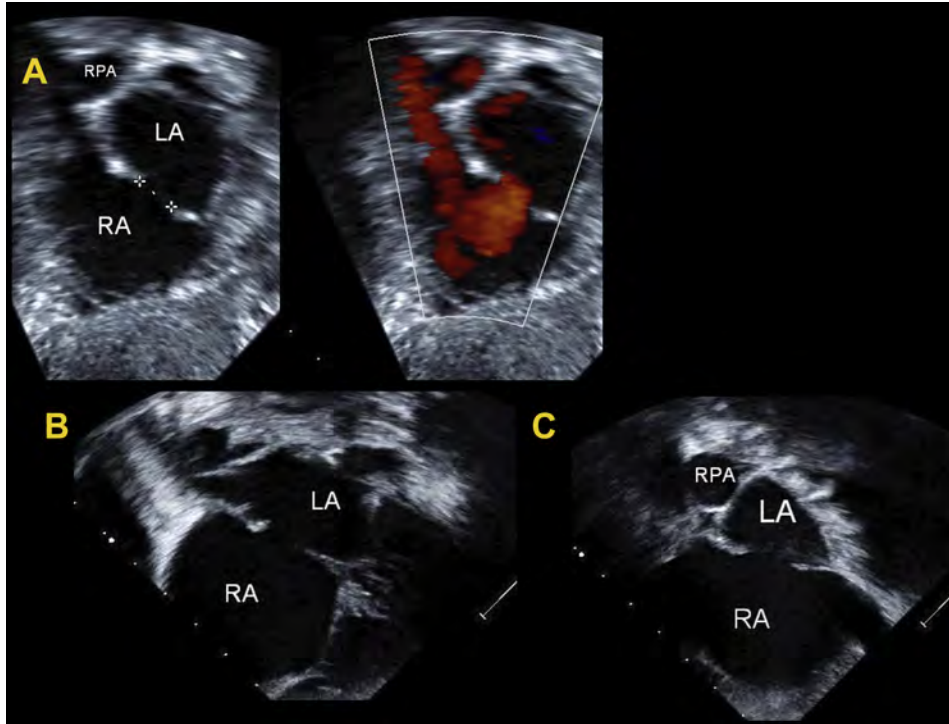


Figure 28 (A and B) Examples of ostium secundum by 2D TTE (*left*) and with color Doppler (*right*) in the subcostal left anterior oblique view. (A) Measurement of the ASD diameter (*left*) and left to right color Doppler flow (*right*). (C) Sagittal subcostal view in a patient with secundum ASD. RPA, right pulmonary artery.

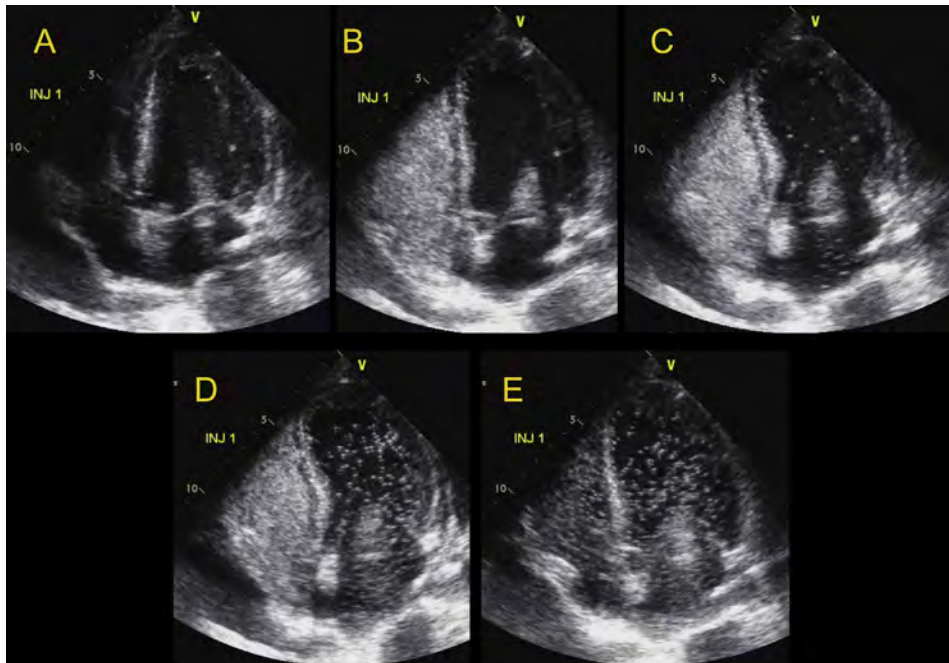
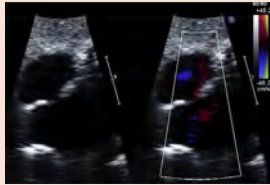
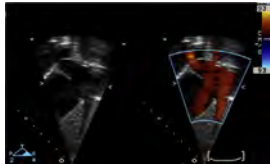
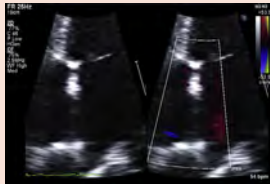
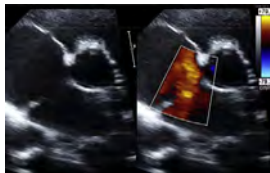


Figure 29 TTE of an apical four-chamber view during saline contrast injection. (A) Initial images demonstrate prominent artifact over mitral valve. (B) Complete opacification of the RA and RV. (C) Delayed entry of contrast into the LA and LV, consistent with a pulmonary arteriovenous malformation. If the bubbles cross within the first three cardiac cycles, an intracardiac shunt is present. Subsequent cardiac cycles (D and E) demonstrate continued opacification of the LA and LV consistent with intrapulmonary shunting. See also Videos 15 and 16. Video 14 demonstrates the above sequence. Video 16 is an ICE image demonstrating a PFO, with immediate passage of saline contrast from right to left, seen clearly to cross a PFO. INJ, injection.

Table 3 TTE views for assessment of atrial septal anatomy

| View | Example | Septal anatomy | Procedural assessment |
|---|---|--|--|
| Subxiphoid long-axis (frontal) or left anterior oblique (45°) |  | Right pulmonary vein ASD rim, atrial septal defect diameter, and atrial septum length | Position of device with regard to right pulmonary veins and assessment for residual leak |
| Subxiphoid short-axis (sagittal) |  | SVC and IVC rim and atrial septal defect diameter | Position of device with regard to SVC and IVC and assessment for residual leak |
| Apical four-chamber |  | Rim of defect to AV valves, assessment of RV dilation RV pressure estimate from tricuspid regurgitation jet | Position of device with regard to AV valves |
| Parasternal short-axis |  | Aortic and posterior atrial wall rim, atrial septal defect diameter, assessment of RV dilation | Device relationship to aortic valve, assessment for impingement on aorta or straddle, and relationship of device to posterior wall |

pronounced echocardiographic finding associated with this left-to-right shunt is dilatation of the RV.

RV linear dimensions are best measured from a RV-focused apical four-chamber view. Care should be taken to obtain the image demonstrating the maximum diameter of the RV without foreshortening. This can be accomplished by ensuring that the crux and apex of the heart are in view. An RV diameter greater than 41 mm at the base and greater than 35 mm at the midlevel indicates RV dilatation. Similarly, a longitudinal dimension greater than 83 mm indicates RV enlargement.¹¹⁵

The RV area has been shown to correlate with the cardiac magnetic resonance-derived RV volume and can serve as a semiquantitative surrogate for the identification of RV dilatation.^{116,117} The 3D echocardiographically derived RV volume is the most accurate echocardiographic method to estimate the RV volume compared with cardiac magnetic resonance. Compared with 2D techniques, 3D echocardiography results in better reproducibility and less underestimation of the RV volume.¹¹⁸⁻¹²⁰ An RV end-diastolic volume indexed to the body surface area of 87 mL/m² or greater for men and 74 mL/m² or greater for women is considered increased.¹²¹ In the setting of significant RV dilatation, it can be difficult to enclose the entire RV in the 3D volume of interest for calculation of the volume.

The interventricular septal shape/ventricular configuration is another marker of RV size. As the RV dilates in the setting of volume overload, such as left-to-right shunting through an ASD, the interventricular septum becomes displaced toward the LV in diastole, resulting in a flattened appearance compared with the normal round appearance in the normal heart. In addition to the diastolic septal flattening associated with RV volume overload, systolic septal flattening can also be present in those patients with an ASD who have associated pulmonary hypertension. Visual assessment of the diastolic and systolic ventricular septal curvature, looking for a D-shaped pattern, should be used to help in the diagnosis of RV volume and/or pressure overload. Although a D-shaped ventricle formed by flattening of the septum is not diagnostic in RV overload. With its presence, additional emphasis should be placed on the confirmation, as well as the determination, of the etiology and severity of right-sided pressure and/or volume overload.⁹ The severity of septal flattening increases with increasing RV dilatation and has been quantified with an eccentricity index derived from the perpendicular LV minor axis dimensions from the parasternal short-axis view.¹²² The ratio of the minor axis diameter parallel to the ventricular septum compared with the minor axis diameter that bisects the ventricular septum can be calculated at end-diastole. A ratio greater than 1 is associated with RV volume overload.

Pulmonary Artery Hypertension

The pulmonary vasculature normally accommodates the increased volume of flow secondary to ASD without a significant increase in PA pressure. With continued RV volume overload and increased PA flow over time, a small percentage of patients will develop pulmonary hypertension, with an even smaller percentage developing irreversible pulmonary vascular disease.¹²³ The type of ASD is also associated with the frequency and rapidity of development of pulmonary hypertension, with the sinus venosus defect more frequently associated with pulmonary hypertension than secundum ASD and at younger ages.¹²⁴ Evaluation for pulmonary hypertension is therefore an important part of the echocardiographic evaluation of an ASD before intervention. The systolic PA pressure is best estimated from the RV systolic pressure using the tricuspid regurgitation jet velocity (V) and the simplified Bernoulli equation: RV systolic pressure = $4(V)^2$ + estimated RA pressure. The normal peak RV systolic pressure should be less than 30–35 mm Hg. The PA diastolic pressure can be similarly estimated from the pulmonary regurgitation end-diastolic velocity, and the mean PA pressure can be estimated from the peak PA velocity.^{125,126} Although accurate estimates of PA pressure can be calculated using noninvasive techniques, noninvasive estimation of the pulmonary vascular resistance is more problematic. However, it has been described using a ratio of peak tricuspid regurgitation velocity (in meters per second) compared with the RV outflow tract VTI (in centimeters).¹²⁵

RV Function

In general, RV function (systolic or diastolic) is not adversely affected by the presence of an ASD; however, in some settings, RV function will be impaired, such as in the presence of significant pulmonary hypertension. When an evaluation of RV systolic function is required, the methods available include dP/dt , myocardial performance index, tricuspid annular plane systolic excursion, RV fractional area change, RV ejection fraction from 3D volumetric evaluation, Doppler tissue imaging (DTI) S' velocity, DTI isovolumic myocardial acceleration, and deformation evaluation with RV strain and strain rate. For evaluation of RV diastolic function, the methods include transtricuspid E and A wave velocities, E/A ratio, DTI E' and A' velocities, E/ E' ratio, isovolumic relaxation time, and deceleration time. The reader is referred to the recent Guidelines describing the "Echocardiographic Assessment of the Right Heart in Adults" for details regarding the performance of these techniques and their strengths and weaknesses.⁹

LV Function

Age-related LV diastolic dysfunction can lead to increased left-to-right shunting across an ASD with associated worsening of RV volume overload and late presentation of symptoms in older adults. These patients are also at increased risk of acute heart failure with pulmonary edema after closure of their ASD. This acute presentation is thought to be secondary to the combination of acute volume loading of the left heart in the setting of LV diastolic dysfunction that becomes unmasked with closure of the ASD.^{127,128} Preprocedural echocardiographic evaluation of LV diastolic function with assessment of mitral inflow and annular velocities can identify some of these patients at risk of post-ASD closure heart failure and pulmonary congestion. However, LV diastolic dysfunction can be masked by the ASD and pressure equalization between the left heart and right heart.¹²⁹ In those cases, invasive test occlusion of the ASD and measurement of the LA pressure can identify those patients at risk of developing pulmonary edema. Pre-ASD closure treatment with di-

uretics and afterload reduction will help prevent post-ASD closure heart failure. If medical therapy is not adequate to decrease the LA pressure, a fenestrated ASD closure device can be used to avoid the development of acute left heart failure.

KEY POINTS

- The direction of shunting through an ASD by color Doppler is typically left to right. The color scale settings should be optimized for the expected low velocity of shunt flow (i.e., 25–40 cm/sec).
- ASD shunt flow can be right to left or bidirectional in the setting of significant pulmonary hypertension or impaired RV compliance. Pulse wave spectral Doppler can be used for detection of bidirectional shunting in addition to color Doppler.
- Color flow Doppler can detect shunting across a PFO when it has been stretched open by differences in atrial pressure; however, the shunting is often intermittent and might not be readily detectable using color flow Doppler.
- TTE with first-generation contrast can be used to detect a PFO; however, TEE is considered the reference standard for detection of a PFO.
- Whether using TTE or TEE, accuracy will be improved by the use of a standardized contrast protocol that includes multiple injections of agitated saline with provocative maneuvers to transiently increase the RA pressure.
- The appearance of microbubbles in the LA after 3–6 beats indicates intrapulmonary shunting, such as an arteriovenous malformation.
- Bubble studies can provide false-negative findings owing to inadequate opacification of the RA, an inadequate Valsalva maneuver, a prominent eustachian valve directing venous return from the IVC to the IAS and preventing microbubbles entering from the SVC to cross the IAS, an inability to increase the RA pressure above the LA pressure, and poor image quality.
- TCD is an alternative method for the detection of a PFO with advantages that include increased patient comfort (compared with TEE), semiquantitative assessment of shunt size, and the ability to identify extracardiac and intracardiac shunting.
- The most pronounced echocardiographic finding associated with a left-to-right shunt is dilatation of the RV, for which multiple echocardiographic methods are available for measurement.
- Echocardiographic assessment of the magnitude of shunting by Q_p/Q_s estimation and the assessment of RV function completes the assessment of patients with an ASD.

IMAGING OF IAS AND SEPTAL DEFECTS


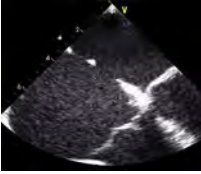


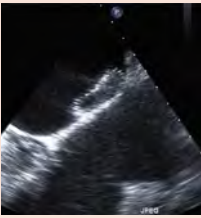
Patent Foramen Ovale

The occurrence of a PFO is common, present in 20%–25% of the population,^{5,130} and the anatomy has been extensively discussed earlier in the present document. PFO has been associated with cryptogenic stroke, decompression sickness, platypnea-orthodeoxia syndrome, and migraine headache.^{131–138} Controversy exists regarding the role of PFO in these syndromes, and currently, the Food and Drug Administration (FDA) has not approved a role for transcatheter procedures to close the PFO in an attempt to decrease the incidence of these problems. Echocardiography has a central role in the evaluation of PFO and monitoring/guidance of PFO closure, similar to its role in ASD closure.

A TTE evaluation of PFO, including the use of agitated saline contrast, is primarily used to identify the presence or absence of a PFO according to the presence or absence of right-to-left shunting. Once a PFO has been identified, and percutaneous device closure is being considered, a detailed evaluation of the atrial septal anatomy is performed using TEE. TEE can also be used if a PFO is suspected; however, TTE is technically inadequate to rule out the presence of a PFO.

The TEE views used for the evaluation of a PFO are similar to those used for the evaluation of an ASD. Starting in the transverse plane at the mid-esophagus with settings optimized to visualize the atrial septum, the TEE imaging plane should be rotated or steered, starting

Table 4 Views for assessment of ASD by TEE

| View | Example | Atrial septal anatomy | Procedural assessment | Suggested multiplane angles | Esophageal position |
|------------------|---|---|--|-----------------------------|---|
| Basal transverse |  | SVC, superior aortic, RUPV | Device relationship in atrial roof | 0°, 15°, 30°, 45° | Mid- to upper esophagus |
| Four-chamber |  | Posterior and AV rims, maximal ASD diameter | Device relationship to AV valves | 0°, 15°, 30° | Mid-esophagus |
| Short-axis |  | Posterior and aortic rims, maximal ASD diameter | Device relationship to AoV and posterior atrial wall | 30°, 45°, 60°, 75° | Mid- to upper esophagus |
| Bicaval |  | IVC and SVC rims, maximal ASD diameter | Device relationship to RA roof/dome | 90°, 105°, 120° | Mid- to upper esophagus and deep transgastric |
| Long-axis |  | Dome/roof of LA | Device relationship to LA dome/roof | 120°, 135°, 150° | Mid- to upper esophagus |

at a 0° multiplane angle, in 15° increments, for complete evaluation of the atrial septum. Side-by-side imaging with color Doppler at a low color Doppler scale is helpful for identifying flow through the PFO and possible additional defects in the atrial septum. The probe will need to be withdrawn for better evaluation of the atrial septum near the SVC and inserted for better evaluation of the atrial septum near the IVC. Alternatively, an initial evaluation of the atrial septum can be performed in the transverse plane, starting at the high esophageal level at the SVC and advancing the probe in the esophagus, imaging through the fossa ovalis and ending at the level of the IVC. A similar maneuver can be performed with the imaging plane at 90°–120°.

Starting at 30°–50°, with the AoV in cross-section, the PFO should be visualized adjacent to the aorta. Rotation of the imaging plane in 15° increments should line the imaging plane with the pathway or tunnel of the PFO. From this angle, the length of the PFO tunnel can be assessed. The thickness of the septum secundum can also be evaluated from this view.

With the PFO visualized, agitated saline contrast is injected to evaluate for right-to-left shunting, as described in the section on Techniques, Standards, and Characterization Visualization of Shunting: TTE and TEE. Provocative maneuvers such as the Valsalva maneuver should be performed to transiently increase the

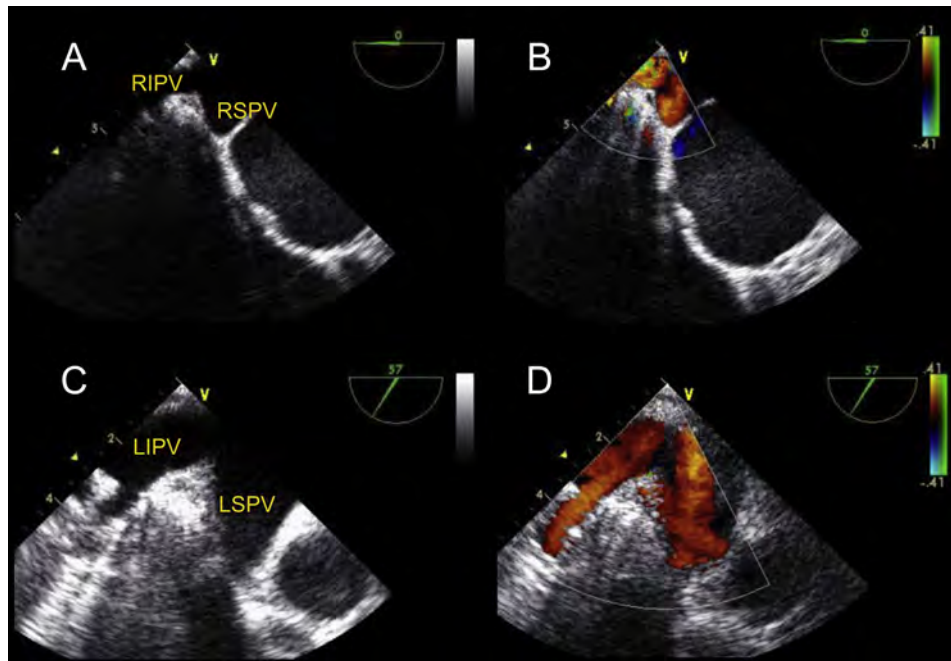


Figure 30 TEE demonstrating from the upper esophageal short-axis view demonstrating the right pulmonary veins at (A) 0° without and (B) with color Doppler and (C) without and (D) with color Doppler at 60°. LIPV, left inferior pulmonary vein; LSPV, left superior pulmonary vein; RIPV, right inferior pulmonary vein; RSPV, right superior pulmonary vein.

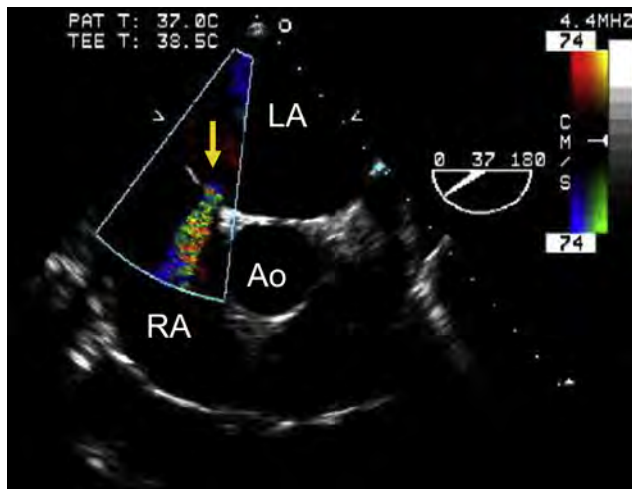


Figure 31 TEE of small ostium secundum ASD (yellow arrow) at the midesophageal aortic valve short-axis view from the midesophagus. Ao, ascending aorta.

RA pressure over the LA pressure. Sedated patients could have difficulty performing an adequate Valsalva maneuver (see the section on Techniques, Standards, and Characterization Visualization of Shunting: TTE and TEE).

Important anatomic details of the atrial septum that should be evaluated because they can influence device candidacy and selection include the location of the PFO (although, unlike secundum ASD, the location of a PFO is fairly consistent in the anterior or superior portion of the fossa ovalis), thickness and extent of septum secundum, total length of the atrial septum, length of the PFO tunnel, size of the PFO at the RA and LA ends, distance of the PFO from the venae cavae, presence of ASA (see the section on Imaging of IAS and Septal Defects: Atrial Septal Aneurysm), and presence of additional

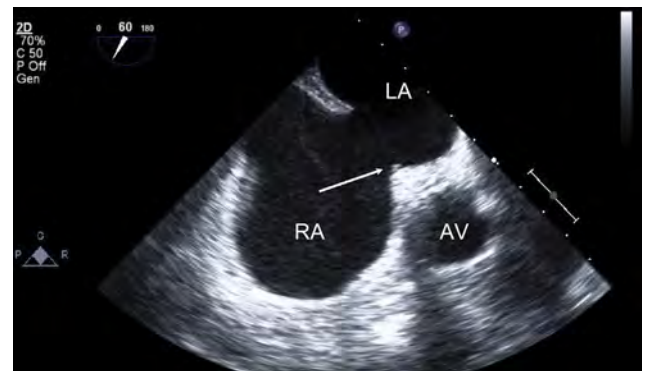


Figure 32 TEE of large ostium secundum ASD from midesophageal AoV short-axis view. Short-axis view of ostium secundum ASD. Note aortic rim (arrow). AV, aortic valve/aorta.

atrial septal fenestrations or defects. As with ASD, partial anomalous pulmonary venous connection should be excluded.

Real-time 3D (RT3D) TEE has been used to better define PFO variations compared with 2D TEE.⁸² RT3D TEE has shown that the shape of the PFO is elliptical, not circular, and that the flow area decreases traversing from the RA to the LA. As with secundum ASD, the area of the PFO changes during the cardiac cycle and is larger during ventricular systole than diastole.⁸² RT3D TEE has also been used for procedural guidance of closure with en face views of the atrial septum showing the relationship of the PFO and device with the surrounding structures in the RA and LA¹³⁹ (Figure 44).

Specific anatomic characteristics of a PFO should be evaluated when deciding on device selection for PFO closure.¹⁴⁰ Specifically, the diameter of the fossa ovalis, length of the PFO tunnel, presence and size of an ASA, thickness of the septum secundum, and maximum size of the PFO during the cardiac cycle are all important in appropriate patient selection for transcatheter closure. In one series,

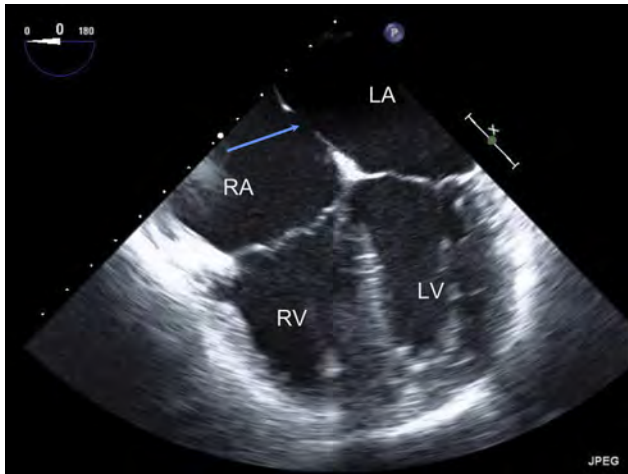


Figure 33 TEE of large ostium secundum ASD from midesophageal four-chamber view. Note ASD (*blue arrow*).



Figure 34 TEE of closure device in ostium secundum ASD from midesophageal four-chamber view. Note relationship between AV valves. Note ASD closure device (*blue arrow*).

using these parameters to choose from among four types of closure devices resulted in an improved closure rate and a decreased incidence of complications compared with the use of a single-device strategy for all PFOs.¹⁴⁰

Atrial Septal Aneurysm

An ASA is a redundancy or saccular deformity of the atrial septum associated with increased mobility (Figures 7 and 10). An ASA is defined as an excursion of 10 mm from the plane of the atrial septum into the RA or LA or a combined excursion right and left of 15 mm. M-mode can be used to document this motion when the cursor can be aligned perpendicular to the plane of the septum (Figure 45). A more detailed classification system (that has not been widely clinically adopted) has divided ASAs into five groups based on the excursion exclusively into the RA or LA, predominantly into the RA or LA, or with equal excursion right and left.¹⁴¹

ASA has been associated with the presence of a PFO or ASD, an increased size of a PFO, and an increased prevalence of cryptogenic stroke and other embolic events. ASA has also been associated with multiple septal fenestrations. TEE is a more sensitive method than TTE for evaluation of an ASA. The presence and extent of an ASA is a factor in device selection for PFO closure. A device can be chosen

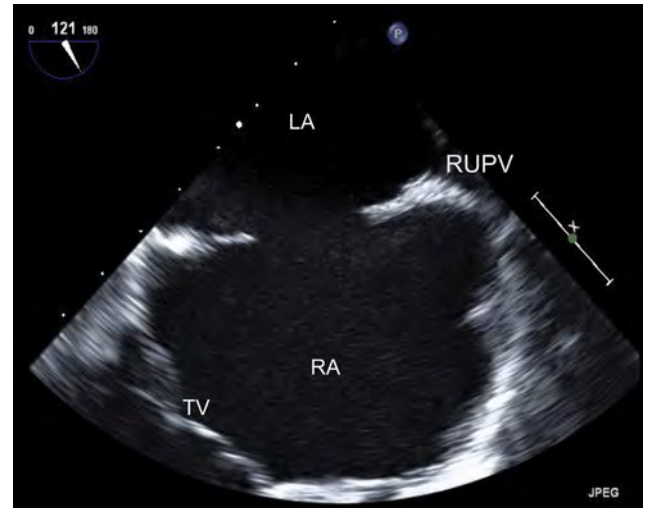


Figure 35 TEE of large ostium secundum ASD from midesophageal modified bicaval view (includes the tricuspid valve). See also Video 17.

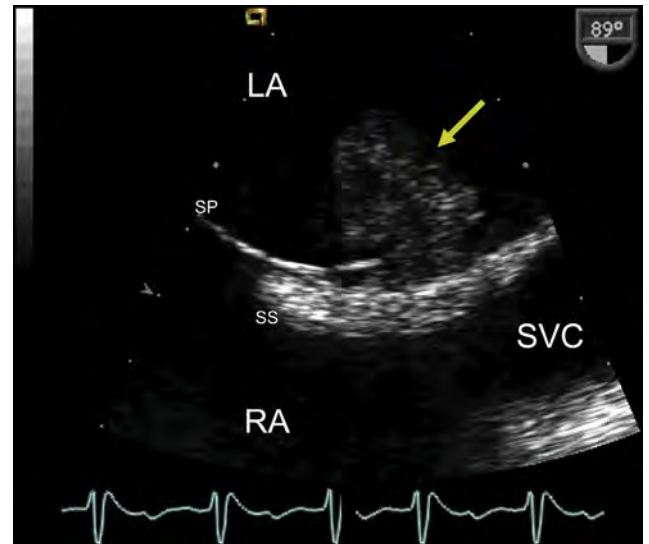


Figure 36 Zoomed bicaval TEE view of thrombus (*yellow arrow*) attached to the IAS at the left atrial septal pouch. This might represent a thrombus in transit crossing a PFO (paradoxical embolism) or an in situ thrombus in the left atrial septal pouch. SP, septum primum; SS, septum secundum.

that is relatively large to encompass and stabilize the atrial septum or a smaller and softer device might be chosen for better conformation with the ASA.

The excursion of the atrial septum can be documented using 2D imaging, as well as M-mode assessment when the M-mode cursor can be aligned perpendicular to the plane of the IAS. This can be done in the subcostal four-chamber views on TTE, in the bicaval views on TEE, and in the septal long-axis views on ICE (Figure 45).

Eustachian Valve and Chiari Network

The eustachian valve extends anteriorly from the IVC–RA junction and is best visualized on TTE from the subxiphoid coronal and sagittal views. On TEE, the eustachian valve is best visualized in the longitudinal plane. The size of the eustachian valve and proximity to the IAS

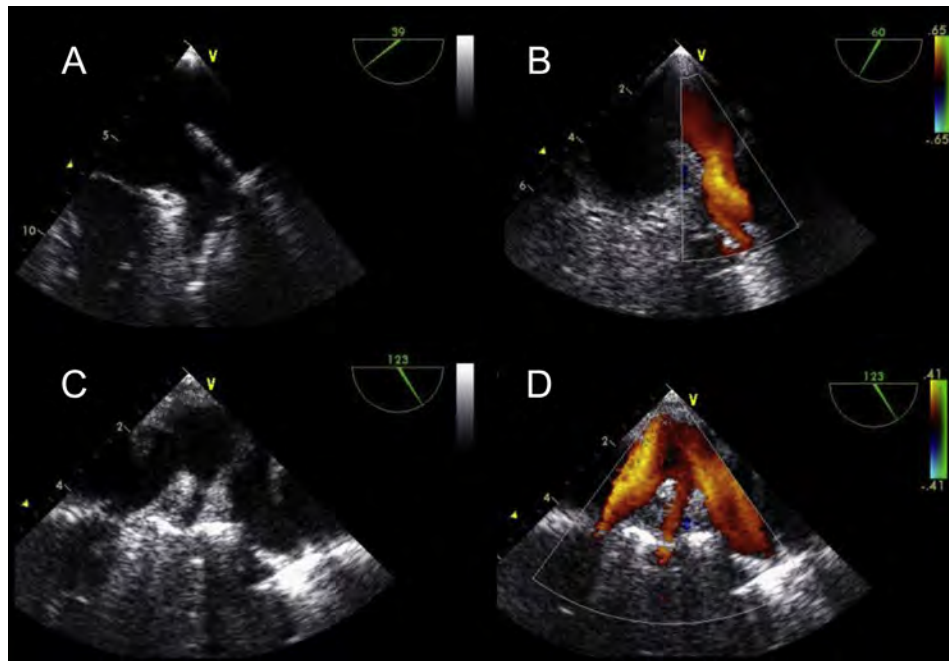


Figure 37 TEE demonstrating left pulmonary veins in two different views. Midesophageal views (A) without and (B) with color flow Doppler obtained at 60° (mitral commissural view) with the probe then rotated slightly to the left to reveal the left-sided pulmonary veins. Midesophageal long-axis views with the probe rotated toward the left pulmonary veins at 120° (C) without and (D) with color Doppler.

should be noted on the echocardiographic evaluation, because a large eustachian valve that is close to the IAS can interfere in the deployment of the RA side of a closure device.

A Chiari network is a remnant of the right valve of the sinus venosus and appears as a filamentous structure in various places in the RA, including near the mouth of the IVC and coronary sinus (Figure 20). A Chiari network can interfere in the passage through the RA of wires, catheters, sheaths, cables, and the device. Therefore, the identification of the presence of a Chiari network should be a part of the echocardiographic evaluation before device closure of an ASD or a PFO.¹⁴²

Assessment of ASDs: Standards and Characterization

ASDs represent a diverse group of differing anatomic lesions that all result in intracardiac shunting. The types of ASDs and other interatrial communications have been fully described in previous sections. The common features of all ASD types that should be systematically evaluated and reported for all ASD types are listed in Table 7. These include the type of ASD (primum or secundum) or other atrial communication (venosus or unroofed coronary sinus), the presence and direction of Doppler flow through the defect, and associated findings such as anomalous pulmonary vein drainage, the presence and size of an eustachian valve or a Chiari network, the size and shape of the defect or defects, the location in the septum, the presence or absence of multiple fenestrations, and the size of the ASD at end-systole and end-diastole.

Ostium secundum ASD is the most common defect encountered and most commonly occurs as a deficiency in septum primum.²⁸ Secundum ASDs can vary considerably in their size, shape, and configuration, as has been described previously. A small ASD is typically described as less than 5 mm in the maximal measured ASD diameter.¹⁴³ With favorable anatomic features, ostium secundum ASDs can be amenable to percutaneous transcatheter closure. This topic is specifically

reviewed later in the present document.³⁰⁻³³ Secundum ASDs have a variable amount of surrounding tissue that borders the defect, and these “rims” of surrounding tissue are named for the corresponding surrounding adjacent anatomic structures. By convention, there are six anatomically named rims of surrounding tissue. These rims should be assessed carefully using echocardiography in all patients and, in particular, before consideration of percutaneous closure. A rim length of 5 mm or more is considered a favorable characteristic for percutaneous transcatheter closure of a secundum ASD. An ASD rim length of less than 5 mm is described as “deficient” and could present challenges for transcatheter closure. Secundum ASD rims can be defined as follows:

1. Aortic rim: the superior/anterior rim between the ASD and the AoV annulus and aortic root
2. AV valve rim: the inferior/anterior rim between the ASD and the AV valves
3. SVC rim: the superior/posterior rim between the ASD and the SVC
4. IVC rim: the inferior/posterior rim between the ASD and the IVC
5. Posterior rim: the posterior rim between ASD and posterior atrial walls
6. Right upper pulmonary vein (RUPV) rim: the posterior rim between the ASD and the RUPV

Having adequate superior, inferior, and anterior rims (SVC, RUPV, IVC, and AV valve rims) is particularly important for successful transcatheter ASD closure. A deficient aortic rim has been implicated as a potential risk factor for erosion,^{103,104} although it might not represent an absolute contraindication to device closure. Erosion is discussed in greater detail in the section on Device Embolization and Erosion. TEE evaluates these six ASD rims in the upper esophageal short-axis, midesophageal short-axis, four-chamber, and bicaval views, and TTE provides similar views. The TEE views and corresponding rims evaluated are listed in Table 4. Although TTE might be adequate for the evaluation of rims in smaller pediatric patients, in larger pediatric and adult patients, it will typically be inadequate. Therefore, TEE is recommended for

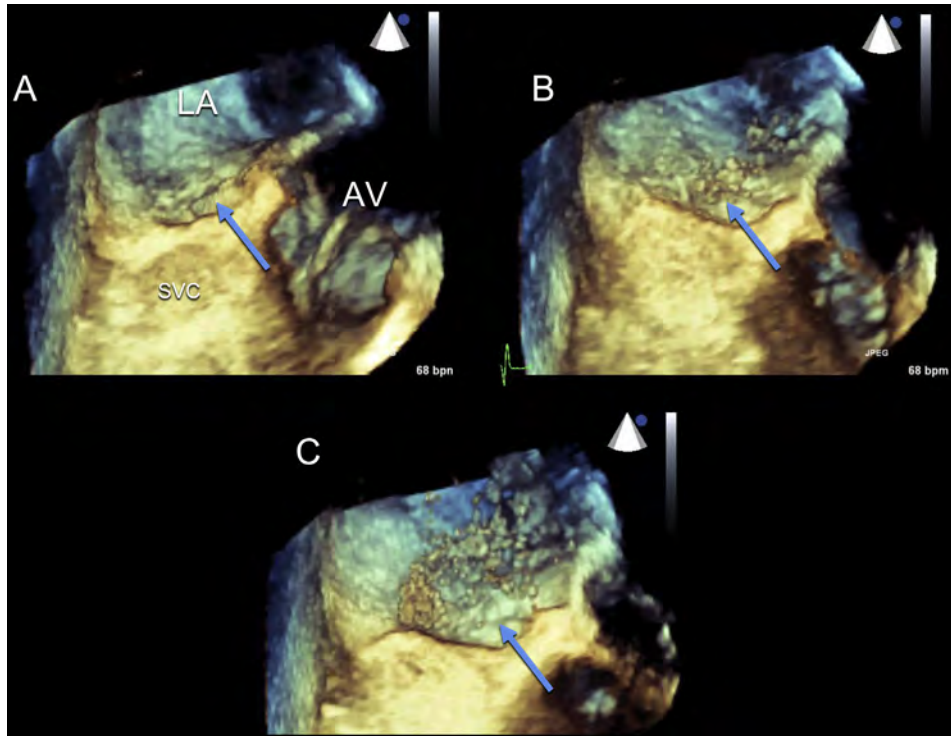


Figure 38 Real-time 3D TEE images from the midesophageal short-axis views of a PFO during a saline contrast study. The PFO exit into the LA is apparent (*blue arrow*). This is performed to help localize the site of bubble entry into the LA and not to quantify the size of the shunt. **(A–C)** Progressive saline contrast microbubbles crossing through the PFO into the LA. *Blue arrow* indicates PFO tunnel. See also [Video 18](#).

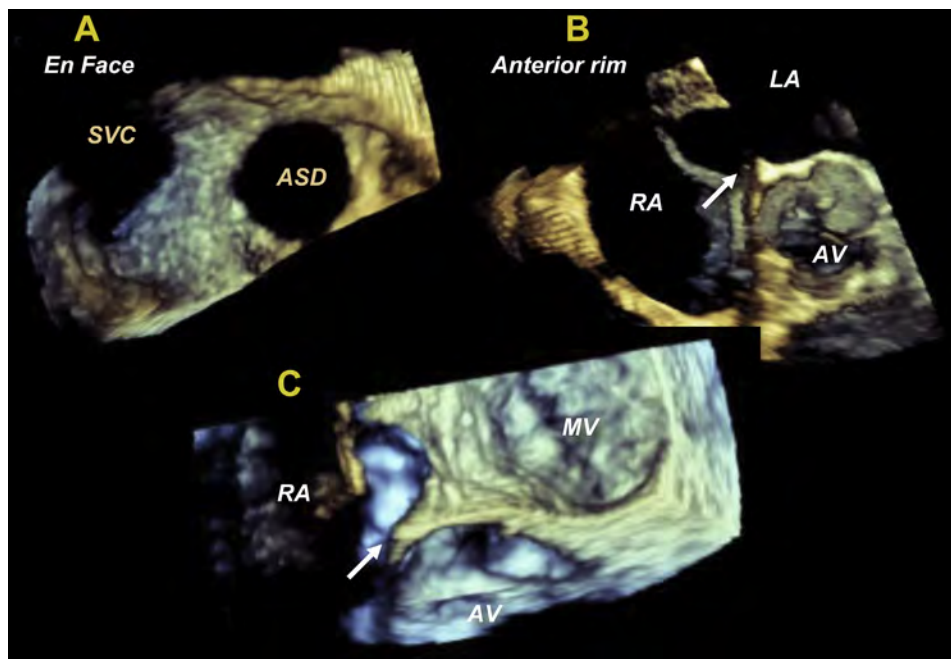


Figure 39 Real-time 3D TEE images of an ostium secundum ASD from the **(A)** RA perspective demonstrating an ASD en face from the midesophageal short-axis view, **(B)** RA perspective demonstrating the aortic rim (*arrow*) from the midesophageal short-axis view, and **(C)** LA perspective from the four-chamber view also demonstrating the aortic rim. *MV*, mitral valve.

these patients to assess these rims before transcatheter closure. ICE has been demonstrated to provide images of the ASD rims similar to those with TEE, although no true four-chamber view is possible

with ICE. TEE with 3D imaging, if available, should be considered for all patients under consideration for percutaneous closure—even if an ICE-guided closure procedure is being planned.

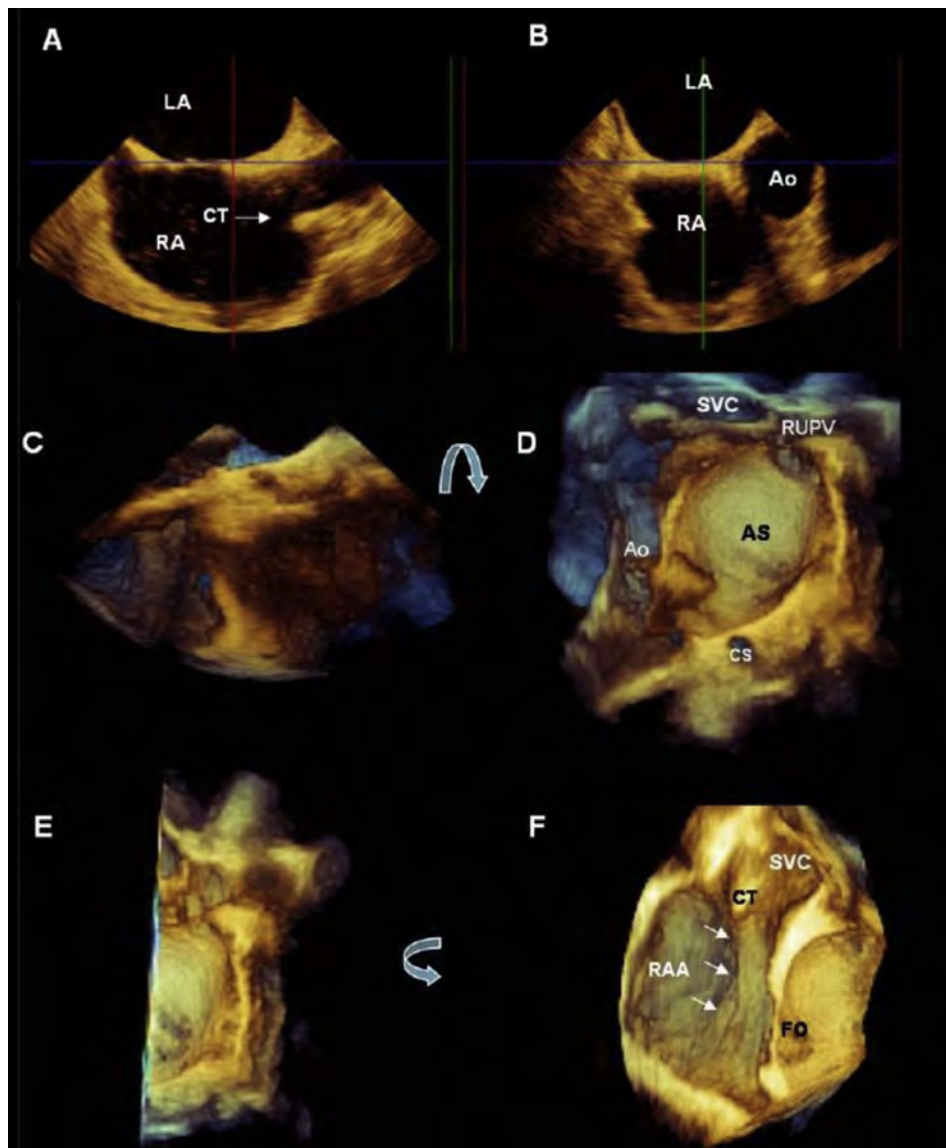


Figure 40 Still image depicting the two perpendicular 2D TEE planes (**A and B**) used to acquire a zoomed 3DE data set of the IAS (**C**). The left side of the atrial septum is shown in the en face perspective visualized after a 90° up–down rotation (*curved arrow*) of the data set (**D**). Image **D** can be cropped to remove the left half of the atrial septum (**E**) and when rotated 90° counterclockwise (*curved arrow*) (**F**), the entire course of the crista terminalis from the SVC toward the IVC (*arrows*) can be visualized. Ao, aorta; AS, atrial septum; CS, coronary sinus; CT, crista terminalis; FO, fossa ovalis; RAA, right atrial appendage.

KEY POINTS

- TTE evaluation of a PFO, including the use of agitated saline contrast, is used to identify the presence or absence of a PFO according to the presence of right-to-left shunting.
- Once a PFO has been identified, if catheter closure is being contemplated, a detailed evaluation of the atrial septal anatomy should be performed using TEE or ICE.
- With the PFO in view, agitated saline contrast is injected to evaluate for right-to-left shunting (see the section on Techniques, Standards, and Characterization Visualization of Shunting: TTE and TEE). Provocative maneuvers such as the Valsalva maneuver should be performed to transiently increase the RA pressure over the LA pressure. Sedated patients might have difficulty performing an adequate Valsalva maneuver.
- The anatomic details of the atrial septum when a PFO is present that should be routinely evaluated include the location of the PFO, thickness and extent of septum secundum, total length of the atrial septum, length of the PFO tunnel, size of the PFO at the RA and LA ends, distance of the PFO from the venae cavae, presence of an ASA, and presence of additional atrial septal fenestrations or defects.

- An ASA is defined as excursion of 10 mm from the plane of the atrial septum into the RA or LA or a combined excursion right and left of 15 mm.
- The common features of all ASDs and other septal defect types that should be evaluated systematically are listed in [Table 7](#).
- Ostium secundum ASDs have six defined rims of tissue surrounding them (aortic, AV valve, SVC, IVC, posterior, and RUPV).
- A ostium secundum ASD rim of less than 5 mm is considered deficient for purposes of transcatheter closure but does not represent an absolute contraindication to the procedure.

ROLE OF ECHOCARDIOGRAPHY IN TRANSCATHETER DEVICE CLOSURE

Echocardiography is commonly used for imaging guidance during percutaneous transcatheter closure of ASDs and PFOs.^{8,57,62,75,83,88,144-146} Real-time intraprocedural echocardiography

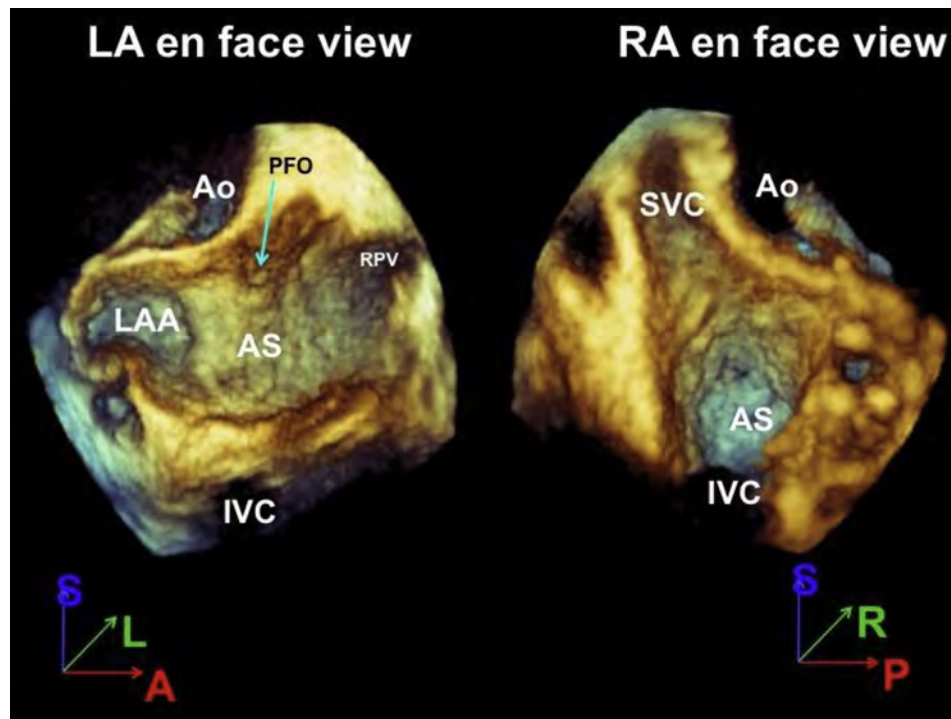


Figure 41 The interatrial septum when viewed from the LA (*left*). The atrial septum should be oriented with the right upper pulmonary vein at the 1-o'clock position. When displayed as viewed from the right atrium (*right*), the SVC should be located at the 11-o'clock position. A, anterior; AS, atrial septum, Ao, aorta; L, left; LAA, left atrial appendage; P, posterior; R, right; S, superior.

with TTE, TEE, 3D imaging, and ICE provides important incremental information before, during, and after deployment of the device. Although each modality has its own advantages and disadvantages, echocardiographic augmentation of fluoroscopic imaging offers significant information in patient selection, device selection, procedural guidance, monitoring for complications, and assessment of the results.

Description of Available Transcatheter Devices and Techniques

The American College of Cardiology/American Heart Association guidelines have recommended ASD closure for patients with RA and RV enlargement, regardless of symptoms (class I).¹⁴⁷ Small ASDs (i.e., an ASD diameter of less than 5 mm) with no evidence of RV enlargement or pulmonary hypertension do not require closure, because they are not considered significant enough to affect the clinical course or hemodynamics of these individuals. Smaller ASDs that are associated with paradoxical embolism or platypnea-orthodeoxia can be considered for closure according to guideline recommendations (class IIa). The only absolute contraindication for ASD closure pertains to patients with irreversible pulmonary hypertension (pulmonary vascular resistance greater than 8 Woods units) and no evidence of left-to-right shunting (class III).¹⁴⁷ Sinus venosus and ostium primum defects are not suitable for percutaneous device closure because of poor anatomic and rim characteristics and the lack of randomized controlled trial data supporting this approach. The indications and contraindications to ASD and PFO closure are listed in [Table 8](#).


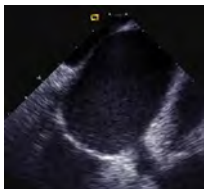


Numerous devices exist for percutaneous transcatheter closure of ASDs and PFOs ([Figure 46](#)). However, no transcatheter closure device has yet been approved by the U.S. FDA for the percutaneous

transcatheter closure of PFOs. The two types of devices currently approved in the United States for transcatheter closure of secundum ASDs are the Helex (W.L. Gore, Newark, DE) and Amplatzer (St. Jude Medical, Plymouth, MN) septal occluder devices ([Figure 46](#)). Only secundum ASDs have been approved by the FDA to be treated with these percutaneous transcatheter closure devices. Thus, patients with sinus venosus and primum defects should be evaluated for surgical repair, if appropriate.

The Helex occluder (W.L. Gore) is composed of expanded polytetrafluoroethylene patch material supported by a single nitinol wire frame. The device bridges and eventually occludes the septal defect as cells infiltrate and ultimately cover the expanded polytetrafluoroethylene membrane. The Helex occluder (W.L. Gore) is not recommended for closure of defects larger than 18 mm in diameter or those in which the rim is absent over more than 25% of the circumference of the defect.

The Amplatzer septal occluder (ASO) and Amplatzer multifenestrated "cribriform" septal occluder (St. Jude Medical) are double-disc devices composed of nitinol mesh and polyester fabric. These devices are designed to appose the septal wall on each side of the defect, creating a platform for tissue ingrowth after implantation. The ASO (St. Jude Medical) is a self-centering device with a waist sized to fill the diameter of a single ASD. The narrow waist of the cribriform device is specifically designed to allow placement through the central defect of a fenestrated septum; the matched disc diameters positioned on either side of the septum maximize coverage of multiple fenestrations. The ASO (St. Jude Medical) is contraindicated in patients in whom a deficiency (defined as less than 5 mm) of septal rim is present between the defect and the right pulmonary vein, AV valve, or IVC. Although a deficiency of the aortic rim is not considered an absolute contraindication to the use of the

Table 5 Intracardiac echocardiographic views for assessment of IAS

| ICE view | Example | Position of ICE catheter | Anterior–posterior flexion | Right–left flexion | Visualized structures |
|-----------------------------|---|-------------------------------------|----------------------------|--------------------|---|
| Home view |  | Mid-RA | Neutral | Neutral | RA, TV, RV, PV, RVOT, lower IAS |
| Septal view |  | Mid-RA | Posterior tilt | Rightward tilt | Inferior and superior IAS, septum primum, septum secundum, relationship to MV |
| Septal long-axis or bicaval |  | Upper RA | Posterior tilt | Rightward tilt | IAS, septum primum, septum secundum, SVC |
| Septal short-axis |  | Mid-RA, turn toward tricuspid valve | Posterior tilt | Leftward tilt | AoV, IAS, posterior–anterior plane of ASD, posterior and AV rims |

MV, mitral valve; RVOT, right ventricular outflow tract; TV, tricuspid valve.

Table 6 Features of currently available intracardiac ultrasound systems

| Ultrasound method/ name of catheter | Catheter size (F) | Imaging frequency range (MHz) | Viewing sector (°) | Depth of field (cm) | Steering (°) | Doppler | RT3D available | Cost |
|--|-------------------|-------------------------------|--------------------|---------------------|--|---------|-------------------------|------|
| Rotational/UltralCE* | 9 | 9 | 360 | 5 | No | No | No | + |
| Phased array/Viewflex Plus† | 9 | 4.5–8.5 | 90 | 21 | Anterior–posterior (120) | Yes | No | ++ |
| Phased array/AcuNav‡ | 8 or 10 | 5–10 | 90 | 16 | Anterior, posterior, left, and right (160) | Yes | Yes (10F catheter only) | ++ |

*Boston Scientific, Natick, MA.

†St. Jude Medical, St. Paul, MN.

‡Siemens Medical Solutions USA, Inc., Malvern, PA.

device, it has been suggested that this could increase the risk of device erosion.

A significant proportion of defects are associated with absent or deficient aortic rims, and although erosion after ASD device closure

occurs most often in these patients, the great majority of these defects can be successfully closed by a device without subsequent erosion. The Helix septal occluders (W.L. Gore) and ASOs (St. Jude Medical) are deployed using their unique delivery systems by way

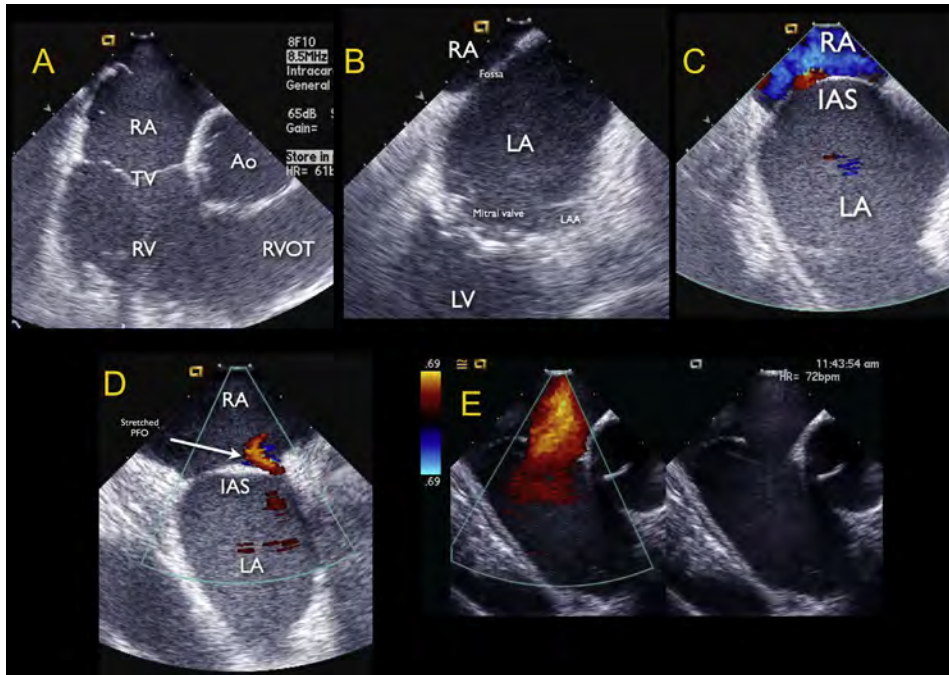


Figure 42 Intracardiac echocardiographic evaluation of the IAS (see the section on Intracardiac Echocardiographic Imaging Protocol for IAS for details). **(A)** Home view. **(B)** Septal long-axis view. **(C)** Bicaval view. **(D)** Septal short-axis view of PFO. **(E)** Septal short-axis view of ostium secundum ASD. The *white arrow* indicates the direction of PFO flow through stretched PFO. LAA, left atrial appendage; RVOT, right ventricular outflow tract; TV, tricuspid valve. See also [Video 19](#).

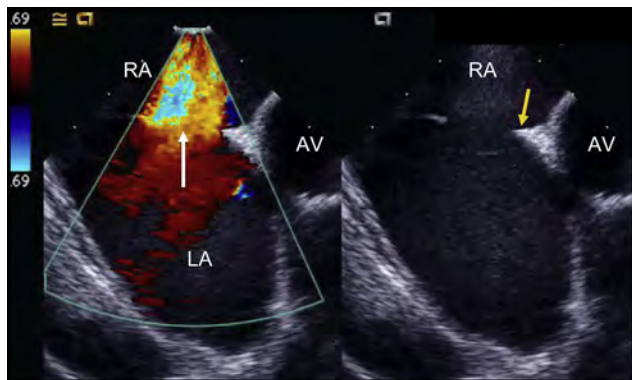


Figure 43 Intracardiac echocardiogram of an ostium secundum ASD with left to right flow with and without color Doppler mapping. The *white arrow* indicates the direction of ASD flow; *yellow arrow*, the aortic rim. AV, aortic valve.

of venous access after careful assessment of the atrial septum and sizing of the defect. The distinctions between techniques in device delivery and assessment of appropriate positioning are discussed in the subsequent sections.

Device Embolization and Erosion

Complications of percutaneous PFO and ASD closure devices are rare and include device embolization, cardiac perforation, tamponade, and device erosion.^{148,149} Device embolization occurs in approximately 0.1%–0.4% of cases and is most common with ASD closure devices.¹⁴⁹ Device embolization is a potential life-threatening complication requiring immediate removal by percuta-

Table 7 Specific characteristics of ASD that should be routinely measured and reported

| |
|--|
| ASD type—PFO, primum ASD, secundum ASD, or other atrial communication (sinus venosus defect, unroofed coronary sinus, anomalous pulmonary vein drainage) |
| Doppler flow—presence of left to right, right to left or bidirectional flow |
| Presence or absence of ASA |
| Associated findings—eustachian valve or Chiari network |
| ASD size—maximal and minimal diameters (optimally measured from 3D volume data sets), ASD area |
| ASD location in septum (i.e., high secundum ASD, sinus venosus defect SVC or IVC type) |
| Measurement of all rims—aortic, RUPV, superior, posterior, inferior, AV septal |
| Shape of ASD—round, oval, irregular |
| Presence of multiple fenestrations |
| Dynamic nature of ASD—measurement of area and maximum/minimal diameters in end-systole and end-diastole |
| Stop-flow diameter of ASD (when balloon sizing is used for percutaneous transcatheter closure) |

neous or surgical intervention. Device embolization can be readily diagnosed by routine surveillance TTE. The risk factors for device embolization include an undersized ASD device, deficient rims of surrounding tissue, and device malpositioning. Immediate embolization can occur after device deployment and most likely results from device malpositioning or an incorrect device size. TTE and TEE are invaluable tools in evaluating the precise location of a dislodged device and the physiologic sequelae (e.g., inflow/outflow obstruction, valve disruption) that result from the embolization.

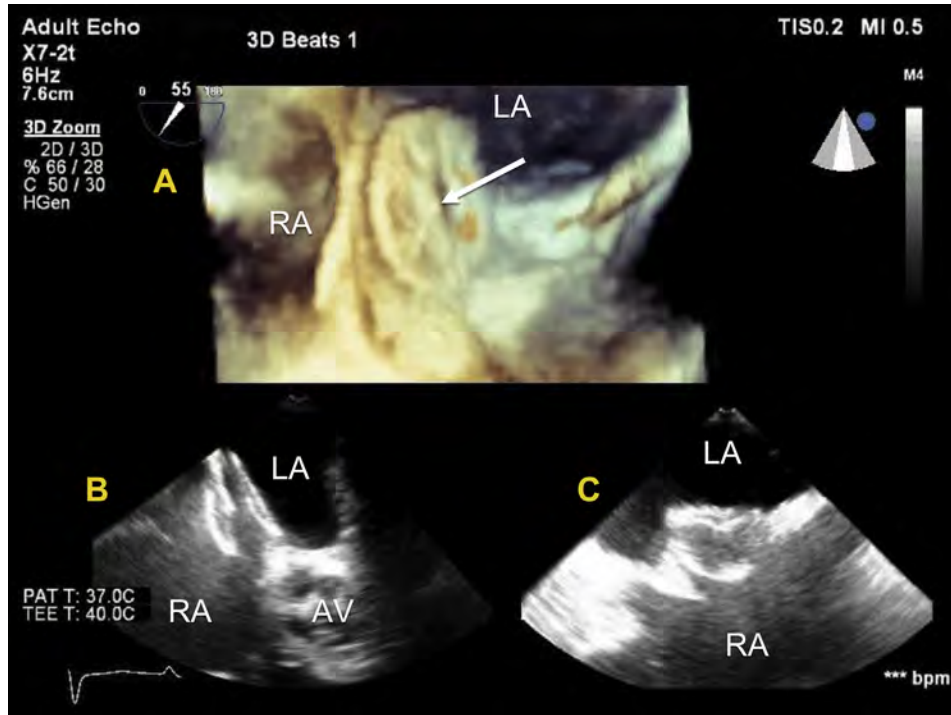


Figure 44 Triplane (A, 3D; B, biplane orthogonal short-axis, and C, biplane orthogonal long-axis views) of cribriform closure device deployed during PFO closure. The white arrow indicates LA disc of closure device. AV, aortic valve.

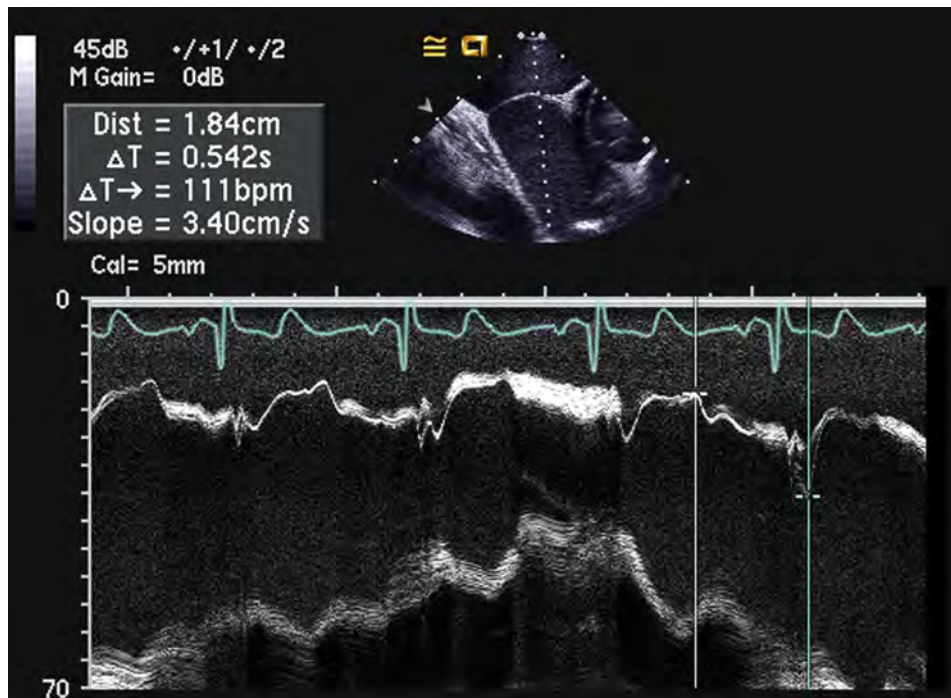


Figure 45 M-mode of an ASA demonstrating greater than 15 mm mobility of the fossa on ICE imaging.

Device erosion is a rare but potentially fatal event. Erosion has been reported to occur with multiple devices, including the ASO (St. Jude Medical), the atrial septal defect occluder system, and the Angel-Wings device (Microvena Corp., White Bear Lake, MN). Of these, only the ASO (St. Jude Medical) is currently approved

for use in the United States.^{63,150,151} The estimated rate of erosion with the ASO (St. Jude Medical) is 0.1%–0.3%.^{150,152–154} Device erosion can occur at the roof of the RA or LA or at the junction of the aorta and can result in hemopericardium, tamponade, aortic fistula, and/or death.¹⁵⁴ Device erosion can begin as a

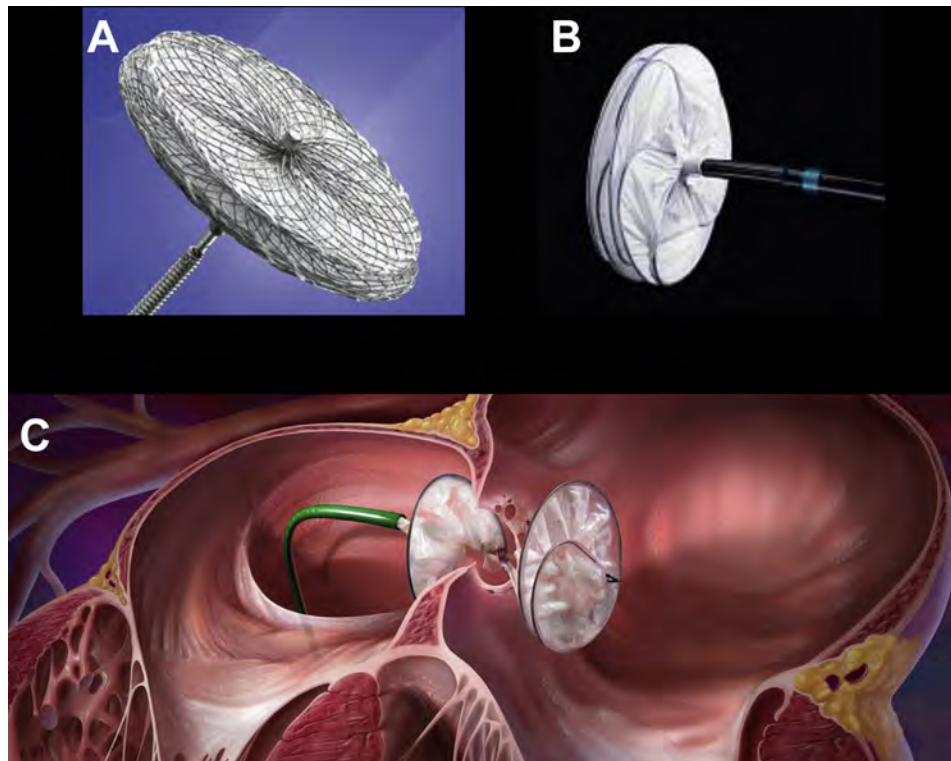


Figure 46 Examples of ASD closure devices. **(A)** ASO (St. Jude Medical). **(B)** Helex occluder (W.L. Gore). **(C)** Cartoon depicting deployment of ASD device. 4C, four-chamber (view); Ao, aorta; SAX, short-axis (view).

Table 8 Indications and contraindications for ASD and PFO closure

| |
|---|
| Potential Indications for ASD and PFO closure |
| Isolated secundum ASD with a pulmonary/systemic flow (Qp/Qs) ratio 1.5:1, signs of right ventricular volume overload |
| PFO—cryptogenic stroke and evidence of right to left shunt (currently still under investigation and not FDA approved) |
| Contraindications (absolute or relative) |
| PFO or small ASD with Qp/Qs <1.5:1 or no signs of RV volume overload |
| A single defect too large for closure (>38 mm) |
| Multiple ASDs unsuitable for percutaneous closure |
| Defect too close to SVC, IVC, pulmonary veins, AV valves, or coronary sinus |
| Anterior, posterior, superior, or inferior rim <5 mm |
| Abnormal pulmonary venous drainage |
| Associated congenital abnormality requiring cardiac surgery |
| ASD with severe pulmonary arterial hypertension and bidirectional or right-to-left shunting |
| Intracardiac thrombi diagnosed by echocardiography |

subclinical event, with the device impinging on the surrounding structures, tenting the atrial or aortic tissue, or resulting in a subclinical pericardial effusion. Erosion can also manifest clinically with chest pain, syncope, shortness of breath, the development of a hemopericardium, cardiac tamponade, hemodynamic compromise, and death.^{151,154}

Most cases of erosion have been reported to occur within 72 hours of device implantation, but late erosion cases have been reported greater than 6 years after deployment.¹⁵⁵ Most erosions occur in the first week after implantation.^{63,151} Although not well defined, it has been assumed that erosion is related to the abrasive mechanical

forces between the human tissue and the device (in contrast to inflammation).

The cause of erosions is unknown. A thorough understanding of this serious problem has been hampered by the infrequency of this complication and the absence of data from control populations. Extensive reviews of imaging and device data from series of cases in which erosions occurred have been performed. From such information and expert consensus, the factors can be broadly divided into those generally thought to be more significant such as device oversizing (present in up to 40% cases), the complete absence of the aortic rim, a high/superior septal location of the defect, and a deficient anterior rim with

Table 9 Proposed possible risk factors for Amplatzer device erosion

| |
|---|
| Deficient aortic rim in multiple views, absent aortic rim at 0° (“bald aorta”) Deficient superior rim in multiple views Superior location of secundum ASD Oversized ASD device (device diameter >1.5 times static stop-flow diameter) Dynamic ASD (50% change in size of ASD) Use of 26-mm ASO device Malaligned defect Tenting of atrial septal free wall after placement of device (into transverse sinus) Wedging of device disc between posterior wall and aorta Pericardial effusion present after device placement |
|---|

associated insufficiency of the posterior rim.¹⁵⁴ Other morphologic risk factors that have been proposed to predict erosion include a specific ASD orientation such as malalignment of the defect with the aorta, a dynamic ASD (one that changes size more than 50% throughout the cardiac cycle), a deficient or an absent aortic rim (present in up to 90% of cases), and a device that straddles or splays around the aorta.¹⁵⁴ No consensus has been reached, however, in the interventional community regarding the root cause of erosion.^{31,152} It is important to note, for example, that a deficient aortic rim is prevalent among populations of patients who have undergone successful device closure of ASD with the ASO (St. Jude Medical) (40% in a recent report).^{31,153,154} Important risk factors for erosion after device placement have been suggested from a retrospective review of available data on confirmed cases and include deformation of the closure device at the aortic root and pericardial effusion seen within 24 hours of deployment. The proposed risk factors for erosion of the Amplatzer device are listed in [Table 9](#).

No one risk factor or echocardiographic feature therefore can define the absolute risk of erosion. Thus, no clear “echocardiographic contraindications” exist for device closure. In one conceptual framework, for example, erosion might result from the unique combination of certain specific high-risk ASD morphologic features that are then combined with an oversized device and subsequent remodeling of the heart and closure device. Echocardiographic imaging therefore might help to identify patients at risk of erosion (e.g., aortic rim deficiencies, device–patient mismatch at the atrial roof, or impingement of the aorta before release).¹⁵⁴ The FDA and the manufacturer have concurred that an additional postapproval study of the ASO (St. Jude Medical) would be beneficial to better evaluate the risk factors for erosion. A standardized rigorous protocol for the evaluation of the atrial septum and associated rims, such as described in the present document, has the potential to increase the quality and consistency of the data used to analyze the root cause and prevent this rare, but serious, complication.

Imaging Modalities in Transcatheter Guidance: TTE, TEE, ICE

Regardless of modality, echocardiography is essential in the monitoring of transcatheter procedure guidance and postprocedural complications. A comprehensive list of all potential complications of transcatheter closure and the appropriate imaging modality to assist with the diagnosis is provided in [Table 10](#).

Table 10 Acute and chronic complications of percutaneous transcatheter closure and role of echocardiography in diagnosis and treatment

| Complication | Consequence | Acuity | Treatment | Role of echocardiography | Preferred echocardiographic modality |
|-------------------------|-------------------------------------|------------------|------------------------------------|---|--|
| Cardiac perforation | Tamponade | Acute | Surgery | Diagnosis | TTE, TEE, or ICE |
| Device embolization | Embolization, valve obstruction | Acute or chronic | Percutaneous or surgical retrieval | Diagnosis, guidance of percutaneous retrieval | TTE, TEE, or ICE for diagnosis; TEE or ICE for retrieval |
| Bleeding | Hypovolemia, shock, death | Acute | Transfusion, surgical intervention | Excluding other diagnoses | TTE |
| Pulmonary embolism | Respiratory failure, death | Acute | Anticoagulation | Evaluating for right heart strain | TTE |
| Device erosion | Hemopericardium, tamponade, death | Chronic or late | Surgical | Diagnosis | TTE (effusion or hematoma); TEE (erosion) |
| Device thrombosis | Embolism, stroke | Chronic or late | Anticoagulation | Diagnosis | TEE |
| Infectious endocarditis | Embolism, sepsis, abscess, death | Chronic or late | Antibiotics, surgery | Diagnosis | TEE |
| Device fracture | Cardiac erosion, perforation, shunt | Chronic or late | Surgical exploration | Diagnosis | TEE |

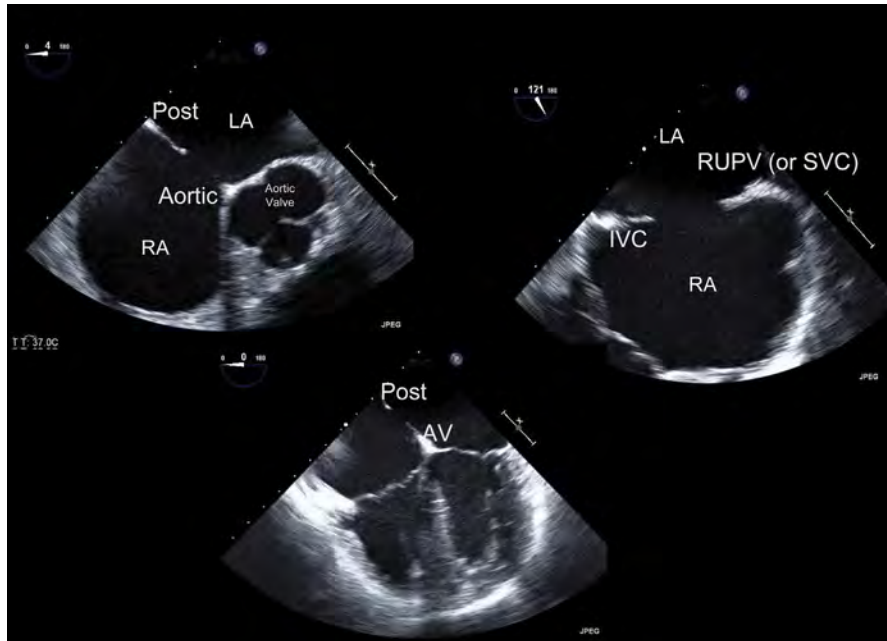


Figure 47 Images representing three (of five) key views for assessment of ASD by TEE. Short-axis views are critical for the assessment of the aortic rim and device interaction with the aorta. Bicaval and long-axis views (not shown) are critical for the assessment of the relationship of the device with the roofs of the atrium. AV, atrioventricular valve rim; Post, posterior rim.

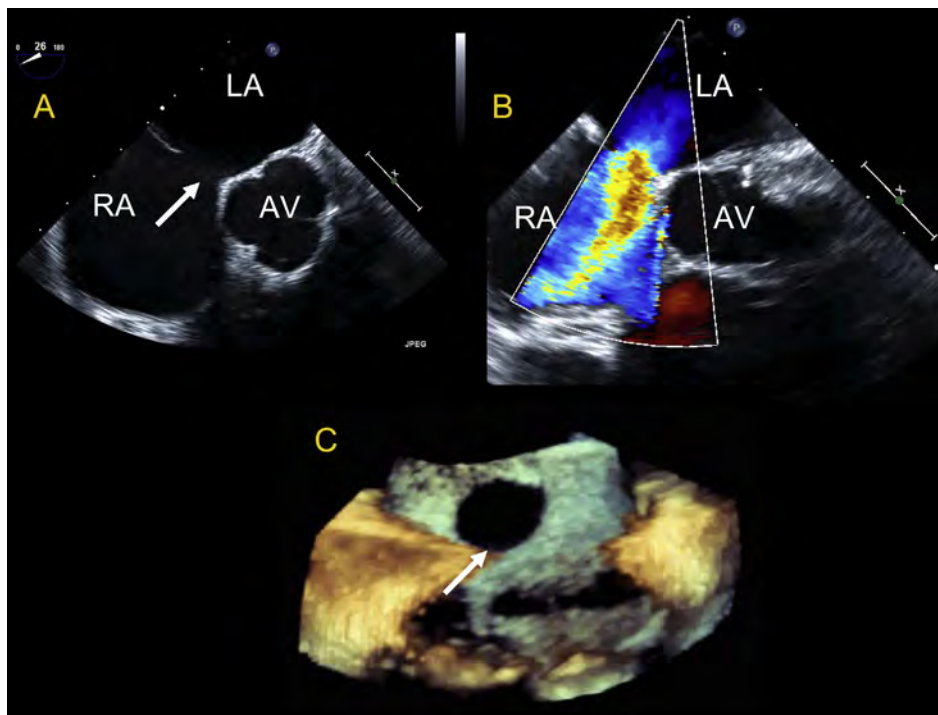


Figure 48 Three-dimensional TEE of medium size ostium secundum ASD with a mildly deficient aortic rim. **(A)** Midesophageal aortic valve short-axis view demonstrating ASD and aortic rim deficiency. **(B)** Similar view demonstrating brisk left to right color Doppler flow. **(C)** Zoom acquisition of ASD en face from RA perspective. White arrow indicates ASD. AV, aortic valve.

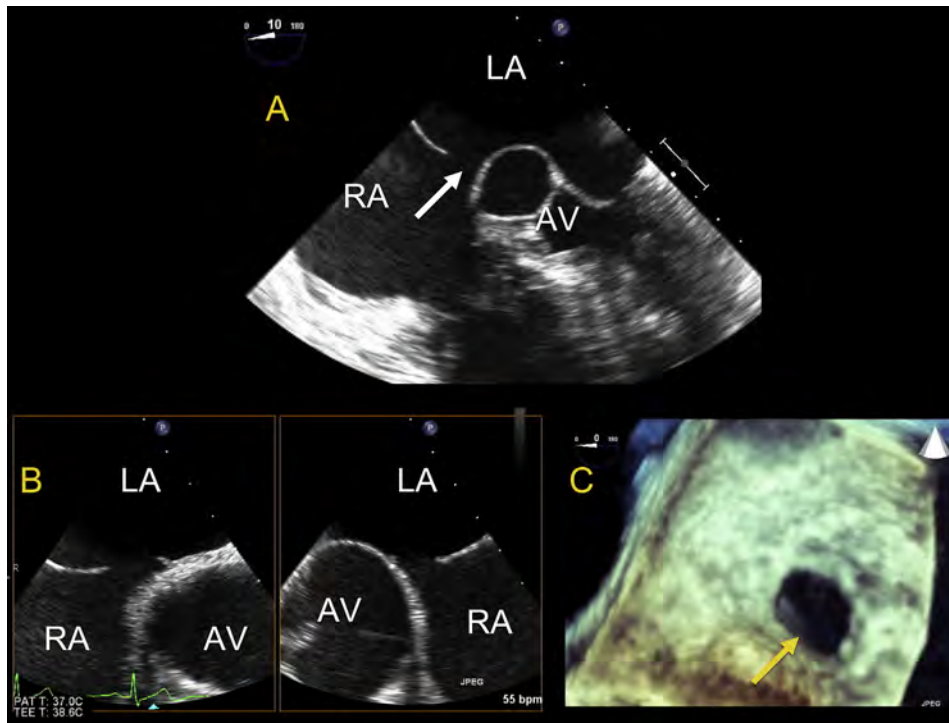


Figure 49 Three-dimensional TEE of medium size ostium secundum ASD with a deficient aortic rim. **(A)** Modified midesophageal four-chamber view. **(B)** Biplane image demonstrating multiple areas of deficiency. **(C)** Zoom acquisition of ASD en face from LA perspective. *Yellow arrow* indicates a deficient rim; *white arrow*, ASD. AV, aortic valve. See also [Videos 20 and 21](#).

Transthoracic echocardiography is the least invasive imaging modality for percutaneous transcatheter closure and could be adequate for procedure guidance in smaller patients.⁶² Its limitations include suboptimal imaging in larger patients and interference of the echocardiographic probe with fluoroscopy. In addition, the implanted device creates artifacts, frequently precluding interrogation of the lower rim of the atrial septal tissue above the IVC.

Transesophageal echocardiography provides detailed imaging findings during percutaneous transcatheter closure.^{7,8,63,66,80,90,145} General anesthesia can be used when TEE is performed to enhance patient comfort and reduce the aspiration risk. In addition to anesthesia support personnel, a dedicated echocardiographer is required to perform the TEE during the closure procedure. Conscious sedation can also be used for selected cases.

Intracardiac echocardiography has emerged as an alternative, and in some centers, the preferred, imaging modality for transcatheter closure guidance.^{65,83,85,88,91,92,146,156} ICE offers imaging that is comparable to TEE and superior to TEE with respect to LA structures and the posterior–inferior rim of the septum. An additional 8F–11F sheath is required for the intracardiac echocardiographic system. If the patient’s weight is more than 35 kg, the sheaths for both the device delivery and the ICE systems can be placed in the same femoral vein using two separate punctures several millimeters from each other. In smaller patients, venous access for the ICE catheter should be obtained in the contralateral vein. Although separate echocardiographic expertise is often used to provide assistance during the procedure, it is not required, because the interventionalist performing the septal closure can also manipulate the catheter. Its advantages include avoidance of general anesthesia, shorter procedure and fluoroscopy times, and comparable or lower cost to TEE-guided percutaneous closure

when general anesthesia is used for those undergoing TEE-guided closure.^{65,83,90,146} Three-dimensional ICE has been recently introduced, and the preliminary results reported from evaluating patients with structural heart disease are beginning to emerge.^{95,97}

Three-dimensional TEE offers RT3D imaging of the atrial septum, providing a comprehensive analysis of the defect and its relationship to the surrounding structures. Direct visualization of the deployed device from both atria augment the postdeployment assessment of the efficacy and potential complications associated with the procedure.^{6,7,31,63,65}

Intraprocedural Guidance of Transcatheter Interventions

All patients undergoing percutaneous transcatheter closure of septal defects require preprocedural echocardiographic imaging with either TTE or TEE, as outlined, to comprehensively assess the septal anatomy and determine the suitability of an atrial defect for device closure. This includes a thorough echocardiographic investigation of the entire IAS and surrounding structures using multiple sequential planes, as previously defined. The type of defect (ASD type, ASA, PFO, stretched PFO) and the number of defects (up to 13% of patients could have more than one defect), defect size, location, morphology, and the surrounding atrial septal tissue (rims) should be defined ([Table 7](#)). Any associated abnormalities of the surrounding structures such as the pulmonary veins, IVC, SVC, coronary sinus, eustachian valve, and AV valves should be characterized or excluded.

The IAS defect and surrounding rims of atrial tissue should be carefully and thoroughly interrogated. Using TEE with the midesophageal four-chamber view (starting from 0° multiplane and moving in 15° multiplane increments), the inferior–anterior and

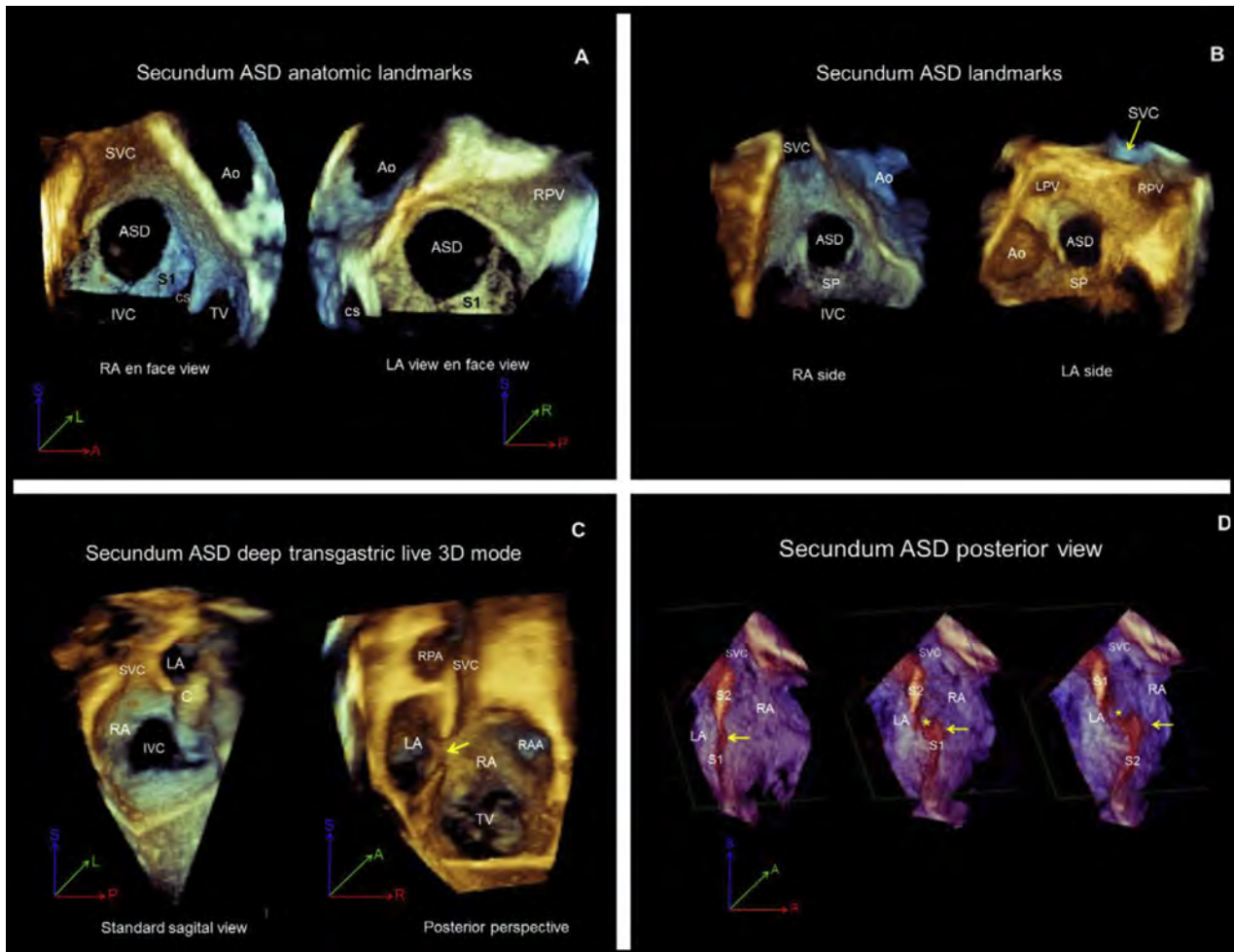


Figure 50 Representative views and anatomic landmarks in an ostium secundum ASD. **(A)** RA and LA en face views. **(B)** Another example of RA and LA en face views. **(C)** Transgastric sagittal bicaval view acquired in live 3D mode from the standard perspective (*left*) and posterior perspective (*right*). **(D)** Posterior aspect views demonstrating the variable alignment between the septum primum and septum secundum over the cardiac cycle. (*Left*) Alignment between the septum secundum and septum primum (*arrow*) components. Mild malalignment (*middle*) and more malalignment (*right*) present between the septal components. As the malalignment increases, the size of the interatrial communication (*asterisk*) increases. In the orientation icon, *blue* designates the *y* plane, *red*, the *x* plane, and *green*, the *z* plane. *A*, anterior; *Ao*, aorta; *C*, catheter; *CS*, coronary sinus; *L*, left; *LPV*, left pulmonary vein; *P*, posterior; *R*, right; *RAA*, right atrial appendage; *RPA*, right pulmonary artery; *S*, superior; *S1*, septum primum; *S2*, septum secundum; *TV*, tricuspid valve. Reproduced with permission from Roberson et al.⁷²

superior–posterior rims can be defined (Figures 47–49). The anterior (retro-aortic) and posterior rims are measured in the midesophageal AoV short-axis view (starting at 30°–45° multiplane and moving in 15° increments). The midesophageal bicaval view (110°–130°) is used to most clearly visualize the superior and inferior rims. Imaging with 3D echocardiography allows for acquisition of similar sets of data but without the need for serial assessment in multiple stepwise views (Figures 50 and 51). Transgastric imaging could be required to visualize the inferior rim of an ASD in some cases and can be used to define the relationship of the inferior aspects of the device and the IAS.

ICE Guidance of PTC

When using ICE guidance, a full assessment of the defect and surrounding tissue rims should be performed. The probe is initially positioned

such that the tricuspid valve is identified. From this position, a posterior deflection of the posterior/anterior knob with a slight rightward rotation of the right–left knob will obtain the septal view (Figures 42C, 43). Advancing the catheter cephalad produces the bicaval view, from which the superior and inferior rims and the defect diameter and configuration are measured (Figure 52A). Rotation of the entire handle clockwise until the intracardiac transducer is near the tricuspid valve, followed by a slight leftward rotation of the right–left knob until the AoV appears creates a view similar to the TEE short-axis plane, with the difference being the near field with ICE is the RA versus that with TEE showing the LA (Figure 52B). From this view, the diameter of the defect and the aortic and posterior rims can be measured.

A complete “neutral” sweep should be performed starting at the “home view” and ending back at the home view. This will, in many instances, effectively exclude sinus venosus SVC-type ASDs, evaluate any AV valve regurgitation, and provide a comprehensive overview of

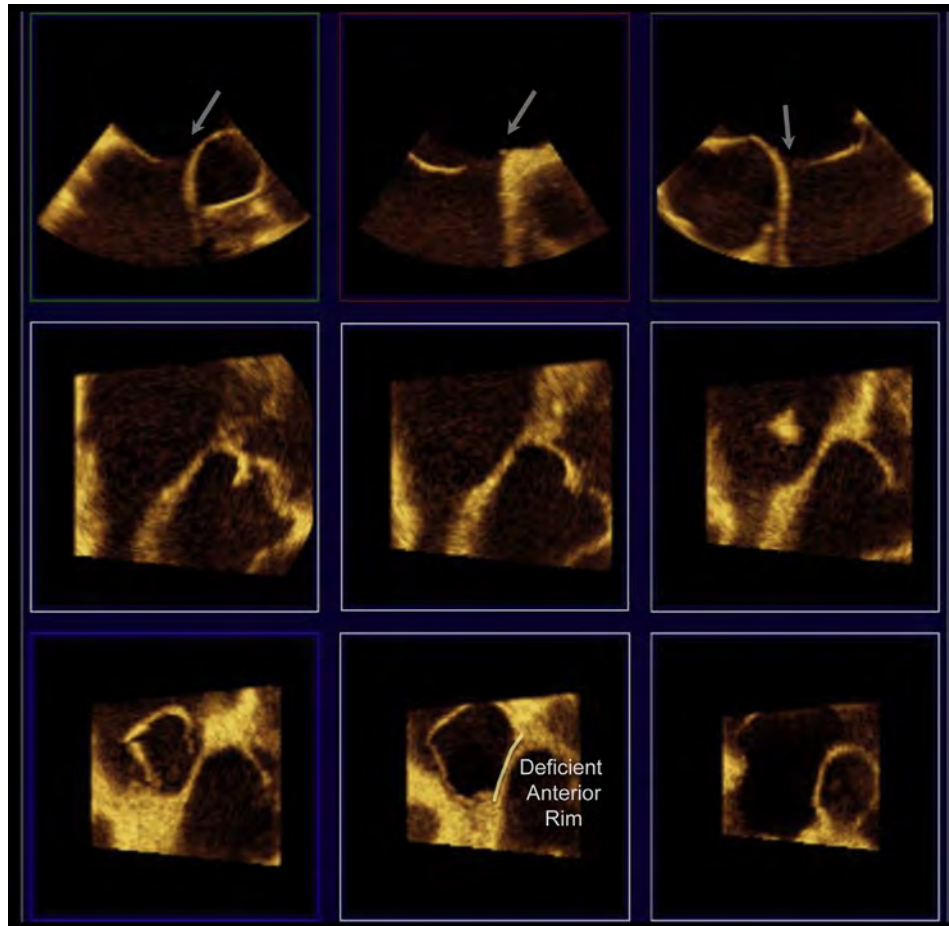


Figure 51 Three-dimensional TEE facilitates en face assessment of ASD shape and size and can characterize the degree of deficiency of the rims. The aortic rim is shown to be deficient in the *bottom center image slice*.

the atrial septum. This should be performed before and after device placement, again to evaluate for mitral regurgitation and tricuspid regurgitation after device placement. A full sweep both of the bicaval and AoV views usually can be done with the catheter having a posterior tilt and pointing directly anterior in the RA.

The initial echocardiographic assessment should include measurement of the defect diameter in the orthogonal planes, overall septal length, and defect rims (retro-aortic, inferior–IVC, and posterior–pulmonary vein). If multiple defects are present, each should be characterized and the distance separating them measured.

In addition to echocardiographic data, a thorough right and left heart hemodynamic assessment is performed to determine the physiologic significance of the defect and exclude any anatomic or physiologic contraindications to septal closure. Right upper pulmonary venous angiography (35° left anterior oblique with 35° cranial angulation) can be performed to profile the atrial septum and serve as a fluoroscopic road map during device deployment.

Balloon sizing of the defect with fluoroscopic and echocardiographic imaging is recommended for all ASD device closure cases; however, some operators might choose not to perform balloon sizing owing to the dimensions of the defect. The stop-flow technique involves placement of a sizing balloon (St. Jude sizing balloon, St. Jude Medical; or NuMED sizing balloon, NuMED Inc., Hopkinton, NY) across the interatrial defect. During imaging with color Doppler, slow inflation of the balloon is performed until color

flow across the defect has completely ceased (Figure 53A). The diameter of the balloon within the atrial septum is measured in several imaging planes at the point at which flow across the defect has been eliminated. In addition, it is essential to interrogate the septum during balloon occlusion of the defect in two orthogonal views (short axis and bicaval) to identify or exclude the presence of additional defects.

Once sizing has been completed, the ICE catheter is moved back to the long axis to monitor the various steps of closure (Figure 53B–E).

Imaging the IAS Immediately After the Procedure

Echocardiographic guidance during deployment of both the ASO (St. Jude Medical) and the Helex (W.L. Gore) septal occlusion devices is used to monitor all stages of device delivery. The most useful views with TEE are the four-chamber and short-axis views. With ICE, the bicaval view gives a panoramic image of the entire LA (Figure 53).

For the ASO (St. Jude Medical), a device between the stop-flow diameter and up to 2 mm greater is typically selected. The delivery system is introduced through the venous sheath and advanced into the left upper pulmonary vein (Figures 52 and 53). The wire and the dilator are slowly withdrawn, taking care to eliminate the possibility of air embolism. The device is loaded and advanced to

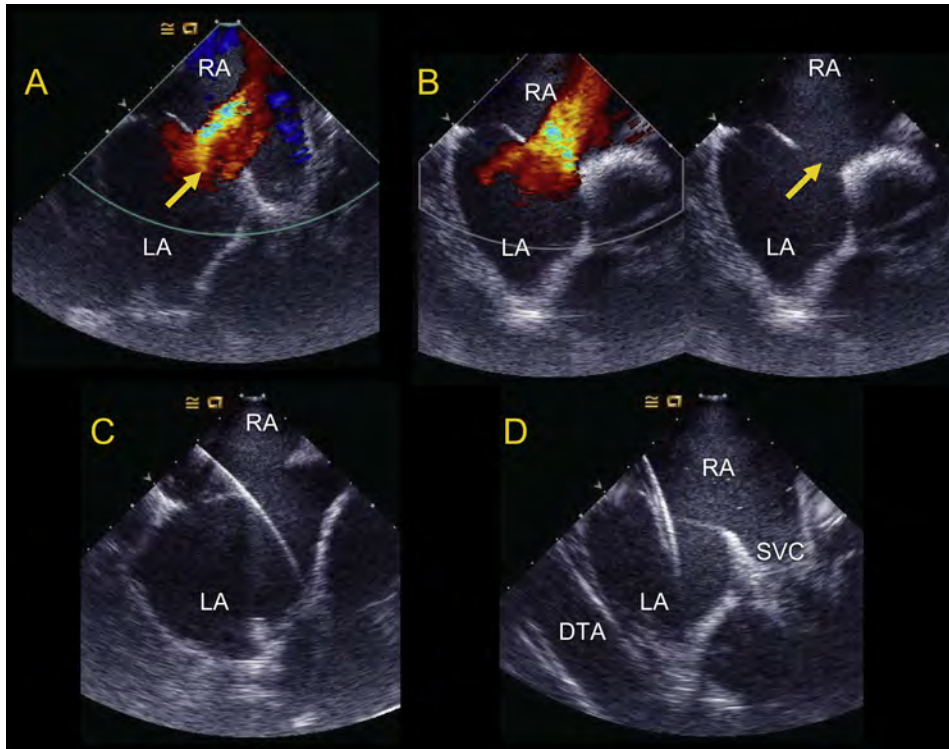


Figure 52 Intracardiac echocardiographically guided ASD closure of ostium secundum defect. **(A and B)** Preprocedure images demonstrating ostium secundum ASD. *Yellow arrow* indicates ASD. **(C)** Passage of guidewire into left superior pulmonary vein. **(D)** Passage of guide catheter into LA. DTA, descending thoracic aorta. See also [Videos 22 and 23](#).

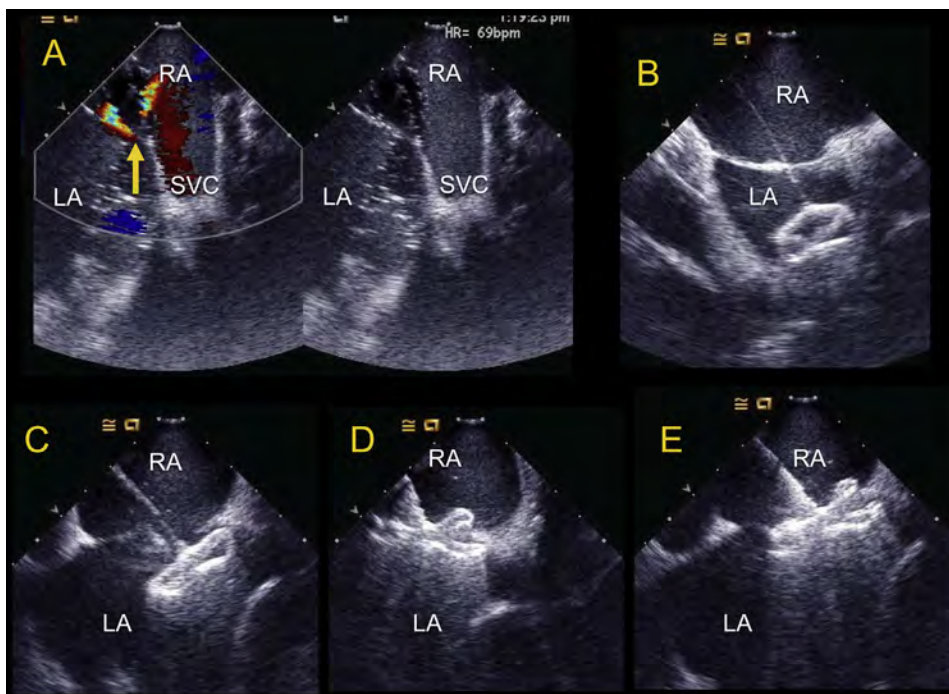


Figure 53 Intracardiac echocardiographically guided ASD closure of ostium secundum defect. **(A)** Balloon sizing of the defect with and without color Doppler. *Arrow* indicates a small degree of flow around the sizing balloon. **(B)** Left atrial disc opens and is withdrawn to the interatrial septum. **(C)** Withdrawal of the LA disc toward the IAS. **(D and E)** Both discs are opened and the position is checked carefully to ensure the septum is “sandwiched” between the discs. See also [Videos 24–28](#). [Video 28](#) represents a sweep through the ASD resulting in an en face view of a stable device.

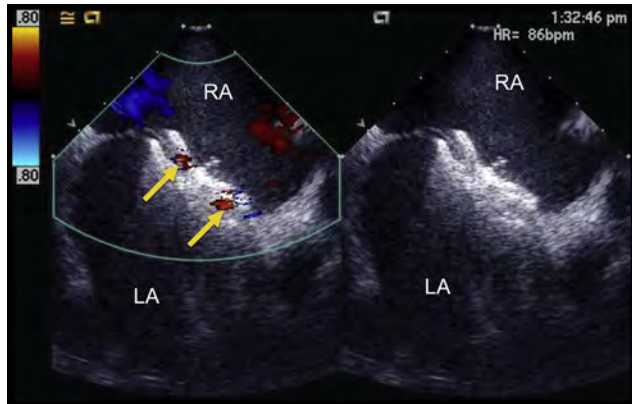


Figure 54 Intracardiac echocardiographically guided ASD closure of ostium secundum defect. See the section on Imaging the IAS Immediately After the Procedure for details. The final position of device (after release from guiding cable) demonstrating normal small residual leak (arrows) through the device (before thrombosis and endothelialization).

the tip of the sheath. The delivery sheath is then repositioned into the body of the LA from the pulmonary vein. The interventionalist fixes the cable and retracts the sheath, thus deploying the LA disc (Figure 53B). It is critical that echocardiography demonstrates to the operator at this stage that the LA disc is remote from the pulmonary veins or LA appendage. Once the left disc is within a few millimeters from the septum, the connecting waist is deployed partially in the LA with continuous traction toward the defect (Figure 53C). The objective is to “stent” the defect with the waist. Next, with continuous traction toward the RA, the RA disc is deployed (Figure 53D and E). Once the entire disc is free of the sheath, the delivery cable is advanced toward the septum to bring the two discs of the device into approximation (Figure 53E).

For the Helex septal occluder (W.L. Gore), the ratio of the device to defect diameter should exceed 2:1, and the selected diameter of the device should be no more than 90% of the measured septal length. Under fluoroscopic and echocardiographic visualization, the catheter tip of the Helex delivery system (W.L. Gore) is advanced across the ASD until the radiopaque marker is positioned within the LA. The left atrial occluder disc is formed in the body of the LA. The interventionalist relies primarily on fluoroscopic imaging for this maneuver. If TEE is being used, it might be beneficial to pull the probe back out of the fluoroscopic field. Once the LA disc has been formed, echocardiographic imaging is used to guide the positioning of the device against the LA aspect of the septum. The LA disc is fixed against the septum while the delivery catheter is withdrawn into the RA and the RA disc is formed. Echocardiographic assessment is performed to confirm that both right and left discs appear planar and apposed to the septum with septal tissue between the discs.

For both the Helex (W.L. Gore) and the ASO (St. Jude Medical) devices, a complete assessment of the device, atrial septum, and surrounding structures is performed before release of the device. Two orthogonal views are obtained to verify that the LA and RA discs are located in the correct chamber. Color Doppler interrogation is performed to exclude residual flow at the device margins, the presence of which suggests inappropriate device size or position (Figure 54). Careful imaging is performed to identify the presence of atrial septal tissue between the LA and RA device discs. Although the aortic rim is generally easily seen, care must be taken

to identify the presence of posterior and inferior tissue. Interference with the pulmonary veins, coronary sinus, AV valve function, and deformation of the aortic root are carefully assessed and excluded before release. Possible device interaction with the aorta and surrounding tissues should be noted. After release of the device, the identical assessments should be performed again. The role of 3D ICE has not yet been clearly defined, but it offers potential for additional anatomic delineation at the transcatheter closure (Figure 55).⁹⁷

Follow-Up

A TTE study should be performed before hospital discharge (and repeated in 1 week when the Amplatzer device has been used). Attention should be given to the device position, any residual shunt, and any evidence of erosion, device instability, or deformation of the surrounding structures. The presence of a pericardial effusion of even modest size could be an indication of device erosion. A 12-lead electrocardiography study should also be performed because rare cases of heart block have been reported with large devices.^{157,158} An increased incidence of atrial arrhythmias and conduction abnormalities early after device closure has been reported.¹⁵⁸

Follow-up evaluations, including TTE, should be performed at 1, 6, and 12 months after the procedure, with a subsequent evaluation every 1–2 years. For the Helex septal occluder (W.L. Gore), attention should also be given toward the stability of the device, because a lack of device stability could indicate wire frame fractures. In instances in which device stability is questionable, fluoroscopic examination without contrast is recommended to identify and assess wire frame fractures. The RV size will typically improve rapidly in the first month after termination of the left-to-right shunt; however, long-standing RV dilation might improve more slowly and also might not normalize completely.¹⁵⁹

KEY POINTS

- TTE is the least invasive imaging modality for percutaneous transcatheter closure and might be adequate for procedure guidance in smaller patients.
- TEE provides detailed imaging during percutaneous transcatheter closure.
- ICE has emerged as an alternative to TEE and, in some centers, is the preferred imaging modality for transcatheter closure guidance.
- 3D TEE offers RT3D imaging of the atrial septum, providing a comprehensive analysis of the defect and its relationship to surrounding structures.
- Regardless of modality used, a complete assessment of the defect and surrounding tissue rims should be performed (Table 7).
- Balloon sizing of the ASD is recommended before closure. During imaging with color Doppler, slow inflation of the balloon is performed until the color flow across the defect has completely ceased. The diameter of the balloon within the atrial septum is measured in several imaging planes at the point at which the flow across the defect has been eliminated.
- A complete assessment of the closure device, atrial septum, and surrounding structures should be performed before release of the device.
- Careful imaging should be performed to identify the presence of atrial septal tissue between the LA and RA device discs. Although the aortic rim is generally easily seen, care must be taken to identify the presence of posterior and inferior tissue.
- TTE should be performed on all patients before hospital discharge (and repeated in 1 week when the ASO device has been used).
- Follow-up evaluations with TTE should be performed at 1, 6, and 12 months after the procedure, with a subsequent evaluation every 1–2 years.

CONCLUSION

As presented in the present document, a comprehensive systematic echocardiographic evaluation of the atrial septal anatomy and associated abnormalities includes the detection and quantification of the

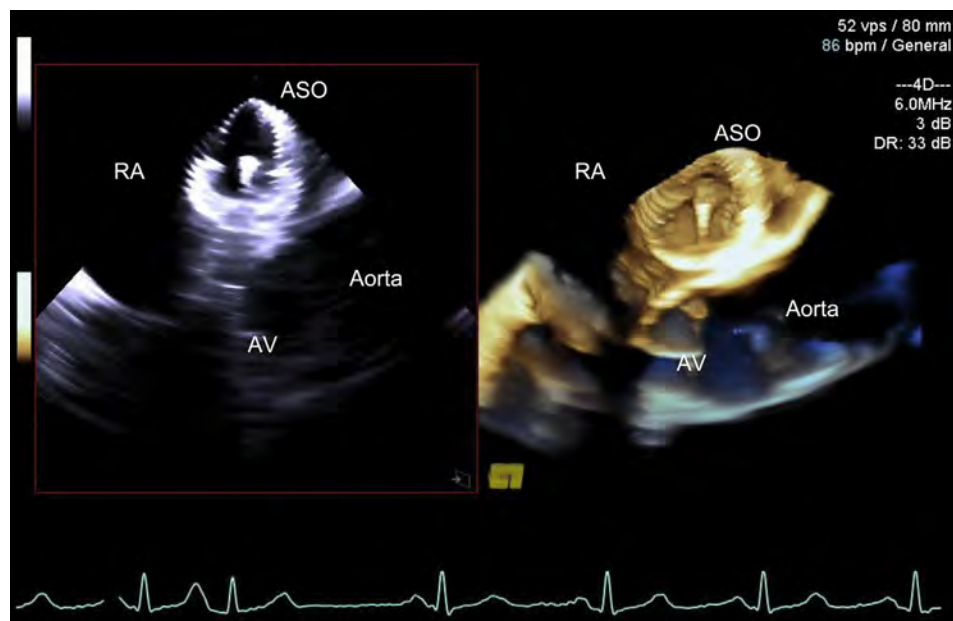


Figure 55 Three-dimensional ICE demonstrating the relationship of the atrial septal occluder to the aorta in 2D (left) and 3D (right) imaging modes. ASO, atrial septal occluder.

size and shape of all defects, the rims of tissue surrounding the defect, the degree and direction of shunting, and the remodeling and changes in size and function of the cardiac chambers and pulmonary circulation. This requires integration of findings across TTE, TEE, and/or ICE imaging for the complete assessment of patients with atrial septal abnormalities. A standardized imaging approach and nomenclature has been presented in the present document to facilitate the comprehensive assessment of these abnormalities.

The emergence of 3D visualization and characterization of normal and abnormal septal anatomy has contributed significantly to the evaluation of the IAS and percutaneous and surgical therapeutic intervention. Future imaging directions include continued refinement of 3D imaging techniques across all modalities (TTE, TEE, ICE), fusion of echocardiography with other imaging modalities such as cardiac computed tomography and fluoroscopy for guidance of transcatheter closure, additional refinement of the methodology in the assessment and quantification of interatrial shunting, and additional delineation of the pathophysiologic relationship of PFO with cryptogenic stroke. Imaging has the potential to contribute to and enhance the understanding of factors that lead to successful device implantation and the risk factors for erosion and device embolization.

NOTICE AND DISCLAIMER

This report is made available by the ASE and the Society for Cardiac Angiography and Intervention (SCAI) as a courtesy reference source for members. This report contains recommendations only and should not be used as the sole basis of medical practice decisions or for disciplinary action against any employee. The statements and recommendations contained in this report were primarily based on the opinions of experts, rather than on scientifically verified data. ASE and SCAI make no express or implied warranties regarding the completeness or accuracy of the information in this report, including the warranty of merchantability or fitness for a particular purpose. In no event shall

ASE or SCAI be liable to you, your patients, or any other third parties for any decision made or action taken by you or such other parties in reliance on this information. Nor does your use of this information constitute the offering of medical advice by ASE or SCAI or create any physician–patient relationship between ASE or SCAI and your patients or anyone else.

SUPPLEMENTARY DATA

Supplementary data related to this article can be found at <http://dx.doi.org/10.1016/j.echo.2015.05.015>.

REFERENCES

1. Samánek M. Children with congenital heart disease: probability of natural survival. *Pediatr Cardiol* 1992;13:152-8.
2. Therrien J, Webb G. Clinical update on adults with congenital heart disease. *Lancet* 2003;362:1305-13.
3. Samánek M, Vorísková M. Congenital heart disease among 815,569 children born between 1980 and 1990 and their 15-year survival: a prospective Bohemia survival study. *Pediatr Cardiol* 1999;20:411-7.
4. Brickner ME, Hillis LD, Lange RA. Congenital heart disease in adults. First of two parts. *N Engl J Med* 2000;342:256-63.
5. Hagen PT, Scholz DG, Edwards WD. Incidence and size of patent foramen ovale during the first 10 decades of life: an autopsy study of 965 normal hearts. *Mayo Clin Proc* 1984;59:17-20.
6. Pushparajah K, Miller OI, Simpson JM. 3D echocardiography of the atrial septum: anatomical features and landmarks for the echocardiographer. *JACC Cardiovasc Imaging* 2010;3:981-4.
7. Song BG, Park SW, Lee S-C, Choi J-O, Park S-J, Chang S-A, et al. Real-time 3D TEE for multiperforated IAS. *JACC Cardiovasc Imaging* 2010;3:1199.
8. Silvestry FE, Kerber RE, Brook MM, Carroll JD, Eberman KM, Goldstein SA, et al. Echocardiography-guided interventions. *J Am Soc Echocardiogr* 2009;22:213-31; quiz 316-317.

9. Rudski LG, Lai WW, Afilalo J, Hua L, Handschumacher MD, Chandrasekaran K, et al. Guidelines for the echocardiographic assessment of the right heart in adults: a report from the American Society of Echocardiography. *J Am Soc Echocardiogr* 2010;23:685-713; quiz 786-788.
10. Shanewise JS, Cheung AT, Aronson S, Stewart WJ, Weiss RL, Mark JB, et al. ASE/SCA guidelines for performing a comprehensive intraoperative multiplane transesophageal echocardiography examination: recommendations of the American Society of Echocardiography Council for Intraoperative Echocardiography and the Society of Cardiovascular Anesthesiologists Task Force for Certification in Perioperative Transesophageal Echocardiography. *J Am Soc Echocardiogr* 1999;12:884-900.
11. Hahn RT, Abraham T, Adams MS, Bruce CJ, Glas KE, Lang RM, et al. Guidelines for performing a comprehensive transesophageal echocardiographic examination: recommendations from the American Society of Echocardiography and the Society of Cardiovascular Anesthesiologists. *J Am Soc Echocardiogr* 2013;26:921-64.
12. Lang RMR, Badano LPL, Tsang WW, Adams DHD, Agricola EE, Buck TT, et al. EAE/ASE recommendations for image acquisition and display using three-dimensional echocardiography. *J Am Soc Echocardiogr* 2012;25:3-46.
13. Johri AM, Rojas CA, El-Sherief A, Witzke CF, Chitty DW, Palacios IF, et al. Imaging of atrial septal defects: echocardiography and CT correlation. *Heart* 2011;97:1441-53.
14. Anderson RH, Brown NA, Webb S. Development and structure of the atrial septum. *Heart* 2002;88:104-10.
15. Geva T. Anomalies of the atrial septum. In: Lai WW, Mertens L, Cohen MS, Geva T, editors. *Echocardiography in Pediatric and Congenital Heart Disease: From Fetus to Adult*. Hoboken, NJ: Wiley-Blackwell; 2009. pp. 158-74.
16. Calvert PA, Rana BS, Kydd AC, Shapiro LM. Patent foramen ovale: anatomy, outcomes, and closure. *Nat Rev Cardiol* 2011;8:148-60.
17. Martins JDF, Anderson RH. The anatomy of interatrial communications—what does the interventionist need to know? *Cardiol Young* 2000;10:464-73.
18. Patel AR, DAlessandro L, Weinberg PM. Anatomy of the atrial septum. In: Hijazi ZM, Feldman T, Abdullah Al-Qbandi MH, Sievert H, editors. *Transcatheter Closure of ASD and PFO*. 1st ed. Minneapolis: Cardiotext Publishers; 2010. pp. 3-15.
19. Schneider B, Zienkiewicz T, Jansen V, Hofmann T, Noltenius H, Meinertz T. Diagnosis of patent foramen ovale by transesophageal echocardiography and correlation with autopsy findings. *Am J Cardiol* 1996;77:1202-9.
20. Rigatelli G, Magro B, Oliva L. Anatomic-functional characterization of IAS for catheter-based interventions. *Am J Cardiovasc Dis* 2011;1:227-35.
21. Kedia G, Tobis J, Lee MS. Patent foramen ovale: clinical manifestations and treatment. *Rev Cardiovasc Med* 2008;9:168-73.
22. Krishnan SC, Salazar M. Septal pouch in the left atrium: a new anatomical entity with potential for embolic complications. *JACC Cardiovasc Interv* 2010;3:98-104.
23. Tugcu A, Okajima K, Jin Z, Rundek T, Homma S, Sacco RL, et al. Septal pouch in the left atrium and risk of ischemic stroke. *JACC Cardiovasc Imaging* 2010;3:1276-83.
24. Strachinaru M, Morissens M, Latifyan S, Costescu I. Left atrial septal pouch thrombus assessed on three-dimensional transoesophageal echocardiography. *Eur Heart J Cardiovasc Imaging* 2012;13:967.
25. Wong JM, Lombardo D, Handwerker J, Fisher M. Cryptogenic stroke and the left atrial septal pouch: a case report. *J Stroke Cerebrovasc Dis* 2014;23:564-5.
26. Strachinaru M, Wauthy P, Sanoussi A, Morissens M, Costescu I, Catez E. The left atrial septal pouch as a possible location for thrombus formation. *J Cardiovasc Med* 2013;14:1-2.
27. Shimamoto K, Kawagoe T, Dai K, Inoue I. Thrombus in the left atrial septal pouch mimicking myxoma. *J Clin Ultrasound* 2014;42:185-8.
28. McCarthy K, Ho S, Anderson R. Defining the morphologic phenotypes of atrial septal defects and interatrial communications. *Images Paediatr Cardiol* 2003;5:1-24.
29. Lock JE, Rome JJ, Davis R, Van Praagh S, Perry SB, Van Praagh R, et al. Transcatheter closure of atrial septal defects: experimental studies. *Circulation* 1989;79:1091-9.
30. Wilson NJ, Smith J, Prommete B, O'Donnell C, Gentles TL, Ruygrok PN. Transcatheter closure of secundum atrial septal defects with the Amplatzer septal occluder in adults and children—follow-up closure rates, degree of mitral regurgitation and evolution of arrhythmias. *Heart Lung Circ* 2008;17:318-24.
31. Tobis J, Shenoda M. Percutaneous treatment of patent foramen ovale and atrial septal defects. *J Am Coll Cardiol* 2012;60:1722-32.
32. Rastogi N, Smeeton NC, Qureshi SA. Factors related to successful transcatheter closure of atrial septal defects using the Amplatzer septal occluder. *Pediatr Cardiol* 2009;30:888-92.
33. Fu YC, Hijazi ZM. The Amplatzer® septal occluder, a transcatheter device for atrial septal defect closure. *Expert Rev Med Devices* 2008;5:25-31.
34. Charuzi Y, Spanos PK, Amplatz K, Edwards JE. Juxtaposition of the atrial appendages. *Circulation* 1973;47:620-7.
35. Kirby ML. Endocardium, cardiac cushions, and valve development. In: *Cardiac Development*. Oxford UK: Oxford University Press; 2007. pp. 119-31.
36. Raghbi G, Ruttenberg HD, Anderson RC, Amplatz K, Adams P, Edwards JE. Termination of left superior vena cava in left atrium, atrial septal defect, and absence of coronary sinus: a developmental complex. *Circulation* 1965;31:906-18.
37. Sun T, Fei H-W, Huang H-L, Chen O-D, Zheng Z-C, Zhang C-J, et al. Transesophageal echocardiography for coronary sinus imaging in partially unroofed coronary sinus. *Echocardiography* 2014;31:74-82.
38. Geggel RL, Perry SB, Blume ED, Baker CM. Left superior vena cava connection to unroofed coronary sinus associated with positional cyanosis: successful transcatheter treatment using Gianturco-Grifka vascular occlusion device. *Catheter Cardiovasc Interv* 1999;48:369-73.
39. Santoro G, Gaio G, Russo MG. Transcatheter treatment of unroofed coronary sinus. *Catheter Cardiovasc Interv* 2013;81:849-52.
40. Ferdman DJ, Brady D, Rosenzweig EB. Common atrium and pulmonary vascular disease. *Pediatr Cardiol* 2011;32:595-8.
41. Gorani DR, Kamberi LS, Gorani NS. Common atrium associated with polydactyly and dwarfism in middle age male patient. *Med Arh* 2011;65:170-2.
42. Jiang H, Wang H, Wang Z, Zhu H, Zhang R. Surgical correction of common atrium without noncardiac congenital anomalies. *J Card Surg* 2013;28:580-6.
43. Agmon Y, Khandheria BK, Meissner I, Gentile F, Whisnant JP, Sicks JD, et al. Frequency of atrial septal aneurysms in patients with cerebral ischemic events. *Circulation* 1999;99:1942-4.
44. Giannopoulos A, Gavras C, Sarioglou S, Agathagelou F, Kassapoglou I, Athanassiadou F. Atrial septal aneurysms in childhood: prevalence, classification, and concurrent abnormalities. *Cardiol Young* 2014;24:453-8.
45. Scaffa R, Spaziani C, Leporace M, Leonetti S, Di Roma M, Gasparone A, et al. Voluminous atrial septal aneurysm may mask a large double atrial septal defect. *Ann Thorac Surg* 2012;93:e41.
46. Krumsdorf U, Keppeler P, Horvath K, Zadan E, Schrader R, Sievert H. Catheter closure of atrial septal defects and patent foramen ovale in patients with an atrial septal aneurysm using different devices. *J Interv Cardiol* 2001;14:49-55.
47. Schuchlenz HW, Saurer G, Weihs W, Rehak P. Persisting eustachian valve in adults: relation to patent foramen ovale and cerebrovascular events. *J Am Soc Echocardiogr* 2004;17:231-3.
48. Schneider B, Hofmann T, Justen MH, Meinertz T. Chiari's network: normal anatomic variant or risk factor for arterial embolic events. *J Am Coll Cardiol* 1995;26:203-10.
49. Lu J-H, Hsu T-L, Hwang B, Weng Z-C. Visualization of secundum atrial septal defect using transthoracic three-dimensional echocardiography in children: implications for transcatheter closure. *Echocardiography* 1998;15:651-60.
50. Attaran RR, Ata I, Kudithipudi V, Foster L, Sorrell VL. Protocol for optimal detection and exclusion of a patent foramen ovale using transthoracic echocardiography with agitated saline microbubbles. *Echocardiography* 2006;23:616-22.

51. Lange A, Walayat M, Turnbull CM, Palka P, Mankad P, Sutherland GR, et al. Assessment of atrial septal defect morphology by transthoracic three dimensional echocardiography using standard grey scale and Doppler myocardial imaging techniques: comparison with magnetic resonance imaging and intraoperative findings. *Heart* 1997;78:382-9.
52. Konstantinides S, Kasper W, Geibel A, Hofmann T, Köster W, Just H. Detection of left-to-right shunt in atrial septal defect by negative contrast echocardiography: a comparison of transthoracic and transesophageal approach. *Am Heart J* 1993;126:909-17.
53. Monte I, Grasso S, Licciardi S, Badano LP. Head-to-head comparison of real-time three-dimensional transthoracic echocardiography with transthoracic and transesophageal two-dimensional contrast echocardiography for the detection of patent foramen ovale. *Eur J Echocardiogr* 2010;11:245-9.
54. Daniëls C, Weytjens C, Cosyns B, Schoors D, De Sutter J, Paelinck B, et al. Second harmonic transthoracic echocardiography: the new reference screening method for the detection of patent foramen ovale. *Eur J Echocardiogr* 2004;5:449-52.
55. Mesihović-Dinarević S, Begić Z, Halimić M, Kadić A, Gojak R. The reliability of transthoracic and transesophageal echocardiography in predicting the size of atrial septal defect. *Acta Med Acad* 2012;41:145-53.
56. Mehta RH, Helmcke F, Nanda NC, Pinheiro L, Samdarshi TE, Shah VK. Uses and limitations of transthoracic echocardiography in the assessment of atrial septal defect in the adult. *Am J Cardiol* 1991;67:288-94.
57. Oto A, Aytemir K, Ozkutlu S, Kaya EB, Yorgun H, Canpolat U, et al. Transthoracic echocardiography guidance during percutaneous closure of patent foramen ovale. *Echocardiography* 2011;28:1074-80.
58. Siostrzonek P, Zangeneh M, Gössinger H, Lang W, Rosenmayr G, Heinz G, et al. Comparison of transesophageal and transthoracic contrast echocardiography for detection of a patent foramen ovale. *Am J Cardiol* 1991;68:1247-9.
59. Kronzon I, Tunick PA, Freedberg RS, Trehan N, Rosenzweig BP, Schwinger ME. Transesophageal echocardiography is superior to transthoracic echocardiography in the diagnosis of sinus venosus atrial septal defect. *J Am Coll Cardiol* 1991;17:537-42.
60. Zhu W, Cao QL, Rhodes J, Hijazi ZM. Measurement of atrial septal defect size: a comparative study between three-dimensional transesophageal echocardiography and the standard balloon sizing methods. *Pediatr Cardiol* 2000;21:465-9.
61. Belohlavek M, Foley DA, Gerber TC, Greenleaf JF, Seward JB. Three-dimensional ultrasound imaging of the atrial septum: normal and pathologic anatomy. *J Am Coll Cardiol* 1993;22:1673-8.
62. Zaout M, Suys B, De Wilde H, De Wolf D. Transthoracic echocardiography guidance of transcatheter atrial septal defect closure in children. *Pediatr Cardiol* 2009;30:992-4.
63. Yared K, Baggish AL, Solis J, Durst R, Passeri JJ, Palacios IF, et al. Echocardiographic assessment of percutaneous patent foramen ovale and atrial septal defect closure complications. *Circ Cardiovasc Imaging* 2009;2:141-9.
64. Bhan A, Kapetanakis S, Pearson P, Dworakowski R, Monaghan MJ. Percutaneous closure of an atrial septal defect guided by live three-dimensional transesophageal echocardiography. *J Am Soc Echocardiogr* 2009;22:753.e1-3.
65. Bartel T, Müller S. Device closure of interatrial communications: per-interventional echocardiographic assessment. *Eur Heart J Cardiovasc Imaging* 2013;14:618-24.
66. Taniguchi M, Akagi T, Watanabe N, Okamoto Y, Nakagawa K, Kijima Y, et al. Application of real-time three-dimensional transesophageal echocardiography using a matrix array probe for transcatheter closure of atrial septal defect. *J Am Soc Echocardiogr* 2009;22:1114-20.
67. Belkin RN, Pollack BD, Ruggiero ML, Alas LL, Tatini U. Comparison of transesophageal and transthoracic echocardiography with contrast and color flow Doppler in the detection of patent foramen ovale. *Am Heart J* 1994;128:520-5.
68. Topçuoğlu MA, Palacios IF, Buonanno FS. Contrast M-mode power Doppler ultrasound in the detection of right-to-left shunts: utility of submandibular internal carotid artery recording. *J Neuroimaging* 2003;13:315-23.
69. Corrado G, Massironi L, Torta D, Rigo F, Beretta S, Sansalone D, et al. Contrast transthoracic echocardiography versus transcranial Doppler for patent foramen ovale detection. *Int J Cardiol* 2011;150:235-7.
70. Woods TD, Patel A. A critical review of patent foramen ovale detection using saline contrast echocardiography: when bubbles lie. *J Am Soc Echocardiogr* 2006;19:215-22.
71. Thanigaraj S, Valika A, Zajarias A, Lasala JM, Perez JE. Comparison of transthoracic versus transesophageal echocardiography for detection of right-to-left atrial shunting using agitated saline contrast. *Am J Cardiol* 2005;96:1007-10.
72. Dragonski B, Bliersch W, Holmer S, Koch H, May A, Bogdahn U, et al. Detection of cardiac right-to-left shunts by contrast-enhanced harmonic carotid duplex sonography. *J Ultrasound Med* 2005;24:1071-6.
73. Rosenzweig BP, Nayar AC, Varkey MP, Kronzon I. Echo contrast-enhanced diagnosis of atrial septal defect. *J Am Soc Echocardiogr* 2001;14:155-7.
74. Soliman OII, Geleijnse ML, Meijboom FJ, Nemes A, Kamp O, Nihoyannopoulos P, et al. The use of contrast echocardiography for the detection of cardiac shunts. *Eur J Echocardiogr* 2007;8:S2-12.
75. Vigna C, Marchese N, Zanchetta M, Chessa M, Inchingolo V, Pacilli MA, et al. Echocardiographic guidance of percutaneous patent foramen ovale closure: head-to-head comparison of transesophageal versus rotational intracardiac echocardiography. *Echocardiography* 2012;29:1103-10.
76. Abdel-Massih T, Dulac Y, Taktak A, Aggoun Y, Massabuau P, Elbaz M, et al. Assessment of atrial septal defect size with 3D-transesophageal echocardiography: comparison with balloon method. *Echocardiography* 2005;22:121-7.
77. Seo J-S, Song J-M, Kim Y-H, Park D-W, Lee S-W, Kim W-J, et al. Effect of atrial septal defect shape evaluated using three-dimensional transesophageal echocardiography on size measurements for percutaneous closure. *J Am Soc Echocardiogr* 2012;25:1031-40.
78. Roberson DA, Cui W, Patel D, Tsang W, Sugeng L, Weinert L, et al. Three-dimensional transesophageal echocardiography of atrial septal defect: a qualitative and quantitative anatomic study. *J Am Soc Echocardiogr* 2011;24:600-10.
79. Magni G, Hijazi ZM, Pandian NG, Delabays A, Sugeng L, Laskari C, et al. Two- and three-dimensional transesophageal echocardiography in patient selection and assessment of atrial septal defect closure by the new DAS-Angel Wings device: initial clinical experience. *Circulation* 1997;96:1722-8.
80. Vaidyanathan B, Simpson JM, Kumar RK. Transesophageal echocardiography for device closure of atrial septal defects: case selection, planning, and procedural guidance. *JACC Cardiovasc Imaging* 2009;2:1238-42.
81. Price MJ, Smith MR, Rubenson DS. Utility of on-line three-dimensional transesophageal echocardiography during percutaneous atrial septal defect closure. *Catheter Cardiovasc Interv* 2010;75:570-7.
82. Tanaka J, Izumo M, Fukuoka Y, Saitoh T, Harada K, Harada K, et al. Comparison of two-dimensional versus real-time three-dimensional transesophageal echocardiography for evaluation of patent foramen ovale morphology. *Am J Cardiol* 2013;111:1052-6.
83. Kim SS, Hijazi ZM, Lang RM, Knight BP. The use of intracardiac echocardiography and other intracardiac imaging tools to guide noncoronary cardiac interventions. *J Am Coll Cardiol* 2009;53:2117-28.
84. Zanchetta M, Onorato E, Rigatelli G, Pedon L, Zennaro M, Carrozza A, et al. Intracardiac echocardiography-guided transcatheter closure of secundum atrial septal defect: a new efficient device selection method. *J Am Coll Cardiol* 2003;42:1677-82.
85. Luxenberg DM, Silvestry FE, Herrmann HC, Cao Q-L, Rohatgi S, Hijazi ZM. Use of a new 8 French intracardiac echocardiographic catheter to guide device closure of atrial septal defects and patent foramen ovale in small children and adults: initial clinical experience. *J Invasive Cardiol* 2005;17:540-5.
86. Bocalandro F, Baptista E, Muench A, Carter C, Smalling RW. Comparison of intracardiac echocardiography versus transesophageal echocardiography guidance for percutaneous transcatheter closure of atrial septal defect. *Am J Cardiol* 2004;93:437-40.

87. Rigatelli G, Dell'Avvocata F, Cardaioli P, Giordan M, Dung HT, Nghia NT, et al. Safety and long-term outcome of modified intracardiac echocardiography-assisted "no-balloon" sizing technique for transcatheter closure of ostium secundum atrial septal defect. *J Interv Cardiol* 2012;25:628-34.
88. Rigatelli G, Dell'Avvocata F, Cardaioli P, Giordan M, Vassiliev D, Nghia NT, et al. Five-year follow-up of intracardiac echocardiography-assisted transcatheter closure of complex ostium secundum atrial septal defect. *Congenit Heart Dis* 2012;7:103-10.
89. Koenig PR, Abdulla R-I, Cao Q-L, Hijazi ZM. Use of intracardiac echocardiography to guide catheter closure of atrial communications. *Echocardiography* 2003;20:781-7.
90. Rao PS. Why, when and how should atrial septal defects be closed in adults. In: Rao PS, editor. *Atrial Septal Defects*; 2012; pp. 121-38.
91. Awad SM, Cao Q-L, Hijazi ZM. Intracardiac echocardiography for the guidance of percutaneous procedures. *Curr Cardiol Rep* 2009;11:210-5.
92. Kim NK, Park S-J, Shin JI, Choi JY. Eight-French intracardiac echocardiography—safe and effective guidance for transcatheter closure in atrial septal defects. *Circ J* 2012;76:2119-23.
93. Mallula K, Amin Z. Recent changes in instructions for use for the Amplatzer atrial septal defect occluder: how to incorporate these changes while using transesophageal echocardiography or intracardiac echocardiography. *Pediatr Cardiol* 2012;33:995-1000.
94. Stapf D, Franke A, Schreckenber M, Schummers G, Mischke K, Marx N, et al. Beat to beat 3-dimensional intracardiac echocardiography: theoretical approach and practical experiences. *Int J Cardiovasc Imaging* 2013; 29:753-64.
95. Kadakia MB, Silvestry FE, Herrmann HC. Intracardiac echocardiography guided transcatheter aortic valve replacement. *Catheter Cardiovasc Interv* 2015;85:497-501.
96. Lee W, Griffin W, Wildes D, Buckley D, Topka T, Chodakauskas T, et al. A 10-Fr ultrasound catheter with integrated micromotor for 4-D intracardiac echocardiography. *IEEE Trans Ultrason Ferroelectr Freq Control* 2011;58:1478-91.
97. Silvestry FE, Kadakia MB, Willhide J, Herrmann HC. Initial experience with a novel real-time three-dimensional intracardiac ultrasound system to guide percutaneous cardiac structural interventions: a phase I feasibility study of volume intracardiac echocardiography in the assessment of patients with structural heart disease undergoing percutaneous transcatheter therapy. *J Am Soc Echocardiogr* 2014;27:978-83.
98. Faletta F, Scarpini S, Moreo A, Ciliberto GR, Austoni P, Donatelli F, et al. Color Doppler echocardiographic assessment of atrial septal defect size: correlation with surgical measurements. *J Am Soc Echocardiogr* 1991;4: 429-34.
99. Kitabatake A, Inoue M, Asao M, Ito H, Masuyama T, Tanouchi J, et al. Noninvasive evaluation of the ratio of pulmonary to systemic flow in atrial septal defect by duplex Doppler echocardiography. *Circulation* 1984;69:73-9.
100. Rufino Nascimento LG, Dehant P, Jimenez M, Dequeker JL, Castela E, Choussat A. Calculation of the pulmonary to systemic flow ratio using echo-Doppler in septal defects—correlation with oximetry. *Rev Port Cardiol* 1989;8:35-40.
101. Lin YF, Awa S, Hishi T, Akagi M, Dodo H, Ishii T, et al. Two-dimensional pulsed Doppler echocardiographic technique for estimating pulmonary to systemic blood flow ratio in children with atrial septal defect and patent ductus arteriosus. *Acta Paediatr Jpn* 1989;31:314-22.
102. Joyner CR. In: *Ultrasound in the Diagnosis of Cardiovascular Pulmonary Disease*. Chicago: Year Book Medical Publishers; 1974.
103. Gramiak R, Shah PM, Kramer DH. Ultrasound cardiography: contrast studies in anatomy and function. *Radiology* 1969;92:939-48.
104. Fraker TD, Harris PJ, Behar VS, Kisslo JA. Detection and exclusion of interatrial shunts by two-dimensional echocardiography and peripheral venous injection. *Circulation* 1979;59:379-84.
105. Di Tullio M, Sacco RL, Venketasubramanian N, Sherman D, Mohr JP, Homma S. Comparison of diagnostic techniques for the detection of a patent foramen ovale in stroke patients. *Stroke* 1993;24:1020-4.
106. Johansson MC, Helgason H, Dellborg M, Eriksson P. Sensitivity for detection of patent foramen ovale increased with increasing number of contrast injections: a descriptive study with contrast transesophageal echocardiography. *J Am Soc Echocardiogr* 2008;21:419-24.
107. Marriott K, Manins V, Forshaw A, Wright J, Pascoe R. Detection of right-to-left atrial communication using agitated saline contrast imaging: experience with 1162 patients and recommendations for echocardiography. *J Am Soc Echocardiogr* 2013;26:96-102.
108. Fan S, Nagai T, Luo H, Atar S, Naqvi T, Birnbaum Y, et al. Superiority of the combination of blood and agitated saline for routine contrast enhancement. *J Am Soc Echocardiogr* 1999;12:94-8.
109. Johansson MC, Eriksson P, Guron CW, Dellborg M. Pitfalls in diagnosing PFO: characteristics of false-negative contrast injections during transesophageal echocardiography in patients with patent foramen ovales. *J Am Soc Echocardiogr* 2010;23:1136-42.
110. Rahmouni HW, Keane MG, Silvestry FE, St John Sutton MG, Ferrari VA, Scott CH, et al. Failure of digital echocardiography to accurately diagnose intracardiac shunts. *Am Heart J* 2008;155:161-5.
111. Spencer MP, Moehring MA, Jesurum J, Gray WA, Olsen JV, Reisman M. Power M-mode transcranial Doppler for diagnosis of patent foramen ovale and assessing transcatheter closure. *J Neuroimaging* 2004;14: 342-9.
112. Lao AY, Sharma VK, Tsivgoulis G, Frey JL, Malkoff MD, Navarro JC, et al. Detection of right-to-left shunts: comparison between the international consensus and Spencer logarithmic scale criteria. *J Neuroimaging* 2008;18:402-6.
113. Caputi L, Carriero MR, Falcone C, Parati E, Piotti P, Materazzo C, et al. Transcranial Doppler and transesophageal echocardiography: comparison of both techniques and prospective clinical relevance of transcranial Doppler in patent foramen ovale detection. *J Stroke Cerebrovasc Dis* 2009;18:343-8.
114. Siostrzonek P, Lang W, Zangeneh M, Gössinger H, Stümpflen A, Rosenmayr G, et al. Significance of left-sided heart disease for the detection of patent foramen ovale by transesophageal contrast echocardiography. *J Am Coll Cardiol* 1992;19:1192-6.
115. Lang RM, Badano LP, Mor-Avi V, Afilalo J, Armstrong A, Ernande L, et al. Recommendations for cardiac chamber quantification by echocardiography in adults: an update from the American Society of Echocardiography and the European Association of Cardiovascular Imaging. *J Am Soc Echocardiogr* 2015;28:1 e14-3914.
116. Alghamdi MH, Grosse-Wortmann L, Ahmad N, Mertens L, Friedberg MK. Can simple echocardiographic measures reduce the number of cardiac magnetic resonance imaging studies to diagnose right ventricular enlargement in congenital heart disease? *J Am Soc Echocardiogr* 2012;25:518-23.
117. Brown DW, McElhinney DB, Araoz PA, Zahn EM, Vincent JA, Cheatham JP, et al. Reliability and accuracy of echocardiographic right heart evaluation in the U.S. Melody valve investigational trial. *J Am Soc Echocardiogr* 2012;25:383-4.
118. Gopal AS, Chukwu EO, Iwuchukwu CJ, Katz AS, Toole RS, Schapiro W, et al. Normal values of right ventricular size and function by real-time 3-dimensional echocardiography: comparison with cardiac magnetic resonance imaging. *J Am Soc Echocardiogr* 2007;20:445-55.
119. Lu X, Nadvoretzkiy V, Bu L, Stolpen A, Ayres N, Pignatelli RH, et al. Accuracy and reproducibility of real-time three-dimensional echocardiography for assessment of right ventricular volumes and ejection fraction in children. *J Am Soc Echocardiogr* 2008;21:84-9.
120. Jenkins C, Chan J, Bricknell K, Strudwick M, Marwick TH. Reproducibility of right ventricular volumes and ejection fraction using real-time three-dimensional echocardiography: comparison with cardiac MRI. *Chest* 2007;131:1844-51.
121. Tamborini G, Marsan NA, Gripari P, Maffessanti F, Brusoni D, Muratori M, et al. Reference values for right ventricular volumes and ejection fraction with real-time three-dimensional echocardiography: evaluation in a large series of normal subjects. *J Am Soc Echocardiogr* 2010;23: 109-15.
122. Ryan T, Petrovic O, Dillon JC, Feigenbaum H, Conley MJ, Armstrong WF. An echocardiographic index for separation of right ventricular volume and pressure overload. *J Am Coll Cardiol* 1985;5:918-27.

123. Steele PM, Fuster V, Cohen M, Ritter DG, McGoon DC. Isolated atrial septal defect with pulmonary vascular obstructive disease—long-term follow-up and prediction of outcome after surgical correction. *Circulation* 1987;76:1037-42.
124. Vogel M, Berger F, Kramer A, Alexi-Meshkishvili V, Lange PE. Incidence of secondary pulmonary hypertension in adults with atrial septal or sinus venosus defects. *Heart* 1999;82:30-3.
125. Abbas AE, Fortuin FD, Schiller NB, Appleton CP, Moreno CA, Lester SJ. A simple method for noninvasive estimation of pulmonary vascular resistance. *J Am Coll Cardiol* 2003;41:1021-7.
126. Masuyama T, Kodama K, Kitabatake A, Sato H, Nanto S, Inoue M. Continuous-wave Doppler echocardiographic detection of pulmonary regurgitation and its application to noninvasive estimation of pulmonary artery pressure. *Circulation* 1986;74:484-92.
127. Schubert S, Peters B, Abdul-Khaliq H, Nagdyman N, Lange PE, Ewert P. Left ventricular conditioning in the elderly patient to prevent congestive heart failure after transcatheter closure of atrial septal defect. *Catheter Cardiovasc Interv* 2005;64:333-7.
128. Gruner C, Akkaya E, Kretschmar O, Roffi M, Corti R, Jenni R, et al. Pharmacologic preconditioning therapy prior to atrial septal defect closure in patients at high risk for acute pulmonary edema. *J Interv Cardiol* 2012;25:505-12.
129. Masutani S, Senzaki H. Left ventricular function in adult patients with atrial septal defect: implication for development of heart failure after transcatheter closure. *J Card Fail* 2011;17:957-63.
130. Homma S, Sacco RL. Patent foramen ovale and stroke. *Circulation* 2005;112:1063-72.
131. Calvet D, Mas J-L. Closure of patent foramen ovale in cryptogenic stroke: a never ending story. *Curr Opin Neurol* 2014;27:13-9.
132. Dao CN, Tobis JM. PFO and paradoxical embolism producing events other than stroke. *Catheter Cardiovasc Interv* 2011;77:903-9.
133. Blanche C, Noble S, Roffi M, Testuz A, Müller H, Meyer P, et al. Platypnea-orthodeoxia syndrome in the elderly treated by percutaneous patent foramen ovale closure: a case series and literature review. *Eur J Intern Med* 2013;24:813-7.
134. Tobis J. Management of patients with refractory migraine and PFO: Is MIST I relevant? *Catheter Cardiovasc Interv* 2008;72:60-4.
135. Ailani J. Migraine and patent foramen ovale. *Curr Neurol Neurosci Rep* 2014;14:426.
136. Azarbal B, Tobis J, Suh W, Chan V, Dao C, Gaster R. Association of interatrial shunts and migraine headaches: impact of transcatheter closure. *J Am Coll Cardiol* 2005;45:489-92.
137. Volman M, Mojadidi MK, Gevorgyan R, Kaing A, Agrawal H, Tobis J. Incidence of patent foramen ovale and migraine headache in adults with congenital heart disease with no known cardiac shunts. *Catheter Cardiovasc Interv* 2013;81:643-7.
138. Khessali H, Mojadidi MK, Gevorgyan R, Levinson R, Tobis J. The effect of patent foramen ovale closure on visual aura without headache or typical aura with migraine headache. *JACC Cardiovasc Interv* 2012;5:682-7.
139. Rana BS, Shapiro LM, McCarthy KP, Ho SY. Three-dimensional imaging of the atrial septum and patent foramen ovale anatomy: defining the morphological phenotypes of patent foramen ovale. *Eur J Echocardiogr* 2010;11:i19-25.
140. Rigatelli G, Dell'avvocata F, Daggubati R, Dung HT, Nghia NT, Nanjiundappa A, et al. Impact of interatrial septum anatomic features on short- and long-term outcomes after transcatheter closure of patent foramen ovale: single device type versus anatomic-driven device selection strategy. *J Interv Cardiol* 2013;26:392-8.
141. Olivares-Reyes A, Chan S, Lazar EJ, Bandlamudi K, Narla V, Ong K. Atrial septal aneurysm: a new classification in two hundred five adults. *J Am Soc Echocardiogr* 1997;10:644-56.
142. Cooke JC, Gelman JS, Harper RW. Chiari network entanglement and herniation into the left atrium by an atrial septal defect occluder device. *J Am Soc Echocardiogr* 1999;12:601-3.
143. Hausmann D, Daniel WG, Mügge A, Ziemer G, Pearlman AS. Value of transesophageal color Doppler echocardiography for detection of different types of atrial septal defect in adults. *J Am Soc Echocardiogr* 1992;5:481-8.
144. Chen FL, Hsiung MC, Hsieh KS, Li YC, Chou MC. Real time three-dimensional transthoracic echocardiography for guiding Amplatzer septal occluder device deployment in patients with atrial septal defect. *Echocardiography* 2006;23:763-70.
145. Mazic U, Gavora P, Masura J. The role of transesophageal echocardiography in transcatheter closure of secundum atrial septal defects by the Amplatzer septal occluder. *Am Heart J* 2001;142:482-8.
146. Ali S, George LK, Das P, Koshy SKG. Intracardiac echocardiography: clinical utility and application. *Echocardiography* 2011;28:582-90.
147. Warnes CA, Williams RG, Bashore TM, Child JS, Connolly HM, Dearani JA, et al. ACC/AHA 2008 Guidelines for the Management of Adults with Congenital Heart Disease: Executive Summary: a report of the American College of Cardiology/American Heart Association Task Force on Practice Guidelines (writing committee to develop guidelines for the management of adults with congenital heart disease). *Circulation* 2008;118:e714-833.
148. Chessa M, Carminati M, Butera G, Bini RM, Drago M, Rosti L, et al. Early and late complications associated with transcatheter occlusion of secundum atrial septal defect. *J Am Coll Cardiol* 2002;39:1061-5.
149. Abaci A, Unlu S, Alsancak Y, Kaya U, Sezenoz B. Short and long term complications of device closure of atrial septal defect and patent foramen ovale: meta-analysis of 28,142 patients from 203 studies. *Catheter Cardiovasc Interv* 2013;82:1123-38.
150. Amin Z, Hijazi ZM, Bass JL, Cheatham JP, Hellenbrand WE, Kleinman CS. Erosion of Amplatzer septal occluder device after closure of secundum atrial septal defects: review of registry of complications and recommendations to minimize future risk. *Catheter Cardiovasc Interv* 2004;63:496-502.
151. Ivens E, Hamilton-Craig C, Aroney C. Early and late cardiac perforation by Amplatzer atrial septal defect and patent foramen ovale devices. *J Am Soc Echocardiogr* 2009;22:1067-70.
152. El-Said HG, Moore JW. Erosion by the Amplatzer septal occluder: experienced operator opinions at odds with manufacturer recommendations? *Cathet Cardiovasc Intervent* 2009;73:925-30.
153. Diab K, Kenny D, Hijazi ZM. Erosions, erosions, and erosions! Device closure of atrial septal defects: how safe is safe? *Catheter Cardiovasc Interv* 2012;80:168-74.
154. Amin Z. Echocardiographic predictors of cardiac erosion after Amplatzer septal occluder placement. *Catheter Cardiovasc Interv* 2014;83:84-92.
155. Taggart NW, Dearani JA, Hagler DJ. Late erosion of an Amplatzer septal occluder device 6 years after placement. *J Thorac Cardiovasc Surg* 2011;142:221-2.
156. Ilkhanoff L, Naidu SS, Rohatgi S, Ross MJ, Silvestry FE, Herrmann HC. Transcatheter device closure of interatrial septal defects in patients with hypoxia. *J Interv Cardiol* 2005;18:227-32.
157. Al-Anani SJ, Weber H, Hijazi ZM. Atrioventricular block after transcatheter ASD closure using the Amplatzer septal occluder: risk factors and recommendations. *Catheter Cardiovasc Interv* 2010;75:767-72.
158. Hill SL, Berul CI, Patel HT, Rhodes J, Supran SE, Cao QL, et al. Early ECG abnormalities associated with transcatheter closure of atrial septal defects using the Amplatzer septal occluder. *J Interv Card Electrophysiol* 2000;4:469-74.
159. Veldtman GR, Razack V, Siu S, El-Hajj H, Walker F, Webb GD, et al. Right ventricular form and function after percutaneous atrial septal defect device closure. *J Am Coll Cardiol* 2001;37:2108-13.